



**THE STUDY OF ORGANIC SEMICONDUCTORS
TOWARDS DEVICE APPLICATIONS**

by

JOHN FORGIE

A thesis submitted in fulfilment of the requirements for the degree of
Doctor of Philosophy in Department of Pure and Applied Chemistry,
University of Strathclyde

2010

Declaration

This thesis is the result of the author's original research. It has been composed by the author and has not been previously submitted for examination which has led to the award of a degree.

The copyright of this thesis belongs to the author under the terms of the United Kingdom Copyright Acts as qualified by University of Strathclyde Regulation 3.50. Due acknowledgement must always be made of the use of any material contained in, or derived from, this thesis.

Signed:

Date:

Acknowledgements

First and foremost I would like to thank my supervisor Prof. Peter Skabara for giving me the opportunity to do this PhD and for all his help, guidance and encouragement over the years. I would especially like to thank Dr Sergey Gordeyev and Jan Lohr for all my electrochemistry training when I started. Thanks also go to Dr Alex Kanibolotsky and Dr Filipe Vilela for always being available to help and to share their knowledge.

For making me feel welcome in the group when I first joined I would also like to thank Dr Hao Pang, Dr Thomas Westgate, Dr Lyuda Kanibolotskya and Dr Asun Luquin. For making it such an enjoyable working environment and friendly group over the years I would like to thank my fellow PhD students and post-docs; Irina Afonina, Iain Wright, Greg McEntee, Diego Cortizo, Sandie Kaur, Saad Elmasly, Zuzka Vobecka, Neil Thomson, Clara Orifino, Neil Findlay and Dr Juntae Kim.

Finally, I would like to say that I am indebted to you all and this thesis could not have been written without your contributions.

Thank you.

Abstract

In recent years, the use of novel organic conjugated materials as semiconductors in electronic devices has become a continually growing and interesting field of research; the attraction derives from the ability of the materials to be easily manipulated and tailored to suit the desired outcome. Organic semiconductors have tunable band gaps and redox properties that can be influenced through variation of the substituents; accompanying this with the ease and reduced cost of processability required for these materials, it makes them very favourable for device fabrication. Organic semiconductors have found use in devices such as electrochromics, light emitting diodes, field effect transistors, photovoltaics, and sensors. In this thesis, the synthesis and characterisation of many compounds suitable for the aforementioned applications are reported.

Chapter two is the characterisation of monomers and polymers based on the incorporation of tetrathianaphthalene and its open and cyclic forms. Chapter three is the study of conjugated monomers and polymers, containing BODIPY in the main chain, towards the use in photovoltaic devices. Chapter four reports on unusual extended conjugated architectures, the first section is the characterisation of two new dendralene compounds that adopt two different conformers in solution and solid state and the second section reports on a new series of diindenothienothiophene based materials with interesting electrochemical and photophysical properties. In chapter five, a series of compounds that contain a benzobisthiazole core are investigated and in chapter six, the development of two new biological sensors are discussed.

Abbreviations

| | |
|--------|---|
| A | analyte / amp |
| Ac | acetyl |
| a* | dimension of colour |
| a.u. | arbitrary units |
| b* | dimension of colour |
| BODIPY | 4,4-difluoro-4-borata-3a-azonia-4a-aza-s-indacene |
| BTEAI | benzyltriethylammonium iodide |
| BTZ | benzobisthiazole |
| Bu | butyl |
| C | colomb |
| cd | candela |
| CIE | commission international de l'éclairage |
| cm | centimetre |
| CV | cyclic voltammetry |
| DCM | dichloromethane |
| DDQ | dichlorodicyanobenzoquinone |
| DFT | density functional theory |
| DMF | <i>N,N</i> -dimethylformamide |
| DMSO | dimethyl sulfoxide |
| DPV | differential pulse voltammetry |
| e | electron |
| EDOT | 3,4-ethylenedioxythiophene |
| EDST | 3,4-ethylenediselenathiophene |

| | |
|----------|---|
| EDTT | 3,4-ethylenedithiathiophene |
| E_p | voltage peak max |
| E_{pa} | anodic current peak |
| E_{pc} | cathodic voltage peak |
| EPR | electron paramagnetic resonance |
| Et | ethyl |
| eV | electron volt |
| Fc | ferrocene |
| Fc^+ | ferrocenium |
| g | gram |
| h | hour |
| HDME | hanging drop mercury electrode |
| HMDS | hexamethyldisilazane |
| HOMO | highest occupied molecular orbital |
| ICT | intramolecular charge transfer |
| I_p | current peak max |
| I_{pa} | anodic current peak |
| I_{pc} | cathodic current peak |
| iPr | isopropyl |
| iR | internal resistance |
| IR | infrared |
| ISC | intersystem crossing |
| ITO | indium tin oxide |
| IUPAC | international union of pure and applied chemistry |
| L | litre |

| | |
|----------|---|
| L* | lightness |
| LCD | liquid crystal display |
| LUMO | lowest unoccupied molecular orbital |
| m | metre |
| M | molar |
| mA | milliamp |
| m-CPBA | <i>meta</i> -chloroperoxybenzoic acid |
| Me | methyl |
| min | minute |
| mL | millilitre |
| mM | millimolar |
| mol | mole |
| mV | millivolt |
| mW | milliwatt |
| n | number of electrons / non-bonding orbital |
| NCS | <i>N</i> -chlorosuccinimide |
| n-doping | negative doping |
| NO | nitric oxide |
| nm | nanometre |
| NREL | national renewable energy laboratory |
| n-type | negative type |
| OFET | organic field effect transistor |
| OLED | organic light emitting diode |
| OSO | ethylenedioxythiophene-ethylenedithiathiophene- ethylenedioxythiophene |

| | |
|----------|--|
| OPV | organic photovoltaic |
| PCBM | [6,6]-phenyl-C ₆₁ -butyric acid methyl ester |
| PCE | power conversion efficiency |
| p-doped | positively doped |
| p-doping | positive doping |
| PEDOT | poly(ethylenedioxythiophene) |
| PEDTT | poly(ethylenedithiathiophene) |
| Ph | phenyl |
| PLQY | photo luminescent quantum yield |
| PM3 | parameterized model number 3 |
| PPA | polyphosphoric acid |
| PPV | polyphenylene vinylene |
| p-type | positive type |
| R | substituent group |
| RT | room temperature |
| s | second |
| S | siemens / singlet states |
| SCE | standard calomel electrode |
| SEC | spectroelectrochemistry |
| SHE | standard hydrogen electrode |
| SOS | ethylenedithiathiophene-ethylenedioxythiophene- ethylenedithiathiophene |
| SUMO | singly unoccupied molecular orbital |
| T | triplet states |
| THF | tetrahydrofuran |

| | |
|----------|------------------------------------|
| TFA | trifluoroacetic acid |
| TTF | tetrathiafulvalene |
| TTN | tetrathianaphthalene |
| UV | ultraviolet |
| v | vibrational state |
| V | volt |
| V_1 | starting voltage |
| V_2 | finishing voltage |
| V_{OC} | open circuit voltage |
| VDOT | vinylendioxythiophene |
| vis | visible |
| vs | versus |
| x | coordinate of chromaticity diagram |
| X^- | counter anion |
| y | coordinate of chromaticity diagram |
| Y | luminance |

Greek

| | |
|--------------------|---|
| α | 1 st position on heterocycle |
| β | 2 nd position on heterocycle |
| Δ_E | energy difference |
| ΔE_{pa-pc} | difference in potential between anodic and cathodic peaks |
| θ | torsion angle |

| | |
|------------------------|--|
| λ | wavelength |
| λ_{ex} | excitation wavelength |
| λ_{max} | maximum absorption wavelength |
| μA | microamp |
| μm | micrometres |
| μW | microwave |
| π | pi bonding orbital |
| π^* | pi anti-bonding orbital / polarizability |
| σ | sigma bonding orbital |
| σ^* | sigma anti-bonding orbital |

Symbol

| | |
|-------------------------|--|
| A | surface area / absorbance |
| \AA | angstrom |
| c | concentration / speed of light |
| $^{\circ}\text{C}$ | degree centigrade |
| C_{O}^{σ} | concentration of oxidised species at electrode surface |
| C_{R}^{σ} | concentration of reduced species at electrode surface |
| D | diffusion coefficient |
| D_i | diffusion coefficient |
| E | electrode potential |
| E^0 | standard electrode potential |
| $E_{1/2}$ | reversible wave |

| | |
|------------------|---|
| $E_{1/2}^{1ox}$ | first reversible oxidation wave |
| $E_{1/2}^{1red}$ | first reversible reduction wave |
| $E_{1/2}^{2ox}$ | second reversible oxidation wave |
| $E_{1/2}^{2red}$ | second reversible reduction wave |
| E^{1ox} | first irreversible oxidation wave |
| E^{1red} | first irreversible reduction wave |
| E^{2ox} | second irreversible oxidation wave |
| E^{2red} | second irreversible reduction wave |
| E^{3ox} | third irreversible oxidation wave |
| E^{3red} | third irreversible reduction wave |
| E_e | equilibrium potential |
| E_F | fermi energy level |
| E_g | band gap / energy gap |
| E^{Int} | intramolecular and interchain interactions |
| E_L | potential of oxidation reaction |
| E_p | average energy of emitted photon |
| E_R | potential of reduction reaction |
| E^{Res} | aromatic resonance |
| E^{Sub} | the push / pull effect of the substituent group |
| E^θ | degree of planarity |
| $E^{\sigma r}$ | bond length alternation |
| F | Faraday constant |
| $Grad_{ST}$ | gradient of standard sample |
| $Grad_X$ | gradient of unknown sample |
| h | Planck's constant |

| | |
|----------------------------------|--|
| i | current density |
| i_0 | exchange current density |
| I | current / light intensity |
| I_0 | original light intensity |
| $I_L^{\lambda(\text{emission})}$ | intensity of luminescence at emission wavelength |
| $I_L^{\lambda(\text{excit})}$ | intensity of light from monochromator |
| I_{mpp} | maximum current in I-V characteristics |
| I_p | current peak max |
| I_{sc} | short circuit current density |
| I_{sd} | source drain current |
| J_i | flux of electroactive species |
| k | rate of electrochemical reaction / proportionality constant / rate constant |
| k_0 | standard electron transfer rate constant |
| l | path length |
| L | channel length |
| O | oxidised species |
| $[O]$ | concentration of oxidised species |
| P_{in} | intensity of irradiating light |
| Q_d | charge passed in electrochromic devices |
| R | reduced species / gas constant |
| $[R]$ | concentration of reduced species |
| R^2 | coefficient of determination |
| S | eye sensitivity |
| T | temperature / transmission |

| | |
|------------------------------------|---|
| v | scan rate |
| V_D | drain voltage |
| V_g | gate voltage |
| V_{mpp} | maximum voltage in I-V characteristics |
| V_{sd} | source drain voltage |
| V_t | threshold voltage |
| W | channel width |
| α_A | anodic transfer coefficient |
| α_C | cathodic transfer coefficient |
| γ | charge balance of emissive layer |
| δ_{Ci} / δ_x | concentration gradient |
| Δ_G | Gibbs free energy |
| Δ_{OD} | change in optical density |
| ϵ | molar extinction coefficient |
| $\epsilon_{\lambda(\text{excit})}$ | molar absorptivity at excitation wavelength |
| η | overpotential / refractive index / colour efficiency |
| η_C | fraction of photons coupled out of organic light emitting diode |
| η_{ext} | external efficiency |
| η_{int} | internal electroluminescent quantum efficiency |
| η_{lum} | luminous efficiency |
| η_{PL} | photoluminescence quantum efficiency |
| η_{pow} | power efficiency |
| η_R | power efficiency |
| $\lambda_{(\text{excit})}$ | excitation wavelength |
| μ | mobility |

| | |
|--------------------|----------------------------------|
| Φ | quantum yield |
| Φ_{PL} | photoluminescent quantum yield |
| Φ_{ST} | quantum yield of standard sample |
| Φ_{X} | quantum yield of unknown sample |
| χ_{s} | singlet fraction |

Table of Contents

| | |
|--|-------|
| Declaration | i |
| Acknowledgements | ii |
| Abstract | iii |
| Abbreviations | iv |
| Table of Contents | xiv |
| List of Figures | xx |
| List of Tables | xxx |
| List of Schemes | xxxii |
| Chapter 1. Introduction and Background. | 1 |
| 1.1 Introduction | 2 |
| 1.2 History of organic electronics | 3 |
| 1.3 Conjugated Polymers | 4 |
| 1.4 Band Theory | 8 |
| 1.5 Polymer Growth | 11 |
| 1.6 Modifying the Band Gap through Substituent Effects | 13 |
| 1.7 3,4-Ethylenedioxythophene (EDOT) and derivatives | 16 |
| 1.8 Electrochemistry..... | 21 |
| 1.9 Cyclic Voltammetry | 25 |
| 1.10 UV-vis Absorption..... | 29 |

| | | |
|--------|---|----|
| 1.11 | Spectroelectrochemistry..... | 31 |
| 1.12 | Calculation of energy levels and band gap | 35 |
| 1.13 | Associated Errors | 36 |
| 1.14 | Photoluminescence Quantum Yield..... | 38 |
| 1.15 | Applications and Devices | 41 |
| 1.15.1 | Electrochromic devices | 41 |
| 1.15.2 | Organic Photovoltaic (OPV) Devices | 45 |
| 1.15.3 | Organic Field Effect Transistors (OFET) | 53 |
| 1.15.4 | Organic Light Emitting Diodes (OLED) | 58 |
| 1.15.5 | Sensors | 62 |

Chapter 2. Electrochemical, Spectroelectrochemical and Comparative Studies of novel organic conjugated monomers and polymers featuring the redox active unit tetrathianaphthalene..... 64

| | | |
|-----|---|----|
| 2.1 | Abstract | 65 |
| 2.2 | Introduction | 66 |
| 2.3 | Experimental | 70 |
| 2.4 | Absorption Spectroscopy and Electrochemistry of Monomers..... | 71 |
| 2.5 | X-ray Crystallography and Molecular Modelling | 75 |
| 2.6 | Electrochemistry of the polymers..... | 83 |
| 2.7 | UV-vis Spectroelectrochemistry | 92 |
| 2.8 | Polymer Stability | 95 |
| 2.9 | Polymer Switching | 97 |

| | | |
|---|--|-----|
| 2.10 | Colourimetry | 101 |
| 2.11 | Conclusions..... | 102 |
| Chapter 3. New Redox Stable Low Band Gap Conjugated Polymers based on Thiophene-BODIPY-Thiophene repeat units..... | | |
| | | 103 |
| 3.1 | Abstract | 104 |
| 3.2 | Introduction | 105 |
| 3.3 | Experimental | 109 |
| 3.4 | Molecular Modelling | 110 |
| 3.5 | Absorption and Electrochemistry of 68..... | 111 |
| 3.6 | Electrochemistry of the polymer | 115 |
| 3.7 | Absorption and Spectroelectrochemistry of poly68 | 119 |
| 3.8 | Stability of poly68 | 122 |
| 3.9 | Switching times and CIE coordinates of poly68 | 123 |
| 3.10 | Quantum Yield Calculation | 127 |
| 3.11 | Summary..... | 134 |
| 3.12 | Modifying the LUMO level: comparison of BODIPY with NO ₂ , without NO ₂ and with Br..... | 135 |
| 3.12.1 | Absorption spectroscopy and Electrochemistry of the monomers..... | 136 |
| 3.12.2 | Electrochemical and Absorption Properties of Polymers | 140 |
| 3.13 | Modifying the HOMO level: Comparison of BODIPY EDOT with EDTT open and closed-ring analogues | 148 |
| 3.13.1 | Absorption spectroscopy and Electrochemistry of the monomers..... | 149 |

| | | |
|---|--|------------|
| 3.13.2 | Electrochemical and Absorption Properties of Polymers | 155 |
| 3.14 | The properties of open and closed BODIPY cores..... | 163 |
| 3.14.1 | Absorption spectroscopy and Electrochemistry of monomers..... | 163 |
| 3.14.2 | Electrochemical and Absorption Properties of Polymers | 167 |
| 3.15 | Conclusions and Further Work | 173 |
| Chapter 4. The Study of Unusual Extended Conjugated Architectures..... | | 175 |
| 4.1 | Abstract | 176 |
| 4.2 | Controlling the Conformational Changes in Donor-Acceptor [4]- Dendralenes through Intramolecular Charge-Transfer Processes..... | 177 |
| 4.2.1 | Introduction | 177 |
| 4.2.2 | Experimental | 180 |
| 4.2.3 | X-ray crystallographic studies of 100 | 181 |
| 4.2.4 | UV-vis absorption studies of 100..... | 183 |
| 4.2.5 | Cyclic voltammetry of 100..... | 185 |
| 4.2.6 | Proposed mechanism for interconversion of 100..... | 187 |
| 4.2.7 | UV-vis absorption studies of 101..... | 188 |
| 4.2.8 | Electrochemistry of 101 | 190 |
| 4.2.9 | Conclusions | 199 |
| 4.3 | Characterisation of New Diindenothienothiophene Based Materials | 200 |
| 4.3.1 | Introduction | 200 |
| 4.3.2 | Experimental | 203 |
| 4.3.3 | Electronic absorption and electrochemical studies | 204 |

| | | |
|-------|--|-----|
| 4.3.4 | Photoluminescence studies..... | 209 |
| 4.3.5 | X-ray crystallography..... | 212 |
| 4.3.6 | Transistor fabrication and measurement | 213 |
| 4.3.7 | Conclusions | 216 |

Chapter 5. An Electronic, Electrochemical, Spectroelectrochemical and

Electrochromic Study of Benzobisthiazole based Monomers and Polymers....217

| | | |
|-----|--|-----|
| 5.1 | Abstract | 218 |
| 5.2 | Introduction | 219 |
| 5.3 | Experimental | 223 |
| 5.4 | Absorption and Cyclic Voltammetry of monomers | 224 |
| 5.5 | Electrochemistry of the Polymers | 230 |
| 5.6 | Absorption spectroscopy and spectroelectrochemical analysis of the polymers..... | 239 |
| 5.7 | Conclusions | 249 |

Chapter 6. The Study of Conjugated Polymers in Biological Applications...251

| | | |
|-------|---|-----|
| 6.1 | Abstract | 252 |
| 6.2 | Biological Sensor Based on Flavin | 253 |
| 6.2.1 | Introduction..... | 253 |
| 6.2.2 | Experimental | 256 |
| 6.2.3 | Computational analysis | 257 |
| 6.2.4 | UV-vis absorption spectroscopy and cyclic voltammetry | 257 |
| 6.2.5 | Conclusions..... | 264 |

| | | |
|-------|--|-----|
| 6.3 | The developement of a nitric oxide sensor..... | 265 |
| 6.3.1 | Introduction..... | 265 |
| 6.3.2 | Experimental..... | 267 |
| 6.3.3 | Electropolymerisation onto glassy carbon electrodes..... | 267 |
| 6.3.4 | Electropolymerisation onto a carbon fibre electrode..... | 271 |
| 6.3.5 | Conclusions and Further Work..... | 275 |
| | Publications | 276 |
| | References | 278 |

List of Figures

| | |
|---|-----------|
| Figure 1.1 Parameters influencing band gap | 5 |
| Figure 1.2 Aromatic to quinoidal transition | 6 |
| Figure 1.3 Aromatic to quinoidal form of poly(isothianaphthalene). | 6 |
| Figure 1.4 Available conformations as depicted for terthiophene | 7 |
| Figure 1.5 Band theory diagram..... | 8 |
| Figure 1.6 p- and n-doping of a semiconductor | 9 |
| Figure 1.7 Doping of polythiophene | 10 |
| Figure 1.8 Dedoping of polythiophene, X = counter-ion..... | 10 |
| Figure 1.9 Mechanism of polymer growth as depicted for polythiophene | 11 |
| Figure 1.10 α - α' and α - β' coupling reactions..... | 12 |
| Figure 1.11 Molecular orbital interaction between donor-acceptor moieties | 15 |
| Figure 1.12 Non-covalent sulfur – oxygen interaction in bis-EDOT..... | 16 |
| Figure 1.13 EDTT and bis-EDTT showing a twist between adjacent units..... | 17 |
| Figure 1.14 Expected O···S interactions for PEDOT , POSO and PSOS | 18 |
| Figure 1.15 Typical cyclic voltammogram graph | 26 |
| Figure 1.16 Illustration of oxidation and reduction in an electrochemical cell..... | 27 |
| Figure 1.17 Ferrocene / ferrocenium redox couple (X is the counter-anion)..... | 28 |
| Figure 1.18 Possible electronic transitions for an organic molecule..... | 29 |
| Figure 1.19 Diagrammatic representation of a UV-vis spectroelectrochemical experiment..... | 32 |
| Figure 1.20 (a) Infrared spectroelectrochemistry and (b) Raman spectroelectrochemistry in reflection mode | 33 |

| | |
|--|-----------|
| Figure 1.21 Diagrammatic representation of an EPR SEC cell and its alignment in the spectrometer | 34 |
| Figure 1.22 Example of onset determination | 37 |
| Figure 1.23 Absorption and emission of a molecule..... | 39 |
| Figure 1.24 Diagram of a typical electrochromic device | 42 |
| Figure 1.25 Polymers used in electrochromics and their colour changes | 43 |
| Figure 1.26 1931 CIE colour coordinates | 44 |
| Figure 1.27 Solar photon flux as a function of wavelength | 46 |
| Figure 1.28 Energy levels of donor and acceptor components in organic photovoltaics | 48 |
| Figure 1.29 Power conversion efficiencies for band gap versus ΔE_{LUMO} | 49 |
| Figure 1.30 Mechanism for charge generation..... | 50 |
| Figure 1.31 Schematic of a bulk heterojunction organic photovoltaic | 51 |
| Figure 1.32 Proposed mechanism of charge separation for polymers with both donor and acceptor units integrated into the polymer structure. | 52 |
| Figure 1.33 Set-up of an OFET configuration in (a) top contact and (b) bottom contact arrangement | 53 |
| Figure 1.34 Graph of current versus potential obtained from a series of OFET measurements at varying gate voltages..... | 55 |
| Figure 1.35 Classical structure of an OLED | 58 |
| Figure 1.36 Electroluminescence in a conjugated polymer | 59 |
| Figure 1.37 Host-guest arrangement of Poly47 and metal analyte | 62 |
| Figure 1.38 Addition of ions inducing planarisation of the polymer chain | 63 |

| | |
|--|-----------|
| Figure 2.1 Oxidation of TTF | 66 |
| Figure 2.2 Square scheme oxidation of 1,4-dithiin ring..... | 67 |
| Figure 2.3 Solution state electronic absorption spectra for monomers 54,55 and 56 | 71 |
| Figure 2.4 Cyclic voltammograms of (a) oxidation and (b) reduction of 54, 55 and 56 | 73 |
| Figure 2.5 Cyclic Voltammograms of 54, 55 and 56 for energy level determination. | 74 |
| Figure 2.6 Molecular structures of compound 54 showing the crystallographic asymmetric unit that consists of two conformers..... | 76 |
| Figure 2.7 Molecular structure of compound 55 . Hydrogen atoms are omitted for clarity..... | 77 |
| Figure 2.8 Geometry-optimized structures of compounds 54, 55 and 56 (left to right, respectively). Calculations were performed at the B3LYP/6-31G* level, starting from the observed crystal structures of compounds 54 (for 54 and 56) and 55 | 77 |
| Figure 2.9 X-ray crystal packing diagram of compound 1 viewed along the b axis. Hydrogen atoms are omitted for clarity | 78 |
| Figure 2.10 X-ray crystal packing diagram of compound 55 | 79 |
| Figure 2.11 (a) HOMO, (b) HOMO-1 and (c) LUMO plots of compound 54 | 80 |
| Figure 2.12 (a) HOMO, (b) HOMO-1 and (c) LUMO plots of compound 55 | 80 |
| Figure 2.13 (a) HOMO, (b) HOMO-1 and (c) LUMO plots of compound 56 | 81 |
| Figure 2.14 SOMO plot of 54 radical cation..... | 82 |
| Figure 2.15 Electrochemical growth of (a) poly 54 , (b) poly 55 and (c) poly 56 | 84 |
| Figure 2.16 Cyclic voltammograms for (a) oxidation and (b) reduction of poly 54 , poly 55 and poly 56 | 85 |

| | |
|--|------------|
| Figure 2.17 Cyclic voltammograms of (a) poly 54 , (b) poly 55 and (c) poly 56 with varying scan rates. (d) Plot of current versus scan rate for polymers. | 89 |
| Figure 2.18 Cyclic voltammograms of Poly 54 , Poly 55 and Poly 56 for energy level determination..... | 90 |
| Figure 2.19 Electronic absorption spectra of poly 54 , poly 55 and poly 56 . Spectra were recorded on thin films deposited on ITO glass. | 91 |
| Figure 2.20 Absorption spectroelectrochemical plots of oxidation of (a) poly 54 , (b) poly 55 , (c) poly 56 and reduction of (d) poly 56 . Potentials are given vs. Ag wire pseudo-reference electrode..... | 94 |
| Figure 2.21 Stability of polymers (a) poly 54 , (b) poly 55 and (c) poly 56 on ITO in monomer-free solution. | 96 |
| Figure 2.22 Change in absorbance upon p-doping at various switching rates for (a) poly 54 , (b) poly 55 and (c) poly 56 . Absorbance was monitored at 755 nm between potentials of -0.4 and 1.5 V. | 100 |
| | |
| Figure 3.1 HOMO (a) and LUMO (b) frontier orbitals of 68 | 110 |
| Figure 3.2 Solution state electronic absorption spectra for 68 | 112 |
| Figure 3.3 Cyclic voltammograms of (a) oxidation and (b) reduction of 68 | 113 |
| Figure 3.4 Cyclic voltammogram of 68 for energy level determination..... | 114 |
| Figure 3.5 Electrochemical growth of poly 68 | 115 |
| Figure 3.6 Cyclic voltammograms of (a) oxidation and (b) reduction of poly 68 . .. | 117 |
| Figure 3.7 Cyclic voltammogram of poly 68 for energy level determination..... | 117 |
| Figure 3.8 (a) Cyclic voltammograms of poly 68 with varying scan rate and (b) current max vs. scan rate. | 119 |

| | |
|---|------------|
| Figure 3.9 Solid state electronic absorption spectrum of poly 68 recorded as a thin film deposited on ITO glass. | 120 |
| Figure 3.10 Absorption spectroelectrochemical plot of poly 68 oxidation..... | 121 |
| Figure 3.11 Colour change of poly 68 (left) neutral and (right) doped..... | 122 |
| Figure 3.12 Stability of (a) oxidation and (b) reduction of poly 68 | 123 |
| Figure 3.13 Change in absorbance upon p-doping at various switching rates of poly 68 . Absorbance was monitored at 560 nm between -0.2 and +1.0 V. | 124 |
| Figure 3.14 CIE plots of (a) y vs. x and (b) b* vs. a* for poly 68 | 126 |
| Figure 3.15 Emission spectra of (a) standard 79 and (b) 68 | 128 |
| Figure 3.16 Integrated fluorescence versus absorbance for (a) 79 standard and (b) 68 | 129 |
| Figure 3.17 Emission spectra of (a) standard 80 and (b) 77 | 131 |
| Figure 3.18 Integrated fluorescence versus absorbance for (a) 80 standard and (b) 77 | 133 |
| Figure 3.19 Solution state absorption spectra of 68 , 81 and 82 | 136 |
| Figure 3.20 Cyclic voltammograms of (a) oxidation and (b) reduction of 68 , 81 and 82 | 138 |
| Figure 3.21 Cyclic voltammograms of 68 , 81 and 82 for energy level determination. | 139 |
| Figure 3.22 Electrochemical growth of (a) poly 81 and (b) poly 82 | 141 |
| Figure 3.23 Cyclic voltammograms of (a) oxidation and (b) reduction of poly 68 , poly 81 and poly 82 | 142 |
| Figure 3.24 Cyclic voltammograms of poly 68 , poly 81 and poly 82 for energy level determination..... | 144 |

| | |
|--|------------|
| Figure 3.25 Cyclic Voltammograms with varying scan rates of (a) poly 81 and (b) poly 82 | 145 |
| Figure 3.26 Plots of current max versus scan rate for (a) poly 81 and (b) poly 82 ... | 146 |
| Figure 3.27 Solid state absorption spectra of poly 68 , poly 81 and 82 | 147 |
| Figure 3.28 Solution state absorption spectra of 68 , 90 and 91 | 150 |
| Figure 3.29 Cyclic Voltammograms of (a) oxidation and (b) reduction and 68 , 90 and 91 | 152 |
| Figure 3.30 Cyclic voltammogram of 68 , 90 and 91 for energy level determination. | 154 |
| Figure 3.31 Electrochemical growth of (a) poly 90 and (b) poly 91 | 155 |
| Figure 3.32 Cyclic voltammograms of (a) oxidation and (b) reduction of poly 68 , poly 90 and poly 91 | 156 |
| Figure 3.33 Alignment of sulfur-nitrogen interactions in poly 91 | 158 |
| Figure 3.34 Cyclic voltammogram s of poly 68 , poly 90 and poly 91 for energy level determination..... | 159 |
| Figure 3.35 Cyclic voltammograms with varying scan rates for (a) poly 90 and (b) poly 91 | 160 |
| Figure 3.36 Plots of current max versus scan rate for (a) poly 90 and (b) poly 91 .. | 161 |
| Figure 3.37 Solid state absorption spectra of poly 68 , poly 90 and poly 91 | 162 |
| Figure 3.38 Solution state absorption spectraof 81 and 89 | 164 |
| Figure 3.39 Cyclic Voltammograms of (a) oxidation and (b) reduction of 81 and 89 | 165 |
| Figure 3.40 Cyclic voltammogram of 81 and 89 for energy level determination. .. | 166 |
| Figure 3.41 Electrochemical growth of poly 89 | 167 |

| | |
|--|------------|
| Figure 3.42 Cyclic voltammograms of (a) oxidation and (b) reduction of poly 81 and poly 89 | 169 |
| Figure 3.43 Cyclic voltammogram of poly 81 and poly 89 for energy level determination..... | 170 |
| Figure 3.44 (a) Cyclic voltammograms of poly 89 with varying scan rate and (b) plot of current max vs. scan rate..... | 171 |
| Figure 3.45 Solid state absorption spectra of poly 81 and poly 89 | 172 |
| | |
| Figure 4.1 Sample structures of dendralene family..... | 177 |
| Figure 4.2 X-ray crystal structures of conformers 100a (top) and 100b (bottom). | 182 |
| Figure 4.3 Evolution of UV-vis absorption spectra of 100a over time whilst the sample is exposed to ambient light | 184 |
| Figure 4.4 Kinetic plot of the rate change of 100 | 184 |
| Figure 4.5 Cyclic voltammograms of 100a over time, inset is an expansion of the oxidation peak | 185 |
| Figure 4.6 Attempted polymer growth of 100 | 186 |
| Figure 4.7 Evolution of UV-vis spectra of 101 | 188 |
| Figure 4.8 Kinetic plot of the rate change of 101 at 455 nm (top) and at 368 nm (bottom)..... | 189 |
| Figure 4.9 Cyclic voltammograms of (a) oxidation and (b) reduction of 101 | 191 |
| Figure 4.10 Electrochemical growth of poly 101 | 191 |
| Figure 4.11 Cyclic voltammogram of poly 101 | 192 |
| Figure 4.12 Differential pulse voltammograms of poly 101 reduction..... | 194 |
| Figure 4.13 (a) Cyclic voltammograms of poly 101 oxidation at varying scan rates and (b) plot of scan rate versus current maximum..... | 195 |

| | |
|---|------------|
| Figure 4.14 UV-vis spectrum of poly 101 in the solid state | 196 |
| Figure 4.15 Oxidative spectroelectrochemistry of poly 101 | 197 |
| Figure 4.16 Reductive spectroelectrochemistry of poly 101 | 198 |
| Figure 4.17 UV-vis spectra of compounds 106 , 107 and 108 in dichloromethane solutions. | 205 |
| Figure 4.18 Solvatochromic effect of 108 | 206 |
| Figure 4.19 Cyclic voltammograms of 106 , 107 , and 108 | 208 |
| Figure 4.20 Solution state normalised absorption and emission of 106 | 210 |
| Figure 4.21 Solution and solid state normalised absorption and emission of 107 .. | 210 |
| Figure 4.22 Solution and solid state normalised absorption and emission of 108 .. | 211 |
| Figure 4.23 Asymmetric unit of compound 106 with labels..... | 212 |
| Figure 4.24 Space-filling diagram of 106 showing π - π stacking | 213 |
| Figure 4.25 Inversion between a dimer of 106 within the one-dimensional stacks | 213 |
| Figure 4.26 Polarised optical microscope image of material 106 vacuum deposited onto an HMDS treated Si/SiO ₂ substrate, after annealing for 4 hours at 125°C in nitrogen | 215 |
| Figure 4.27 Transfer characteristics of bottom-gate, bottom-contact OFET based on 106 . Inset shows schematic representation of bottom-gate, bottom-contact transistor structure used | 215 |
| | |
| Figure 5.1 X-ray structure of 117 showing π - π stacks in two dimensions..... | 220 |
| Figure 5.2 Summary of intermolecular close contacts in the X-ray structure of 117 | 220 |
| Figure 5.3 UV-vis spectra of 117 , 120 , 121 , 122 and 123 | 225 |

| | |
|--|------------|
| Figure 5.4 Cyclic voltammograms of (a) oxidation and (b) reduction of, 117 , 120 , 121 and 122 . The oxidation of 121 at 1 V s^{-1} is in the inset of (a) and the reduction of 123 is in the inset of (b)..... | 227 |
| Figure 5.5 Cyclic voltammograms of 117 , 120 , 121 and 122 for energy level determination..... | 229 |
| Figure 5.6 Electrochemical growth of (a) poly 117 , (b) poly 120 and (c) poly 122 .. | 231 |
| Figure 5.7 Cyclic voltammograms of (a) oxidation and (b) reduction of poly 117 , poly 120 and poly 122 | 232 |
| Figure 5.8 Cyclic voltammograms of poly 117 , poly 120 and poly 122 for energy level determination..... | 233 |
| Figure 5.9 Scan rate experiments of (a) poly 117 , (b) poly 120 , (c) poly 122 . The plot of scan rate versus current maxima of all three polymers is shown in (d). | 236 |
| Figure 5.10 Poly 117 (a) oxidation and (b) reduction stability test..... | 237 |
| Figure 5.11 Poly 120 (a) oxidation and (b) reduction stability test..... | 237 |
| Figure 5.12 Poly 122 (a) oxidation and (b) reduction stability test..... | 238 |
| Figure 5.13 UV-vis spectra of poly 117 , poly 120 and poly 122 in the solid state.... | 239 |
| Figure 5.14 UV-vis spectroelectrochemistry of poly 117 upon p-doping..... | 242 |
| Figure 5.15 UV-vis spectroelectrochemistry of poly 120 upon p-doping..... | 242 |
| Figure 5.16 UV-vis spectroelectrochemistry of poly 122 upon p-doping..... | 243 |
| Figure 5.17 Electrochromic colour change of poly 117 between neutral (left) and doped state (right) | 244 |
| Figure 5.18 Electrochromic colour change of poly 120 between neutral (left) and doped state (right) | 244 |
| Figure 5.19 Electrochromic colour change of Poly 122 between neutral (left) and doped state (right) | 244 |

| | |
|--|------------|
| Figure 5.20 Switching times of (a) poly 117 , (b) poly 120 and (c) poly 122 | 247 |
| Figure 6.1 Hydrogen bonding between poly 133 and 134 | 254 |
| Figure 6.2 Oxidation of flavin..... | 255 |
| Figure 6.3 Reduction of flavin | 255 |
| Figure 6.4 Computational analysis of 135 | 257 |
| Figure 6.5 UV-vis absorbance of 135 | 258 |
| Figure 6.6 Cyclic voltammograms of (a) oxidation and (b) reduction of 135 | 260 |
| Figure 6.7 Cyclic voltammogram of 135 for energy level determination..... | 261 |
| Figure 6.8 Attempted polymer growth of 135 | 262 |
| Figure 6.9 UV-vis absorption spectrum of electrochemically formed film growth and monomer film of 135 | 263 |
| Figure 6.10 Dimer of 135 | 264 |
| Figure 6.11 Electrochemical growth onto a glassy carbon electrode..... | 268 |
| Figure 6. 12 Cyclic voltammograms of polymer in monomer-free solution | 269 |
| Figure 6.13 Cyclic voltammogram showing the addition of NO to the polymer film | 270 |
| Figure 6.14 Stability test of the polymer on glassy carbon electrode to 500 oxidative cycles..... | 271 |
| Figure 6.15 Electrochemical growth of the porphyrin onto a carbon fibre electrode | 272 |
| Figure 6.16 Cyclic voltammograms of the polymer film with injection of NO; the inset shows magnification of the active area..... | 273 |
| Figure 6.17 Stability test of polymer on carbon fibre electrode to 500 oxidative cycles..... | 274 |

List of Tables

| | |
|---|------------|
| Table 2.1 Electrochemical and absorption spectroscopy data for compounds 54 , 55 and 56 | 75 |
| Table 2.2 Electrochemical and absorption spectroscopy data for thin films of poly 54 , poly 55 and poly 56 . Experimental conditions are the same as those given in Figures 2.6 and 2.7. | 91 |
| Table 2.3 Switching times and % change in absorbance..... | 100 |
| Table 2.4 CIE Yxy and L*a*b* color spaces for poly 54 , poly 55 and poly 56 for neutral and doped polymers | 101 |
| | |
| Table 3.1 Energy level determination data for 68 | 115 |
| Table 3.2 Energy level determination of poly 68 | 118 |
| Table 3.3 Switching times and % change in absorbance of poly 68 | 124 |
| Table 3.4 CIE Yxy and L*a*b* colour spaces for poly 68 measured between 0 and +1.0 V..... | 125 |
| Table 3.5 Emission data of 79 standard and 68 | 129 |
| Table 3.6 Emission data for 80 standard and 77 | 132 |
| Table 3.7 Electronic absorption data for 68 , 81 and 82 | 139 |
| Table 3.8 Redox data for 68 , 81 and 82 | 140 |
| Table 3.9 Electrochemical data for poly 68 , poly 81 and poly 82 | 144 |
| Table 3.10 Absorption data for poly 68 , poly 81 and poly 82 | 147 |
| Table 3.11 Electronic and electrochemical data for 68 , 90 and 91 | 150 |
| Table 3.12 Electrochemical data for 68 , 90 and 91 | 154 |
| Table 3.13 Electrochemical data for poly 68 , poly 90 and poly 91 | 159 |

| | |
|---|------------|
| Table 3.14 Absorption data for poly 68 , poly 90 and poly 91 | 162 |
| Table 3.15 Electronic absorption data for 81 and 89 | 164 |
| Table 3.16 Electrochemical data for 81 and 89 | 167 |
| Table 3.17 Electrochemical data for poly 81 and poly 89 | 170 |
| Table 3.18 Absorption data for poly 81 and poly 89 | 172 |
| | |
| Table 4.1 Energy level determination of poly 101 | 193 |
| Table 4.2 Solvatochromic data of compound 108 in selected solvents with π^* values by Kamlet and Taft ²¹⁹ | 206 |
| Table 4.3 Electrochemical and absorption spectroscopy data for compounds 106 , 107 and 108 | 209 |
| Table 4.4 Photoluminescence data for compounds 106 , 107 and 108 | 211 |
| | |
| Table 5.1 Absorption spectroscopy and electrochemical data for monomers 117 , 120 , 121 and 122 | 228 |
| Table 5.2 Energy levels of 117 , 120 , 121 and 122 | 229 |
| Table 5.3 Electrochemical data of poly 117 , poly 120 and poly 122 | 234 |
| Table 5.4 Energy level data of poly 117 , poly 120 and poly 122 | 234 |
| Table 5.5 Absorption spectroscopy data for poly 117 , poly 120 and poly 122 | 240 |
| Table 5.6 Switching times and percentage change in absorbance..... | 248 |
| Table 5.7 Yxy and L*a*b* Colour characteristics for poly 117 , poly 120 and poly 122 | 249 |
| | |
| Table 6.1 Energy levels for 135 derived from cyclic voltammetry..... | 261 |

List of Schemes

| | |
|--|------------|
| Scheme 2.1 Synthesis of 54, 55 and 56 | 69 |
| Scheme 3.1 Synthesis of 68 | 109 |
| Scheme 3.2 Synthesis of 81 and 82 | 135 |
| Scheme 3.3 Synthesis of 90 and 91 | 149 |
| Scheme 4.1 Synthesis of 100 and 101 | 179 |
| Scheme 4.2 Proposed mechanism for the interconversion of 100 | 187 |
| Scheme 4.3 Synthesis of 106, 107 and 108 | 202 |
| Scheme 5. 1 Syntheses of 117, 120, 121, 122 and 123 | 222 |
| Scheme 6.1 Synthesis of 135 | 256 |
| Scheme 6.2 ICT process of 135 | 259 |

Chapter 1. Introduction and Background.

1.1 Introduction

In recent years, the use of novel organic conjugated materials as semiconductors in electronic devices has become a continually growing and interesting field of research; the attraction derives from the ability of the materials to be easily manipulated and tailored to suit the desired outcome. Organic semiconductors have tunable band gaps and redox properties that can be influenced through variation of the substituents; this, together with the ease and reduced cost of processability required for these materials, it makes them very favourable for device fabrication.

Traditionally, organic polymers were generally thought of as insulators; this was until just over three decades ago when it was discovered that conjugated polymers could conduct by allowing a flow of electrons or holes through their π -orbital overlap in the polymer chains.

The main advantage organic semiconductors have over their inorganic equivalents is their low weight, low cost and high mechanical flexibility compared to the rigid and brittle properties of their rivals. Inorganic semiconductors require process techniques that are expensive, such as vacuum vapour deposition, whereas organic materials can be processed through a number of different, less expensive methods, such as spin-coating, stamping and ink-jet printing.

However, one of the main targets and a major driving force in this field is creating organic based devices that can match the performance and stability of their traditional analogous inorganic counterparts, such as amorphous silicon and gallium arsenide-based electronic devices.

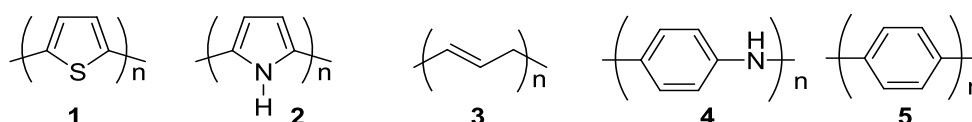
1.2 History of organic electronics

Nearly one hundred years ago, it was predicted that conductivity comparable with metals could be achieved in organic solids, however it took almost sixty years until this was proven correct. The major breakthrough for organic polymers was made by Shirakawa, MacDiarmid and Heeger who discovered that polyacetylene could conduct when oxidised with iodine vapour.¹ This discovery was so important they were awarded the Nobel Prize in 2000.

In the late 1970s and early 1980s, conductivity was achieved in other conjugated polymers such as polypyrrole, polythiophene and polyaniline.^{2,3} Research in this field was still on a relatively small-scale, despite investigation into the possible use of conducting organic materials in electronic devices. The first organic field effect transistor was created in 1986, using electrochemically grown polythiophene.⁴ However, it was not until discovery of the first organic light emitting diode in 1991 that interest in this field really took off.⁵

1.3 Conjugated Polymers

There are many types of conjugated polymers that have been created and analysed over the years, examples include polythiophenes (**1**), polypyrroles (**2**), polyacetylenes (**3**), polyanilines (**4**), and polyphenylenes (**5**).



These polymers have the ability to conduct as the π -electrons in the conjugated double / single bonds in the chain are delocalised, thus giving the polymers a band gap in the semi-conductor range. The polymers can exist as either their aromatic or quinoidal forms and the band gap (E_g) of conjugated polymers are defined and controlled by the following five features, as shown in Figure 1.1:⁶

- (i) bond length alternation ($E^{\sigma r}$)
- (ii) degree of planarity (E^{θ})
- (iii) aromatic resonance energy (E^{Res})
- (iv) the push / pull effect of the substituent groups (E^{Sub})
- (v) intramolecular and interchain interactions (E^{Int})

Therefore:

$$E_g = E^{\sigma r} + E^{\theta} + E^{Res} + E^{Sub} + E^{Int} \quad (1)$$

The bond length alternation is the difference in bond lengths between single and double bonds; if the double and single bonds were the same length in structures **1**, **2**

or **5** then the aromatic and quinoidal form would be identical. This is not the case: the states are not degenerate and in polyacetylene (**3**) the non-absolute delocalisation is caused by Peierls distortion.⁷ The degree of planarity is related to the torsion angle (θ) between adjacent units; bulky substituent (**R**) groups can increase the torsion angle and therefore decrease the degree of planarity. Planarity in the polymer chain is a desired feature that allows a lower band gap and improves the conductivity and the mobility of the polymers. The amount of aromatic resonance energy will influence the band gap and large energies will increase its value as the increase in aromatic stability prevents delocalisation to the quinoidal form.^{8, 9} The **R** group substituent will also influence the band gap through electron-donating and electron-withdrawing effects and these are explained more in section 1.6. The intramolecular (π - π) interactions and interchain (non-covalent bonding) interactions can reduce band gaps through reduction of the torsion angle and therefore help increase delocalisation of the π -electrons.⁹

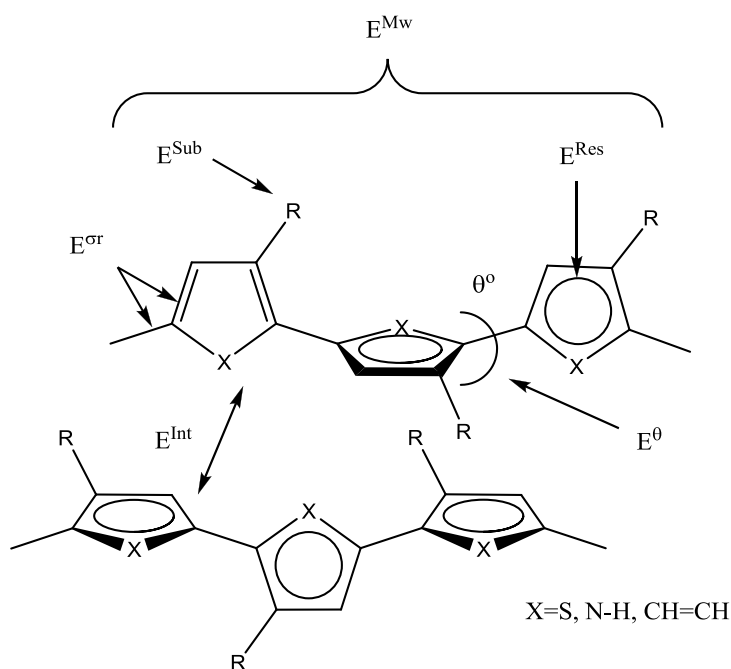


Figure 1.1 Parameters influencing band gap

The quinoidal form of polymers is usually of lower aromatic resonance energy than the aromatic forms,¹⁰ and can be achieved in the neutral state through excitation as shown in Figure 1.2 for polythiophene. Polythiophene exists mostly as the aromatic form giving it a band gap of around 2.1 eV.¹¹

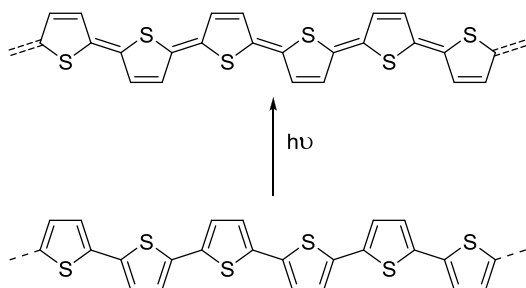


Figure 1.2 Aromatic to quinoidal transition

It is therefore possible to make the band gap of polymers lower by making the quinoidal form more stable, by giving it more aromatic character as shown for poly(isothianaphthalene) (**6**) in Figure 1.3. In the ground state, the thiophene part of the polymer loses aromaticity but in this quinoidal form the benzene unit gains aromaticity resulting in a polymer with a band gap of around 1.1 eV.¹²

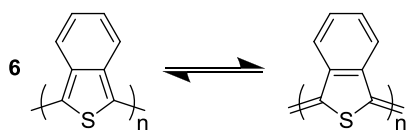


Figure 1.3 Aromatic to quinoidal form of poly(isothianaphthalene).

The conformation of units will also influence the properties in a polymer chain. Monomer units which make up the polymer chain can align in three ways: all-anti, syn / anti and all-syn as shown in Figure 1.4 for some terthiophenes.¹³ The all-anti arrangement is the most common conformer.

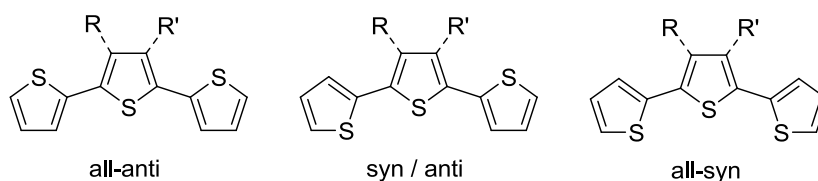
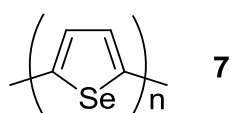


Figure 1.4 Available conformations as depicted for terthiophene

Polythiophene and related aromatic polymers are typically p-type semiconductors and oxidation (p-doping) of these polymers results in the generation of radical cations and / or dication in the chain, which are stabilised through conjugation. However, reduction (n-doping) of these polymers usually results in a chemical reaction between the newly formed radical anion that causes the breakdown of the conjugated chain. n-Doping is generally unstable for most conjugated polymers as they react irreversibly with water and air.

Another, more recent polymer that has been synthesised is polyselenophene (**7**), which has advantages over the equivalent polythiophene with a lower oxidation and reduction potential for both the monomer and polymer forms.¹⁴



Polyselenophenes have a lower band gap because they have a greater effective conjugation length compared to polythiophenes, due to the monomer units in the polymer chain being less likely to twist out of plane with each other.¹⁵ Polythiophenes can twist very easily with little energy required; in many cases, substitution onto the 3,4-positions creates distortion in the chain and this in turn increases the band gap. For polyselenophenes, distortion is less likely to happen and the backbone remains planar with many different substituent groups.

1.4 Band Theory

All materials can be classified as insulators, metals or semiconductors depending on the ability of the material to conduct electricity. The conductivity of the material is determined by the position of its band structures. In band theory, there are three bands: the filled band, the valence band and the conduction band, as depicted in Figure 1.5.

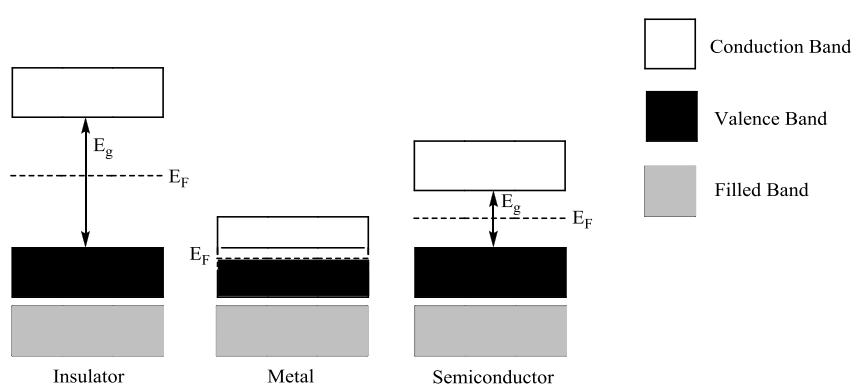


Figure 1.5 Band theory diagram

The lower bands are the filled band(s) which are made up of inner electrons. The valence band which lies above the filled band, is derived from the highest occupied molecular orbital (HOMO) of the material and the upper band is called the conduction band, derived from the lowest unoccupied molecular orbital (LUMO). E_F is the Fermi energy level, the highest occupied state for metals. In between the valence and the conduction band is the forbidden band, essentially the energy gap between the valence and conduction band, known as the band gap. In theory, electrons can move back and forth between the valence and conduction bands, but this ability depends on the band gap and thus determines the conductivity of the material.¹⁶

For insulators, the band gap is too great for thermal energy to promote electrons in the conduction band and such materials therefore do not conduct. In metals there is an overlap of the conduction and valence bands, allowing electrons to pass through the bulk material with minimal resistance. For semiconductors, the band gap is small enough to allow thermal excitation of the electrons to be promoted from the valence to the conduction band. The electrical conductivity of these materials can be enhanced by doping the material.¹⁷

Semiconductors can be doped in two different ways: by p-doping or n-doping. Doping can be carried out chemically or electrochemically. p-Doping is the ejection of an electron(s) to leave positive charges or holes in the valence band, in turn creating a new energy level above the valence band as shown in Figure 1.6. This allows enhanced conductivity since a neighbouring electron can move into the space leaving a hole in its place. n-Doping of a semiconductor is the addition of extra electrons to the valence band. As this band is already full, a new energy level is created that sits below the conduction band (Figure 1.6). The energy gap between this new level and the conduction band is smaller than E_g and so electrons pass from this band to the conduction band more readily and so the conductivity is increased.¹⁸

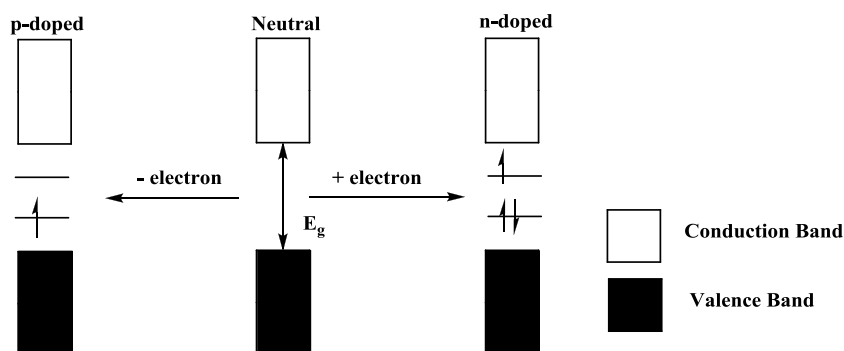


Figure 1.6 p- and n-doping of a semiconductor

The p-doping of a conjugated polymer can be represented chemically, as shown for polythiophene in Figure 1.7. The removal of an electron produces a radical cation species, whilst the second oxidation gives two radical cations which can rearrange to give the more stable dication in the semi-quinoidal form.

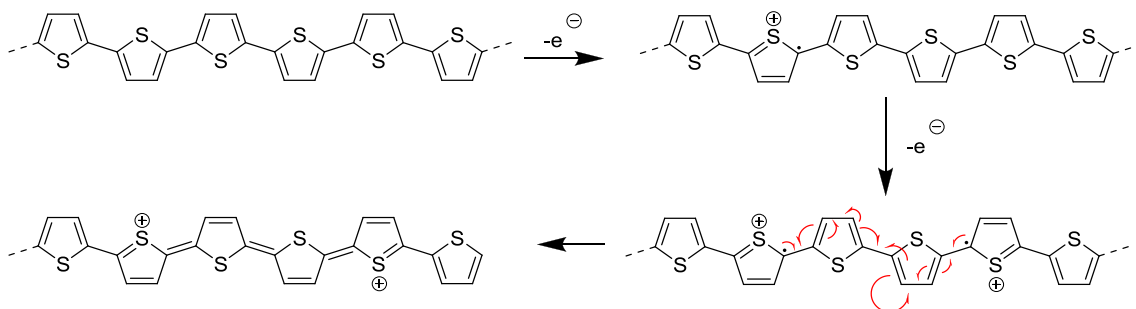


Figure 1.7 Doping of polythiophene

When conjugated polymers are doped in an electrochemical cell or in a solution-state device, the charges can become trapped throughout the chain and kept balanced by counter-ion(s) from the electrolyte. De-doping is a method to reduce/oxidise the polymer back to the neutral state and expel any trapped electrolyte (as shown in Figure 1.8 for p-doped polythiophene) and is achieved by applying a potential in a region of no electroactivity between the first oxidation and reduction processes.¹⁹

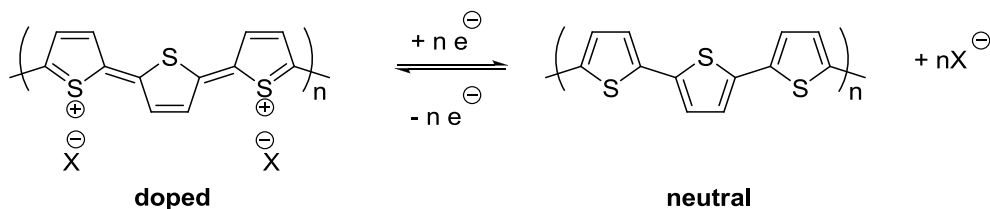


Figure 1.8 De-doping of polythiophene, X = counter-ion

1.5 Polymer Growth

Electropolymerisation is a common technique employed to produce conjugated polymers. The most advantageous method of polymer growth is to grow polymers through repetitive cycling in anodic conditions without a catalyst, with the number of cycles controlling the film thickness.²⁰ The mechanism for polymer growth is similar for many aromatic monomers,¹⁹ and Figure 1.9 shows the growth of polythiophene.

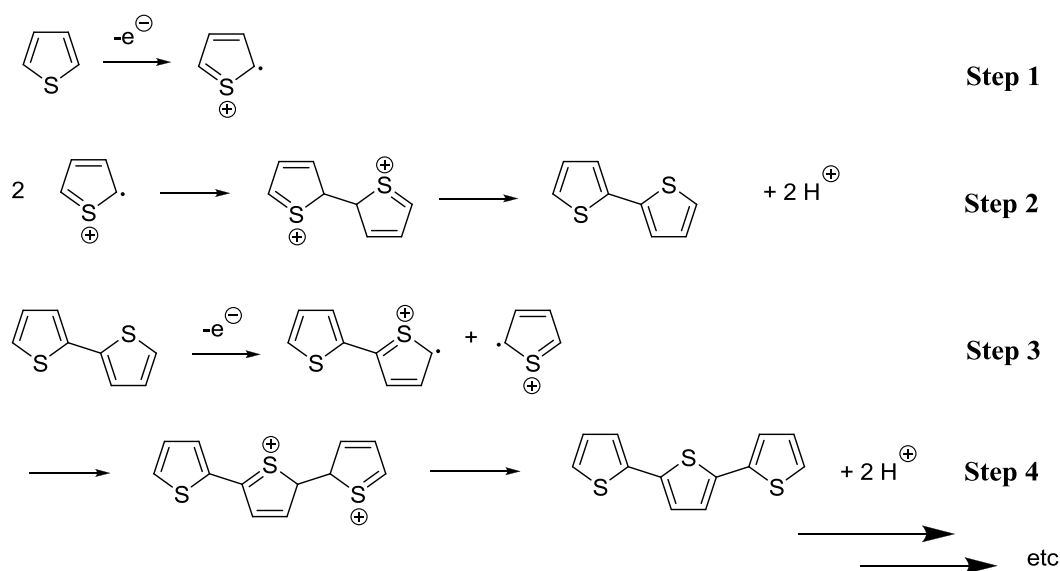


Figure 1.9 Mechanism of polymer growth as depicted for polythiophene

The first step is the removal of an electron from the monomer thiophene to give the radical cation. In the second step, this radical cation can combine with another radical cation monomer to give a dication dimer, as the diffusion of the radical cation back to the bulk solution is slower than that of electron transfer. The dication dimer then re-aromatises and becomes neutral by the loss of two protons.²¹ In the third step, the dimer is oxidised at a lower potential than the monomer and this gives a new radical cation species.¹⁹ This new cation radical can combine with another

monomer cation radical to give a trimer, as shown in step three, and then re-aromatisation produces a terthiophene (step four). The polymer forms through extensive repetition of this sequence until the polymer becomes insoluble in solution and forms a film on the electrode surface.²⁰

Several problems can arise and hinder polymer growth. One issue that can occur is if the radical cation produced is too stable and it diffuses back into the bulk solution. A second problem is the radical produced from the oxidation of the monomer may not reside on the 2,5-positions of thiophene, thus typical polymer growth cannot be achieved. The position of the radical can be discovered through molecular modelling of the singly unoccupied molecular orbital (SUMO) level of the monomer.²²

Another problem that can take place in polymer growth is α - β' coupling instead of α - α' coupling. The former is a non-conjugated bond forming from the 2 or 5 position of one thiophene to the 3 or 4 position of another. This can be prevented by blocking the 3,4' positions as shown in Figure 1.10 to give solely α - α' couplings.

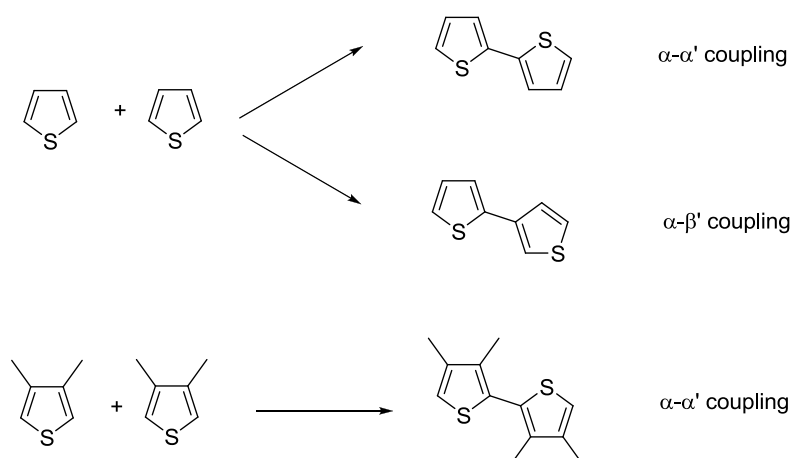


Figure 1.10 α - α' and α - β' coupling reactions

1.6 Modifying the Band Gap through Substituent Effects

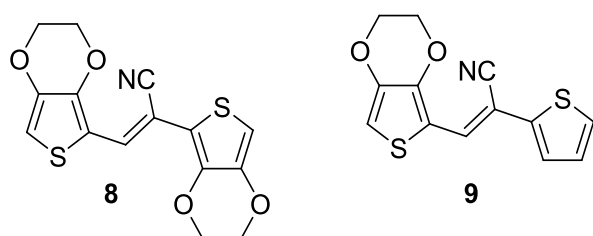
In the simplest cases, methyl or other alkyl groups on the β -positions have shown to decrease the oxidation potential slightly through inductive effects, but they also help prevent unwanted α - β' coupling reactions, lower the band gap and improve the overall conductivity of the conjugated polymer.²³ However, some mono- and dialkyl substituted polymers can actually have the inverse effect through steric hindrance. Steric hindrance in the backbone can cause the monomer units to twist away from each other, breaking the planarity and therefore disrupting the π -orbital overlap and decreasing the conjugation of the polymer.²⁰ Cyclising the alkyl groups is one method to decrease this problem.²⁴ Another option is to synthesise monomers with the desired substituents at the middle unit in a trimer. This has the benefit of both minimising steric hindrance and lowering the oxidation potential of polymer growth through increased conjugation.²⁵

Alkoxy- and alkylthio-substituted monomers have lower oxidation potential than their alkyl equivalents as the lone pairs of the heteroatoms donate electron density to the monomer units.²⁰ The mesomeric donation of electron density has the benefit of lowering the oxidation potential and as a result raises the HOMO level but also raises the LUMO level too.

Electron-withdrawing groups such as halogens, carboxylates, nitro, and nitrate groups have the opposite effect; they make the reduction potential less negative but increase the oxidation potential.

The incorporation of different groups into the main chain is an effective method to influence the energy levels. Fluorinated groups have been shown to lower both the HOMO and LUMO energy levels as well as helping the planarisation of the material.

To alter the reduction potential of the polymer chain greatly, the best way is to incorporate an electron-withdrawing group in the polymer chain.²⁶ Examples include **8** and **9**, where cyano groups between two thiophenes in the polymer chain result in polymers with band gaps below 1.5 eV.²⁷



Creating polymers with alternating donor-acceptor units in the chain has been shown to be an excellent way to achieve low band gaps. The size of the band gap can be influenced by an intramolecular charge transfer process.²⁸ The interactions from the donor and acceptor can result in hybridisation of the HOMO of the donor with the LUMO of the acceptor resulting in a small band gap polymer,²⁹ as shown in Figure 1.11.²⁸ In alternating donor-acceptor polymers, the quinoidal form becomes stabilised as the bond length alternation decreases, thus reducing the band gap.

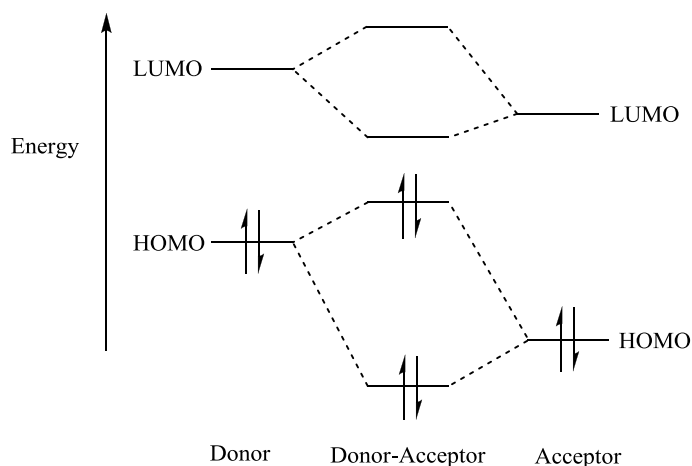
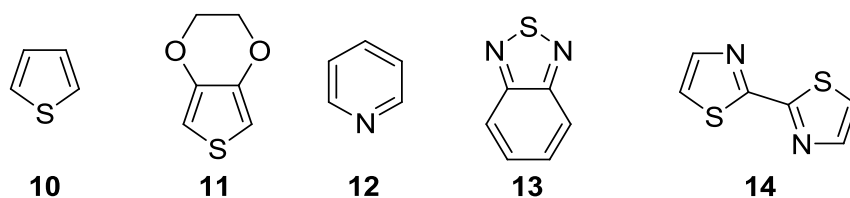
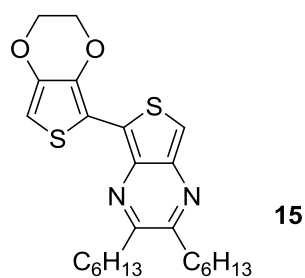


Figure 1.11 Molecular orbital interaction between donor-acceptor moieties

Donors typically used include thiophene (**10**) and ethylenedioxythiophene (EDOT) (**11**) and acceptors are usually nitrogen-based molecules such as pyridine (**12**),³⁰ benzothiadiazole (**13**),³¹ and bis-thiazoles (**14**).³²



One of the smallest band gaps produced for a conjugated polymer is from a polymer polymerised from a bis-thiophene monomer consisting of a donor and acceptor group (**15**). The planarity and the repeating donor-acceptor units result in a band gap of less than 0.4 eV.³³



1.7 3,4-Ethylenedioxythiophene (EDOT) and derivatives

3,4-Ethylenedioxythiophene (EDOT, **11**) and its resultant polymer, poly(ethylenedioxythiophene) (PEDOT) was first synthesised by Bayer nearly twenty years ago.³⁴ This polymer was remarkable as it had a low band gap and was stable to p-doping, with the charged state highly conducting (up to several hundred S cm^{-1}).³⁵ PEDOT has exceptional hole-injection properties,³⁷ and has a band gap of *ca.* 1.6 eV, lower than the analogous polythiophene derivative (*ca.* 2.1 eV).³⁸ The reason for the difference can be attributed to the non-covalent sulfur-oxygen interactions (shown for bis-EDOT (**16**) in Figure 1.12) that hold the polymer planar and thus increasing the effective conjugation length. This allows a lowering of the oxidation and reduction potentials and therefore overall a lower band gap.

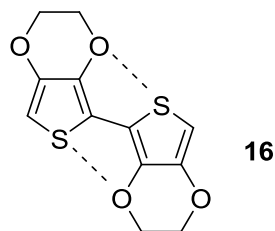


Figure 1.12 Non-covalent sulfur – oxygen interaction in bis-EDOT

The non-covalent interactions have been observed in single crystal X-ray crystallographic data, where the distances between the sulfur and oxygen atoms are shorter than the sum of the van der Waals radii of the interacting atoms (S and O).³⁹ Comparing EDOT with the sulfur version, 3,4-ethylenedithiathiothiophene (EDTT, **17**),³⁸ is the best way to demonstrate the large affect that the non-covalent interaction has on the electrochemical properties of a material. EDTT has a lower oxidation

potential than EDOT. As mentioned above, sulfur is a stronger electron donor than oxygen and the sulfur groups contribute to three-dimensional organisation through intermolecular interactions.^{40, 41} However, the oxidation potential and the band gap of the polymer are higher than those of PEDOT. The reason for this is that there are no interactions between the sulfur of the thiophene and the sulfur of the ethylenedithia bridge to hold the polymer planar, therefore there is a limited effective conjugation length. In fact, the steric hindrance causes distortion and the units twist away from each other as shown in Figure 1.13 for bis-EDTT (**18**).^{39, 42}

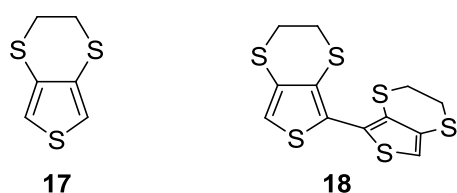
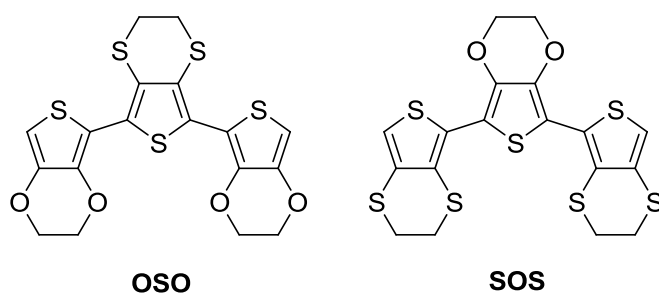


Figure 1.13 EDTT and bis-EDTT showing a twist between adjacent units

In our group we have investigated the effect of successive replacement of oxygen with sulfur in the PEDOT structure through the synthesis and analysis of two new monomers **OSO** and **SOS**.⁴³



The electrochemistry of these two monomers along with EDOT and EDTT and the subsequent polymers of all four showed that PEDOT has the lowest oxidation

potential and the lowest band gap at 1.35 eV, as it has exclusively O \cdots S interactions in the polymer chain making it the most planar structure. The next smallest band gap is POSO (1.47 eV) as it has predominately O \cdots S interactions but also now includes sterically demanding S \cdots S interactions producing a small departure from planarity, restricting the extent of the effective conjugation length. PSOS has more S \cdots S interactions than O \cdots S interactions and this polymer has a much larger band gap (1.89 eV). PSOS is lower in band gap than poly(ethylenedithiathiphene) (PEDTT) (2.19 eV) only because O \cdots S interactions in the trimer units within the backbone provide a longer effective conjugation length (*i.e.* within SOS terthiophenes). The expected interactions are depicted in Figure 1.14.⁴³ We showed that the planarity of the polymer can be retained with a small dilution of EDOT units, *i.e.* at least one interaction between the units. This agrees with research performed by other groups.⁴⁴

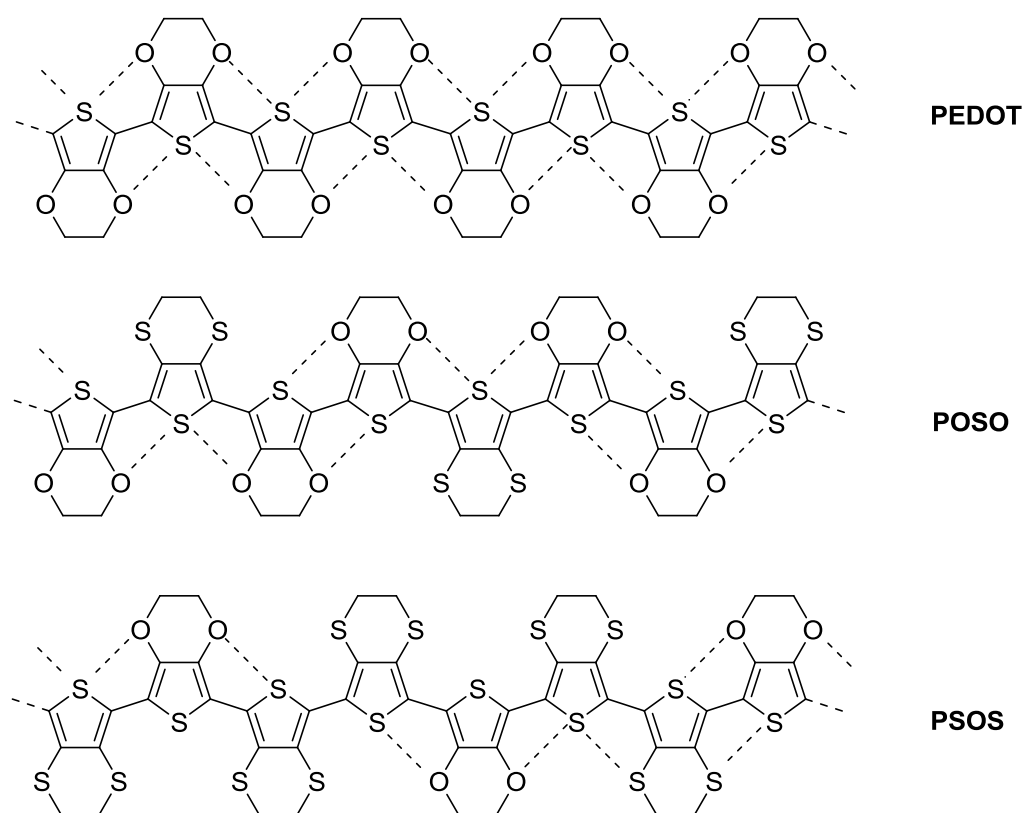
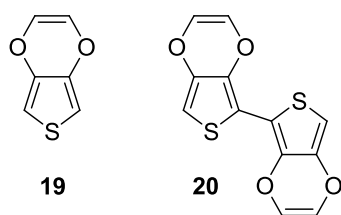


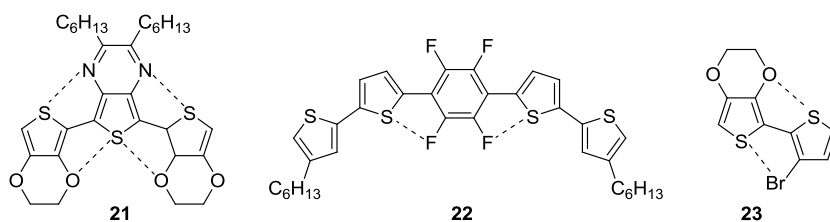
Figure 1.14 Expected O \cdots S interactions for **PEDOT**, **POSO** and **PSOS**

PEDOT has many uses, it can be used in electrochromic displays,⁴⁵ and smart windows,⁴⁶ as it is dark blue when neutral and pale / almost transparent when p-doped. Other applications include use as the hole injection layer in organic light emitting diodes and organic photovoltaics.^{47, 48}

An interesting modification to EDOT is the creation of vinylendioxythiophene (VDOT) (**19**), which is more planar and has a lower oxidation potential than EDOT as the vinylendioxy-bridge is a better electron donor than the ethylene equivalent. However, electropolymerisation of VDOT is not possible and bis-VDOT (**20**) was required to be synthesised and then electro-polymerised. The resultant polymer also supports close non-covalent oxygen-sulfur interactions and overall is similar in band gap to PEDOT.

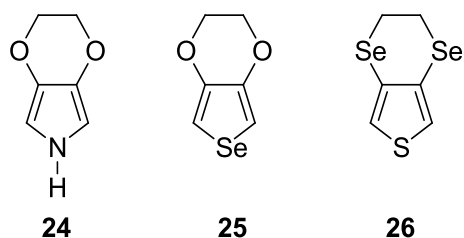


Other non-covalent interactions have been shown to exist and an example is the sulfur-nitrogen interaction. This interaction (along with a sulfur-oxygen interaction) can be seen in the X-ray crystallographic analysis of **21** which is planar and shows bond distances for both interactions smaller than the sum of the van der Waals radii of the corresponding atoms.⁴⁴ Other non-covalent interactions have been shown to exist between sulfur and halogen atoms, such as fluorine (**22**),⁴⁹ and bromine (**23**).⁵⁰



One problem of EDOT based polymers is their insolubility, in an attempt to make them more soluble, alkyl chains can be added to other units in the monomer. However, the addition of long alkyl chains to the sp^3 carbon of the ethylene bridge actually causes disruption of the polymer chains by hindering π -stacking and reduces the polymer's stability to oxygen by making the polymer more permeable.⁵¹

There have been several monomers created that are analogous to EDOT, such as the pyrrole (**24**) and selenophene (**25**) analogues, as well as replacing oxygen with selenium to give EDST (**26**).



The pyrrole derivative of EDOT has a lower oxidation potential but the resulting polymer has a higher band gap which is a result of no nitrogen-oxygen non-covalent interaction to hold the polymer stable and to increase the effective conjugation length.⁵² The selenophene derivative has both a lower oxidation and band gap to the analogous thiophene version, implying that selenium-oxygen non-covalent interactions are present to hold the polymer backbone in a planar conformation.⁵³ In our group, we synthesised and characterised 3,4-ethylenediselenathienophene (EDST) which shows that the polymer form also adopts a planar conformation, unlike the sulfur derivative (PEDTT) and more similar to PEDOT.⁵⁴

1.8 Electrochemistry

This section describes the equations related to electrochemical analysis performed using literature procedures.^{17, 18, 55, 56} In general, an electrochemical cell is made up of at least two electrodes in contact with a solution containing an analyte and electrolyte. Applying a potential difference across the cell causes two different redox reactions to occur at either electrode. Oxidation is the loss of electron(s) from the analyte with n being the number of electrons:



and reduction, the gain of electron(s) is given by the reverse reaction:



where O is the oxidised species and R is the reduced species. The electrode potential for the redox reactions above is given by the Nernst equation:

$$E = E^0 + \frac{RT}{nF} \ln \frac{[\mathbf{O}]}{[\mathbf{R}]} \quad (4)$$

where E^0 the standard electrode potential, R is the gas constant, T is the temperature, F is the Faraday constant ($96,485 \text{ C mol}^{-1}$), $[\mathbf{O}]$ and $[\mathbf{R}]$ are the concentration of the species in the oxidised and reduced forms respectively. The standard electrode potential is the measure of the individual potential of the electrode in a standard. The Gibbs free energy change of an electrochemical reaction is given by the following equation:

$$\Delta G = -nFE_{cell} \quad (5)$$

where n is the number of electrons transferred and

$$E_{cell} = E_R - E_L \quad (6)$$

E_R and E_L is the potential of the reduction and oxidation reactions, respectively. The electrode kinetics can be derived by considering the following equations:



The rate of the electrochemical reaction (k) is related to the current I or current density i , which is related to the current through the area of the electrode surface (A):

$$i = I/A \quad (8)$$

For the forward reaction (reduction):

$$i^{\rightarrow} = nFk^{\rightarrow}C_O^{\sigma} \quad (9)$$

and the reverse reaction (oxidation):

$$i^{\leftarrow} = nFk^{\leftarrow}C_R^{\sigma} \quad (10)$$

where C_O^{σ} and C_R^{σ} are the concentrations of oxidised and reduced species at the electrode surface, respectively. If there is a net current density then:

$$k^{\rightarrow} = k_0 \exp\left(\frac{-\alpha_c n F}{RT}\right) \quad (11)$$

and

$$k^{\leftarrow} = k_0 \exp\left(\frac{(1-\alpha_A)nF}{RT}\right) \quad (12)$$

where α_C and α_A are the cathodic and anodic transfer coefficients, respectively. These coefficients reflect the amount of applied potential which actually goes into reducing the activation barrier for electron transfer in the forward and reverse directions. In simple redox couples, α_C and α_A are equal to one. k_0 is the standard electron transfer rate constant. If the reaction is governed by the rate of electron-transfer, the current is given by the Butler-Volmer equation:

$$i = i_0 \left\{ \exp\left(\frac{(1-\alpha_A)nF\eta}{RT}\right) - \exp\left(\frac{-\alpha_C nF\eta}{RT}\right) \right\} \quad (13)$$

where i_0 is the exchange current density,

$$i_0 = nFk_0 C_0^{\alpha_A} C_R^{\alpha_C} \quad (14)$$

and this gives the amount of electron exchange at the equilibrium potential, E_e for the electron transfer, which is related to the overpotential (η) by the equation:

$$\eta = E - E_e \quad (15)$$

When η is positive, an oxidation reaction occurs and the net current is positive.

When η is negative, reduction occurs and the net current is negative.

Mass transport, the process of at which the electroactive material moves from the bulk solution toward the electrode surface is controlled by three mechanisms: migration, convection and diffusion. Of these three, diffusion is the most important

and follows Fick's first law, where the flux J_i (amount of diffusant per second) of the electroactive species, i , is related to the diffusion coefficient (D_i) by the following equation:

$$J_i = -D_i \left(\frac{\partial c_i}{\partial x} \right) \quad (16)$$

$(\partial c_i / \partial x)$ is the concentration gradient, the change in the concentration of c of the species i per unit distance x . The concentration gradient arises as some of the electroactive species is consumed around the electrode surface and this depletion causes the gradient.⁵⁷ As the current response is related to the diffusion coefficient through the following two equations:

$$i = nFJ_i \quad (17)$$

therefore current is influenced by diffusion as:

$$i = -nFD_i \left(\frac{\partial c_i}{\partial x} \right) \quad (18)$$

A plot of scan rate versus current will determine if the redox response of a material is diffusion related or not. If a linear fit is observed then the material is not diffusion controlled. A non-linear line suggests a diffusion coefficient influences the current response and the current peak will in fact be proportional to the square root of the scan rate. This is seen in the Randles-Sevcik equation which links the peak max (I_p) of current (I) with the concentration (c), the area of the electrode (A), the scan rate (v) and the diffusion coefficient (D):

$$I = -0.4463 nFA \left(\frac{nF}{RT} \right)^{\frac{1}{2}} D^{\frac{1}{2}} c v^{\frac{1}{2}} \quad (19)$$

1.9 Cyclic Voltammetry

There are many types of potential sweep techniques employed for electrochemistry; the most common of these is cyclic voltammetry (CV). CV uses a potentiostat to probe the redox properties of materials by applying a potential in the forward and then reverse direction while recording the current response. Materials can be measured in solution or in the solid state. In a normal electrochemical cell, the flow of current alters the potentials for both electrodes. In CV, only the processes at one electrode are examined and this electrode is known as the working electrode. The redox processes at the other electrode, the counter electrode, are ignored and the purpose of the counter electrode is simply to supply the current required by the working electrode without limiting the response. The current response is measured between these two electrodes. The potential at the working electrode is measured and controlled between that electrode and a separate reference electrode, the reference electrode should not vary and remains at a fixed potential during the experiment, independent of current density.¹⁷

Common electrodes used for the working electrode are glassy carbon, platinum and gold. These can either be various shapes such as disc, spade or cylinder. The counter electrode is typically platinum as either wire or gauze and the reference electrode can be a saturated calomel electrode (SCE), a Ag/AgCl electrode, a pseudo silver wire or a standard hydrogen electrode (SHE).

The experiment involves running a potential varying with time over a desired range, V_1 to V_2 . When V_2 has been reached, the voltage is reversed and swept back to V_1 . As the potential sweeps, any electron transfer processes for the electroactive material

that occur will result in an increase in the current response, peaking at I_p and E_p . The scan rate, v , can be controlled and used as described above to measure the diffusion dependence of the material. A typical graph output is plotted with current versus potential (Figure 1.15). When the material is oxidised the positive current increases and when the potential reaches that of the oxidation potential of the material (E_{pa}) the current peaks at I_{pa} and then lessens as the concentration of the material near the electrode surface decreases. In the reverse mechanism, and in reduction processes, the current peaks at I_{pc} at E_{pc} in the same manner as before.⁵⁷ If the redox process is reversible, the reduction / oxidation back to the neutral state should be of similar size and shape but of opposite current.⁵⁶ For fast electron transfer, these two peaks should lie 57 mV apart.¹⁷

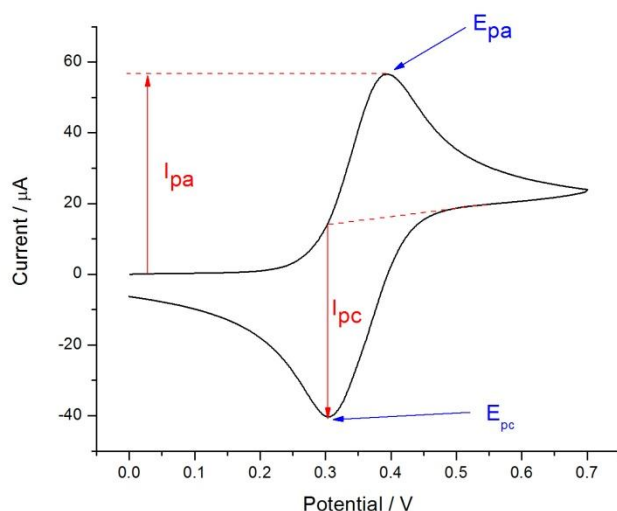
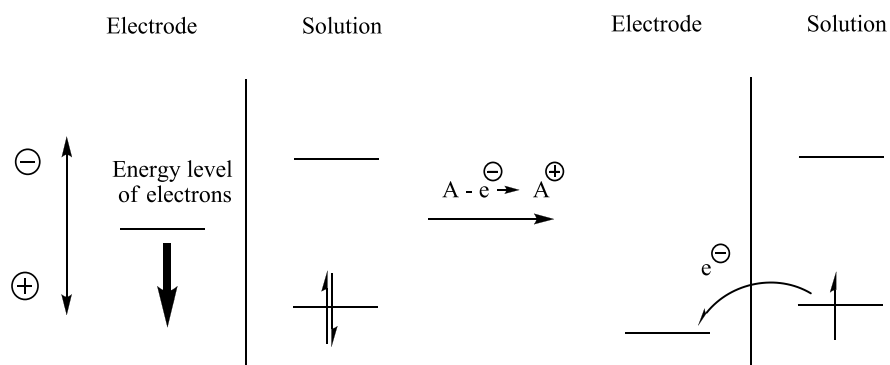


Figure 1.15 Typical cyclic voltammogram graph

In an electrochemical cell, the process of oxidation and reduction of a material can be described by comparing the HOMO and LUMO levels with the energy level of the electrode. In the oxidation process, the energy level of the electrons in the

electrode must be lower (of more positive potential) than the HOMO level of the material being oxidised as shown in Figure 1.16(a). Once the energy level of the electrode is low enough, electron(s) will transfer from the HOMO of the material to the electrode, resulting in an anodic current.

(a) Oxidation:



(b) Reduction:

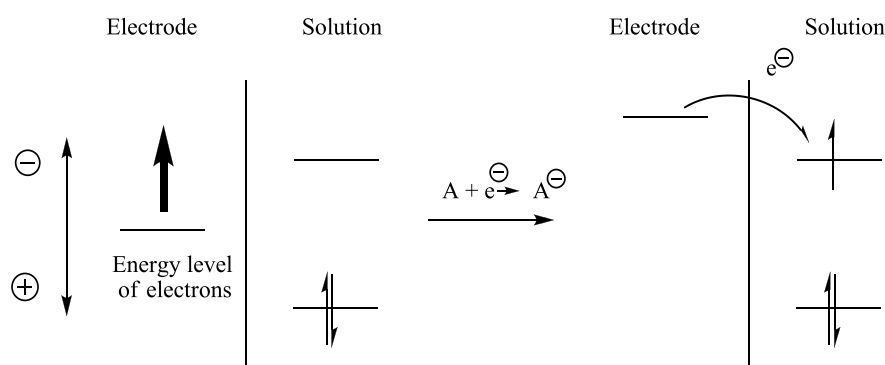


Figure 1.16 Illustration of oxidation and reduction in an electrochemical cell

Reduction of the electroactive species occurs in the same way but in reverse (Figure 1.16(b)). As the energy level of the electrode rises, becoming more negative in potential, there arises a point when it becomes energetically favourable for an electron to move from the electrode and transfer to the LUMO of the species in solution giving a cathodic current.⁵⁶

In solutions of low conductivity, the applied voltage may not be the same as the desired potential at the working electrode. This potential drop is caused by the resistance of the solution between the working and reference electrodes. The potential drop can cause serious error, but can be corrected by applying internal resistance (iR) compensation before running an experiment. The addition of an electrolyte to the system minimises the problem also by increasing conductivity and minimising electrical migration of the electrochemical cell.^{17, 58}

All electrochemical results are referenced against a stable and solvent independent redox couple (Figure 1.17) to allow comparisons. The ferrocene / ferrocenium (Fc/Fc⁺) redox couple is recommended by IUPAC.

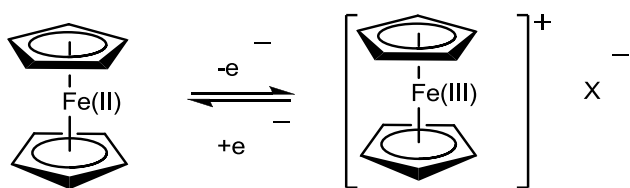


Figure 1.17 Ferrocene / ferrocenium redox couple (X is the counter-anion)

This redox couple was recommended by Strehlow over 25 years ago,⁵⁹ as it matched all but one (ferrocene is not spherical) of the following seven criteria:

- (i) The molecule is spherical and has large a radius as possible
- (ii) The ions carry a low charge
- (iii) The equilibrium is reversible and fast
- (iv) Both components of the redox couple are soluble
- (v) No geometry changes occur
- (vi) The redox potential is in the range of many solvents
- (vii) Both forms are stable.

1.10 UV-vis Absorption

Electrons in a material can be excited from a low electronic state to a higher electronic state through absorbance of ultra violet – visible (UV-vis) light. Transitions can occur from bonding or lone pairs to anti-bonding orbitals.⁶⁰ These transitions can involve σ , π , and n electrons or electrons involved in charge transfer reactions. Non-bonding electrons (n) are found in molecules with hetero-atoms present that have lone pair(s). There are four possible transitions involving σ , π , and n electrons (Figure 1.18).

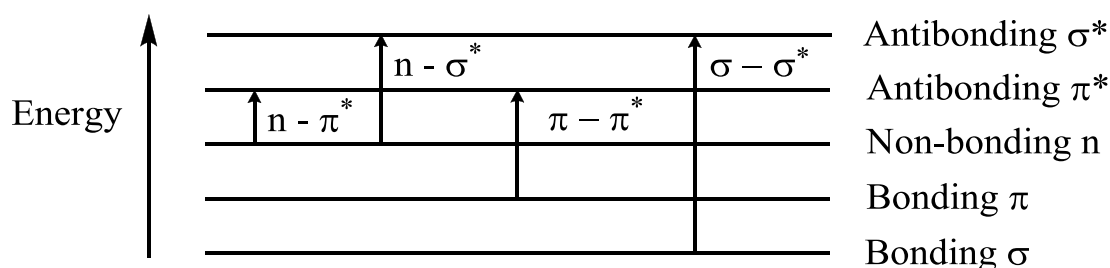


Figure 1.18 Possible electronic transitions for an organic molecule

The energy of the transition, which is the separation between the upper and lower states, corresponds to a wavelength at which that transition absorbs; they are related through the equation:

$$E = hc/\lambda \quad (20)$$

where h is Planck's constant ($6.63 \times 10^{-34} \text{ m}^2 \text{ kg s}^{-1}$) and c is the speed of light ($3 \times 10^8 \text{ m s}^{-1}$). The σ - σ^* transition has an absorption maxima not normally seen in UV-vis spectra as the maxima occur between 100 and 200 nm, the vacuum UV region.

The $n\text{-}\sigma^*$ transition occurs between 150 and 250 nm, whereas $n\text{-}\pi^*$ and $\pi\text{-}\pi^*$ transitions have absorption maxima in the 200 to 700 nm region; these transitions need double bonds in the molecule to provide the π electrons. In molecular systems with a high degree of conjugation, such as the conjugated polymers described earlier, the $\pi\text{-}\pi^*$ transitions have the lowest energy and therefore occur at the highest wavelength.^{6, 60} The intensity of the absorbance depends on the transitions being allowed or forbidden. Allowed transitions absorb strongly and forbidden transitions do not.

In an UV-vis spectrometer, the intensity of light at each wavelength is measured before (I_0) and after (I) it passes through the sample. This percentage transmission ($\%T$) is therefore:

$$\%T = \left(\frac{I}{I_0} \right) \times 100 \quad (21)$$

Thus, from this the absorbance can be calculated:

$$A = -\log (\%T) \quad (22)$$

and from the Beer-Lambert law, the absorbance is related to the molar extinction coefficient, ϵ , a measure of how strongly a species absorbs at that given wavelength:

$$A = \epsilon c l \quad (23)$$

where c is the concentration (mol L^{-1}) and l is the path length (cm).⁶⁰

The effect of conjugation length and substituent groups have on the wavelength is explained via the Woodward-Fieser rules: the longer the conjugation in the molecule,

the higher the wavelength for λ_{max} and substituent groups on the conjugation chain will impart either a bathochromic (red shift) or a hypsochromic shift (blue shift) for electron-donating and electron-withdrawing groups, respectively.^{49, 61}

1.11 Spectroelectrochemistry

Spectroelectrochemistry (SEC) is the combination of either electronic or vibrational techniques such as UV-vis spectroscopy, Infrared (IR) spectroscopy, Raman spectroscopy or Electron Paramagnetic Resonance (EPR) alongside an electrochemical technique such as CV. Spectroelectrochemistry utilises the difference in the spectroscopic signature between the oxidised and reduced form of a system to probe its redox properties. In this project, only UV-vis spectroelectrochemistry is employed as it is a very useful technique for the investigation of materials in electrochromics due to it showing how the absorption spectra of the material changes upon doping.⁶² The graphs are normally plotted as three-dimensional figures with wavelength, absorbance, and potential, as the x, y, and z axes, respectively.

The set-up of a UV-vis spectroelectrochemical experiment is shown in Figure 1.19. The working electrode is a film of a polymer either grown electrochemically or deposited by spin-coating, drop casting or spray-coating. Small molecules deposited onto the surface of indium tin oxide (ITO) can also be studied, as long as they remain adhered onto the electrode surface over the duration of the experiments. Spectroelectrochemical experiments can also be performed on substrates in solution, using a specially adapted electrochemical cell. The counter and reference electrodes

are typically a platinum and silver wire. Spectroelectrochemical experiments are performed in an electrolytic solution in order to complete the circuit and provide counter ions to balance charged states as a result of doping the material under investigation.

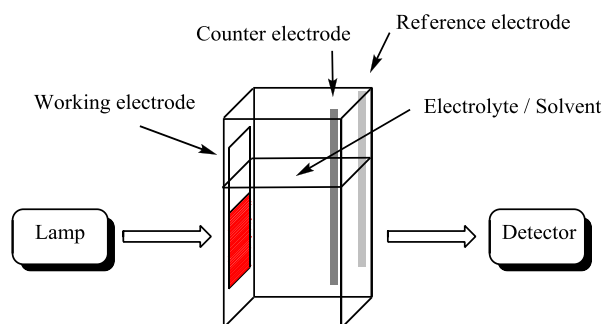


Figure 1.19 Diagrammatic representation of a UV-vis spectroelectrochemical experiment

UV-vis spectroelectrochemistry graphs show the formation of polarons (radical cations) and bipolarons (dications) through oxidation, such species are local gaps in the conjugated chain that absorb in the visible to near-infrared region. The absorption caused by polaronic doped states is due to charge transfer from an oxidised polymer chain to a neutral one. Creating charges along the chain causes a break in the effective conjugation length of the polymer which results in a drop in the π - π^* transition. Sometimes, if the potential at which the polarons and bipolarons form are close in potential then the spectra may show a combination of both in one peak rather than two separate peaks.⁶¹

Infrared spectroelectrochemistry (IR-SEC) is useful for probing bonds that may change with potential; either transmissive or reflective techniques can be used. The transmissive set-up is similar to that of UV-vis SEC with the window being made of either doped tin oxide or silicon.⁵⁵ Boron doped diamond can also be used as a

transmissive electrode as it has a wide electrochemical window and chemical inertness.⁶³ In reflective mode, the redox species are probed at the surface of a metal working electrode which also acts as the reflector (Figure 1.20 (a)).⁵⁶

As most solvents are good absorbers of infrared radiation, the solution layer has to be thin, less than 100 μm in depth.⁵⁶ Infra-red spectroscopy works by measuring vibrations of bonds in molecules. For a vibrating bond to appear as a band in an IR spectrum a net change in dipole must occur. Dipole moment is a quantitative measure of the degree of charge separation in a vibration. Vibrations that are IR active include symmetric and asymmetric stretching, bending or scissoring and rocking.⁶⁰ The frequency of vibrations is the same as the frequency of the absorbed radiation. When the radiation of this frequency falls upon the molecule, it is absorbed and so the bond starts to vibrate. Fourier Transform Infrared (FTIR) spectroscopy is used in preference to Dispersive Infrared spectroscopy as no slits or prisms are required. FTIR has good noise rejection and, as each wavenumber (inverse of wavelength) does not have to be measured successively, analysis times are much shorter.

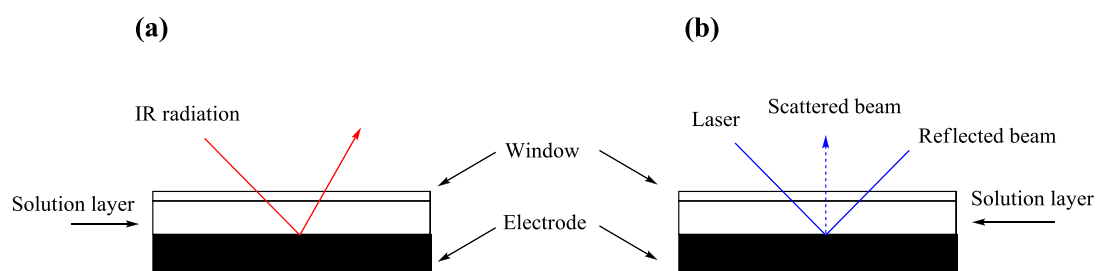


Figure 1.20 (a) Infrared spectroelectrochemistry and (b) Raman spectroelectrochemistry in reflection mode

Even with thin solution layers, Infrared spectroelectrochemistry still has problems with solvents and the window absorbing at low energies. These problems can be

overcome by using Raman spectroscopy. Raman spectroelectrochemistry is analogous to IR-SEC with the set-up in reflectance mode and with the scattered beam collected by the detector as shown in Figure 1.20 (b).⁵⁵

Electron Paramagnetic Resonance spectroelectrochemistry (EPR-SEC), is a more useful technique than the other techniques discussed. EPR measures the interaction of an unpaired electron with a magnetic field. Without a magnetic field, electron spin states are degenerate, but the application of a magnetic field removes the degeneracy. In a single electron transfer process, EPR is useful as an analysis technique as in this reaction either the starting material or the product will be paramagnetic, giving an increase or decrease in signal strength at a particular magnetic field. Information about the site of the redox activity in the material can also be acquired.⁶⁴ The experimental set-up of an *in situ* EPR-SEC (Figure 1.21) is different to that of the other spectroelectrochemistry techniques with the working electrode unable to be in the path of the magnetic field. The working electrode is typically platinum gauze placed in the flat region of the cell; the connecting platinum wire from the gauze is sheathed in polytetrafluoroethylene tubing so that the site of electrolysis only occurs at the gauze. The counter and reference electrodes are usually platinum wire and Ag/AgCl.⁶⁴

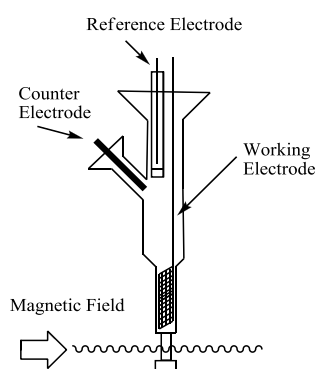


Figure 1.21 Diagrammatic representation of an EPR SEC cell and its alignment in the spectrometer

1.12 Calculation of energy levels and band gap

The HOMO, LUMO and band gap (or HOMO-LUMO gap) of polymers (or monomers) can be calculated experimentally using the following equations. When the graphs are referenced to the ferrocene / ferrocenium redox couple, the onset of the first oxidation peak can be subtracted from the known HOMO of ferrocene (-4.8 eV) to give the HOMO of the monomer or polymer. The same can be applied to calculate the LUMO energy level from the onset of the first reduction peak. The electrochemical HOMO-LUMO or band gap (E_g) for monomers and polymers, respectively, is therefore the difference between the calculated HOMO and LUMO levels.

$$\mathbf{HOMO\ of\ material = -4.8 - onset\ of\ oxidation} \quad (24)$$

$$\mathbf{LUMO\ of\ material = -4.8 - onset\ of\ reduction} \quad (25)$$

$$\mathbf{E_g = LUMO - HOMO} \quad (26)$$

The optical HOMO-LUMO or band gap for monomers and polymers is determined from the absorption spectra of the materials. The optical E_g is determined from the onset of the longest wavelength absorption band (λ),⁶⁵ using the following equations:

$$\mathbf{E_g = \frac{hc}{e\lambda}} \quad (27)$$

where h is Planck's constant, c is the speed of light and e is the charge of an electron (1.602×10^{-19} C), the resultant value is given in eV. As h , c and e are constants, the above equation can be simplified to:

$$\mathbf{E_g = 1240.68 / \lambda} \quad (28)$$

1.13 Associated Errors

Although an associated error is not normally published along with the calculated HOMO, LUMO or energy gap, the uncertainty in the determination can be calculated as follows.

For energy level determination, the uncertainty of the ferrocene reference must first be considered. The $E_{1/2}$ of ferrocene is recorded three times and averaged and thus, the random uncertainty associated with this is:

$$\mathbf{random\ uncertainty} = \pm \frac{\mathbf{max\ measurement - min\ measurement}}{\mathbf{n}} \quad (29)$$

where n is the number of measurements, which in this case is three. The average $E_{1/2}$ for ferrocene is not calculated until three that are within 10 mV range are recorded in succession. Therefore, this would produce a random uncertainty of ± 0.0033 V.

The reading uncertainty of the cyclic voltammetry instrument is ± 1 of the least significant digit, which gives an error reading of ± 0.0001 V. The total uncertainty in the calculation of the $E_{1/2}$ of ferrocene is ± 0.0033 V, which can be calculated from the following equation:

$$\mathbf{total\ uncertainty} = \pm \sqrt{(\mathbf{random\ uncertainty})^2 + (\mathbf{reading\ uncertainty})^2} \quad (30)$$

The cycle used in the energy level determination will also have the same reading uncertainty as that of the ferrocene oxidation. As the calculation of the onset of either the HOMO or LUMO is performed manually, this is where there will be the

greatest error occurs. As shown in Figure 1.22, the onset of this oxidation can be calculated from several positions, with the difference between the possible onset positions up to 15 mV. Thus, giving an onset determination error of ± 0.015 V.

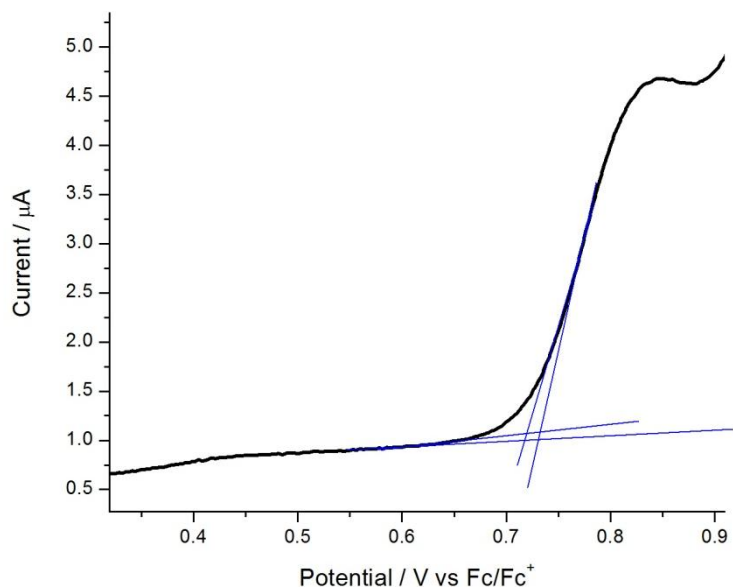


Figure 1.22 Example of onset determination

Overall, the uncertainty for the energy level determination can be calculated using the total ferrocene, the reading and the onset uncertainty as shown:

$$\text{Uncertainty} = \pm\sqrt{(0.0033)^2 + (0.0001)^2 + (0.015)^2} = \pm 0.0154 \text{ eV} \quad (31)$$

Therefore in an energy gap calculation, which encompasses the uncertainty in the HOMO and LUMO determination, there is an associated uncertainty of ± 0.03 eV. For optical energy gap calculations, there will also be an onset uncertainty (± 0.015 nm) and a reading error of ± 0.01 nm in the absorption spectra. As the calculation uses metres, these errors become 1.5×10^{-11} and $\pm 1 \times 10^{-11}$ m, respectively. Therefore, the uncertainty in optical energy gap is negligible.

1.14 Photoluminescence Quantum Yield

When a molecule absorbs a photon of light, an excited state is formed. The deactivation of this excited state back to the ground state can be through several mechanisms and for many organic compounds this results in luminescence. Luminescence is the emission of a photon of light corresponding in energy to the gap between the excited and ground states. Luminescence is bathochromically shifted (compared to absorption) to a longer wavelength / lower energy. This is because energy is lost through non-radiative processes, such as vibrational relaxations, internal conversions and intersystem crossing before emission occurs. Luminescence can either be fluorescence or phosphorescence, depending on the spin state the emission occurred from.⁶⁶

In most molecules, the ground state is a singlet state (S_0) as the electrons are paired in opposite orientations. When excitation occurs, if the electron does not change its spin configuration, then the new state will also be a singlet state (S_1 , S_2 etc.). If the electron changes its spin configuration and becomes parallel with the electron still in the ground state then the excited state will be a triplet state (T_1 , T_2 etc.). This transition is highly forbidden as a change in spin would take place. The triplet state is always lower in energy than the analogous singlet state because of the newly produced electron repulsion. Fluorescence is from a singlet state and is short-lived as it is an allowed transition. Phosphorescence is the emission from a triplet state and is long-lived in comparison to fluorescence as it is a forbidden transition (excited triplet state back to singlet ground state).⁶⁷ A simplified diagram of the absorption and emission of a molecule is shown in Figure 1.23.

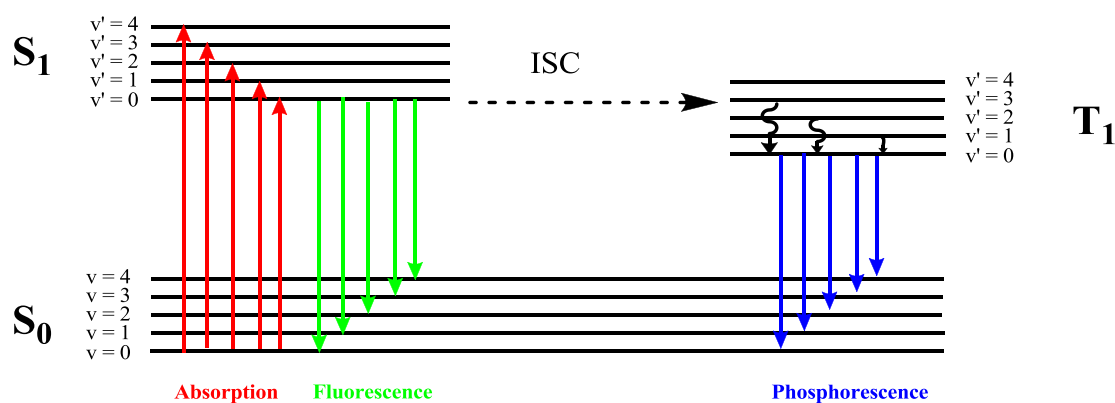


Figure 1.23 Absorption and emission of a molecule

The diagram shows that for each state there are associated vibrational states. Absorption from the ground state can be to any vibrational state in the excited singlet state. Through vibrational relaxation, the electron will relax to the lowest vibrational state ($v' = 0$) before either fluorescing back to S_0 or transferring to an analogous excited triplet state through intersystem crossing (ISC). Once again, vibrational relaxation will cause the electron to relax to the lowest vibrational state of the triplet state before phosphorescing to S_0 . Like fluorescence, phosphorescence can be to any of the vibrational states of S_0 before further possible relaxation to the ground state.⁶⁶

67

Phosphorescence is generally much weaker in intensity than fluorescence, as stated earlier. Intersystem crossing is less likely to occur as it is a spin forbidden process. Also, the lifetime of the molecule is longer in the triplet state, therefore the probability of other non-radiating transitions occurring are greater.

The photoluminescence quantum yield of a molecule is the ratio of photons absorbed to photons emitted and is essentially a measure of the probability of deactivation from an excited state to the ground state from luminescence. The quantum yield (Φ_L)

can be related to the intensity of luminescence at any wavelength ($I_L^{\lambda(emission)}$) through the following equation:

$$I_L^{\lambda(emission)} = k \Phi_L c \varepsilon_{\lambda(excit)} I^{\lambda(excit)} \quad (32)$$

where k is a proportionality constant, c is the concentration, $\varepsilon_{\lambda(excit)}$ is the molar absorptivity of the sample at $\lambda_{(excit)}$ and $I^{\lambda(excit)}$ is intensity of the excitation light that comes from the monochromator and impinges on the sample.⁶⁶ The above equation is only valid for optically dilute samples; if the concentration is too great then self-quenching, an inner filter effect, can occur which is the absorbance by the sample of its own luminescence.⁶⁸

A more reliable method of calculating quantum yields is to use a comparative method,⁶⁹ which compares the quantum yield of an unknown sample (Φ_x) with that of a known standard (Φ_{ST}). In such an experiment, we compare the gradient of the unknown ($Grad_x$) with the standard ($Grad_{ST}$), which can be calculated from a plot of integrated fluorescence *vs.* absorbance of five different dilute samples, while also taking into account the refractive indices of the solvents used (η) and applying these data to the following equation:

$$\Phi_x = \Phi_{ST} \left(\frac{Grad_x}{Grad_{ST}} \right) \left(\frac{\eta_x^2}{\eta_{ST}^2} \right) \quad (33)$$

1.15 Applications and Devices

There are many applications for organic small molecules, monomers and polymers. Years of research have been conducted for each application and progress is still ongoing to improve the efficiency of each device. Organic semiconductors have found use in devices such as electrochromics,⁷⁰⁻⁷³ light emitting diodes,⁷⁴⁻⁷⁷ field effect transistors,⁷⁸⁻⁸¹ photovoltaics,⁸²⁻⁸⁴ and sensors.⁸⁵⁻⁸⁸ Each application and device will now be explained in more detail.

1.15.1 Electrochromic devices

Electrochromics is the one application where organic semiconductors already excel over their inorganic counterparts with their ability to control and fine-tune the colour. Organic based electrochromics have a higher colouration efficiency, greater stability, faster switching times and have the ability to become fully transparent.^{89, 90}

Electrochromic materials can reversibly change from one state of absorption to another by applying a potential; this effect is caused by modifying the band gap of the material, creating doped states in the material and shifting the spectra towards higher wavelengths.^{91, 92} Polythiophene itself is red in the neutral state and blue when p-doped,^{20, 25} and through varying the side group, the three primary colours can be created, thus allowing the development of devices based solely on conjugated polymers.^{93, 94} The band gap of the polymer essentially controls the colour change. Conjugated polymers with E_g above 3 eV are transparent when neutral and will

absorb in the visible region in the doped state. Polymers with band gaps of 1.5 eV and below are highly absorbing and coloured when neutral but upon p-doping the absorption shifts to the near-IR. Thus polymers with band gaps between 1.5 and 3 eV give a change in the visible region.¹⁹

A classical electrochromic device is a simple set-up and is depicted as a seven layer structure (Figure 1.24).⁹⁵ The electrochromic layer can be deposited in several different ways, such as electrochemical growth, spin-coating, drop-casting, or spray-coating.⁹⁶ When a potential is applied, the electrochromic layer becomes either oxidised or reduced, depending on the polarity of the current flow and the new charged state produced is balanced by counter-ions from the electrolyte layer. The change in the material's state is due to the applied potential and results in a change of colour. This colour change can be seen from either side as the substrate and the conductor are transparent.

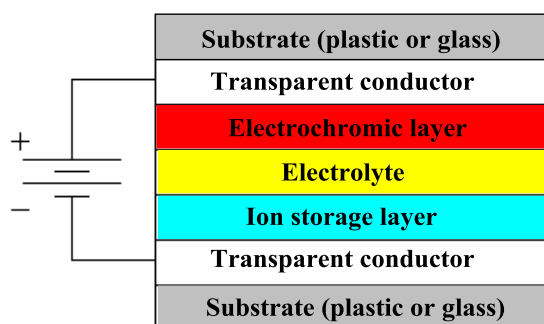


Figure 1.24 Diagram of a typical electrochromic device

Typical polymers used in electrochromics and their colour changes are shown below in Figure 1.25.⁹⁵

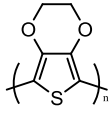
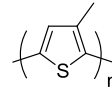
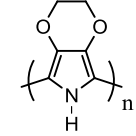
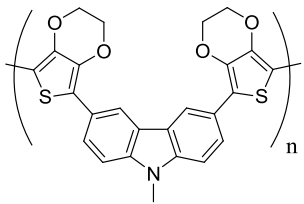
| | <u>Polymer</u> | <u>Neutral</u> | <u>Doped</u> |
|-------|---|----------------|--------------------------|
| PEDOT |  | Dark blue | Transparent / light blue |
| 27 |  | Red | Light blue |
| 28 |  | Pink | Transparent / light blue |
| 29 |  | Yellow | Blue |

Figure 1.25 Polymers used in electrochromics and their colour changes

The switching ability of a polymer, the rate of change of the absorption or transmittance upon fast switches (up to ten seconds) between oxidation and reduction, gives an indication of the material's potential use in an electrochromic device. The rate of change is dependent upon the ability of electrolyte counter-ions to diffuse in and out of the polymer to balance the charge when doped (keeping electro-neutrality) and expelled when neutral. More open polymers possess a better switching ability and have a greater change as a less-packed morphology allows an efficient flow of counter-ions into and out of the polymer film.⁹²

Colourimetry experiments produce colour coordinates of materials in the neutral and doped states, and inbetween if required. Colour coordinates can be given as the 1931 (Yxy) and/or the 1976 ($L^*a^*b^*$) CIE representation of colour space to determine the colour transformation. Y is the luminance of the colour with x and y coordinates of

the chromaticity diagram (Figure 1.26).⁹⁷ L^* is the lightness of the material with a^* and b^* opponent dimensions of colour. A positive a^* is red and a negative a^* is green. A positive b^* is yellow and a negative b^* is blue.⁹⁸

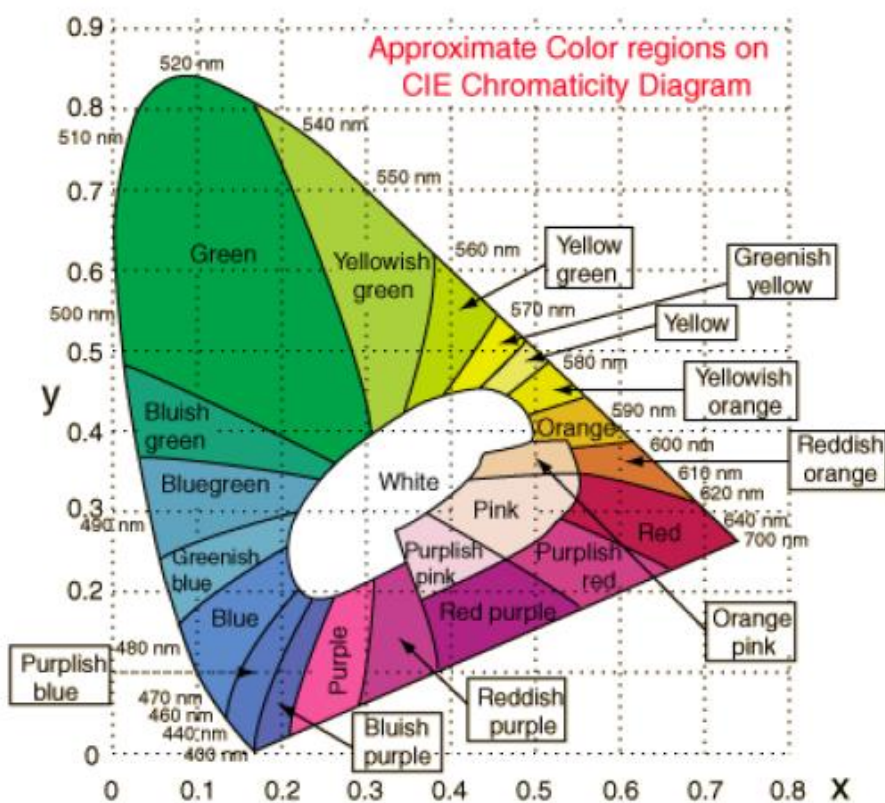


Figure 1.26 1931 CIE colour coordinates

The colour efficiency (η) of polymers can be calculated from the equation:

$$\text{Colour efficiency } (\eta) = \Delta_{OD}/Q_d \quad (34)$$

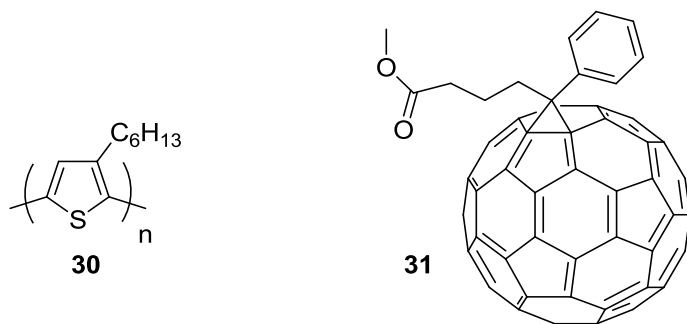
where Δ_{OD} is the change in optical density and Q_d is the charge passed during this process. Δ_{OD} is determined from the percentage transmittance (%T) before and after a full switch and can be calculated using the following equation:

$$\Delta_{OD} = \log(\%T \text{ of bleached state} / \%T \text{ of coloured state}) \quad (35)$$

1.15.2 Organic Photovoltaic (OPV) Devices

The photovoltaic effect in semiconductor junctions is the creation of electricity from light. Photovoltaics or solar cells are designed and manufactured to make use of this effect to create a renewable energy device that harvests light from the sun. Traditional solar cells are made from inorganic materials such as silicon, however, these devices are expensive to produce.⁹⁹ Research focus has turned to the organic versions known as organic photovoltaics (OPV). The semiconducting active layer in OPVs is essentially where the light is absorbed, separated to give electrons and holes, which in turn are then transported to the electrodes.

The active layer in organic photovoltaics is made from the combination of two electroactive components, a donor and an acceptor. The most commonly used donor is regioregular poly(3-hexylthiophene) (**30**) and the acceptor used for organic photovoltaics is [6,6]-phenyl-C₆₁-butyric acid methyl ester (PCBM) (**31**).¹⁰⁰ PCBM was first used in 1995,¹⁰¹ and to date is still the best acceptor found. It can be used alongside donor polymers with a wide range of band gaps ranging between 1.2 and 1.9 eV. The band gap of poly(3-hexylthiophene) is at the edge of this limit with an E_g of 1.9 eV.¹⁰²



However, despite the vast amount of research that has been performed on poly(3-hexylthiophene) and power efficiencies of 5% being achieved, the limiting factor for this polymer is inevitably its large band gap. A band gap of 1.9 eV corresponds to a wavelength of 650 nm and relating this wavelength to the photon flux of the sun (Figure 1.27), means that less than 25% of the sun's available photons are harvested.¹⁰³

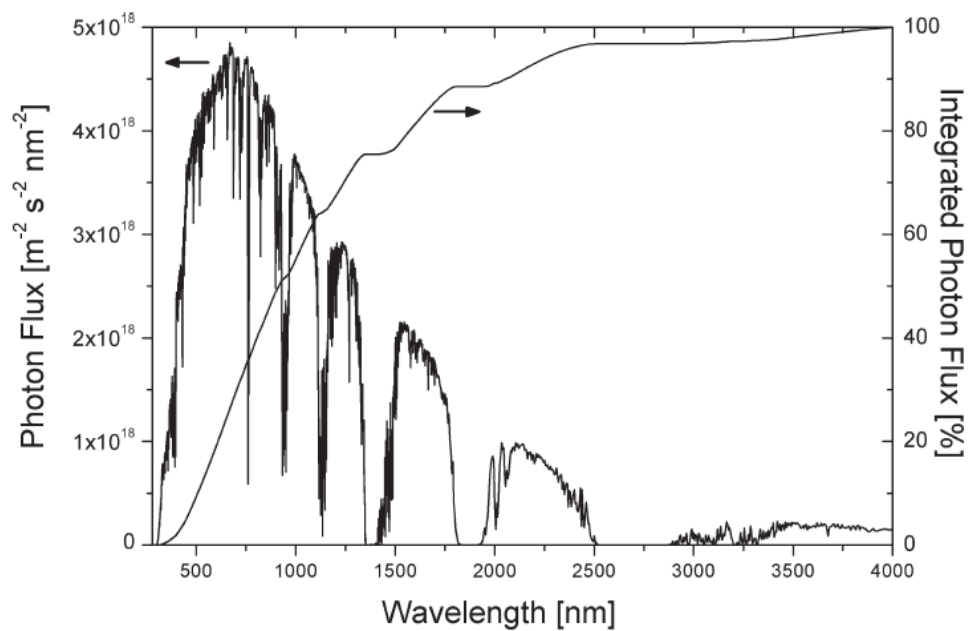


Figure 1.27 Solar photon flux as a function of wavelength

By examining the solar spectrum of the sun under AM 1.5 conditions¹⁰⁴ (the sun at 45° above the horizon, an integrated power density of 100 mW cm⁻² and integrated photon flux of $4.31 \times 10^{21} \text{ s}^{-1} \text{ m}^{-2}$), as shown in Figure 1.27, it can be seen that decreasing the band gap of the donor material will increase the amount of photons that can be absorbed.¹⁰³ However, having too small a band gap is not ideal either as the open circuit voltage (V_{OC}) will be small and overall the power conversion

efficiency (*PCE*) will be low. The optimal band gap has therefore been predicted to be 1.4 eV.¹⁰⁵

The power conversion efficiency (η_R) of organic photovoltaics can be calculated from a current-voltage (I-V) graph using the following equation:

$$\eta_R = I_{sc} V_{oc} (FF) / P_{in} \quad (36)$$

where I_{sc} is the short circuit current density (mA / cm²), the current at V = 0 V, which is dependent on the photon absorption of the active layer. V_{oc} is the open circuit voltage, which is the voltage at zero current and also the difference between the HOMO of the donor and the LUMO of the acceptor (see Figure 1.28). P_{in} is the intensity of the irradiating light (mW / cm²), AM 1.5 standardised. *FF* is the fill factor, which is determined by the balanced charge transport and recombination properties of the donor and acceptor. The fill factor can be calculated from the following equation:

$$FF = \max\{I_{mpp} V_{mpp}\} / I_{sc} V_{oc} \quad (37)$$

where I_{mpp} is the maximum current and V_{mpp} is maximum voltage in the I-V characteristics.

The energy levels of the donor and acceptor units should be offset and the ideal configuration is depicted in Figure 1.28. V_{oc} , as stated above, is proportional to the difference between the HOMO of the donor and LUMO of the acceptor.¹⁰⁶ For optimum efficiency of charge separation, ΔE_{LUMO} (energy difference between the LUMO of the donor and LUMO of the acceptor) should be 0.3 eV and matching this

value to the correct band gap donor will give theoretical efficiencies of 10%.¹⁰⁷ The graph in Figure 1.29, shows that the efficiency of a bulk heterojunction organic photovoltaic is at its highest when the ΔE_{LUMO} is 0.3 eV and the band gap of the donor is between 1.2 and 1.7 eV. If the acceptor is PCBM with an assumed LUMO of -4.3 eV (although this value varies considerably in the literature) then the optimum LUMO of the donor should be -4.0 eV.¹⁰⁶

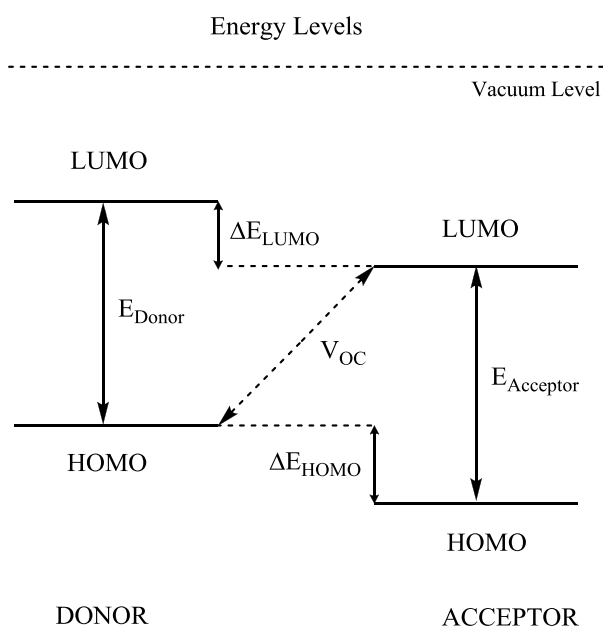


Figure 1.28 Energy levels of donor and acceptor components in organic photovoltaics

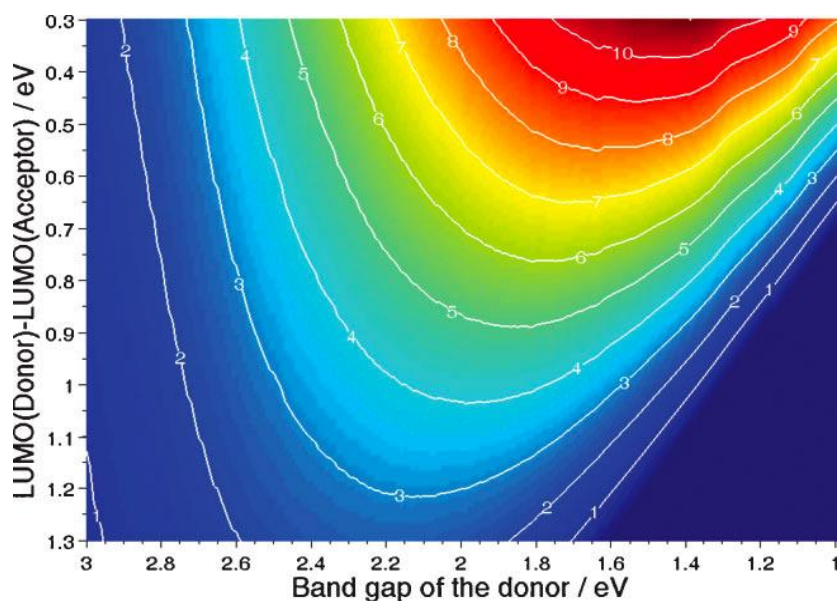


Figure 1.29 Power conversion efficiencies for band gap versus ΔE_{LUMO}

The mechanism for charge generation in an organic photovoltaic device is shown in Figure 1.30, along with a depiction of how energy can be lost through four different pathways.¹⁰³ The red and blue levels represent the HOMO (lower) and the LUMO (upper) energy levels of the donor and acceptor units in a photovoltaic junction, respectively. In part (a), a photon is absorbed creating an exciton. The exciton travels towards the donor-acceptor interface in part (b) and in part (c), an electron is transferred to the LUMO of the acceptor. Through a coulombic interaction, the charges are still attracted to each other until they are separated by an electric field as depicted in part (d). Part (e) shows that if the charges live long enough they are transported towards the electrodes and part (f) is the collection of the charges at the anode and cathode electrodes.

Energy can be lost in four ways: (1) represents photons that have energy greater than that of the donor band gap and are not absorbed and usually dissipated as heat.

Excitons that are created too far away from the donor-acceptor interface will recombine as shown in step (2). Even after separation, geminate recombination (3) or bimolecular recombination (4) can occur.¹⁰³ The acceptor units need to be close together so that a series of electron transfer steps can take place to carry charges to the electrode from the bulk. To avoid the premature recombination of electrons and holes, the semiconductor must be highly pure and defect free.

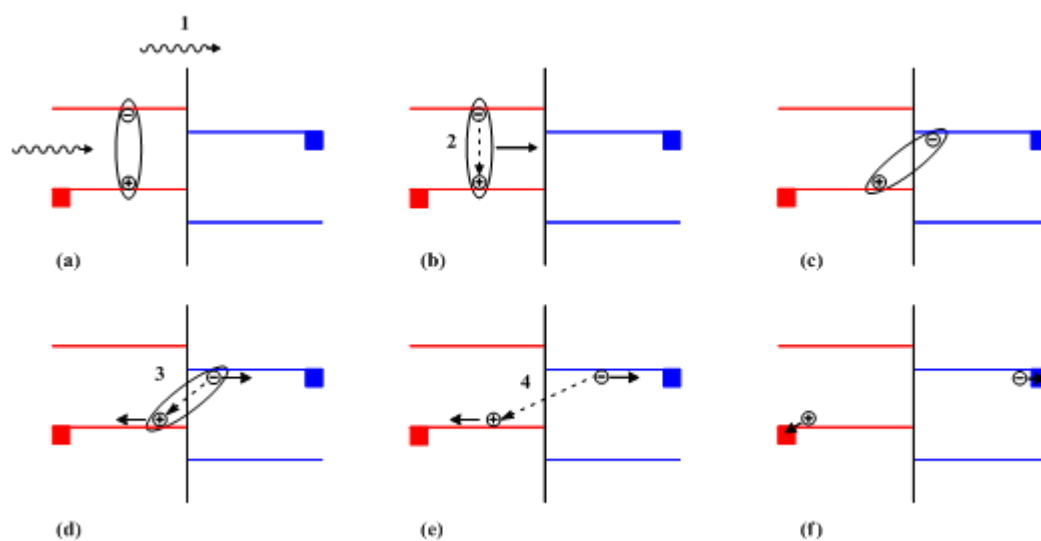


Figure 1.30 Mechanism for charge generation

Bilayer OPVs (donor and acceptor layers coated on top of each other) are inefficient as the area of donor-acceptor interface is very small and as a consequence solution-processed bulk heterojunction OPVs are predominately used.¹⁰¹ This device structure is better as the interface between donor and acceptor has increased greatly and therefore, as a result, so has the number of charge separation sites. A typical structure of a bulk heterojunction is shown in Figure 1.31.

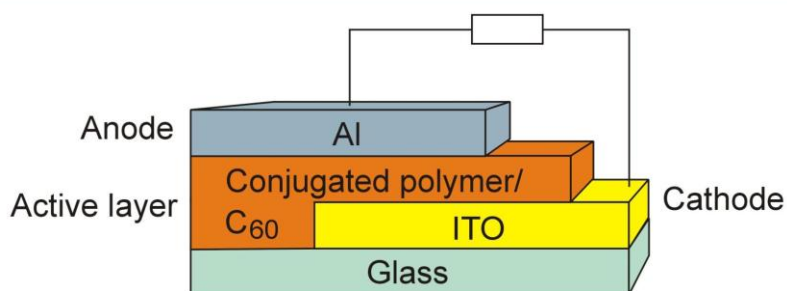
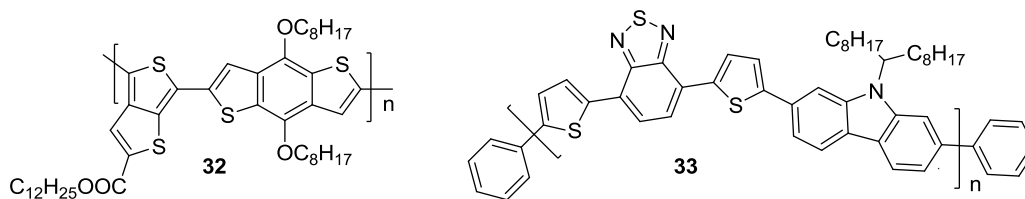


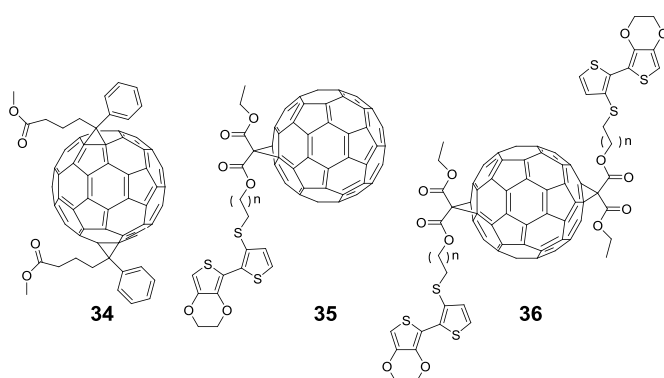
Figure 1.31 Schematic of a bulk heterojunction organic photovoltaic

Improving the processing of the materials is the best way to optimise the power efficiency; this can be done by mixing the donor and acceptor in many different ratios,¹⁰⁸ annealing after coating and through the addition of other additives to improve the morphology and reduce phase separation.¹⁰⁹ Controlling the thickness of the active layer is also important. In simple terms, increasing the thickness would increase the amount of light absorbed and the number of charge separations but consequently the resistance would increase along with a decrease in the fill factor.¹¹⁰

Other donors that have been investigated with promising results are **32**,¹¹¹ and **33**.¹¹² These new donors showed 4.76% and 6% efficiency, with C₆₀ and C₇₀, as acceptors, respectively. To date, the best power conversion efficiency of 7.9% has been reported by Solarmer Energy and confirmed by the National Renewable Energy Laboratory (NREL).¹¹³



Alternative acceptors to molecular based systems include n-type polymers,¹¹⁴ but the best acceptor materials are based on C₆₀ and C₇₀. An example includes the modification of PCBM, creating the bi-substituted version (**34**) that in comparison has raised the LUMO level by 100-200 mV,¹¹⁵ thus increasing the open circuit voltage and allowing a better ΔE_{LUMO} for most donor polymers. A more unusual strategy is the creation of polythiophenes connected directly to C₆₀-fullerene groups (via monomers **35** and **36**).¹¹⁶



It is postulated that the charges separate and pass in opposite directions in the same polymer (Figure 1.32). However, these are not as good as separate donor-acceptor heterojunctions, but the strategy does have promise.¹¹⁷

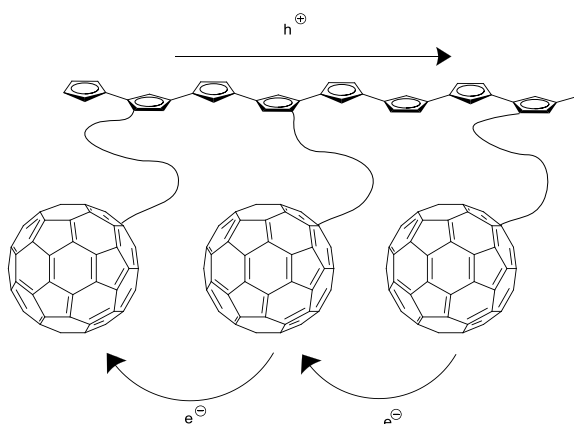


Figure 1.32 Proposed mechanism of charge separation for polymers with both donor and acceptor units integrated into the polymer structure.

1.15.3 Organic Field Effect Transistors (OFET)

Field effect transistors are effectively an on-off switch used in electronic circuits. Organic field effect transistors are based mainly on two types: small molecules and conjugated polymers. The main criteria are materials that possess a low threshold voltage, a high on / off ratio, high mobility and are stable under ambient and operating conditions.¹¹⁸

A typical device structure for an organic field effect transistor (OFET) is shown in Figure 1.33. An OFET is a three terminal device in either (a) top contact or (b) bottom contact arrangement.¹¹⁹ The difference between these two arrangements is that the source and drain electrodes can either be evaporated onto the top of the organic semiconductor (top contact) or evaporated onto the dielectric before the deposition of the semiconductor (bottom contact).¹²⁰

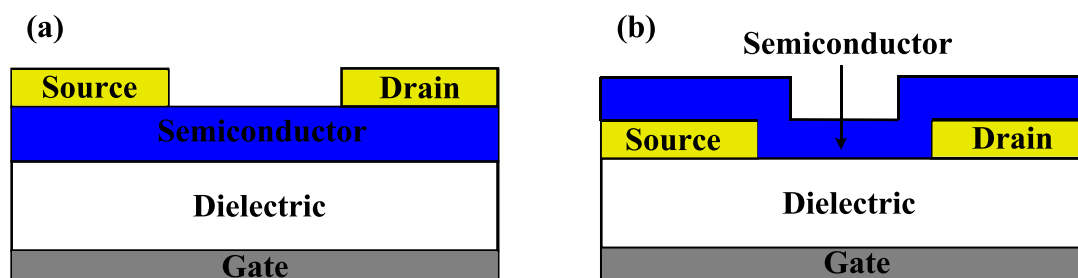


Figure 1.33 Set-up of an OFET configuration in (a) top contact and (b) bottom contact arrangement

The gate voltage (V_g) determines how much current can travel from the source to drain through the semiconductor material. When no potential is applied to the gate voltage there is little conductivity through the semiconductor and therefore very little current flowing between the source and drain. This is the OFET in the off state.

When an increase in potential in either polarity is applied, an electric field is induced, causing a potential gradient and resulting in a build-up of charges at the dielectric-semiconductor interface. The charges can now move and current can be drawn through the device by applying a voltage across the source and drain. The transistor is now in the on state.^{120, 121}

The polarity of the voltage determines the type of semiconductor, if a negative voltage is applied at the gate then the semiconductor will be p-type as the HOMO and LUMO levels of the organic semiconductor will shift upwards with respect to the Fermi level of the metal. When the HOMO and the Fermi level are resonant then holes will flow from the HOMO to the metal. n-Type behaviour is achieved by applying a positive potential at the gate, resulting in a shifting of energy levels down with respect to the Fermi level of the metal, when the LUMO of the semiconductor and the Fermi level are resonant then electrons will flow from the metal to the LUMO of the organic semiconductor. Materials that can behave as both p- and n-type are termed ambipolar semiconductors.¹²²

Crucial parameters that govern the performance of an OFET are the charge carrier mobility (μ), the on-off ratio and the threshold or turn-on voltage (V_t). Mobility is a measure of the charge carrier drift velocity per unit of electric field; the on-off ratio is the ratio of current in the accumulation mode over the current in the depletion mode and the threshold voltage is the minimum voltage at the gate electrode when the conduction channel starts to form. A typical OFET measurement is shown in Figure 1.34, where the source drain current (I_{sd}) is measured with respect to the source drain voltage (V_{sd}) at different gate voltages. The graphs are split into two sections, the linear regime when I_{sd} is linearly proportional to V_{sd} , and the saturation regime when I_{sd} is independent of V_{sd} .

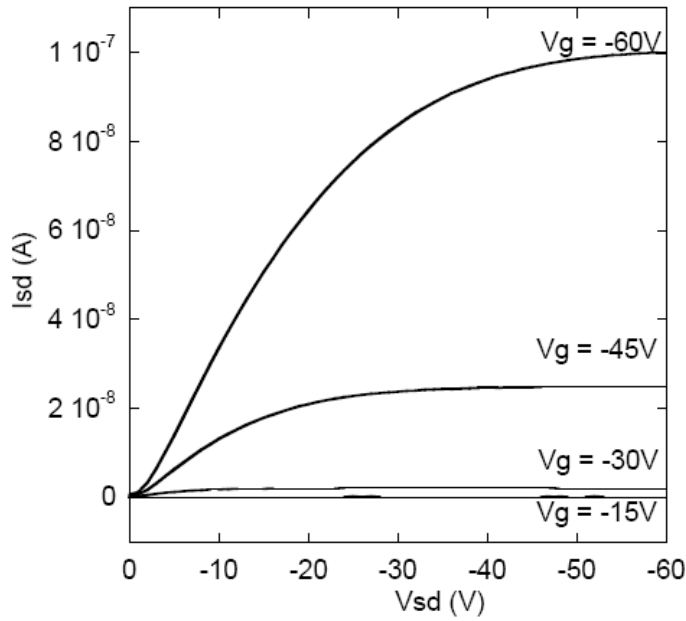


Figure 1.34 Graph of current versus potential obtained from a series of OFET measurements at varying gate voltages

The mobility of the semiconductor can be determined from the following two equations which relate to the two different sections of the graph.^{120, 123}

Linear regime:

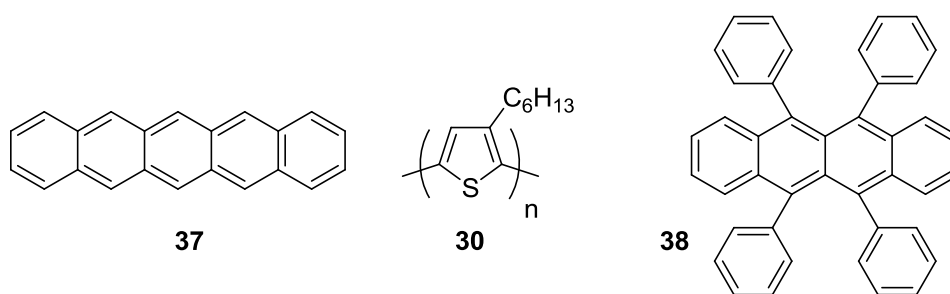
$$I_{sd} = \frac{W}{L} \mu C V_{sd} \left(V_g - V_t - \frac{1}{2} V_{sd} \right) \quad (38)$$

Saturation regime:

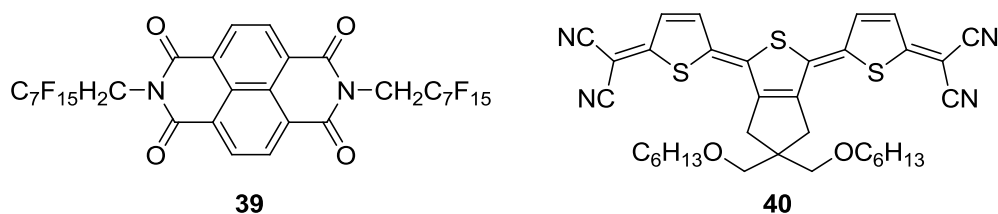
$$I_{sd} = \frac{W}{2L} \mu C (V_g - V_t)^2 \quad (39)$$

where W is the width of the channel, L is the channel length, C is the capacitance of the insulating (dielectric) layer, V_g is the applied gate voltage and V_t is the threshold voltage. The threshold voltage is determined from the onset of source-drain current.

Organic field effect transistors have the advantage of the semiconductor being easy to apply in device fabrication by either spin-coating or drop-casting. The choice of semiconductor is limited not only by the solubility, but also by the ability of the material to self-assemble in the solid state as this can maximise charge transport through π -stacking.¹²⁴ Flat molecules such as pentacene (**37**) are a good example of materials with self-assembling properties.¹²⁵ Pentacene is a well known p-type semiconductor and other heavily studied p-type semiconductors include polythiophene derivatives (mainly regioregular poly(3-hexylthiophene) (**30**)),¹²⁶ and rubrene (**38**).¹²⁷ A device consisting of rubrene has shown an incredibly high mobility of $15 \text{ cm}^2 \text{ V}^{-1} \text{ s}^{-1}$ compared to those of pentacene ($1 \text{ cm}^2 \text{ V}^{-1} \text{ s}^{-1}$) and poly(3-hexylthiophene) ($0.1 \text{ cm}^2 \text{ V}^{-1} \text{ s}^{-1}$).

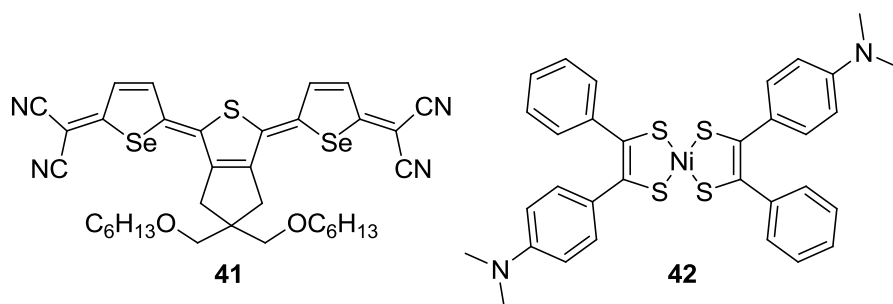


n-Type semiconductors for use in OFETs suffer from environmental quenchers such as oxygen and water, as they react with the radical anion produced from the transfer of an electron.¹²⁸ This instability limits the use of many compounds in OFETs but commonly used n-type semiconductors include fluoro- and cyano-substituted compounds such as **39**,¹²⁹ and **40**.¹³⁰



There are very few ambipolar semiconductors. Two recent examples were reported by Takimiya *et al* (**41**),¹³¹ and Anthopoulos *et al* (**42**) and both are air-stable.¹³² Other p-type, n-type and ambipolar organic semiconductors are given in recent reviews.^{120,}

121, 133



The choice of metal for the electrodes is an important choice. For p-type semiconductors, the metal should have a high work function (*e.g.* gold and platinum), whereas for n-type semiconductors, the metal should have a low work function (*e.g.* aluminium).¹³⁴ Choosing an appropriate metal to match the behaviour of the semiconductor allows efficient charge injection (holes or electrons). The work function is the energy required to remove an electron from the metal's Fermi level to the vacuum level.¹²⁰ Typical dielectrics used in OFETs are SiO₂ based networks or non-conducting polymers such as poly(methyl methacrylate).¹²¹

1.15.4 Organic Light Emitting Diodes (OLED)

Electroluminescence is the conversion of electrical energy into light. Materials that have this ability and conduct are used in light emitting diodes. The organic light emitting diode (OLED) has become the focus of much research for the next generation of commercial televisions, as it has several advantages compared to the current market leader, liquid crystal display (LCD) televisions. These advantages include being ultra thin, thus more portable with the possibility of being flexible. They are solution processable, have faster switching speeds, run on low voltages and are an emissive technology that requires no back light or filters.

OLEDs are assembled as small devices (Figure 1.35) in a multilayer structure. The organic emitters are embedded between thin electrodes, one of which has to be transparent. Typically, ITO coated glass is used as the anode and aluminium as the cathode. The two other layers, hole conducting and electron transport layers, are inserted to assist the transport of charges from the electrodes to the semiconductor.⁹⁵

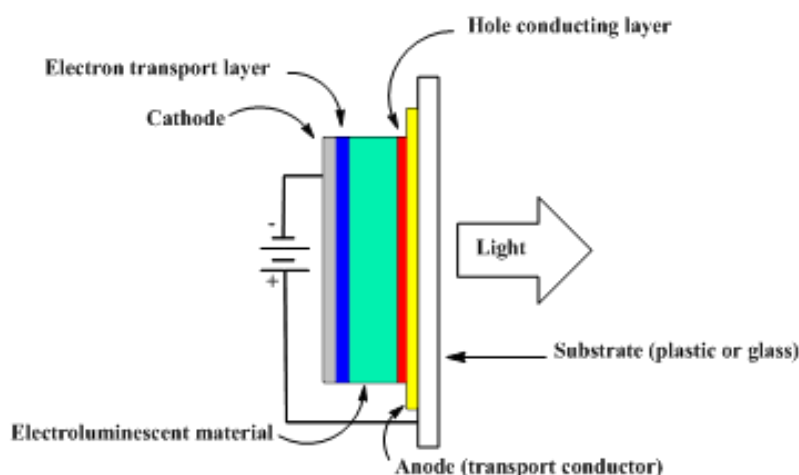


Figure 1.35 Classical structure of an OLED

When a potential difference is applied between the electrodes, electrons are injected from the low work function cathode and holes from the high work function anode. These charges are transported through the semiconductor and when they combine in the semiconductor, an exciton is formed and the relaxation from either a singlet or triplet state to the ground state triggers either fluorescence or phosphorescence, respectively. Figure 1.36 shows fluorescence emission from an excited singlet state in an OLED set-up.¹³⁵

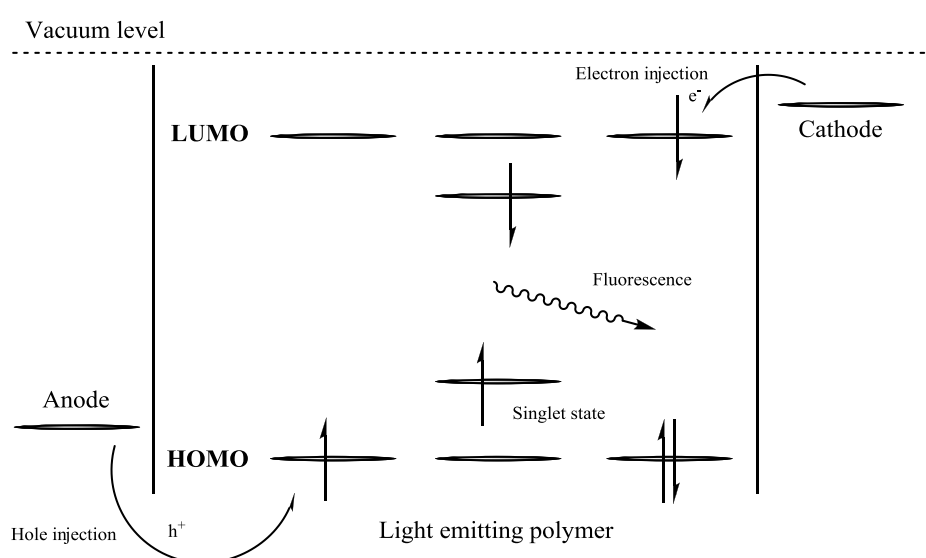
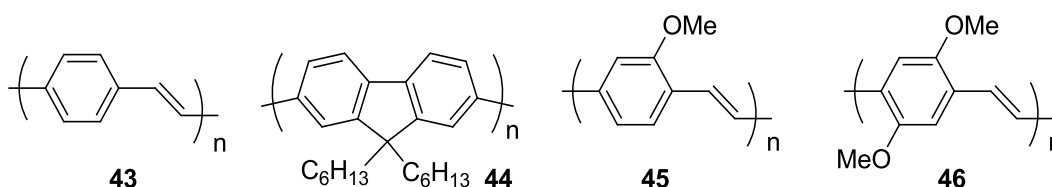


Figure 1.36 Electroluminescence in a conjugated polymer

The colour of the electroluminescent light is dependent on the HOMO-LUMO gap of the emitting material, which is related to the effective conjugation length and therefore is tailorable. Blue-shifted emissions are from short π -conjugated polymers and red-shifted emissions are from longer π -conjugated polymers.¹³⁶ The HOMO-LUMO gap of the conjugated semiconductor used should be between 1.65 and 3.2 eV for emission in the visible region.

Two of the most common emitting layers are shown below. Polyphenylene vinylene (PPV) (**43**) gives a green emission,¹³⁷ and polyfluorenes (**44**) provide strong blue emission.¹³⁸ The colour of the emission, as already mentioned, can be tuned. The addition of one (**45**),¹³⁹ or two methoxy groups (**46**),¹⁴⁰ to PPV gives yellow and orange-red emissions, respectively. For other examples of OLED materials, there are many reviews published.^{135, 141} Combining all three colours or just red and blue emitters gives 3- or 2-colour white light. White OLEDs themselves are being researched for large-scale solid-state lighting.¹⁴²



The efficiencies of OLEDs can be quoted in several ways: internal electroluminescent quantum efficiency, power efficiency or luminous efficiency.⁷⁶ Each efficiency is related to the external electroluminescent quantum efficiency, which is the ratio of photons emitted compared to the charge injected as a percentage of emission per unit current (cd A⁻¹), or as the efficiency of the device at the maximum brightness (cd m⁻²).¹³⁵ The external efficiency (η_{ext}) can be calculated from the following equation:

$$\eta_{ext} = \gamma \eta_{PL} \eta_C \chi_S \quad (40)$$

where, γ relates to the charge balance in the emissive layer, η_{PL} is the photoluminescence quantum efficiency of the emitter, η_C is the fraction of photons coupled out of the device and χ_S is the singlet fraction. When electrons and holes

recombine, the excited state can either be a singlet or triplet state in a ratio of 1:3. For organic polymers, the triplet state is long-lived with a low emission probability. The effective maximum efficiency for a conjugated polymer is therefore only 25%.^{143, 144} The internal electroluminescent quantum efficiency (η_{int}) can be calculated using the external quantum efficiency in the following equation:

$$\eta_{int} = 2n^2\eta_{ext} \quad (41)$$

The $2n^2$ factor is included as all photons emitted cannot be perceived due to refraction of the organic material (n is the refractive index) and are diminished by this amount. The power efficiency (η_{pow}) is the ratio of the output light to input power and can be calculated from the following equation:

$$\eta_{pow} = \eta_{ext} E_p V^{-1} \quad (42)$$

where, E_p is the average energy of the emitted photons and V is the applied voltage. The luminous efficiency (η_{lum}) is determined by multiplication of the power efficiency with the eye sensitivity curve S as defined by CIE:

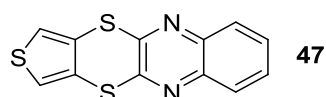
$$\eta_{lum} = \eta_{pow} S \quad (43)$$

The S value accounts for the sensitivity of the human eye to different colours.⁷⁶

1.15.5 Sensors

Conjugated polymers can be used as sensors, working on the principle that a host-guest arrangement between the receptor (conjugated polymer) and the analyte changes the behaviour of the polymer through either a change in the redox potential, the current response or the electronic properties.¹⁴⁵

In our group, we have shown that a conjugated polymer, electrochemically grown from **47**, can detect Ag^+ and Hg^{2+} ions at levels as low as 10^{-4} M through an increase in current and potential (up to $5\mu\text{A}$ and 400 mV respectively).



The change in the redox potential can be attributed to the coordination of the sp^2 nitrogen atoms and the possibility of sulfur-metal interactions with the two sulfur atoms in the dithiophene ring, as shown in Figure 1.37.⁸⁵

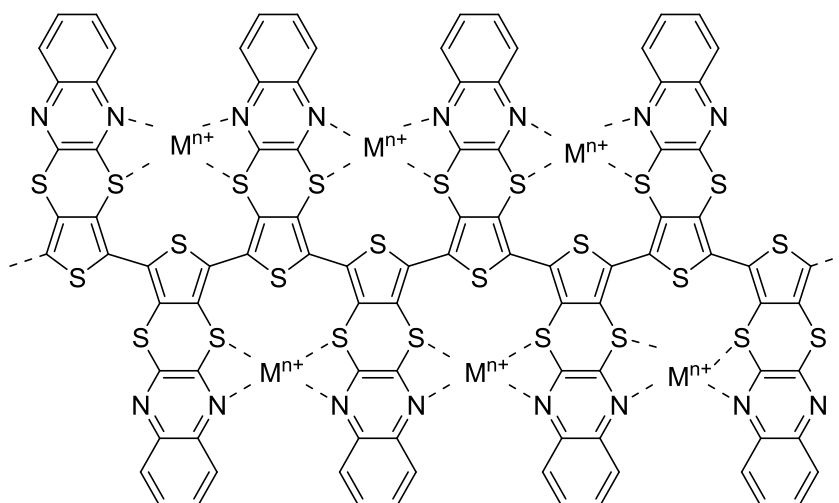


Figure 1.37 Host-guest arrangement of Poly**47** and metal analyte

In most cases, addition of ions to a conjugated polymer disrupts the effective conjugation length by breaking planarity in the polymer chain. This results in an increase in the anodic potential and a hypsochromic shift in the absorption maximum.¹⁴⁶ However, there are examples (such as **48** in Figure 1.38) where cation complexation with the crown ether in the polymer side-group induces planarisation in a twisted chain, producing a polymer with a longer effective conjugation length and therefore a decrease (0.1 V) in the required anodic potential.¹⁴⁷

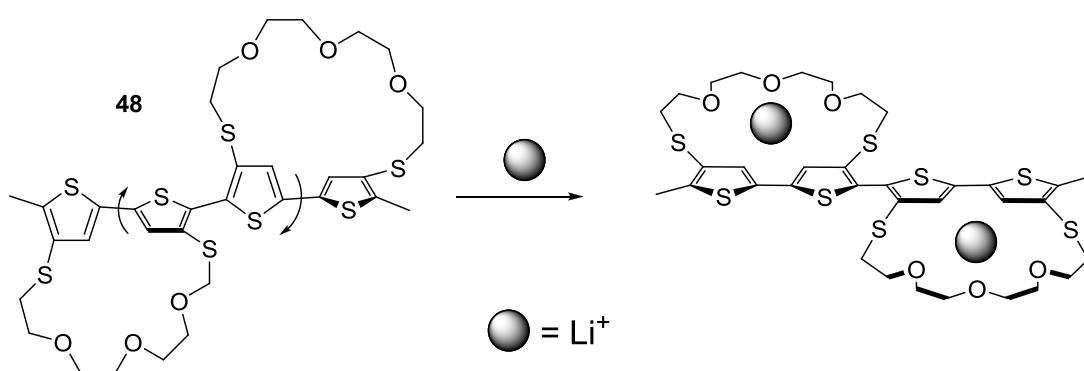
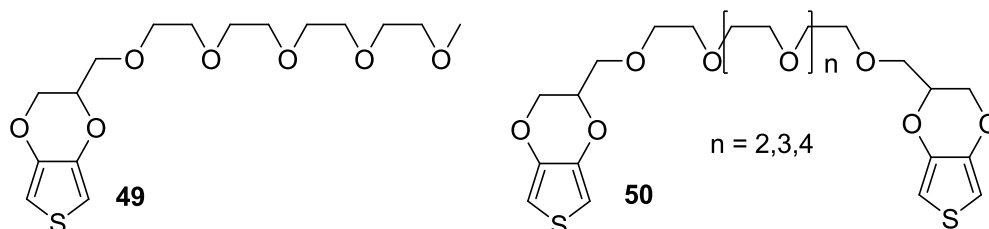


Figure 1.38 Addition of ions inducing planarisation of the polymer chain

The above situation only works for Li⁺ ions. There are many conjugated polymers (such as those derived from monomers **49** and **50**), that can detect several cation and dication metals, *e.g.* Bu₄N⁺, Na⁺, Ca²⁺, Ba²⁺ and Sr²⁺ by a shift in the anodic peak (several hundred millivolts).¹⁴⁸



**Chapter 2. Electrochemical,
Spectroelectrochemical and Comparative Studies of
novel organic conjugated monomers and polymers
featuring the redox active unit tetrathianaphthalene.**

2.1 Abstract

A series of monomers has been synthesised and characterised on the basis of the incorporation of tetrathianaphthalene (**54**) and its saturated (**55**) and open cyclic (**56**) forms as fused side groups onto polythiophene chains. The X-ray crystal structures of compounds **54** and **56** are reported. Tetrathianaphthalene (TTN) is an isomer of tetrathiafulvalene (TTF); however, monomer and polymer versions of **54** do not show any similarity to TTF in cyclic voltammetry (CV) or spectroelectrochemical measurements. CV experiments have shown that **54** and **56** are easier to oxidise than **55**, whereas **54** also has an additional reduction peak, giving it a smaller HOMO-LUMO gap than the other two monomers.

All three polymers of **54-56** have nearly the same oxidation and reduction potentials as well as band gaps; small variations can be attributed to the differences in the side groups. Spectroelectrochemical measurements revealed that the polymers showed electrochromic behaviour; switching times and colourimetry measurements are reported. From this data, all three polymers have a colour change of red to yellow with poly(**56**) having the best colour contrast and percentage change in absorbance from various switching times.

2.2 Introduction

Tetrathiafulvalene (TTF) (**51**) is one of the most studied electroactive organic materials over the last thirty five years and is well known for its easily accessed $\text{TTF}^{+\cdot}$ and TTF^{2+} oxidation states,¹⁴⁹ as shown in Figure 2.1. TTF and its derivatives have traditionally been used in the search for new superconductors and charge transfer salts,^{150, 151} but in recent years, they have also been incorporated into conjugated polymers, with examples including grafting of TTF to thiophene,^{120, 152, 153} and polythiophene backbones.¹⁵⁴⁻¹⁵⁶

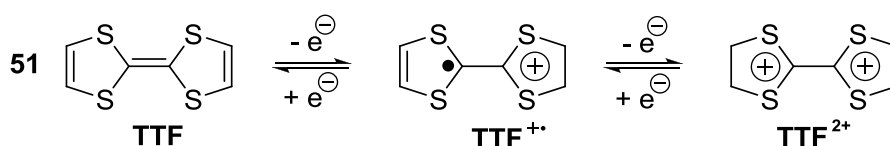
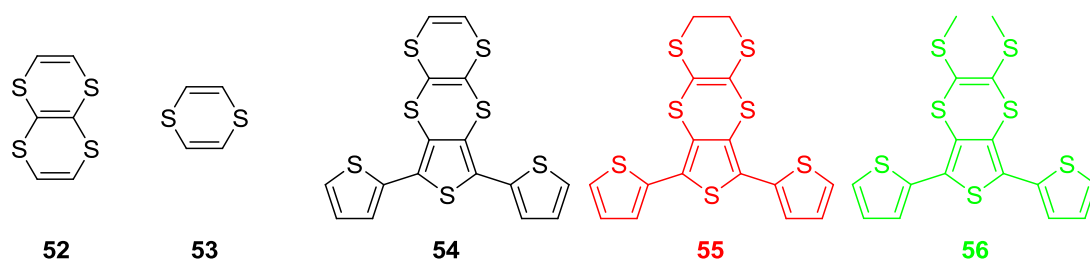


Figure 2.1 Oxidation of TTF

Tetrathianaphthalene (TTN) (**52**), comprising two fused 1,4-dithiin rings (**53**), is an isomer of TTF and is often used as a precursor in the synthesis of TTF.¹⁵⁷ To date, there has been no electrochemical analysis on TTN incorporated into conjugated polymers. In this chapter, the synthesis and characterisation of three monomers (**54**, **55**, and **56**) and their electrochemically prepared polymers are reported. In this comparative study, monomer **54** has a TTN group attached to a terthiophene unit, whereas monomer **55** is the saturated form of **54** and monomer **56** is the open bridge form.



In previous work, it was shown that TTN and 1,4-dithiin adopt boat conformations in the neutral state and planar conformations when oxidised.¹⁵⁸⁻¹⁶⁰ The 1,4-dithiin ring is an eight π -electron anti-aromatic heterocycle that can lose two electrons when oxidised to give an aromatic dication and this process is sometimes irreversible.¹⁵⁸ However, the oxidation can become complicated and the resulting voltammogram will change depending on the scan rate. The situation is best explained using a square scheme as shown in Figure 2.2.¹⁵⁸

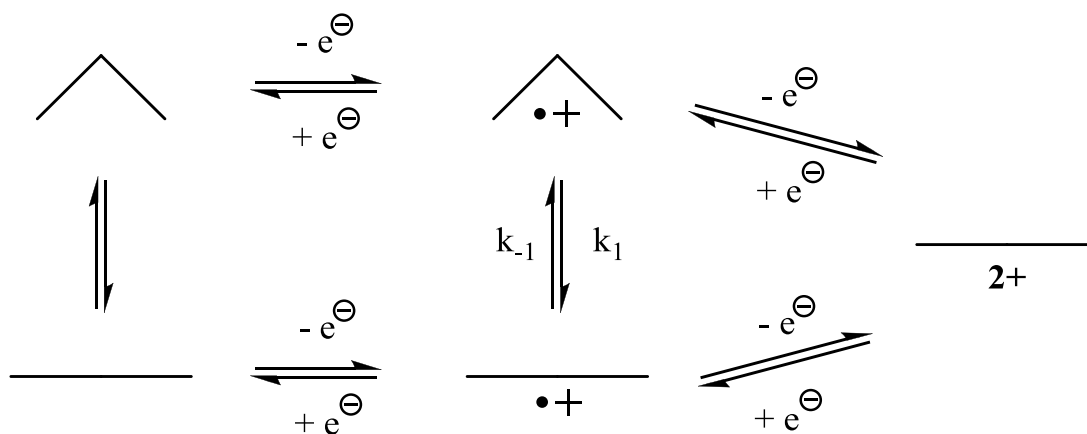


Figure 2.2 Square scheme oxidation of 1,4-dithiin ring

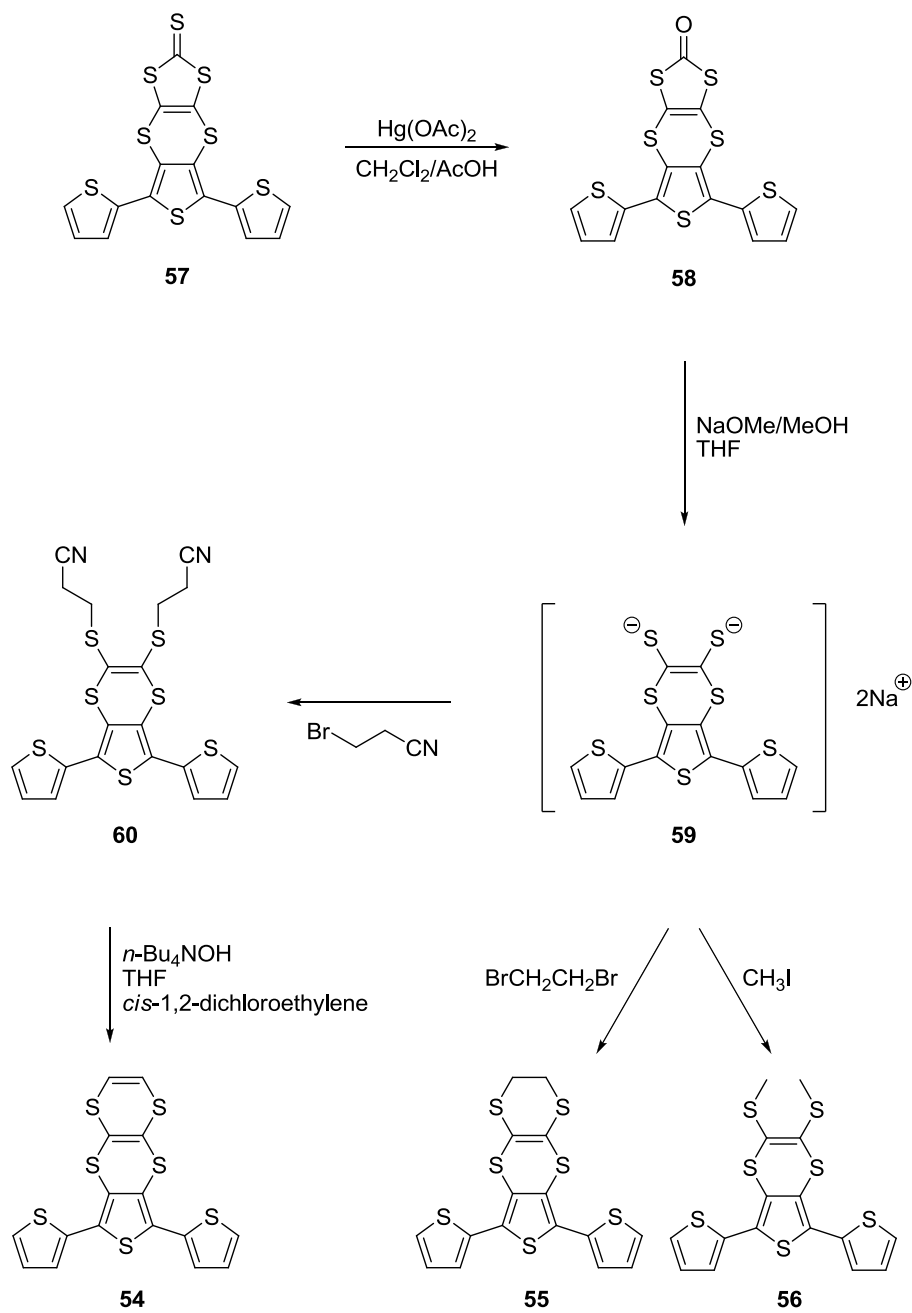
If the scan rate is fast, the top route is observed, but when the scan rate is slow enough to allow the conversion from the boat to the planar conformation then the

bottom route is preferred. The different oxidation potentials for the second electron loss is variable due to the two different available routes. The boat radical cation has the driving force of becoming planar and therefore the oxidation is lower than that of the equivalent planar version. In some cases, varying the scan rate does not have an affect on the conformation and it is likely that the boat conformer goes to the planar conformation at all scan rates after the loss of the first electron.¹⁶¹

TTF is more electron-donating than TTN and is therefore more easily oxidised ($E_{1/2}^{1ox} = +0.34$ and $E_{1/2}^{2ox} = +0.71$ V vs. SCE for TTF,¹⁶² and $E_{1/2}^{1ox} = +0.69$ and $E_{1/2}^{2ox} = +1.16$ V vs. SCE for TTN).¹⁶³ Moses *et al.*^{164, 165} have shown that TTN can be electrochemically transformed to give TTF through oxidation and then rearrangement. However, Sugimoto *et al.*¹⁶⁶ have shown that this reaction will not occur if there is extended conjugation; therefore, monomer **54** would be unlikely to take part in any rearrangement reactions when oxidised.

The synthetic procedures for monomers, **54**, **55** and **56** are summarised and shown in Scheme 2.1 and the electronic, electrochemical, X-ray crystallographic and computational analysis are presented and reported for all three monomers. The polymers grown electrochemically are characterised through electrochemical, absorption and spectroelectrochemical techniques. All three polymers were also investigated as potential electrochromic materials by measurement of the percentage change in absorbance through different switching times and CIE colour coordinates.

Scheme 2.1 Synthesis of **54**, **55** and **56**



2.3 Experimental

Monomers **54**, **55** and **56** were prepared synthetically by Alexander Kanibolotsky (University of Strathclyde). X-ray crystallography measurements were performed and solved by Simon Coles, Michael Hursthouse (University of Southampton), Ross Harrington and William Clegg (Newcastle University). Computational Analysis was performed by Peter Skabara (University of Strathclyde).

Cyclic voltammetry measurements were performed on a CH Instruments 660A electrochemical workstation with *iR* compensation using anhydrous dichloromethane as the monomer solvent and acetonitrile for monomer-free solvent. The electrodes were glassy carbon, platinum wire, and silver wire as the working, counter, and reference electrodes, respectively. All solutions were degassed (Ar) and contained monomer substrates *ca.* 10^{-4} M, together with *n*-Bu₄NPF₆ as the supporting electrolyte. All measurements are referenced against the $E_{1/2}$ of the Fc/Fc⁺ redox couple. Spectroelectrochemical and switching experiments were conducted on indium tin oxide (ITO) coated glass. Absorption spectra and CIE coordinates were recorded on a UNICAM UV 300 instrument.

2.4 Absorption Spectroscopy and Electrochemistry of Monomers.

The electronic absorption spectra for the three monomers in dichloromethane are shown in Figure 2.3. The absorption maxima are all similar given their near identical structures. Compounds **54** (356 nm), **55** (360 nm), and **56** (362 nm) give expected absorption maxima for the π - π^* transition of standard terthiophenes with heterocyclic side chains. The onset of the absorption edge gives the optical HOMO-LUMO gap for the monomers. The values calculated were found to be 2.95 eV for monomer **56** and 2.99 eV for monomers **54** and **55**, indicating that the different side groups have little effect on the π - π^* transitions.

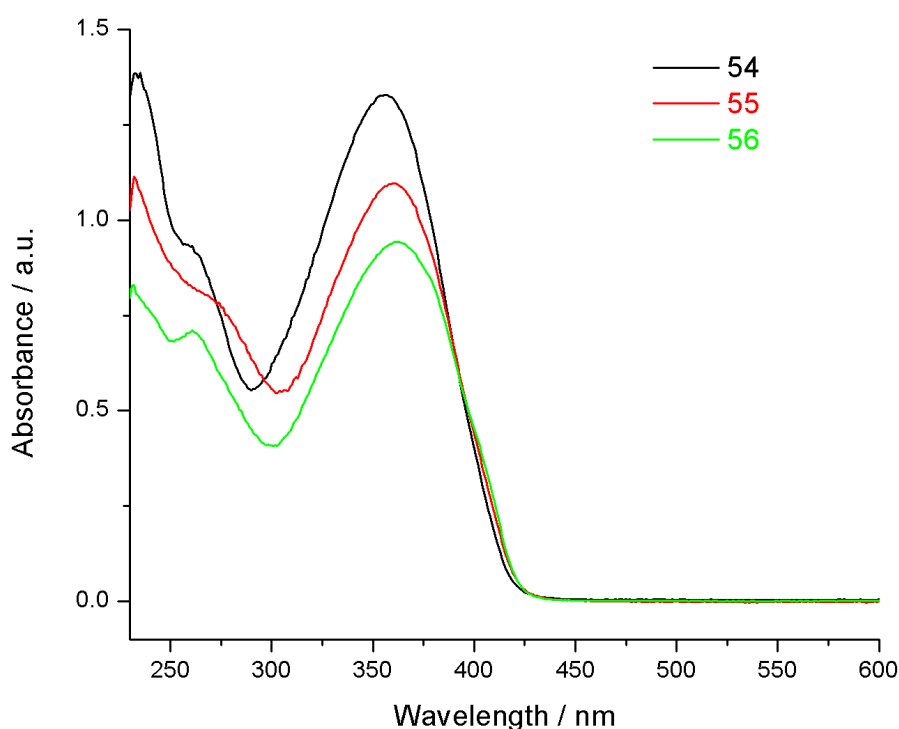


Figure 2.3 Solution state electronic absorption spectra for monomers **54**, **55** and **56**.

The electrochemistry of the monomers was studied by cyclic voltammetry. The oxidation and reduction of the monomers are shown in Figure 2.4; the oxidation shows one reversible and one irreversible wave in all three cases. The first wave is a two-electron loss, which results in a dication with the second wave a one-electron oxidation. In comparison with TTF, monomer **54** does not show the famous two-reversible oxidation to the radical cation then dication. Instead the results suggest that the electrons are removed from the terthiophenes and the TTN unit simultaneously. Despite the similarity between the structures, the potentials at which oxidation occurs varies between the monomers (Table 2.1). Monomers **54** and **56** have reversible first oxidations at $E_{1/2}^{1ox} = +0.68$ V and $+0.64$ V, respectively, whereas monomer **55** has a higher first oxidation wave ($E_{1/2}^{1ox} = +0.71$ V). The differences are accounted for by the different side group structures. Monomer **54** has a lower potential compared with monomer **55** because there are two additional π electrons and oxidation tends towards a charged aromatic intermediate within two dithiin rings. The lowering of the oxidation of **56** is somewhat unexpected but can possibly be explained, as the alkyl sulfyl groups are open and able to twist allowing the π -orbitals of the open alkyl sulfyl groups to align with the π -orbitals of the dithiin ring creating an inductive effect, thus lowering the oxidation potential. Similarly, the potential for the second oxidation waves is higher for **55** (+1.12 V) compared with that for **54** (+0.99 V) and **56** (+0.98 V).

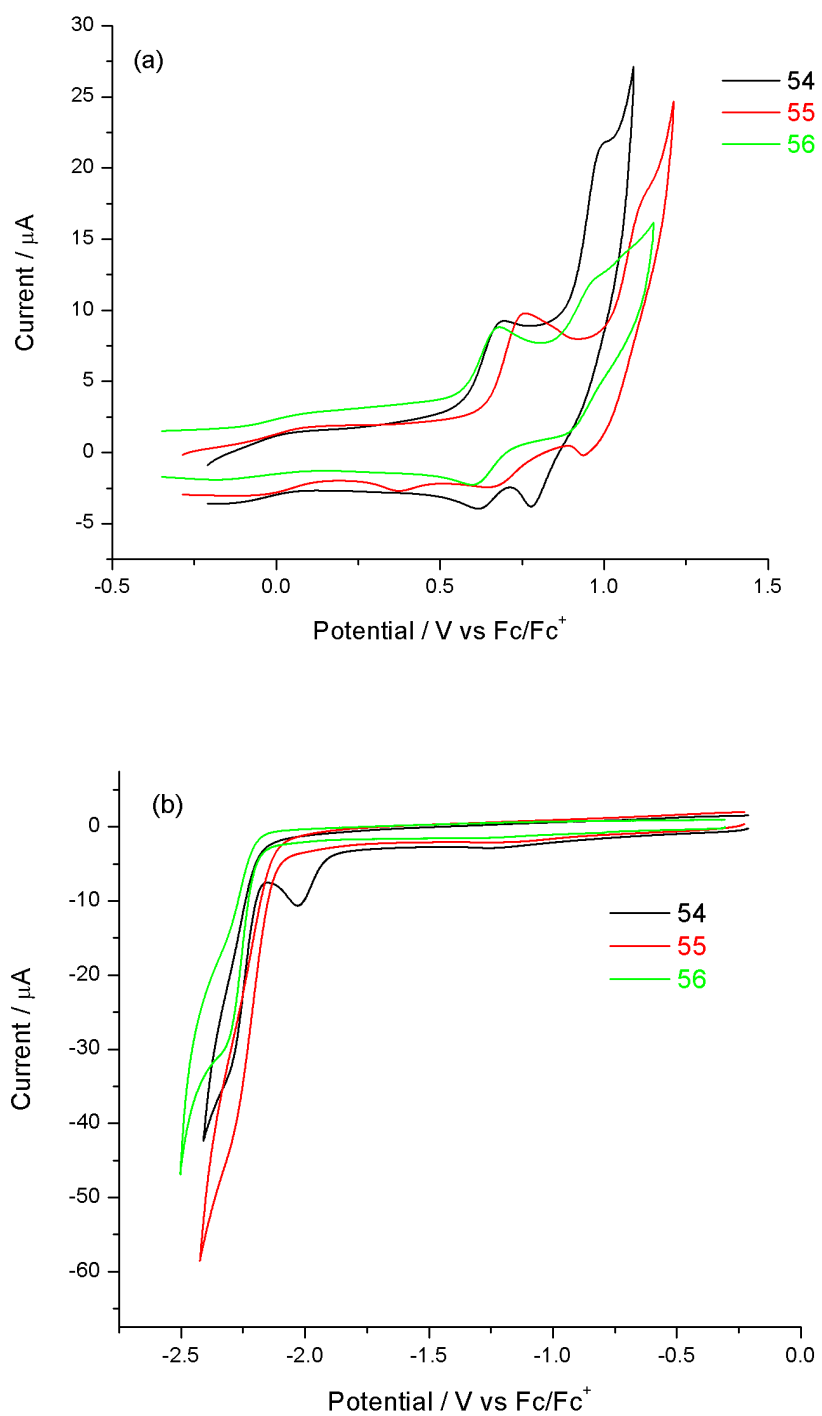


Figure 2.4 Cyclic voltammograms of (a) oxidation and (b) reduction of **54**, **55** and **56**

Irreversible reduction of the monomers (Figure 2.4 (b)) occurs at -2.28, -2.27 and -2.30 V for **54**, **55** and **56** respectively. However, compound **54** shows an additional reduction peak (-2.03 V) that corresponds to the irreversible reduction of the TTN group.

The electrochemical HOMO-LUMO gaps of the monomers were calculated from the difference in the onsets of the first oxidation and reduction peaks. Using data referenced to the ferrocene / ferrocenium redox couple, HOMO and LUMO levels were calculated by subtracting the onsets from the HOMO of ferrocene, which has a known value of -4.8 eV. A summary of these data can be seen in Table 2.1.

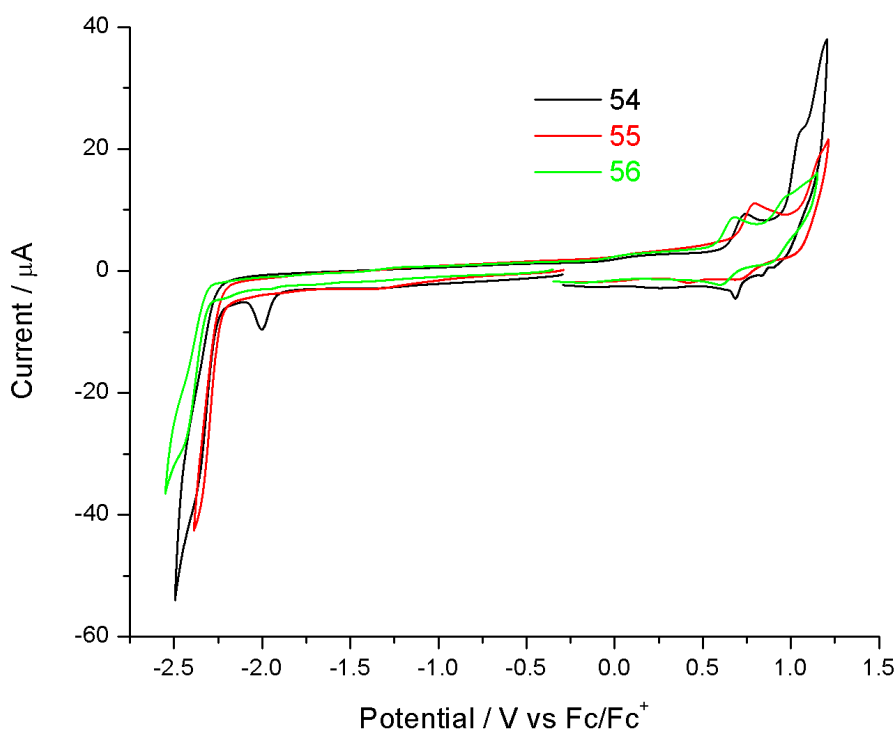


Figure 2.5 Cyclic Voltammograms of **54**, **55** and **56** for energy level determination.

The HOMO-LUMO gaps are similar for **55** and **56**, with **54** being smaller due to the extra reduction peak at lower potential. An interesting comparison is the electrochemical HOMO-LUMO gap with the value determined from absorption spectroscopy. For monomers **55** and **56**, the experimental gaps for both techniques are very similar, but for **54**, there is a significant difference between optical (2.99 eV) and electrochemical (2.56 eV), suggesting that the TTN group shows some reductive electro-activity that is independent of the terthiophene chain.

Table 2.1 Electrochemical and absorption spectroscopy data for compounds **54**, **55** and **56**.

| Monomer | E^{1ox} / V | E^{2ox} / V | E^{1red} / V | E^{2red} / V | HOMO / eV ^a | LUMO / eV ^a | E_g / eV^b |
|-----------|---------------|--------------------|--------------------|--------------------|------------------------|------------------------|--------------|
| 54 | +0.69/+0.66 | +0.99 ⁱ | -2.03 ⁱ | -2.28 ⁱ | -5.44 | -2.88 | 2.56 |
| 55 | +0.75/+0.66 | +1.12 ⁱ | -2.27 ⁱ | - | -5.49 | -2.56 | 2.93 |
| 56 | +0.68/+0.60 | +0.98 ⁱ | -2.30 ⁱ | - | -5.38 | -2.49 | 2.89 |

^aHOMO and LUMO values are calculated from the onset of the first peak of the corresponding redox wave and referenced to ferrocene, which has a HOMO of -4.8 eV. ^b E_g is the HOMO-LUMO energy gap. ⁱIrreversible peak.

2.5 X-ray Crystallography and Molecular Modelling.

The structure of the TTN derivative (**54**) was determined by single-crystal X-ray diffraction studies using synchrotron radiation. The asymmetric unit consists of two molecules, differing slightly in geometry (conformers A and B, Figure 2.6). Of particular note is the fact that the three C-C bonds within the dithiin units of conformer A are 0.03 to 0.08 Å shorter than the corresponding bonds in conformer B. Although these differences are individually marginal (with standard uncertainties of ~0.02 Å), there is a systematic pattern: comparing analogous C-S bonds between

the two conformers reveals that almost all of these bonds are longer in A than in B. (The difference ranges from -0.003 to 0.042 Å). Therefore, conformer B appears to have a more delocalised π -electron distribution. A least-squares fit of the three fused rings of conformers A and B shows a root-mean square difference of 0.048 Å, with only small differences in the orientations of the terminal thiophene rings relative to this central core.

In general, dithiin rings adopt boat conformations.¹⁶⁰ The degree of bending in the dithiin rings can be expressed as a folding along the S...S vectors within each ring. The differences between the corresponding folding angles in each conformer of compound **54** are small; the outer dithiin rings have angles of 47.5(4) (S6...S7) and 46.0(5)° (S13...S14), whereas the inner rings have values of 52.1(4) (S4...S5) and 53.7(4)° (S11...S12). The terthiophene units possess a high degree of coplanarity between adjacent thiophene units, with torsion angles of 179.3(9) (S1-C4-C5-S2), 178.5(9) (S2-C8-C9-S3), 176.0(9) (S8-C20-C21-S9), and 179.9(9)° (S9-C24-C25-S10).

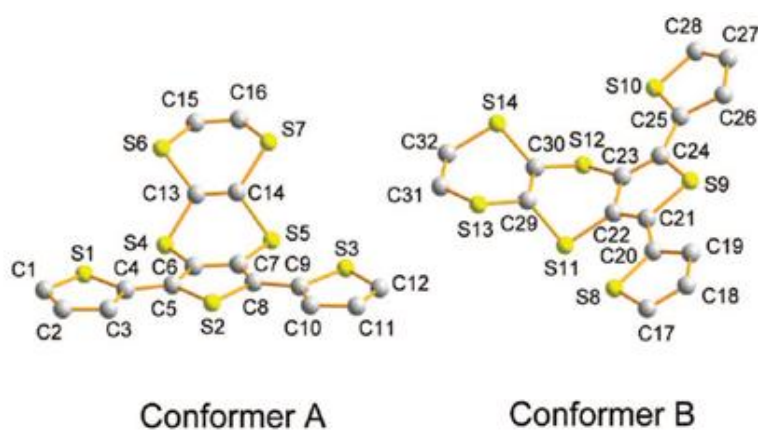


Figure 2.6 Molecular structures of compound **54** showing the crystallographic asymmetric unit that consists of two conformers

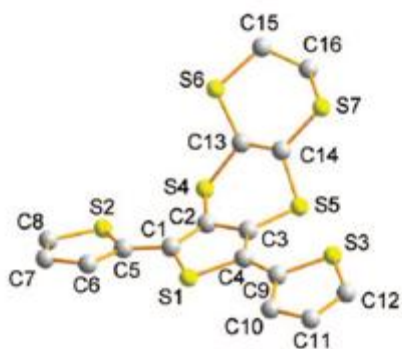


Figure 2.7 Molecular structure of compound **55**. Hydrogen atoms are omitted for clarity

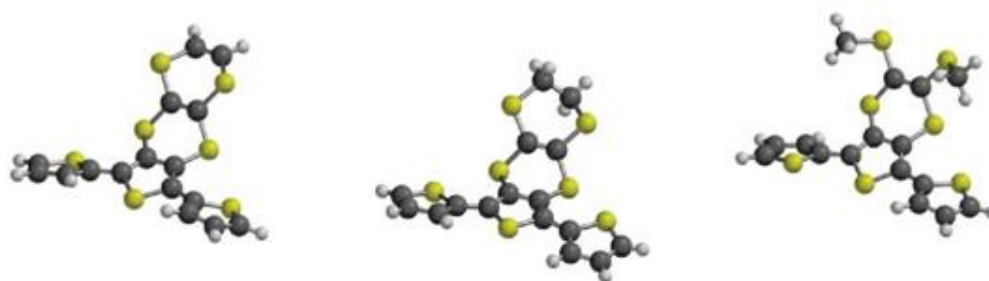


Figure 2.8 Geometry-optimized structures of compounds **54**, **55** and **56** (left to right, respectively). Calculations were performed at the B3LYP/6-31G* level, starting from the observed crystal structures of compounds **54** (for **54** and **56**) and **55**.

In previous studies on 3,4-dithio-substituted terthiophenes in our group,^{13, 43, 154, 167-169} we have found that high degrees of coplanarity within the conjugated chain are formed from an all-anti arrangement of the thiophene rings in which the sulfur atoms of the peripheral rings form close intramolecular S...S contacts with the 3,4-dithio substituents on the central ring. This is elegantly demonstrated in the structure of compound **54**, which has close S...S contacts at distances of 3.182(6) (S1...S4), 3.230(6) (S3...S5), 3.238(6) (S8...S11), and 3.184(7) Å (S10...S12). These values are much smaller than the sum of the van der Waals radii for two sulfur atoms (3.6

Å) and indicate weak bonding between the chalcogens. Finally, one intermolecular short contact exists between the two conformers (S7...S8, 3.506(7) Å,) (Figure 2.9) to link pairs of molecules, but there are no other short intermolecular interactions within the packing diagram.

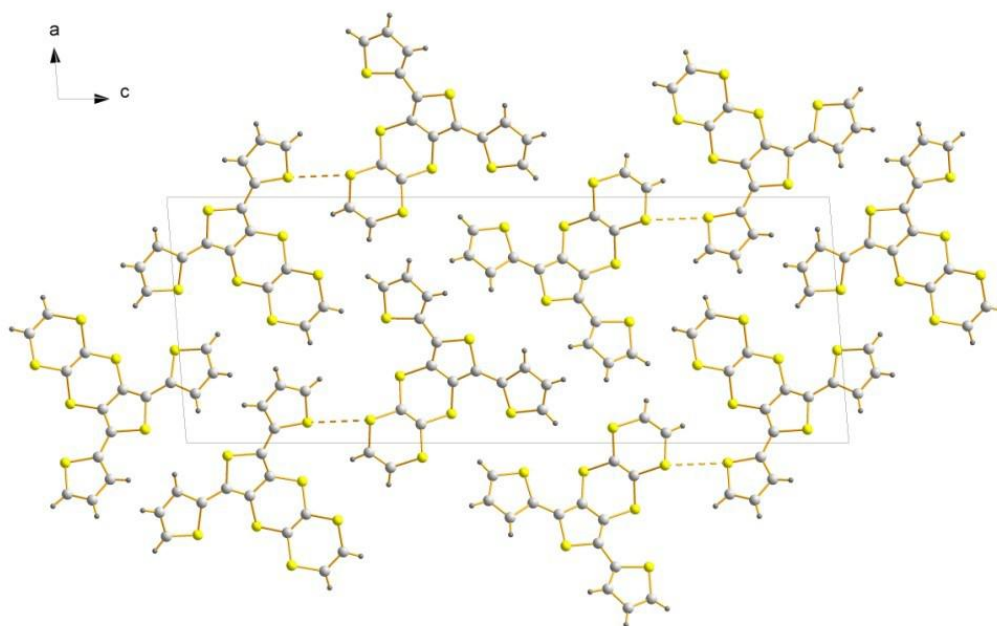


Figure 2.9 X-ray crystal packing diagram of compound 1 viewed along the b axis. Hydrogen atoms are omitted for clarity

In compound **55**, the folding vectors are significantly different between the two types of sulfur heterocycles. For the dithiin ring fused to the central thiophene, the value is similar to those in compound **54** ($51.6(1)^\circ$, S4...S5), whereas the fold in the dihydro-dithiin ring gives a tighter angle ($32.5(2)^\circ$, S6...S7). Again, the conformation within the terthiophene unit is all-anti. The torsion angles between the thiophenes are $168.0(3)^\circ$ (S1-C1-C5-S2) and 175.7° (S1-C4-C9-S3), and the S...S contacts

between peripheral thiophenes and the 3,4-dithio substituents on the central ring are 3.228(2) (S2...S4) and 3.183(2) Å (S3...S5). The molecules pack with no evidence of π - π stacking. However, weak intermolecular contacts between S3 and S5 atoms (3.575(2) Å) give rise to a remarkable packing motif, in which groups of six molecules are held together, almost in a spherical arrangement, to give clusters with a diameter of ca. 2.2 nm (Figure 2.10).

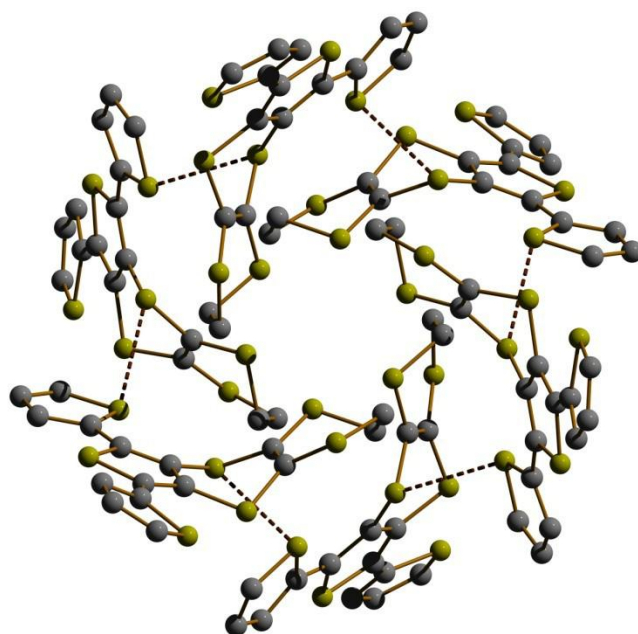


Figure 2.10 X-ray crystal packing diagram of compound **55**.

To assign the redox processes taking place within the series of terthiophenes, computational calculations were performed using density functional theory at the B3LYP/6-31G* level (Spartan '06). Compound **54** was considered from the initial geometry of its crystal structure (conformer A), as was the case for compound **55**. Calculations performed on terthiophene **56** were based on the crystal structure of **54** with SCH₃ groups substituting the vinylene bridge, followed by relaxation to an equilibrium geometry. In almost all cases, the thiophene units retain anti

conformations, apart from one peripheral thiophene in **56**. Compared with the crystal structures of compounds **54** and **55**, planarity is lost in the relaxed structures with torsion angles in the range *ca.* 20-35°. The calculations were performed for molecules in the gas phase, and it can be assumed that crystal packing forces will have a significant effect on the geometry of the molecule. The folding vectors observed in the dithiin rings of **54** and **55** are in the range 48.2-53.2°, whereas that of the dihydro-dithiin is 30.8°; these values are in good agreement with the crystal structure data. According to the HOMO and HOMO-1 plots of all three compounds (Figure 2.11, Figure 2.12 and Figure 2.13), the removal of the first electron from each molecule originates from different sites.

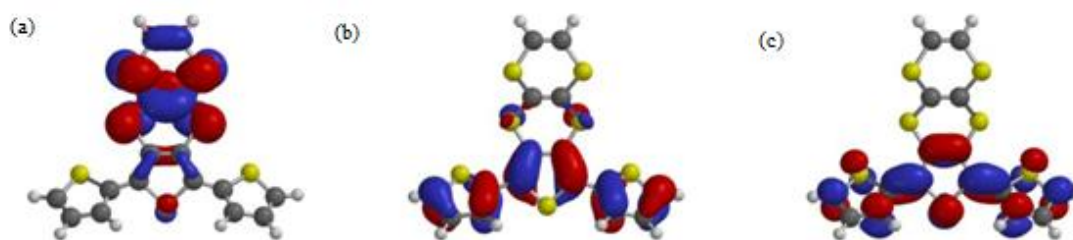


Figure 2.11 (a) HOMO, (b) HOMO-1 and (c) LUMO plots of compound **54**.

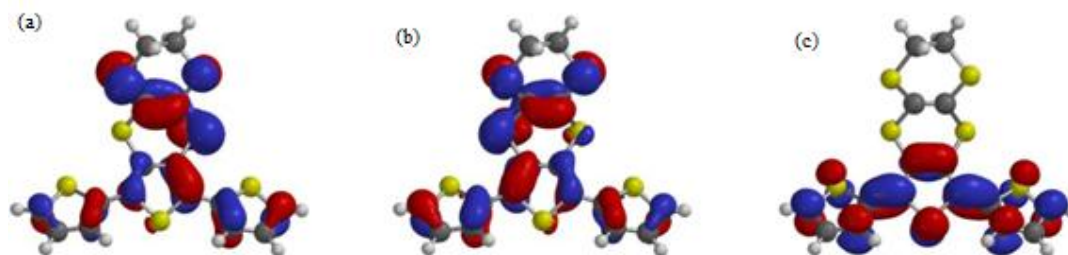


Figure 2.12 (a) HOMO, (b) HOMO-1 and (c) LUMO plots of compound **55**.



Figure 2.13 (a) HOMO, (b) HOMO-1 and (c) LUMO plots of compound **56**.

In compound **54**, the TTN unit is a better electron donor than the terthiophene fragment, and this is similar to the redox behaviour of a closely related TTF-terthiophene-fused analogue (*vide infra*).¹⁵⁴ In **55**, the outer vinylene unit is reduced to a saturated bridge between the corresponding sulfur atoms, and the result is that the electron-donating property of the dihydro-TTN is decreased to the extent that the HOMO is spread over both types of sulfur heterocycles (dithiin and thiophene). For compound **56**, the dithiin ring holds little electron density, and the HOMO is dominant over the terthiophene chain. From the CV data, we observe that the difference between the two oxidation processes is *ca.* 0.35 to 0.40 V. From the computational data, the HOMO and HOMO-1 orbitals are close-lying with differences in the range 0.1 to 0.2 eV. Although the latter cannot be compared directly to the CV data (because there are charges involved in the latter), the HOMO-1 give some indication for the sites of the second oxidation process, For compounds **55** and **56**, the first oxidation already involves the terthiophene unit, indicating that polymerisation can proceed from the cation radical species. Examination of the SOMO of the radical cation of **54** reveals that electron density is localised within the TTN unit (Figure 2.14). Removal of a second electron to give the triplet diradical results in the spin density residing within the terthiophene unit. From these

calculations, it is evident that the dication state must be reached to achieve polymerisation of **54**.

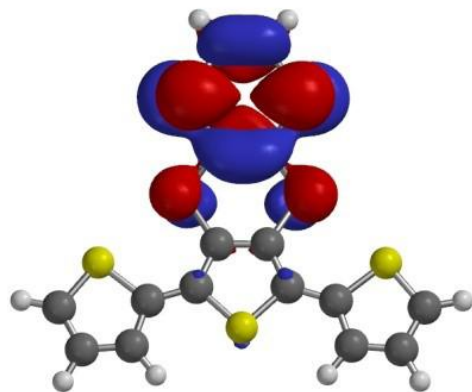
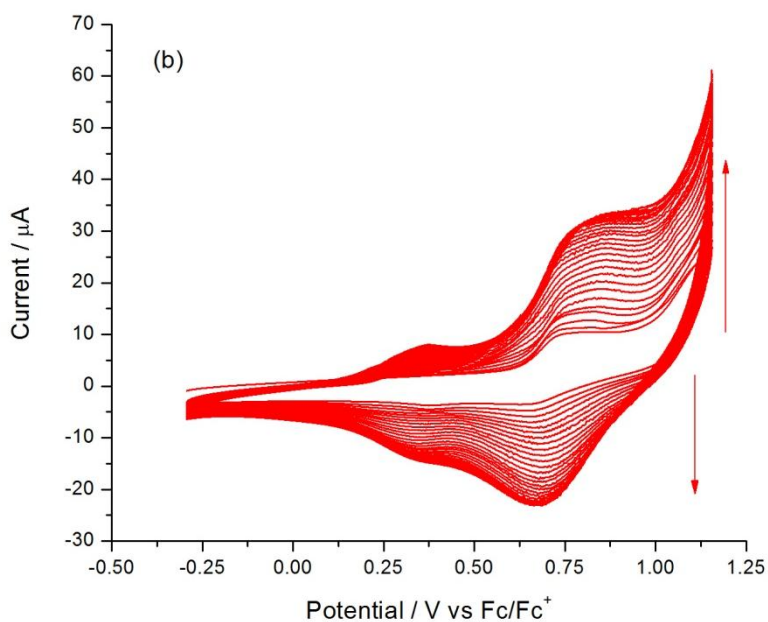
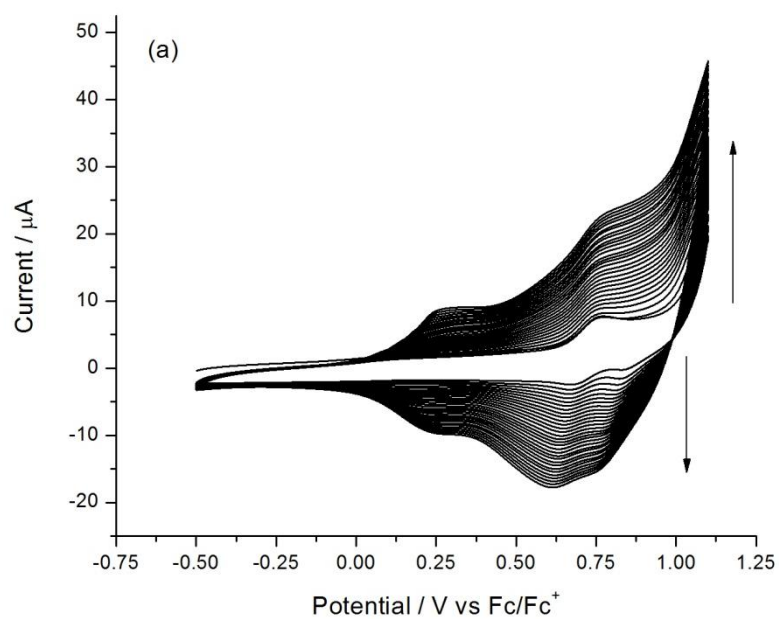


Figure 2.14 SOMO plot of **54** radical cation

2.6 Electrochemistry of the polymers.

The three monomers were polymerised electrochemically by repetitive cycling over both redox-active peaks. All the monomers polymerised readily, and the growth traces for the corresponding polymers are shown in Figure 2.15.



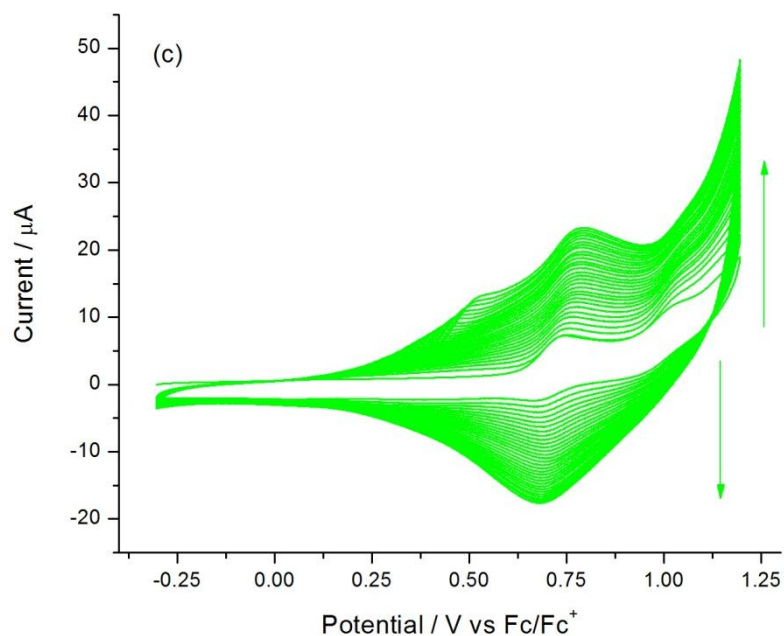
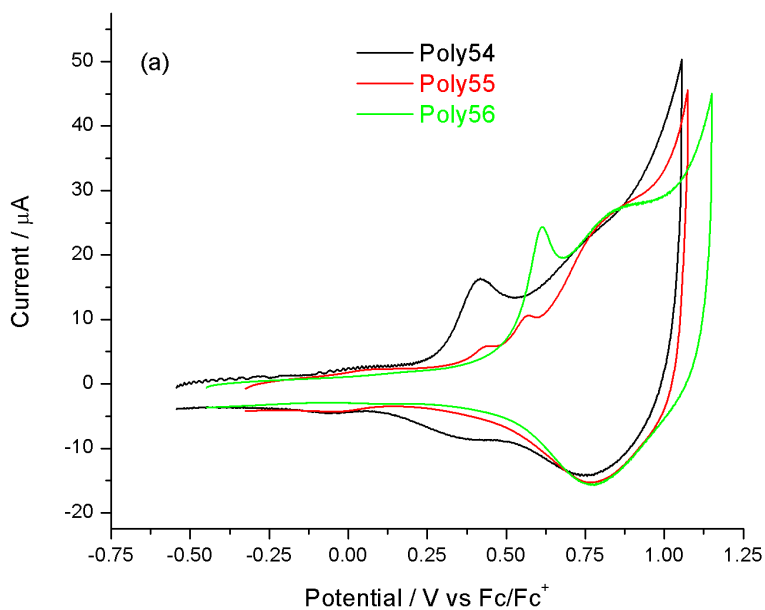


Figure 2.15 Electrochemical growth of (a) poly54, (b) poly55 and (c) poly56

The electrochemistry of the three polymers was investigated in monomer-free acetonitrile with the same concentration of supporting electrolyte as before; the cyclic voltammograms of poly54, poly55 and poly56 are shown in Figure 2.16.



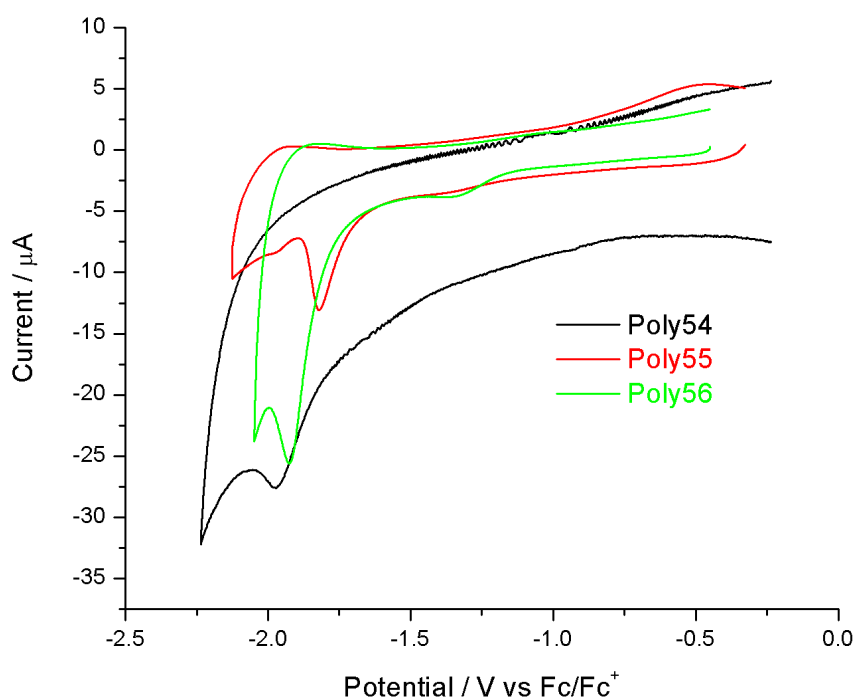


Figure 2.16 Cyclic voltammograms for (a) oxidation and (b) reduction of poly**54**, poly**55** and poly**56**.

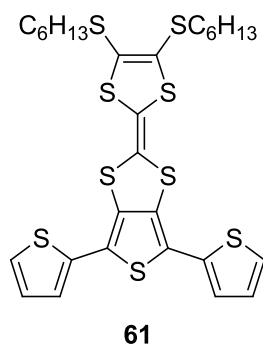
The oxidation of the three polymers is shown in Figure 2.16 (a); in each case the polymers feature a quasi-reversible oxidation wave followed by a large, broad reversible wave. It is unlikely that the first wave represents a localised oxidation of the dithiin side group because this is a fresh peak that emerges with polymer growth. The potentials at which the first oxidation is observed differ with each polymer, with poly**54** considerably lower than its analogues (+0.42 V compared with poly**55** at +0.56 V and poly**56** at +0.60 V). The difference in this behaviour can be attributed to two factors: (i) the electronic contribution of the side group and (ii) the morphology of the polymer films and the subsequent interchain interactions. The second oxidation potentials are similar ($E_{1/2}^{2ox}$ for poly**54**, poly**55** and poly**56** is +0.77, +0.80, and +0.80 V, respectively).

In view of these results, it can be envisaged that the removal of the first electrons from the polymers involves the dithiino-thiophene heterocycle, whereas the second wave arises from the oxidation of the bithiophene units in the polymer chain. This assumption is corroborated by UV-vis spectroelectrochemical measurements (see section 2.7) because the emergence of main-chain polarons is observed only after reaching the second oxidation wave. Furthermore, the quasi-reversible nature of the first oxidation wave could be due to persistent, stabilised conformers generated within the dithiin rings upon removal of an electron. This phenomenon has been demonstrated in a related derivative, in which the dithiin ring becomes stabilised by reaching an aromatic state upon oxidation.¹⁵⁸

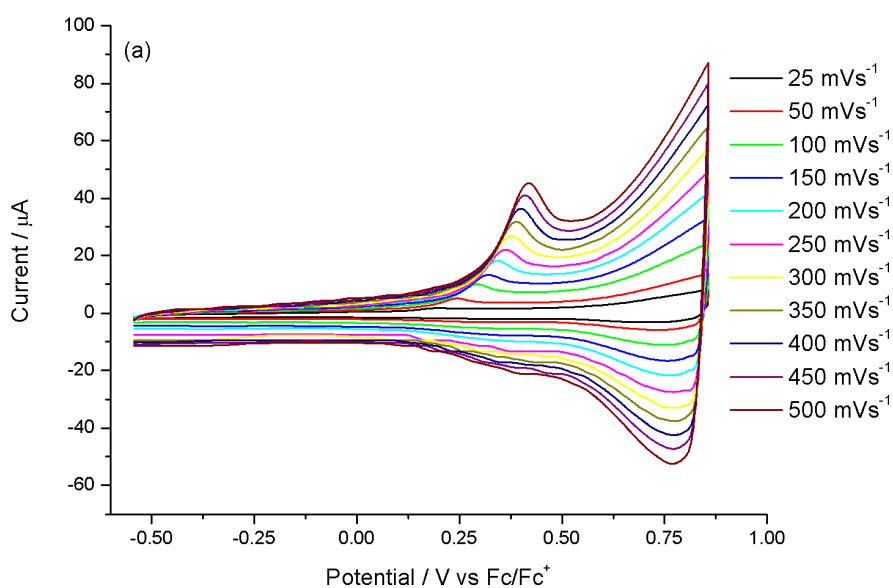
The reduction of the polymers is shown in Figure 2.16 (b); the irreversible reduction of poly**54** occurs at the most negative potential (-1.97 V), compared with the irreversible reductions of poly**55** (-1.82 V) and poly**56** (-1.93 V). Following the computational calculations for the terthiophene monomers, the electrons are added to the polythiophene chain, and the drop in potential (compared to the monomers) is due to the increased ability of the polymers to stabilise a negative polaron. For poly**54**, the small peak that is observed in the monomer would be hidden by the large peak at -1.97 V, so it is impossible to say if this additional reduction process exists in the polymer.

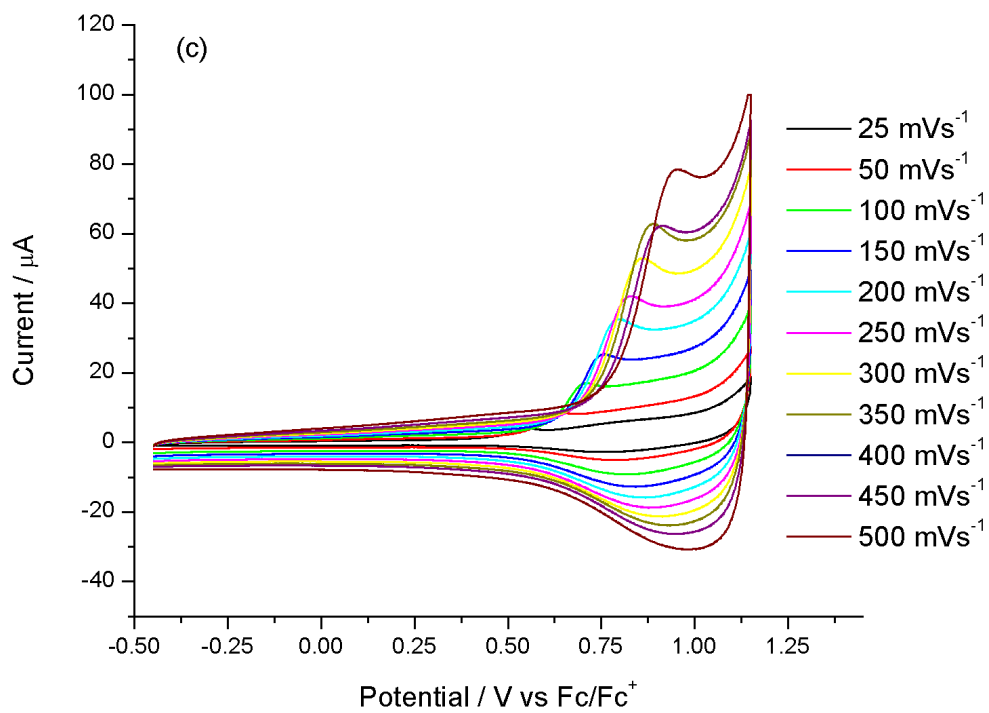
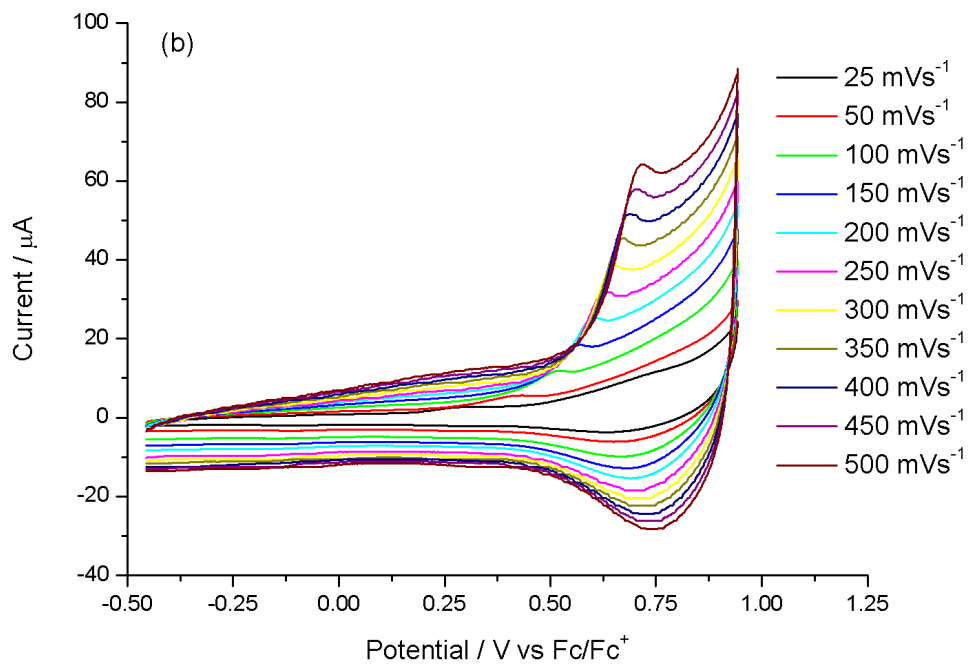
An interesting analogy is the comparison of fused TTN-thiophene with fused TTF-thiophene, by comparing **54** and poly**54** with compound **61** and its polymer, the latter of which had to be prepared from a chemical coupling route because **61** could not be electrochemically polymerised.¹⁵⁴ **61** gives two reversible oxidation waves, $E_{1/2}^{1ox} = +0.24$ and $E_{1/2}^{2ox} = +0.62$ V vs. Fc/Fc⁺. The decrease compared to **54** in the oxidation potentials is because TTF is a better electron donor than TTN. For poly**61**,

the oxidation potentials are $E_{1/2}^{1ox} = +0.29$ and $E_{1/2}^{2ox} = +0.67$ V, which are actually higher than the monomer but still lower than poly**54** (by *ca.* 0.1 V). The electrochemistry of poly**61** is complex; the first oxidation can be assigned to the TTF unit with the second to both TTF and the polythiophene chain.



For each polymer, the relationship between scan rate and peak current was investigated. (Figure 2.17 (a) to (c)). A plot of scan rate versus current maximum gave a linear fit (Figure 2.17 (d)) giving R^2 values of 0.9991, 0.999, and 0.9879 for poly**54**, poly**55** and poly**56**, respectively. This confirms that charge transport through the polymer film is not diffusion limited.¹⁷⁰





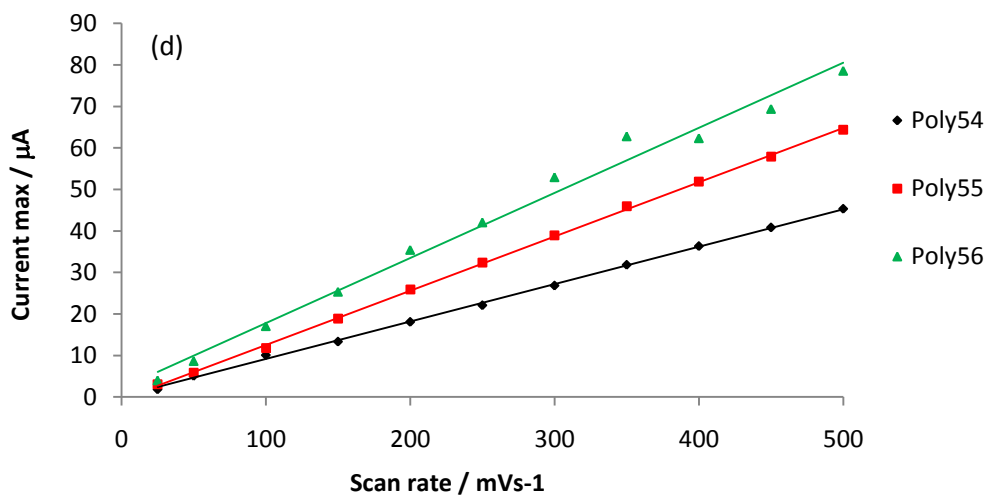


Figure 2.17 Cyclic voltammograms of (a) poly54, (b) poly55 and (c) poly56 with varying scan rates. (d) Plot of current versus scan rate for polymers.

The electrochemical band gaps of all three polymers was determined from the difference of the onset of the first oxidation and reduction processes, which represent the HOMO and LUMO levels respectively (Figure 2.18). To calculate the energy levels of these bands, the onsets were once again subtracted from the HOMO of ferrocene (-4.8 eV). A summary of these data can be seen in Table 2.2.

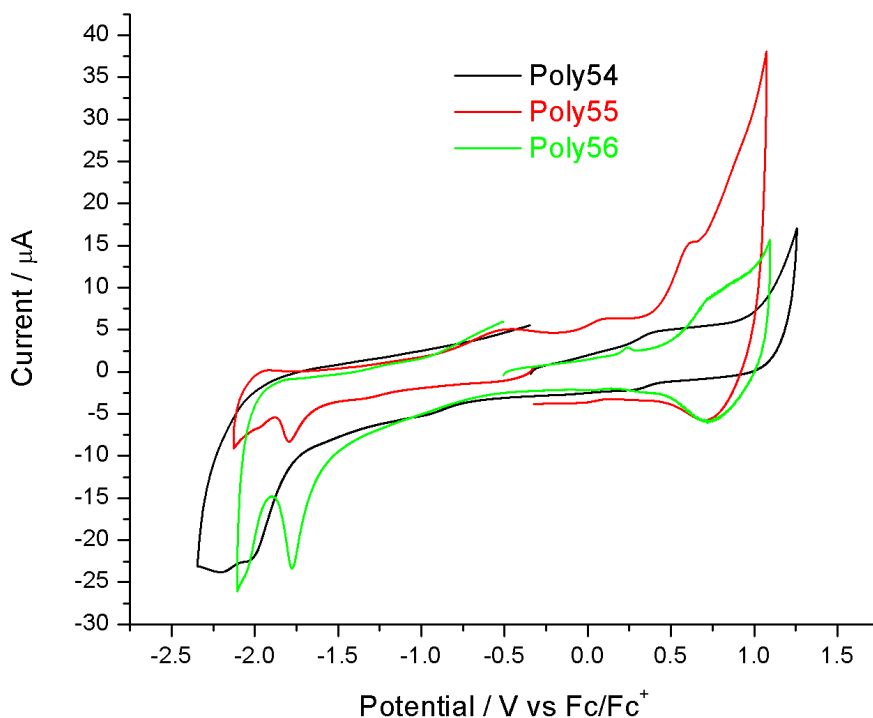


Figure 2.18 Cyclic voltammograms of Poly54, Poly55 and Poly56 for energy level determination.

The three polymers possess similar band gaps ranging from 2.04 to 2.11 eV, which are similar to the optical band gap calculated for the polymers and that of polythiophene itself.^{11, 171} The optical band gap was calculated from the edge of the maximum absorption band of the three polymers measured from films grown on indium tin oxide (ITO) coated glass (Figure 2.19). The values calculated are 1.98, 1.98, and 2.00 eV for poly54, poly55 and poly56, respectively.

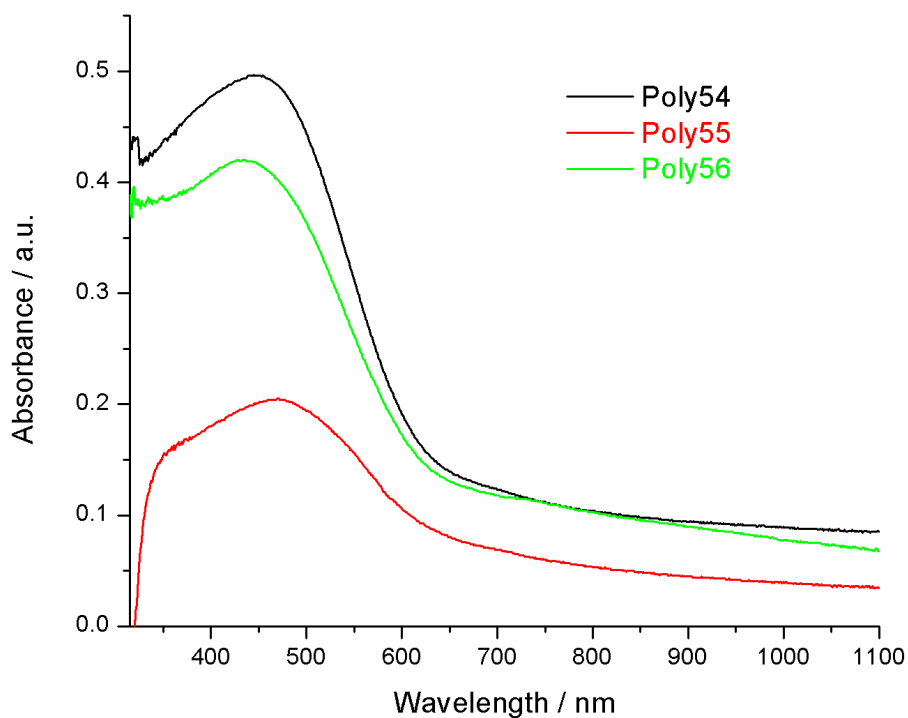


Figure 2.19 Electronic absorption spectra of poly**54**, poly**55** and poly**56**. Spectra were recorded on thin films deposited on ITO glass.

Table 2.2 Electrochemical and absorption spectroscopy data for thin films of poly**54**, poly**55** and poly**56**. Experimental conditions are the same as those given in Figures 2.6 and 2.7.

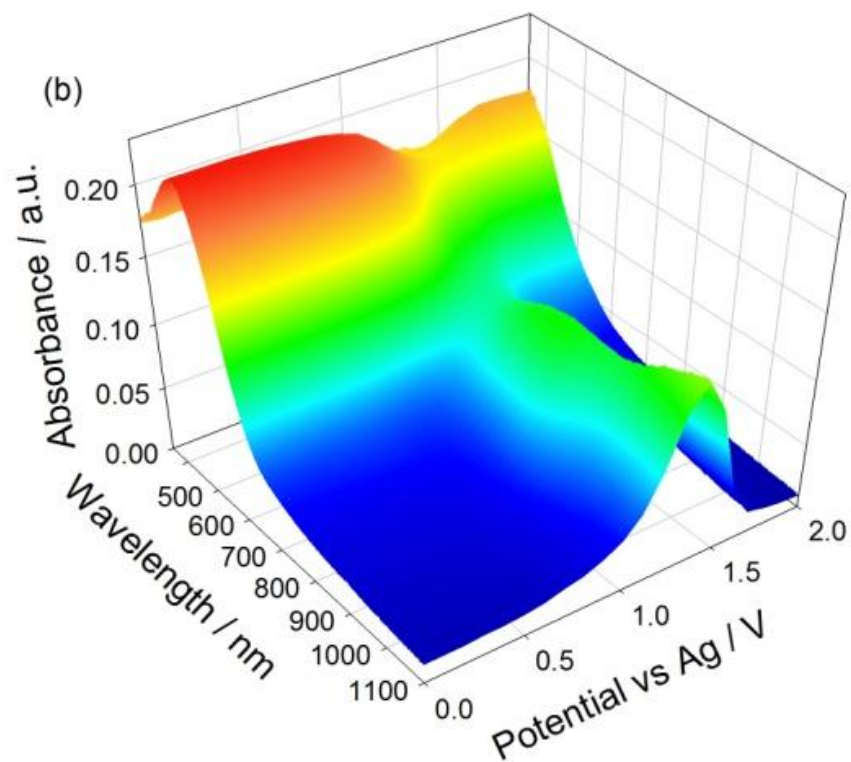
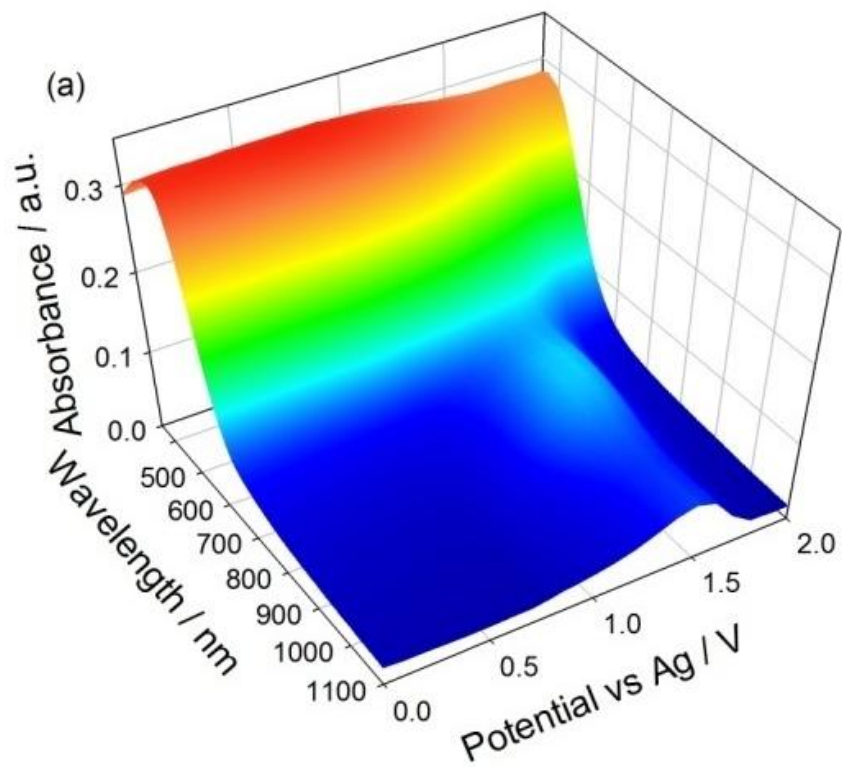
| | E^{1ox}/V | E^{2ox}/V | E^{1red}/V | HOMO/ eV | LUMO/ eV | E_g/ eV | λ_{max}/ nm |
|----------------|-------------|---------------|--------------|----------|----------|-----------|---------------------|
| Poly 54 | +0.42 | +0.78 / +0.75 | -1.97 | -5.05 | -3.01 | 2.04 | 436 |
| Poly 55 | +0.56 | +0.82 / +0.77 | -1.82 | -5.21 | -3.14 | 2.07 | 471 |
| Poly 56 | +0.60 | +0.83 / +0.77 | -1.93 | -5.30 | -3.19 | 2.11 | 450 |

^aHOMO and LUMO values are calculated from the onset of the first peak of the corresponding redox wave and referenced to ferrocene, which has a HOMO of -4.8 eV. ^b E_g is the HOMO-LUMO energy gap. ⁱIrreversible peak.

2.7 UV-vis Spectroelectrochemistry

UV-vis spectroelectrochemical measurements were performed on films grown on ITO glass and then dedoped. The spectroelectrochemical plots of oxidation of poly**54**, poly**55** and poly**56** (Figure 2.20 (a), (b) and (c), respectively) all show similar p-doping. There are no changes in the absorption spectra over the first oxidation peak, suggesting that the first electrons removed are not from the π -conjugated chain. New absorption waves form at +0.9 V in the wavelength region 600 – 800 nm and *ca.* 900 nm, attributed to the formation of polarons. Increasing oxidation leads to a disruption of the polymer π -conjugated chain and hence a decrease in the π - π^* transition. For poly**54**, there is very little decrease in the π - π^* transition band (5% change compared with 17 and 8% change for poly**55** and poly**56**), suggesting that oxidation involves the TTN side group instead of the polythiophene chain. This tends toward the effect seen with TTF attached to polythiophene in which the electroactivity is dominated by the TTF unit, however, TTF spectroelectrochemistry also shows a band at 390 nm which is not seen with p-doping of poly**54**.^{154, 172}

Reduction spectroelectrochemistry measurements were performed for all three polymers, but the only film that showed any significant change was poly**56** (Figure 2.20 (d)), which gave a slight broadening of the absorbance in the range of -0.8 to -1.2 V accompanied by a decrease in the π - π^* transition after -1.0 V. These effects can be attributed to the n-doping of the polythiophene chain.



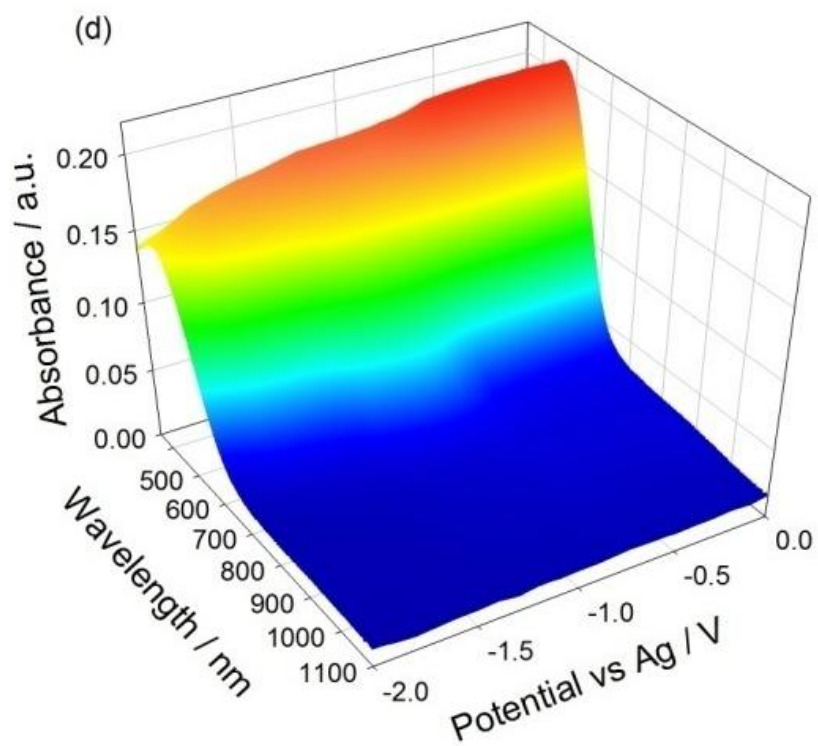
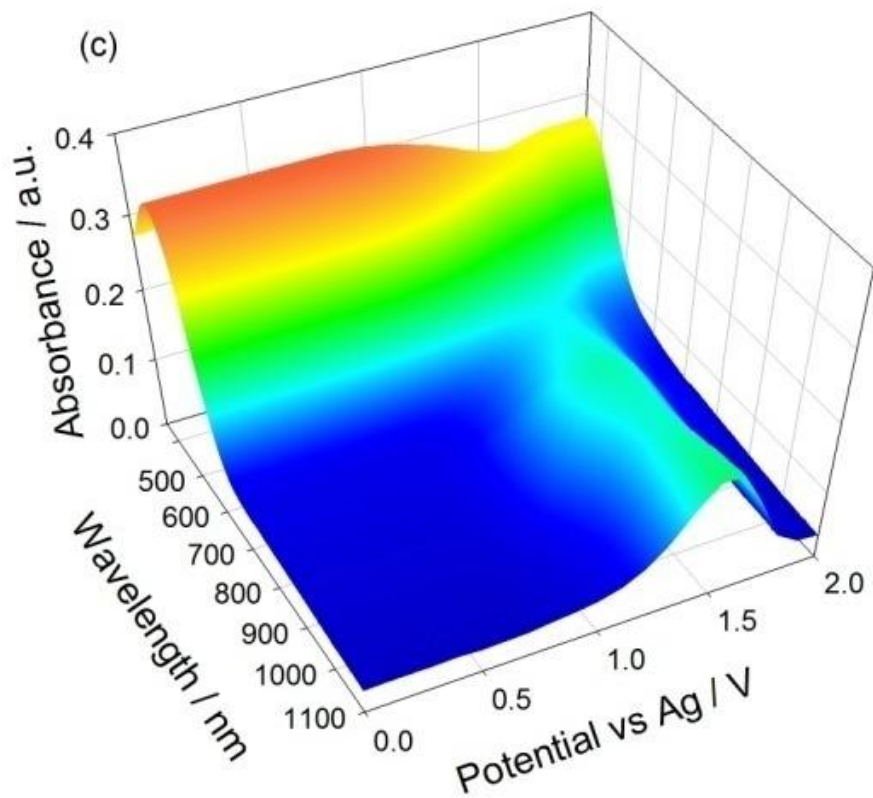
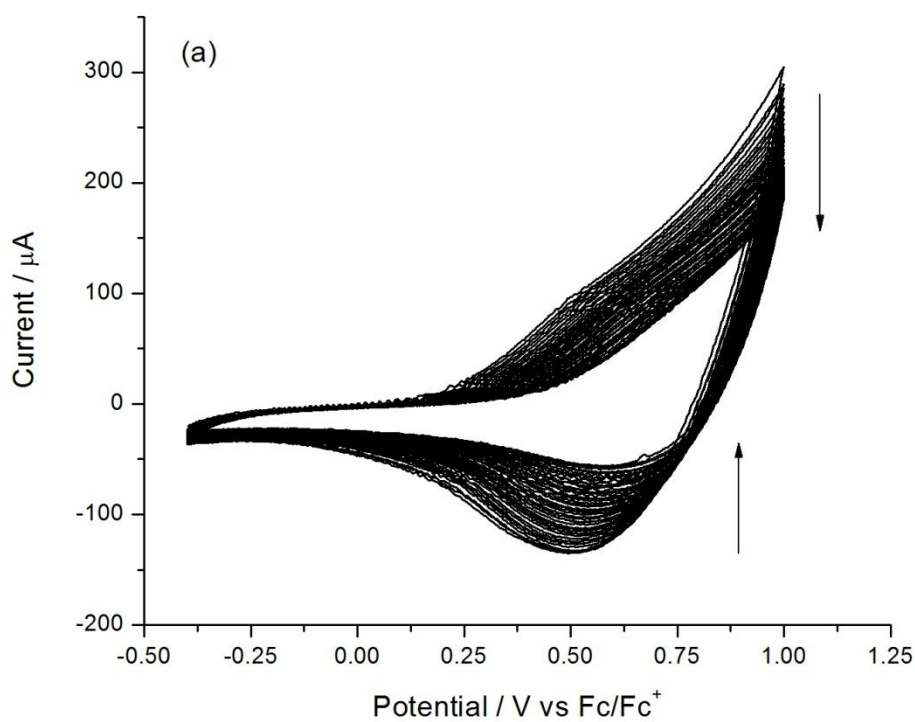


Figure 2.20 Absorption spectroelectrochemical plots of oxidation of (a) poly54, (b) poly55, (c) poly56 and reduction of (d) poly56. Potentials are given vs. Ag wire pseudo-reference electrode.

2.8 Polymer Stability

The stability of the three polymers was measured on ITO glass in monomer-free solution (Figure 2.21) by subjecting the materials to repetitive oxidation cycles. It can be seen that poly55 is the most stable toward p-doping with a decrease of only 17% in current response compared to a 49% decrease for poly54 and a 64% decrease for poly56.



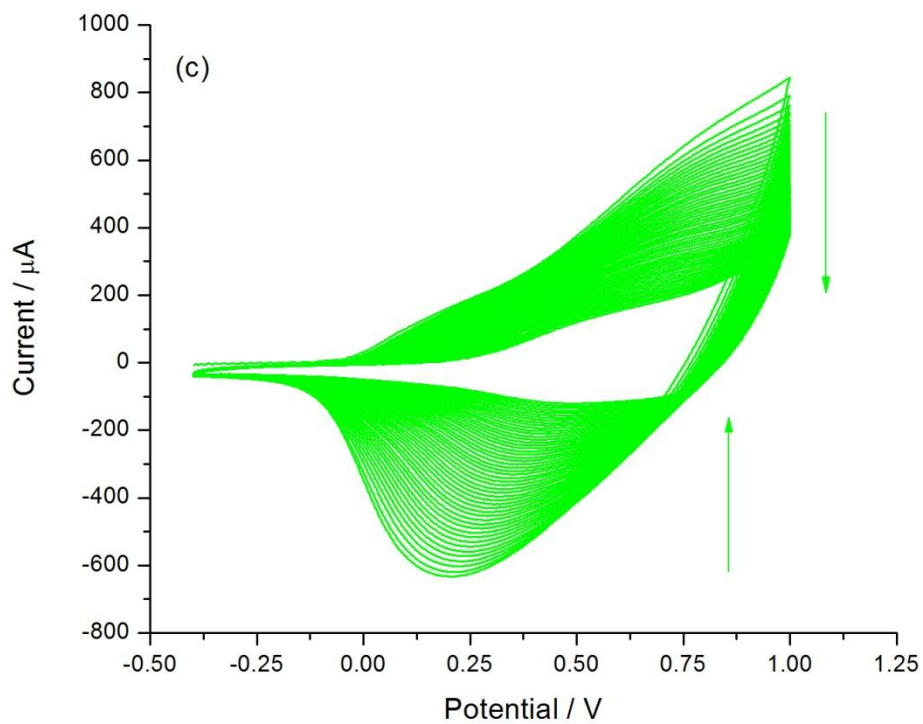
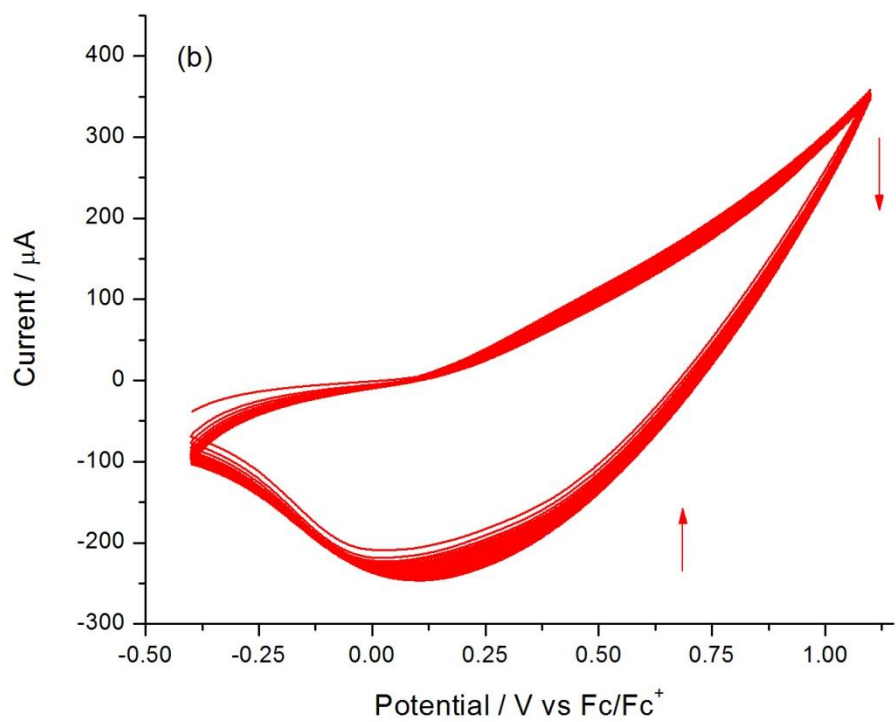
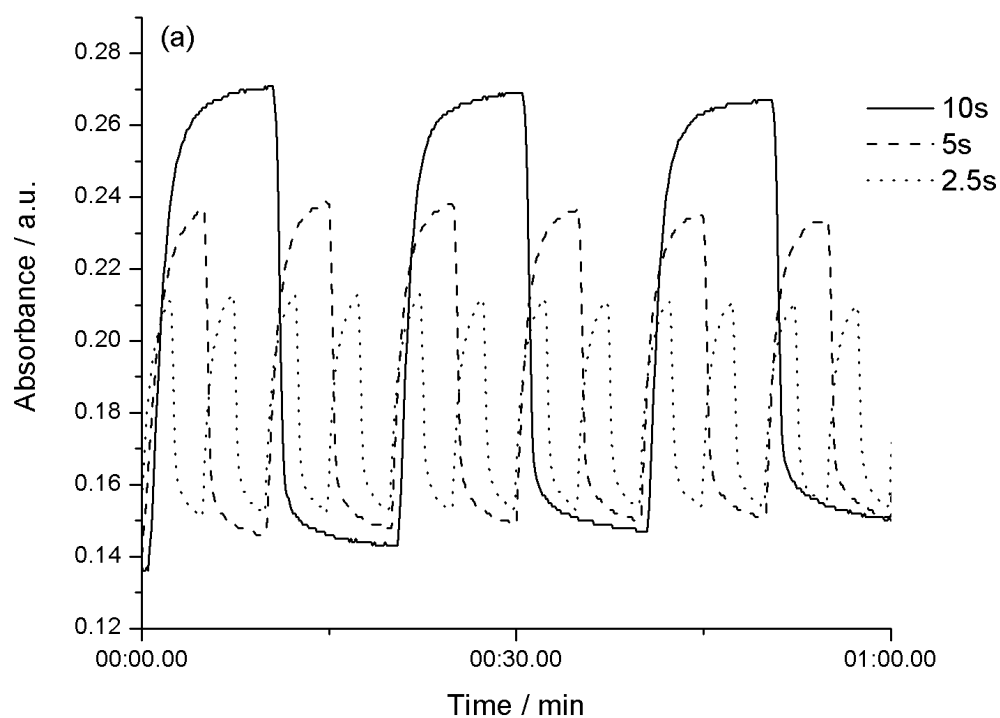
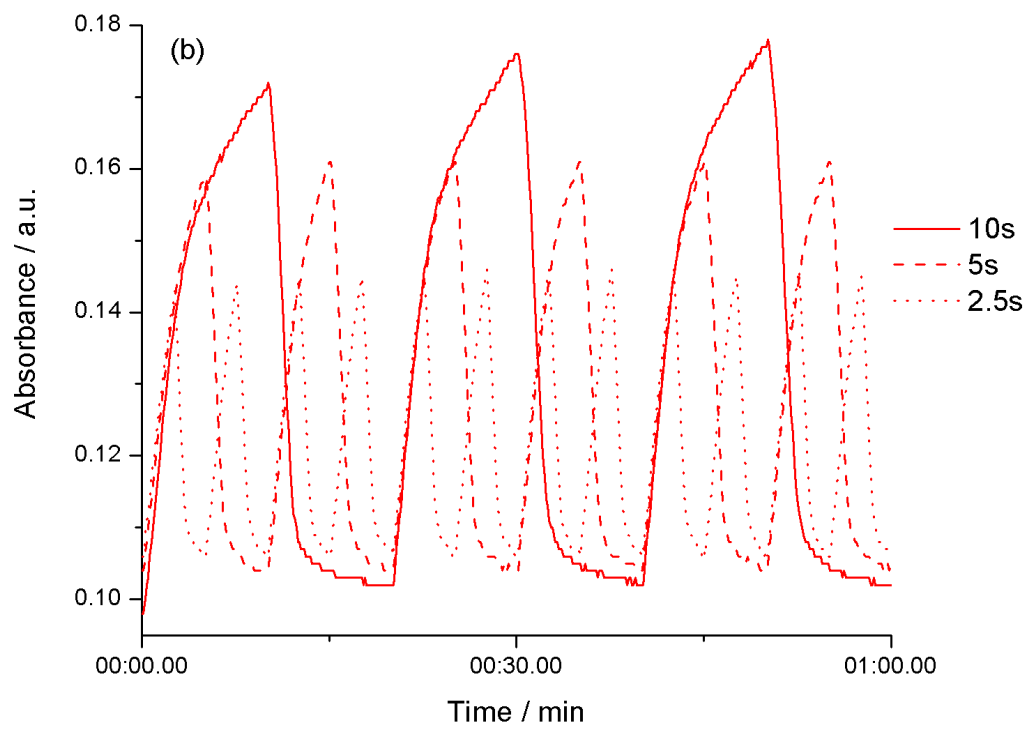
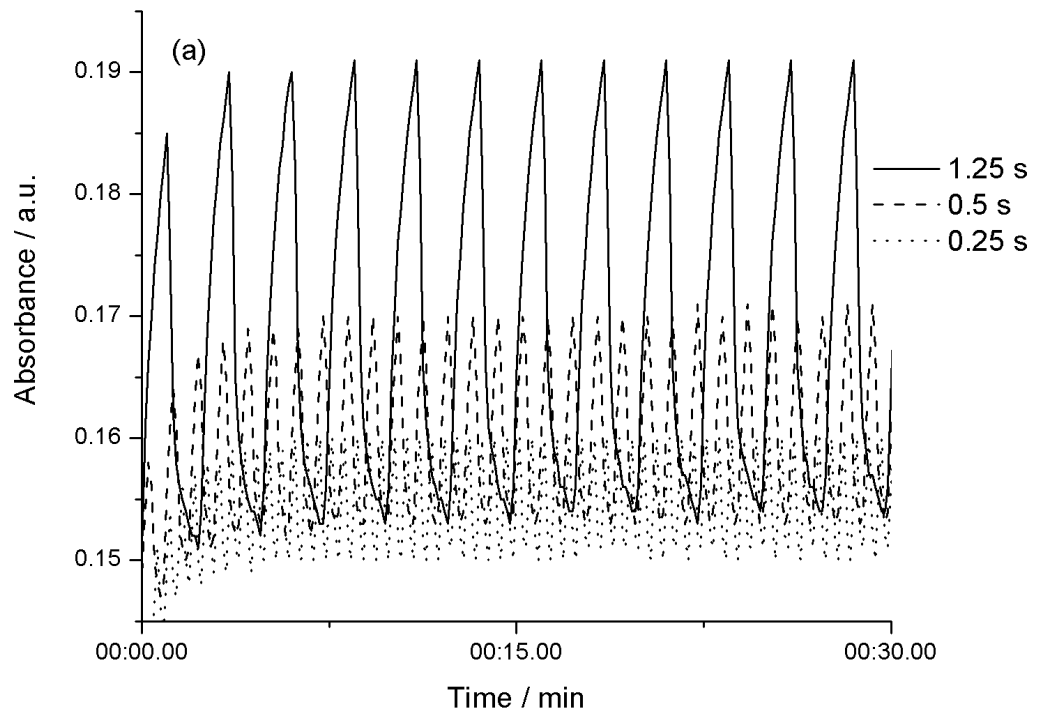


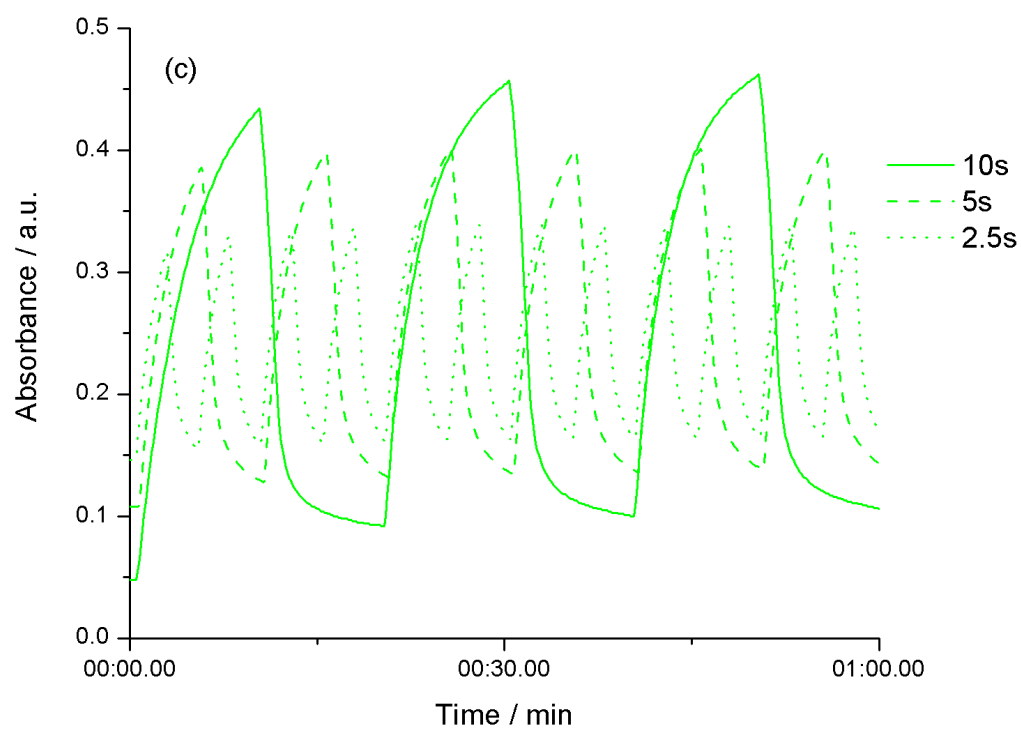
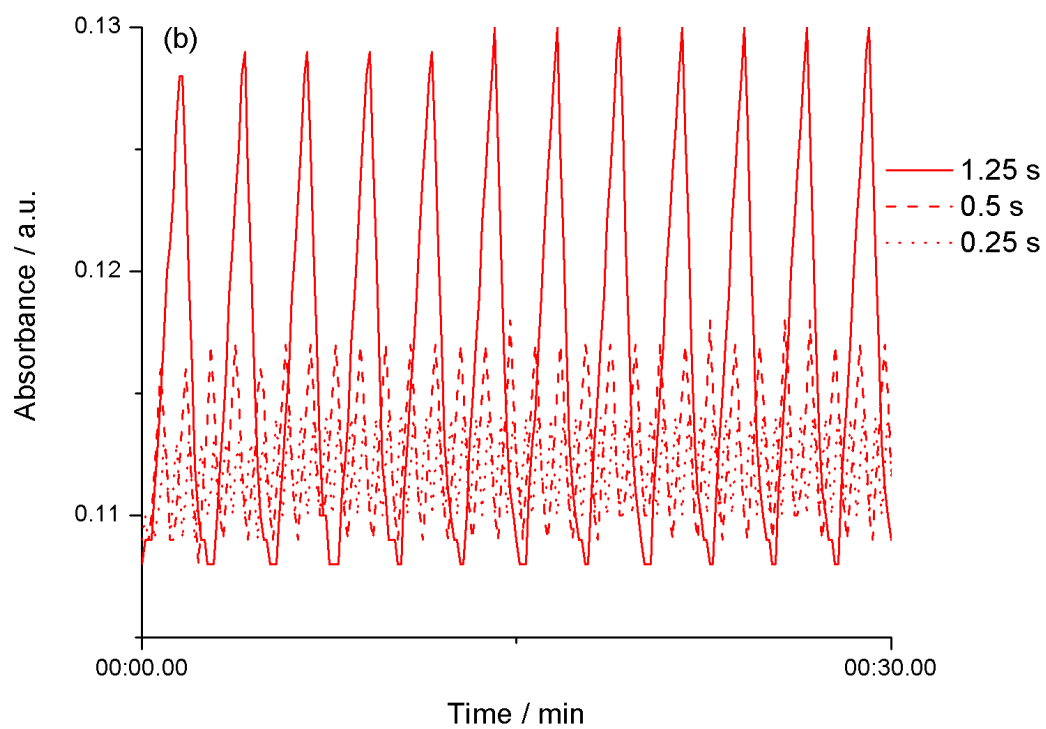
Figure 2.21 Stability of polymers (a) poly54, (b) poly55 and (c) poly56 on ITO in monomer-free solution.

2.9 Polymer Switching

The switching ability of all three polymers was performed by monitoring the absorbance of each polymer between two different potentials that will change the state from neutral to p-doped. The polymers were grown afresh on ITO and dedoped. The potential was switched between -0.4 and 1.5 V, and the absorbance was measured at 755 nm, which provided the greatest change in absorbance. The switching times measured were 10, 5, 2.5, 1.25, 0.5, and 0.25 s. The changes in absorbance can be seen in Figure 2.22 and are summarised in Table 2.3. Comparison of the percentage change in absorbance for the three polymers shows that poly**56** gives the greatest change; this is not unexpected as more open polymers give faster switching times because a less-packed morphology allows an efficient flow of counterions into and out of the polymer film.







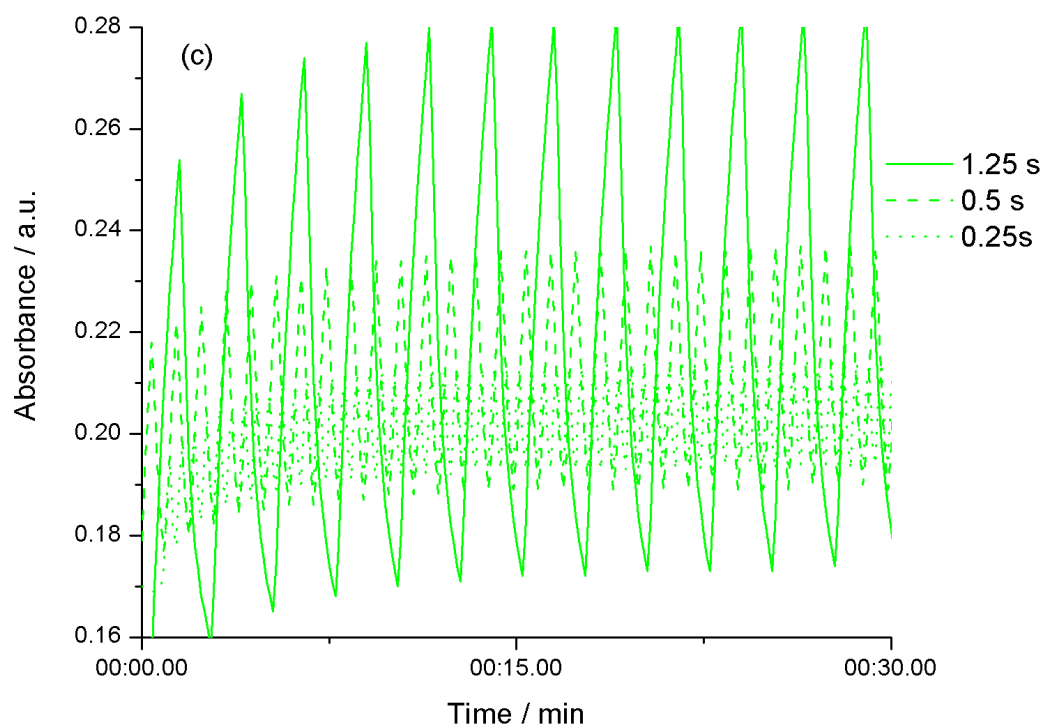


Figure 2.22 Change in absorbance upon p-doping at various switching rates for (a) poly54, (b) poly55 and (c) poly56. Absorbance was monitored at 755 nm between potentials of -0.4 and 1.5 V.

Table 2.3 Switching times and % change in absorbance.

| Switching time / s | % Change Poly54 | % Change Poly55 | % Change Poly56 |
|--------------------|-----------------|-----------------|-----------------|
| 10 | 45.9 | 42.7 | 79.8 |
| 5 | 36.1 | 35.4 | 66.2 |
| 2.5 | 28.2 | 26.9 | 51.6 |
| 1.25 | 18.9 | 16.9 | 39.3 |
| 0.5 | 10.0 | 6.8 | 19.0 |
| 0.25 | 6.3 | 3.5 | 9.3 |

2.10 Colourimetry

Colour characteristics were analysed for all three polymers. Each polymer has a colour change of red (neutral) to yellow (doped). A summary of the data are shown in Table 2.4. Of the three polymers, poly**56** gives the greatest colour contrast.

Table 2.4 CIE Yxy and L*a*b* color spaces for poly**54**, poly**55** and poly**56** for neutral and doped polymers

| | Y | x | y | L* | a* | b* |
|------------------------|--------|--------|--------|--------|-------|------|
| Poly 54 neutral | 47.67 | 0.3393 | 0.3313 | 74.62 | 6.74 | 7.87 |
| Poly 54 doped | 52.72 | 0.3296 | 0.3358 | 77.71 | 1.21 | 8.04 |
| Poly 55 neutral | 81.09 | 0.3212 | 0.3226 | 92.17 | 3.58 | 3.13 |
| Poly 55 doped | 90.22 | 0.3178 | 0.3271 | 96.09 | -0.22 | 4.27 |
| Poly 56 neutral | 117.44 | 0.3145 | 0.3173 | 106.38 | 3.3 | 0.05 |
| Poly 56 doped | 122.93 | 0.3131 | 0.3223 | 108.26 | -0.28 | 1.87 |

2.11 Conclusions

Three new monomers and their respective polymers have been synthesised and characterised by absorption, CV, UV-vis spectroelectrochemistry, electrochromic switching times, and colourimetry. The first monomer (**54**) has a fused TTN side group, which is an isomer of TTF. The other two monomers are the saturated (**55**) and the open cycle form (**56**). Despite the similarity in structure to TTF, monomer **54** does not show any similar oxidation traits, such as the famous TTF two-wave oxidation or the formation of a new band at 390 nm in spectroelectrochemistry measurements upon p-doping.

All three monomers and polymers show differences in oxidation and reduction potentials as well as energy level calculations which can be explained in relation to structure comparisons. All three polymers showed electrochromic behaviour with a visible colour change from red to yellow upon p-doping. Poly**56** showed the best colour contrast between neutral and oxidised states but was the least stable toward repetitive oxidation cycles.

**Chapter 3. New Redox Stable Low Band Gap
Conjugated Polymers based on Thiophene-BODIPY-
Thiophene repeat units.**

3.1 Abstract

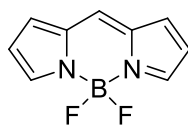
The computational, electronic and electrochemical study of a monomer, compound **68**, which can be electropolymerised to produce a BODIPY conjugated polymer, is reported and discussed. The material is fascinating as it produces a low band gap polymer in which the oxidation and reduction processes are reversible, indicating a potential use in organic photovoltaic devices. The polymer's band gap is too narrow to give a good open circuit voltage, but through structure modification, polymers with wider band gaps were therefore created.

The first modification was the removal of the electron-withdrawing NO₂ group (**81**) and to replace this with an inductive bromine atom (**82**). The second modification was aimed at changing the HOMO level through replacement of the EDOT units with EDTT. The non-planar nature of the bis-EDTT repeat unit in the polymer main chain (poly**90**) provided a lowering of the HOMO level, compared to poly**68**. The effect of the BF₂ moiety was also investigated in the examination of poly**91** and was found to have a greater effect than expected. Further investigation into the effect of removing the BF₂ group was analysed in the third comparison between two monomers and polymers that have EDOT as the polymerisable group (poly**81** and poly**89**).

By examination of the energy levels (with PCBM as the acceptor), poly**90** as a donor would give a theoretical 10% power conversion efficiency in a working photovoltaic device.

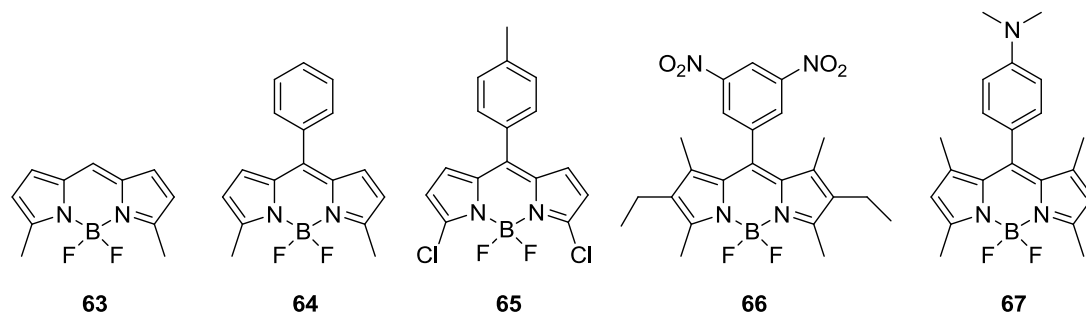
3.2 Introduction

BODIPY (4,4-difluoro-4-borata-3*a*-azonia-4*a*-aza-s-indacene) (**62**) and its many derivatives, are well known and studied for several applications. Such interest stems from the strong absorption, fluorescence and high quantum yields displayed by this group of materials.¹⁷³ BODIPY dyes were first discovered by Trebis and Kreuzer,¹⁷⁴ and have been used in electroluminescent devices,¹⁷⁵ dye sensitised solar cells,¹⁷⁶ sensing of cations,¹⁷⁷ and biological tagging of proteins.¹⁷⁸



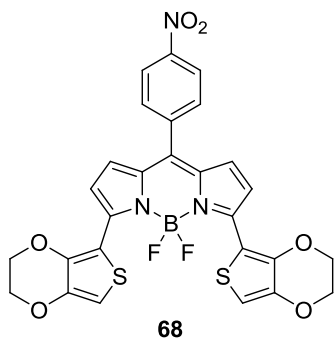
BODIPY
62

The absorption and fluorescence of these dyes can be controlled through the extent of the electron delocalisation around the central cyanine framework by the donor / acceptor characteristics of the attached substituents. BODIPY without substituents (**62**) has recently been synthesised as a stable compound, this structure shows an absorbance λ_{max} at 499 nm, an emission λ_{max} at 535 nm and a quantum yield (Φ_{PL}) of 0.93.¹⁷⁹ The absorption, fluorescence and quantum yields of these dyes can vary greatly depending on the substituent. For example, compound **63**,¹⁸⁰ which has two α -methyl groups, has an absorption λ_{max} at 507 nm, emission λ_{max} at 520 nm and a quantum yield of 0.81.

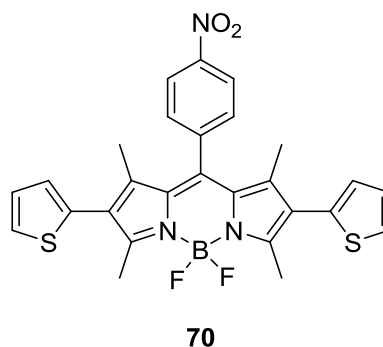
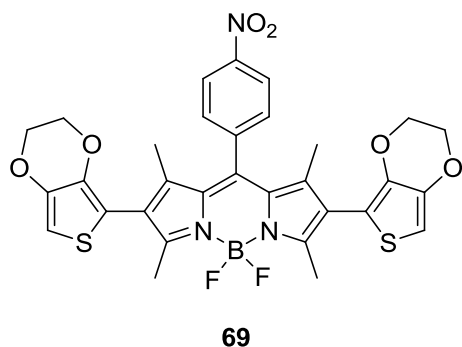


Addition of an aryl group in the *meso* position, **64** does not change the absorption or fluorescence but the quantum yield has greatly decreased ($\Phi_{\text{PL}} = 0.19$). However, the quantum yield can be increased ($\Phi_{\text{PL}} = 0.27$) by chlorination at the 3- and 5- positions (**65**).¹⁷³ Once again, the absorption and fluorescence values are unchanged. Incorporation of an electron-withdrawing group (such as two nitro groups on **66**)¹⁸¹, or an electron-donating group (tertiary amine, **67**)¹⁸² cause an even greater drop in the fluorescence quantum yield ($\Phi_{\text{PL}} = 0.01$ and 0.012 for **66**, and **67**, respectively), through competing electron transfer reactions.

Despite the amount of research and development of BODIPY and its derivatives over the last four decades, there has been very little study of BODIPY groups incorporated into the main chain of π -conjugated polymers with delocalised donor and acceptor groups throughout the main chain. In the first section of this chapter, the computational, electronic and electrochemical study of a monomer, compound **68**, which can be electropolymerised to produce a BODIPY conjugated polymer, is reported and discussed. The attachment of EDOT groups was chosen for the well known facile ability of the EDOT unit to electropolymerise.¹⁸³



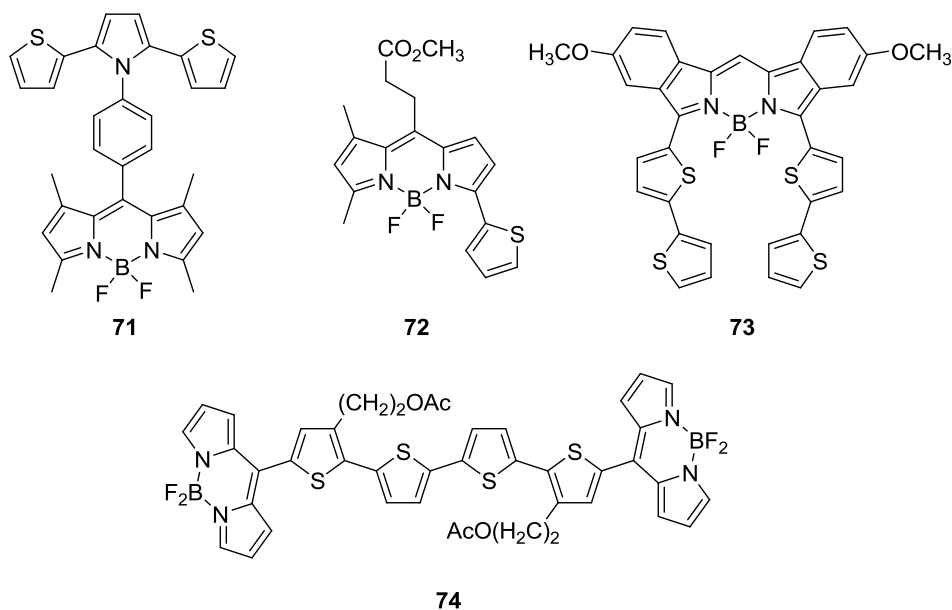
Previous electrochemical analysis of BODIPY compounds have shown that oxidation and reduction of the core can be achieved within normal electrochemical windows,¹⁸⁴ and that if the 2, 4, 6, and 8 positions are blocked then the oxidation and reduction waves can be reversible.¹⁸⁵ There have only been two BODIPY-EDOT polymers reported, both by Cihnaer *et al.*



Compounds **69** and **70**¹⁸⁶ both produce an irreversible oxidation and reversible reduction wave under cyclic voltammetry analysis, as expected. The absorbance of both compounds gives λ_{\max} at 540 and 530 nm, for **69** and **70**, respectively. Unusually, the λ_{\max} is very similar compared to compound **66** (540 nm),¹⁸¹ suggesting that the addition of EDOT or thiophene in this case does not extend the effective conjugation length; this is also shown in the polymers. Monomer **69** electropolymerises directly, but monomer **70** did not and was grown as a copolymer with EDOT.¹⁸⁷ In each case, reversible p- and n-doping are observed. However, the

band gaps are very similar to that of PEDOT (1.35 eV),⁴³ with values of 1.33 and 1.76 eV for poly**69** and poly**70**-EDOT, respectively.

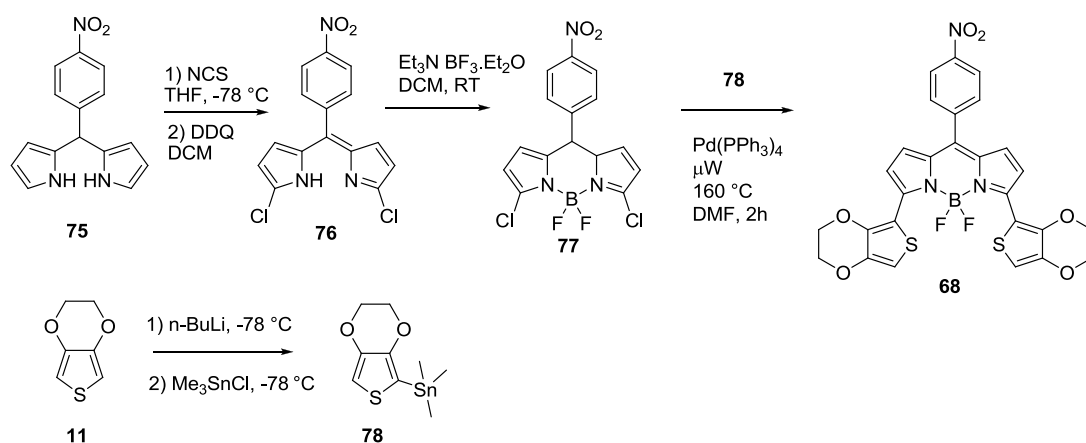
There have been other examples of thiophene functionalised BODIPY compounds such as compounds **71**,¹⁸⁸ **72**,¹⁸⁹ **73**,¹⁹⁰ and **74**.¹⁹¹



Compound **71** was electropolymerised through the thiophene groups, but this results in a polymer in which BODIPY is a side group rather than a component of the main chain.¹⁹² Compounds **72** and **73** were synthesised as dyes, but no electrochemical data was reported. What is noted is that addition of one or more thiophene groups decreases the quantum yield for **72** ($\Phi_{\text{PL}} = 0.19$). Compound **74** incorporates two BODIPY units connected *via* a quaterthiophene. This compound is designed to be a light harvesting system, featuring nonradiative resonance energy transfer from the quaterthiophene donor to the BODIPY acceptor.

The synthetic procedure for monomer **68** is shown in Scheme 3.1.

Scheme 3.1 Synthesis of **68**.



3.3 Experimental

All monomers were prepared synthetically by Zuzana Vobecka and Filipe Vilela (University of Strathclyde), and computational analysis was performed by Peter Skabara.

Cyclic voltammetry measurements were performed on a CH Instruments 660A electrochemical workstation with *iR* compensation using anhydrous dichloromethane as the monomer solvent and acetonitrile for monomer-free solvent. The electrodes were glassy carbon, platinum wire, and silver wire as the working, counter, and reference electrodes, respectively. All solutions were degassed (Ar) and contained monomer substrates *ca.* 10⁻⁴ M, together with *n*-Bu₄NPF₆ as the supporting electrolyte. All measurements are referenced against the E_{1/2} of the Fc/Fc⁺ redox couple.

Spectroelectrochemical and switching experiments were conducted on ITO glass. Absorption spectra and CIE coordinates were recorded on a UNICAM UV300 spectrophotometer. Fluorescence measurements were recorded on a Perkin Elmer LS

45 luminescence spectrometer. Solid state absorption of poly**68** was recorded on a Shimadzu UV-3107PC UV-vis-NIR scanning spectrophotometer at the University of Glasgow.

3.4 Molecular Modelling

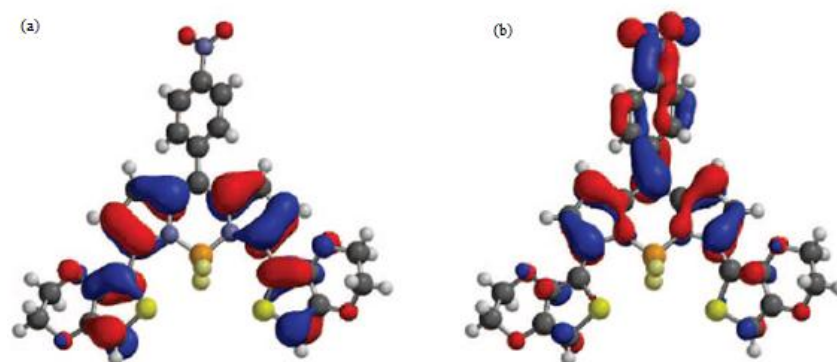


Figure 3.1 HOMO (a) and LUMO (b) frontier orbitals of **68**.

Molecular modelling of **68** was performed using DFT calculations at the B3LYP/6-31G* level (Spartan '08). The calculations indicate that the oxidation site is localised on the EDOT-pyrrole units (Figure 3.1(a)), whilst the electrons are injected into the BODIPY core (Figure 3.1(b)). The LUMO based on the BODIPY core has been seen in other DFT calculations performed by other groups.¹⁸⁸ The HOMO and LUMO plots also clearly indicate that the monomer has an intramolecular charge transfer (ICT) pathway between the two conjugated segments of the molecule, a process which has also been observed in other BODIPY donor-acceptor derivatives.¹⁷⁶

It can be seen in the LUMO plot that there is a considerable contribution from the nitrophenylene group, despite the large twist between this group and the BODIPY core (*ca.* 129°), due to steric repulsion between aromatic protons. The EDOT units

are also twisted out of plane from the BODIPY core (*ca.* 28-35°), and this is due to a non-covalent interaction from the sulfur of the EDOT units with the fluorines of the BF₂ functionality (2.84 Å, sum of the van der Waals radii for S and F = 3.45 Å).¹⁹³ As the fluorine atoms point away from the plane from the pyrroles, this interaction results in a non-planar arrangement between EDOT and pyrrole groups.

3.5 Absorption and Electrochemistry of 68

The absorption spectrum of **68** was performed in dichloromethane solution. The spectrum (Figure 3.2) shows four absorption maxima at 349, 444, and 663 nm with a shoulder at 611 nm. The peak at 444 nm can be assigned to the BF₂ group from the BODIPY core (see 3.13.1 for confirmation of this) and the highest absorption band can be attributed to the intramolecular charge transfer process of the monomer, which is of higher wavelength compared to other basic BODIPY compounds (*ca.* 510 nm). The bathochromic shift is a result of the extended conjugation from the attachment of the two EDOT groups. The onset of the highest wavelength (729 nm) allows the determination of the optical HOMO-LUMO gap. This was calculated to be 1.7 eV which is small for a monomer but can be attributed to the ICT process explained in the molecular modelling section.

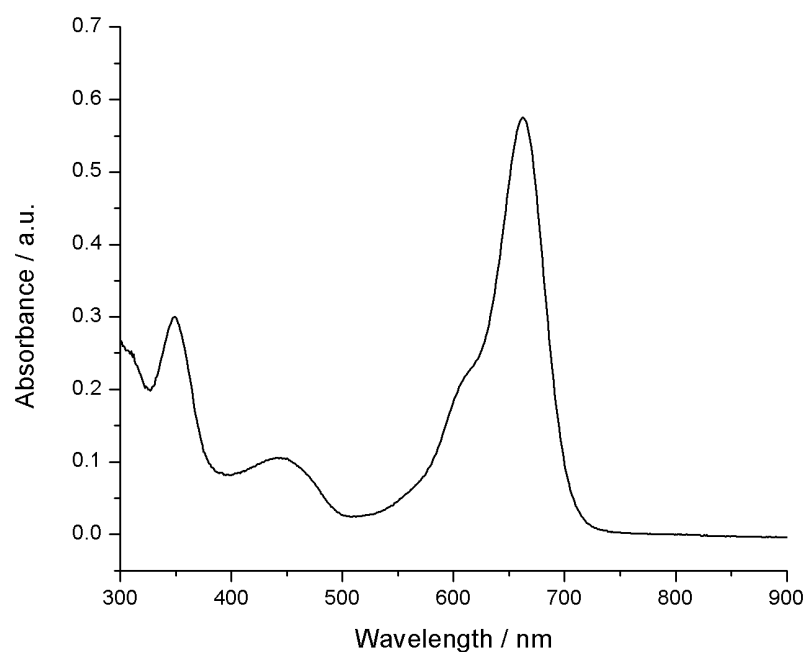


Figure 3.2 Solution state electronic absorption spectra for **68**.

The electrochemical properties of the monomer were investigated using cyclic voltammetry with a glassy carbon working electrode, platinum wire counter electrode and a pseudo silver reference electrode. The substrate concentration was 10^{-4} M with *n*-Bu₄NPF₆ (0.1 M) as the supporting electrolyte and dichloromethane as the solvent. The oxidation and reduction of **68** is shown in Figure 3.3.

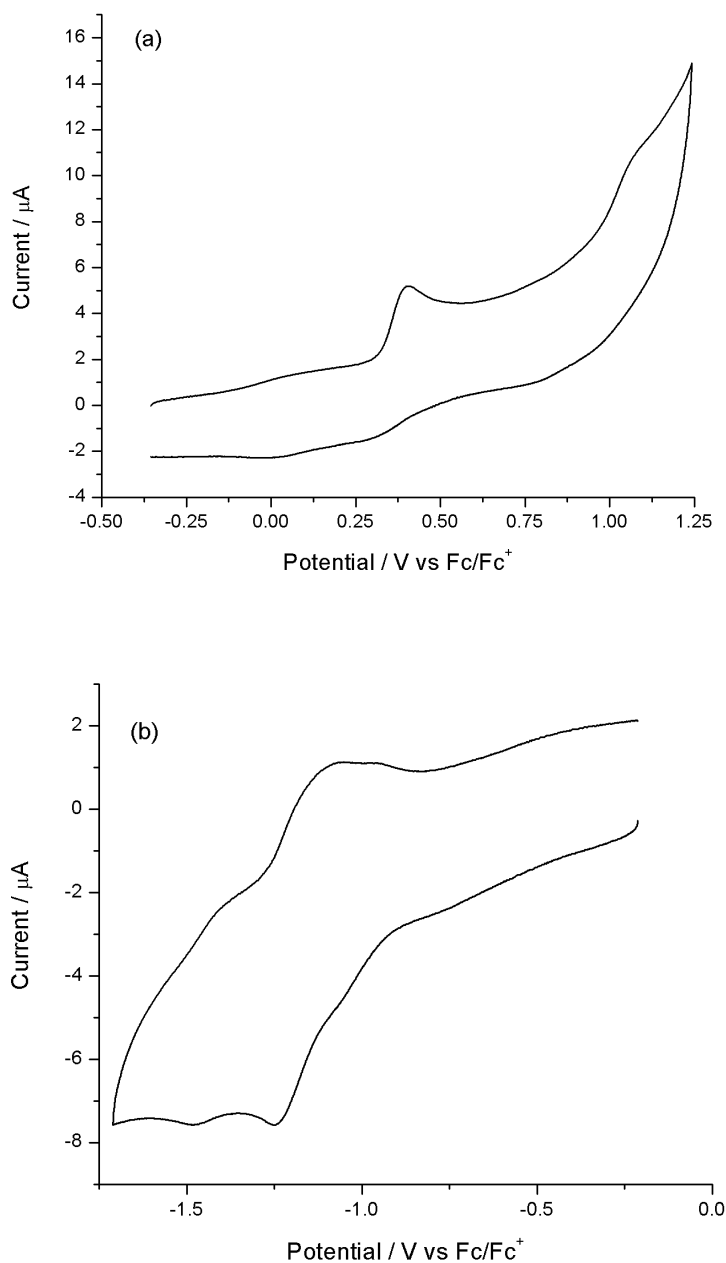


Figure 3.3 Cyclic voltammograms of (a) oxidation and (b) reduction of **68**.

The oxidation graph (Figure 3.3(a)) shows two irreversible peaks at +0.40 and +1.07 V, which can be assigned to the formation of a radical cation (1st wave) and then dication radical (2nd wave) on the two EDOT units. The irreversible nature of these peaks is due to polymer growth beginning to take place. The reduction graph (Figure 3.3(b)) shows two reduction peaks, $E_{1/2}^{1\text{red}} = -1.17$ V and $E_{1/2}^{2\text{red}} = -1.44$ V, attributed

to the formation of the radical anion and dianion on the BODIPY core and the nitrophenylene group. CV analysis of other BODIPY compounds with nitrophenylene groups report only one reduction wave.¹⁸⁶ It is possible that the potential in these cases was not taken low enough to see the second wave. At a more negative potential there is also an irreversible peak (see Figure 3.4), due to the reduction of the EDOT groups.

The electrochemical HOMO-LUMO gap was determined for **68** from the difference in HOMO and LUMO levels. Using data referenced to the ferrocene/ferrocenium redox couple, HOMO and LUMO levels were calculated by subtracting the onsets of the first oxidation and reduction peaks (Figure 3.4) from the known value of ferrocene (-4.8 eV). The data are summarised in Table 3.1. The electrochemical HOMO-LUMO gap of 1.46 eV is in reasonable correlation with the optical HOMO-LUMO gap (1.70 eV).

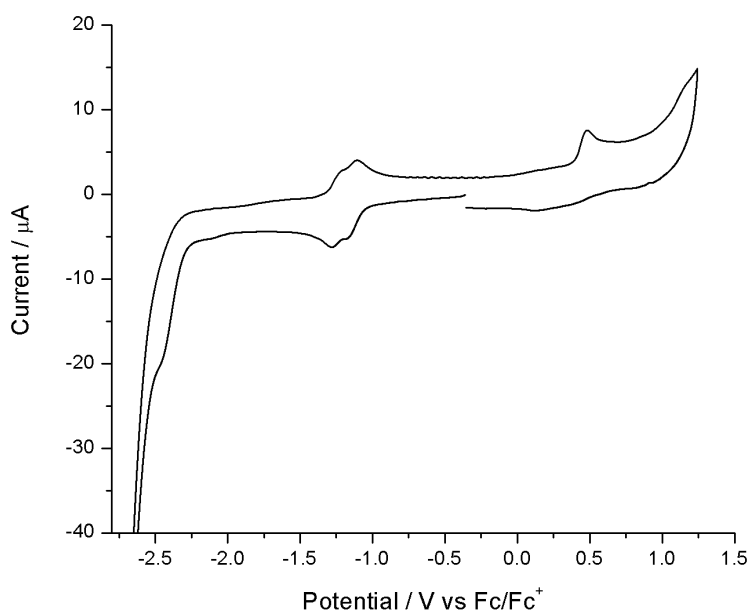


Figure 3.4 Cyclic voltammogram of **68** for energy level determination.

Table 3.1 Energy level determination data for **68**.

| Onset of Oxidation | HOMO | Onset of Reduction | LUMO | HOMO-LUMO gap |
|--------------------|------|--------------------|-------|---------------|
| / V | / eV | / V | / eV | / eV |
| +0.40 | -5.2 | -1.06 | -3.74 | 1.46 |

3.6 Electrochemistry of the polymer

To investigate the electrochemistry of the polymer, it was first electropolymerised onto the glassy carbon working electrode surface by repetitive cycling over the first oxidation peak (Figure 3.5). Polymer growth was monitored with the increase in current over successive cycles and the development of a new peak at lower potential due to the increase in conjugation length and therefore improved electron donor ability of the growing polymer.

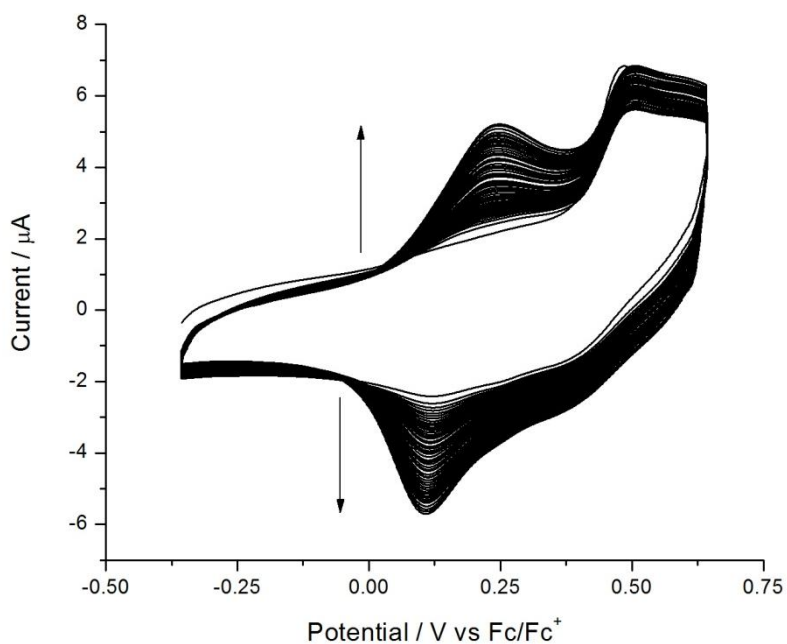
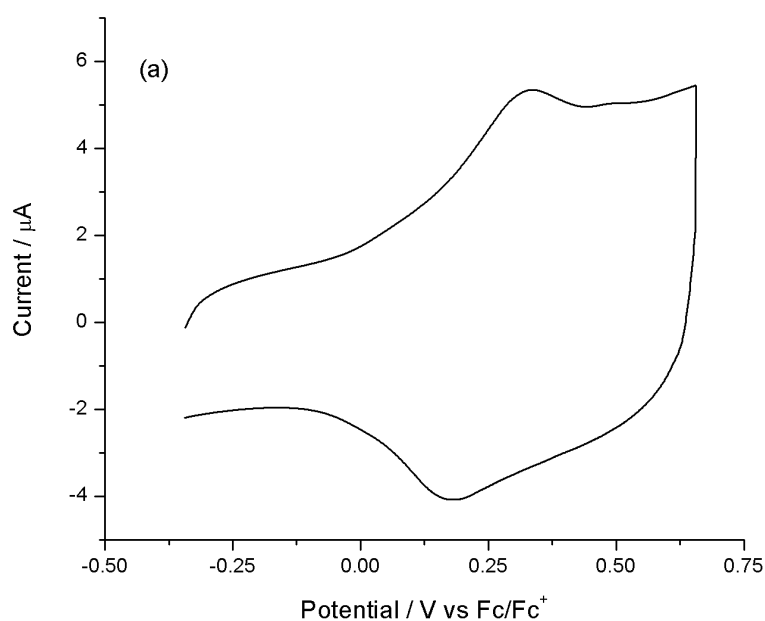


Figure 3.5 Electrochemical growth of poly**68**.

The redox properties of the polymer were measured using cyclic voltammetry in monomer-free acetonitrile solution with $n\text{-Bu}_4\text{NPF}_6$ (0.1 M) as the supporting electrolyte. The oxidation graph (Figure 3.6(a)) shows a reversible wave ($E_{1/2}^{\text{1ox}} = +0.26$ V) attributed to the removal of electrons from the newly formed bis-EDOT units throughout the polymer chain. The reduction graph (Figure 3.6(b)) once again shows two reversible waves ($E_{1/2}^{\text{1red}} = -1.13$ V and $E_{1/2}^{\text{2red}} = -1.27$ V) that have been shifted to a less negative potential due to the increased conjugation of the polymer compared to the monomer.



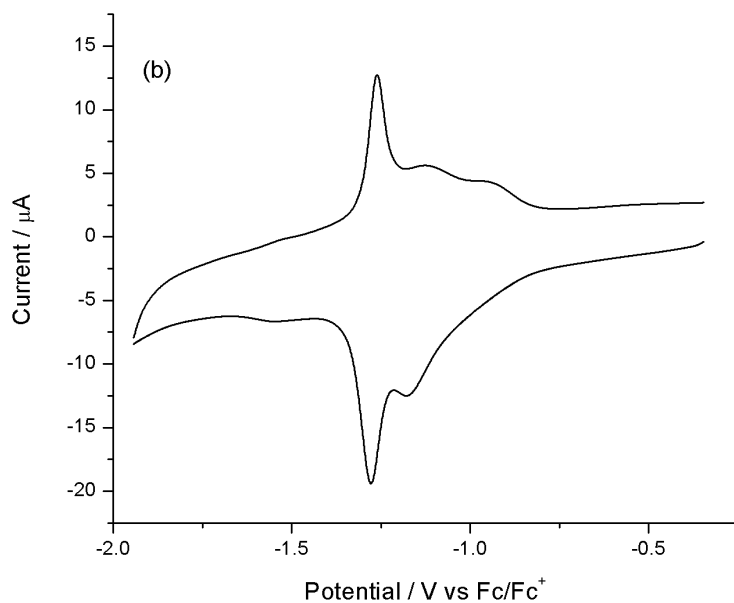


Figure 3.6 Cyclic voltammograms of (a) oxidation and (b) reduction of poly**68**.

The electrochemical band gap of poly**68** was calculated in the same manner as before by subtracting the onsets of the first oxidation and reduction waves from the known HOMO of ferrocene (-4.8 eV) to give the HOMO and LUMO energy levels respectively.

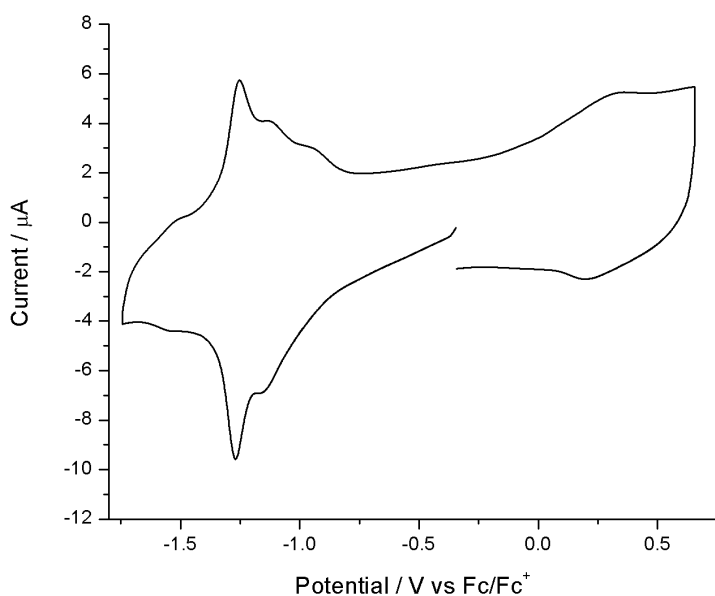


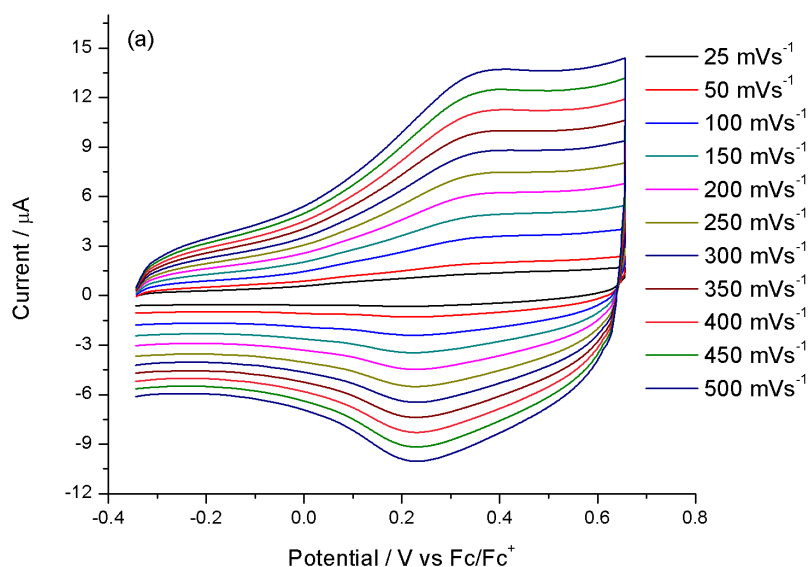
Figure 3.7 Cyclic voltammogram of poly**68** for energy level determination.

The band gap is the difference between the HOMO and LUMO levels and all the data are summarised in Table 3.2. The onset of the oxidation wave (-0.12 V) gives a HOMO value of -4.68 eV and an onset of the first reduction (-0.92 V) gives a LUMO level of -3.88 eV, resulting in an electrochemical band gap of 0.8 eV. This band gap is incredibly small for a conjugated polymer and made even more remarkable by the fact that both the oxidation and reduction processes are reversible.

Table 3.2 Energy level determination of poly**68**.

| Onset of Oxidation / V | HOMO / eV | Onset of Reduction / V | LUMO / eV | Band gap / eV |
|---------------------------|--------------|---------------------------|--------------|------------------|
| -0.12 | -4.68 | -0.92 | -3.88 | 0.8 |

To test the diffusion properties of poly**68**, the oxidation of the polymer was repeated several times with varying scan rates (Figure 3.8(a)). A plot of current maximum versus the scan rate (Figure 3.8(b)) was plotted to compare the current response to the scan rate. A linear regression with a good correlation ($R^2 = 0.997$) proves the polymer is not diffusion limited.



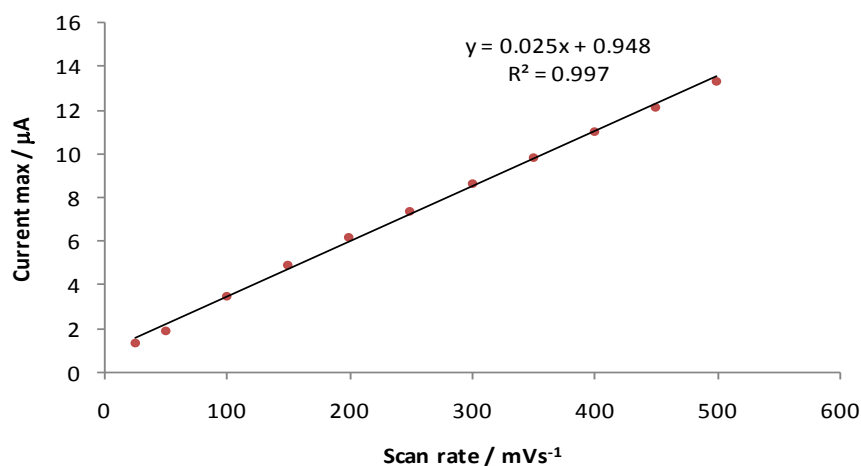


Figure 3.8 (a) Cyclic voltammograms of poly**68** with varying scan rate and (b) current max vs. scan rate.

3.7 Absorption and Spectroelectrochemistry of poly**68**

As the polymer has a low band gap (0.8 eV), the absorption spectrum of this polymer in the solid state is outside the range of our normal spectrometer (Unicam UV 300 range 190 -1100 nm) and therefore the solid state spectrum was measured using a Shimadzu UV-3107PC UV-vis-NIR scanning spectrophotometer at the University of Glasgow (range 200 – 2000 nm).

The solid state spectrum is shown in Figure 3.9 and represents a thin film of poly**68** grown onto ITO coated glass and dedoped beforehand to remove any trapped charge. The spectrum shows three absorption maxima at 421, 582, and 960 nm along with a shoulder at 682 and a broad shoulder between 1290 and 1700 nm. Compared to the monomer (peaks at 349, 444, and 663 nm), all the peaks for poly**68** have been shifted bathochromically by 72, 138, and 297 nm, respectively because of the increase in conjugation.

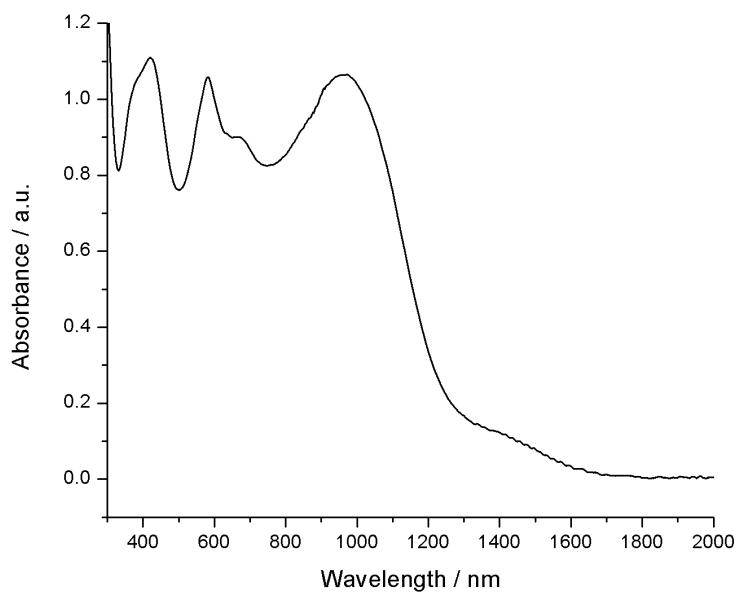


Figure 3.9 Solid state electronic absorption spectrum of poly**68** recorded as a thin film deposited on ITO glass.

The optical band gap of this polymer is a little harder to determine as the band of the highest absorption is broad, but this wavelength range corresponds to a band gap of 0.78 to 0.96 eV which encompasses the electrochemical band gap of 0.8 eV.

A spectroelectrochemical experiment of poly**68** was performed to investigate how the absorption character of the polymer changes with p-doping by growing a fresh polymer onto ITO coated glass. The UV-vis spectroelectrochemical experiment was carried out in the range of 0 to +1.6 V (not referenced to ferrocene) and is shown in Figure 3.10.

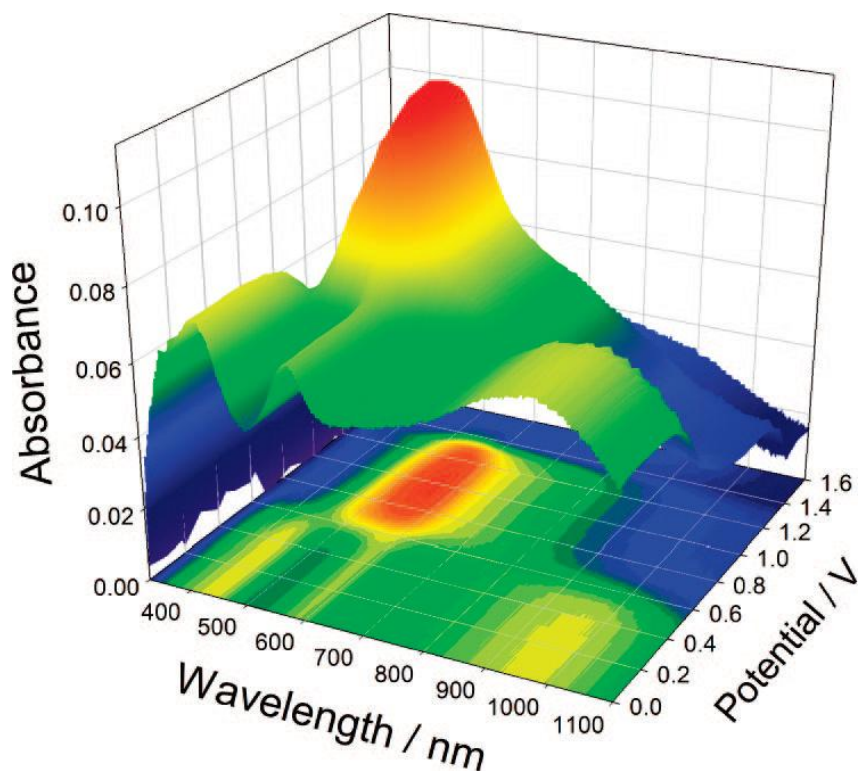


Figure 3.10 Absorption spectroelectrochemical plot of poly68 oxidation.

Upon p-doping, the absorption characteristics of the polymer change spectacularly. As the potential increases, firstly there is a decrease in the intensity of the peaks at 421, 582 and 960 nm from the creation of polarons, disrupting conjugation in the polymer chain and then above +0.6 V there is the development of a new broad peak between 450 and 950 nm (*ca.* 585 nm). This new broad absorbance which peaks at +1.0 V is the signature of a localised bipolaron state, located on the pyrrole-(EDOT)₂-pyrrole repeat unit. This new peak is in a similar wavelength range to the BODIPY core, and as the polymer changes from the neutral to the p-doped state, with localised charges mainly on the bis-EDOT segment, the BODIPY core is allowed to once again absorb in its normal range. Visually, the polymer changes from a transparent green to a pink-violet state (Figure 3.11). Above +1.4 V, the polymer becomes too charged and dissolves into the bulk solution.

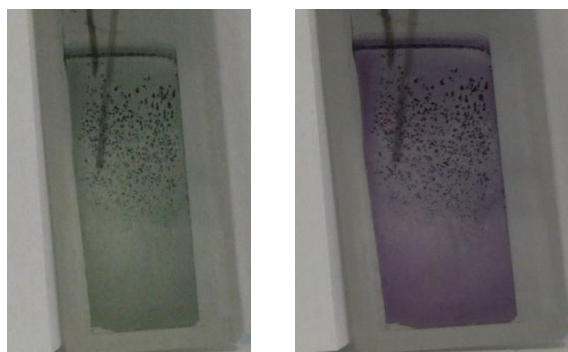
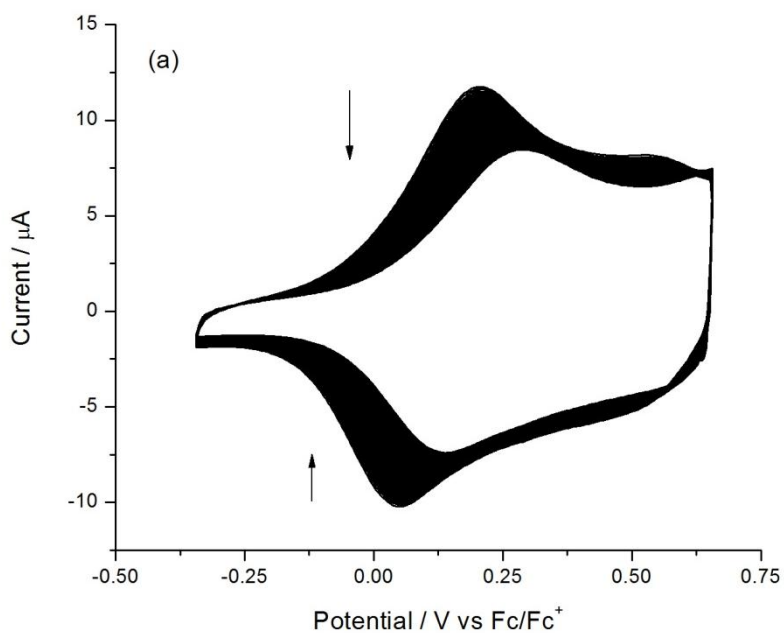


Figure 3.11 Colour change of poly68 (left) neutral and (right) doped

3.8 Stability of poly68

Stability studies of poly68 were performed on ITO coated glass slides cycled 250 times in monomer-free solution to monitor the change in the current response. Figure 3.12 (a) shows that in anodic conditions, poly68 has a 29% decrease in electrochemical activity and Figure 3.12 (b) shows that the electrochemical activity under reductive conditions is 35%.



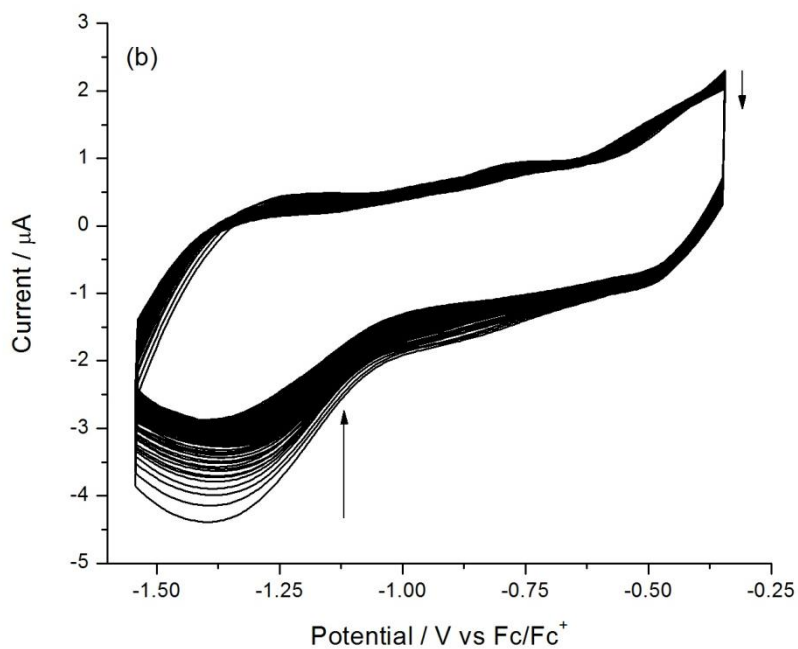


Figure 3.12 Stability of (a) oxidation and (b) reduction of poly68.

3.9 Switching times and CIE coordinates of poly68

As the polymer exhibits a good contrast between colour states, switching times were measured between the neutral (-0.2 V) and the doped state (+1.0 V) with switching times of 10, 5, 2.5, 1.25, 0.5, and 0.25 seconds. Fresh polymers were grown on ITO coated glass and dedoped. The results of the switching time experiment are shown in Figure 3.13 and the data summarised in Table 3.3.

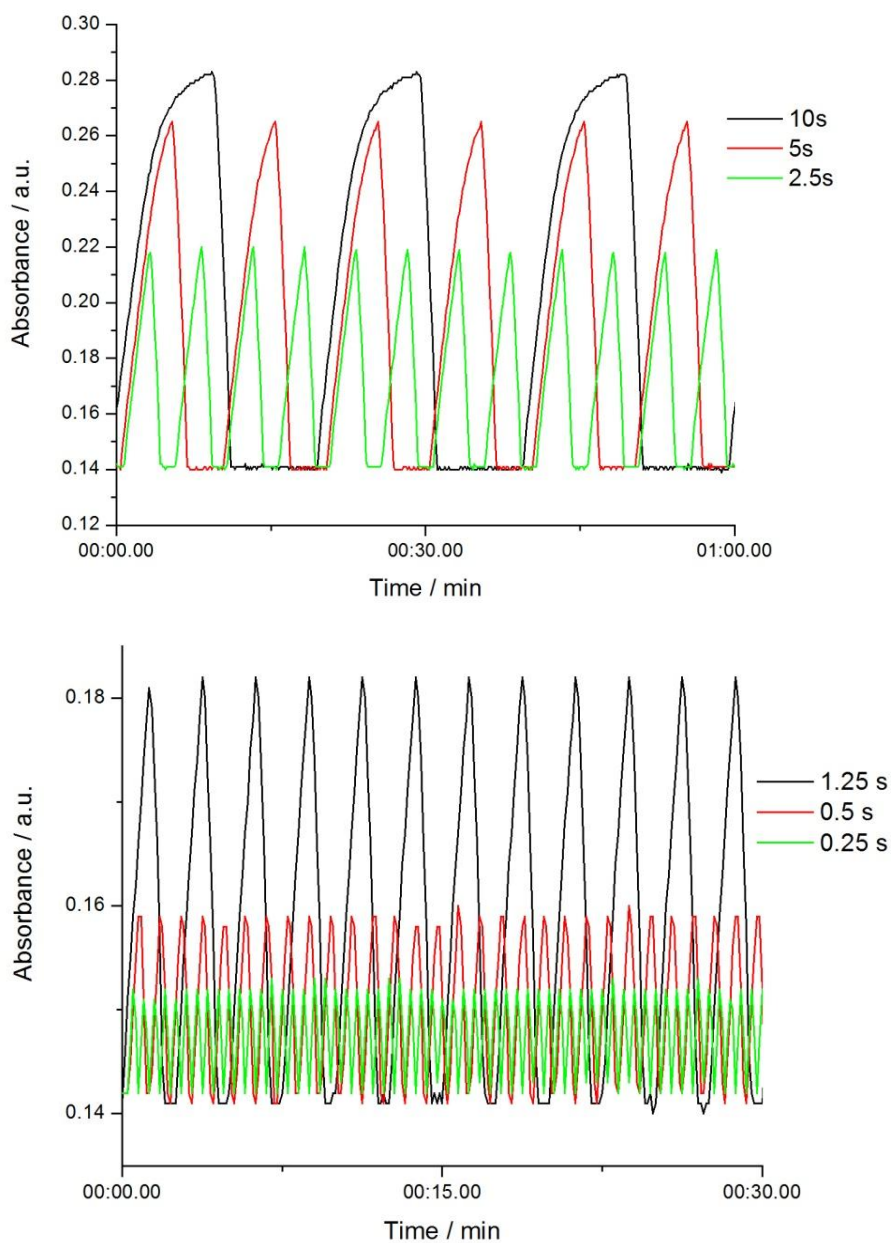
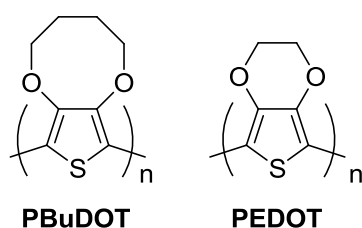


Figure 3.13 Change in absorbance upon p-doping at various switching rates of poly68. Absorbance was monitored at 560 nm between -0.2 and +1.0 V.

Table 3.3 Switching times and % change in absorbance of poly68.

| Switching Time / s | 10 | 5 | 2.5 | 1.25 | 0.5 | 0.25 |
|--------------------|------|------|------|------|------|------|
| % Change | 50.5 | 47.2 | 36.1 | 22.5 | 11.3 | 6.0 |

Although there is a large and significant change in the spectroelectrochemical experiment (Figure 3.10) when comparing the neutral and doped states, the percentage change in absorbance at short times does not give a big enough change to allow this polymer to be realistically considered for electrochromic devices, as it has inferior optical contrast compared to electrochromic polymers such as PBuDOT (63% at 1.3 s) and PEDOT (44% at 2.2 s).⁴⁵



CIE coordinates were however still measured between 0 and +1.0 V for the polymer and the data is summarised in Table 3.4 and plots of x against y and a* against b* are shown in Figure 3.14.

Table 3.4 CIE Yxy and L*a*b* colour spaces for poly**68** measured between 0 and +1.0 V.

| | Y | x | y | L* | a* | b* |
|---------|-------|--------|--------|-------|-------|--------|
| Neutral | 74.4 | 0.3113 | 0.3295 | 89.11 | -4.44 | 3.79 |
| Doped | 54.08 | 0.2972 | 0.2880 | 78.5 | 8.04 | -12.12 |

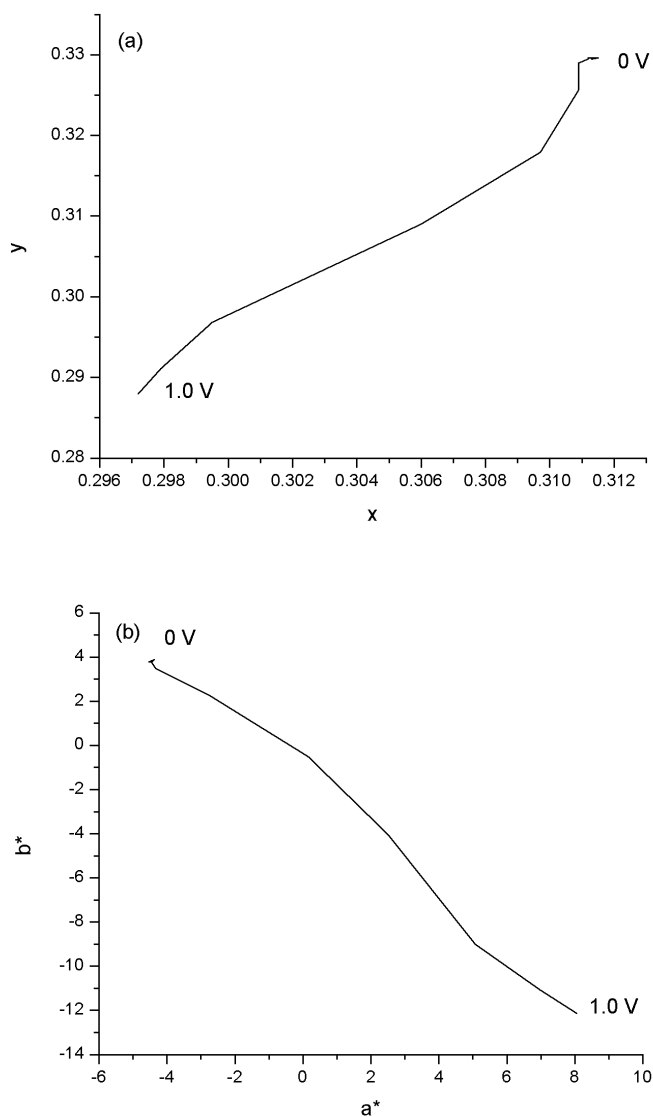


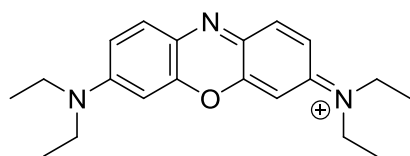
Figure 3.14 CIE plots of (a) y vs. x and (b) b^* vs. a^* for poly68.

The colour coordinates produced, shown in Table 3.4 represent the visual colour change noted for the polymer. In the neutral state, a negative a^* is green, with -4.44 along with $b^* = 3.79$ (giving the polymer a yellow tint) being recorded for poly68; the pink-violet doped state can be seen with a positive a^* (red) and a negative b^* (blue), the CIE points observed were $a^* = 3.79$ and $b^* = -12.12$.

3.10 Quantum Yield Calculation

As BODIPY is a well known fluorescent dye, an interesting study was to measure the quantum yield of **68** to see if the addition of EDOT units to the core quenches the emission compared to the precursor **77**.

To measure quantum yields, a standard with a known PLQY is chosen that matches well with the absorption and emission wavelengths of the compound. Oxazine 1 (**79**) was chosen as the standard for **68** as it excites at 590 nm and emits around 650 nm (**68** excites at 663 and emits around 690 nm).



79

Five concentrations of solutions for both standard and unknown, that have absorbance values that fall between 0.010 and 0.070 a.u., were prepared fresh and the emission spectra for all were recorded. The emission spectra of both **79** and **68** are shown in Figure 3.15; the integrated area of the emission produced was measured and shown in Table 3.5 along with the gradients produced (Figure 3.16). Gradients were produced from plots of absorbance vs integrated fluorescence (Figure 3.16).

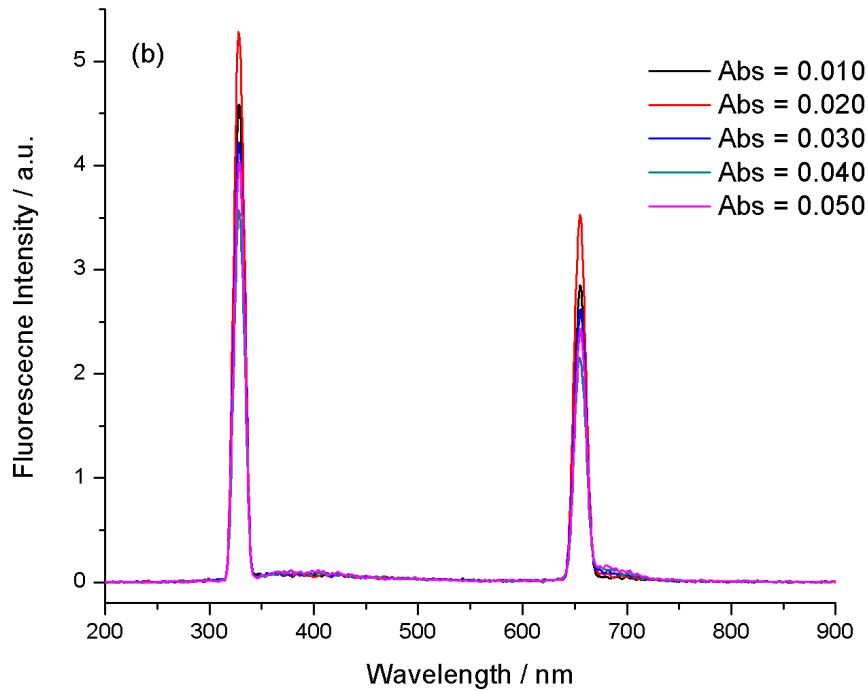
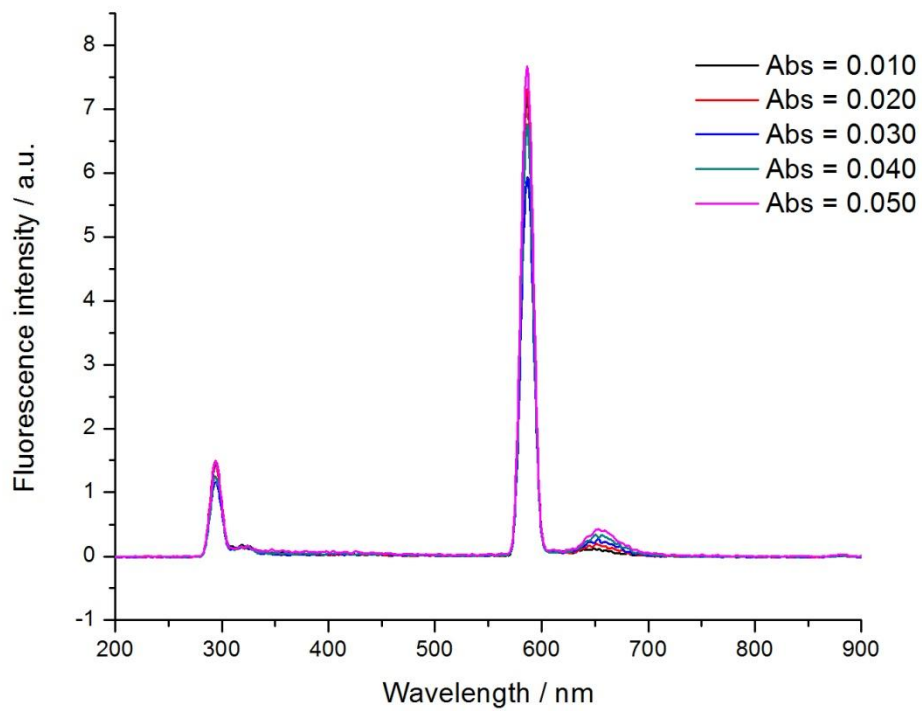


Figure 3.15 Emission spectra of (a) standard **79** and (b) **68**

Table 3.5 Emission data of **79** standard and **68**

| 79 | | 68 | |
|-----------------|-------------------------|-----------------|-------------------------|
| Absorbance | Integrated Fluorescence | Absorbance | Integrated Fluorescence |
| / a.u. | / a.u. | / a.u. | / a.u. |
| 0.01 | 5.91 | 0.01 | 2.65 |
| 0.02 | 7.714 | 0.02 | 4.05 |
| 0.03 | 10.399 | 0.03 | 4.6 |
| 0.04 | 14.147 | 0.04 | 5.714 |
| 0.05 | 19.25 | 0.05 | 7.059 |
| Gradient | 373.41 | Gradient | 150.37 |

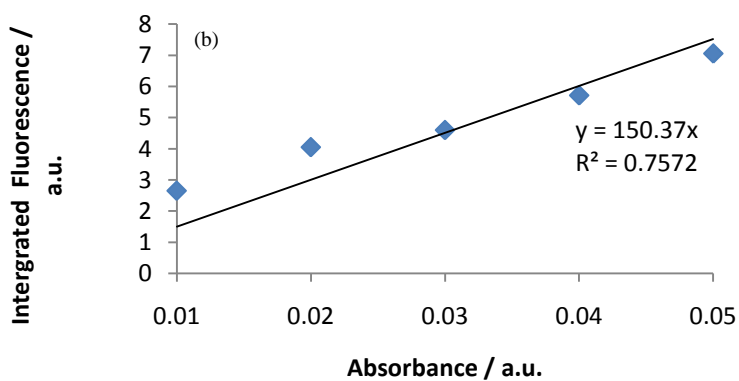
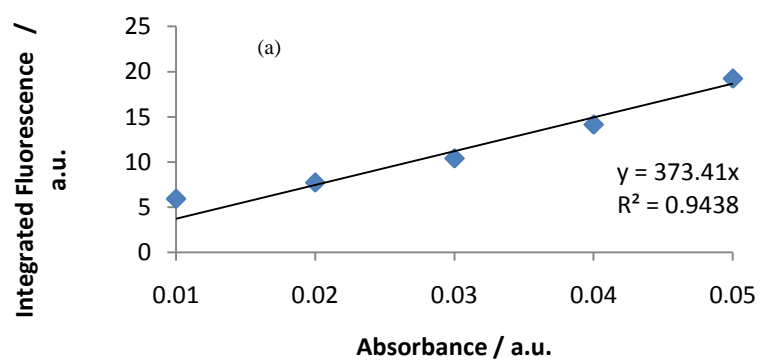


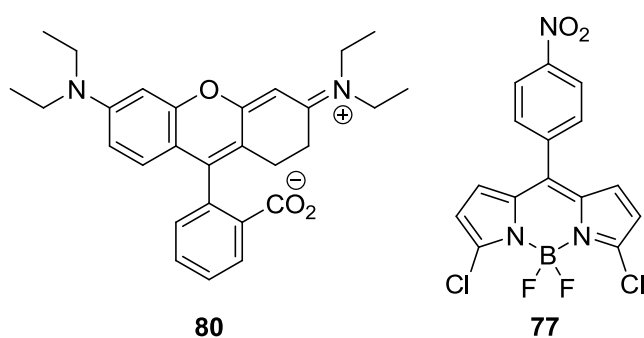
Figure 3.16 Integrated fluorescence versus absorbance for (a) **79** standard and (b) **68**

By using Equation (33) (section 1.14) and taking into account the refractive index (η) of the solvent, the quantum yield of the unknown (x) can be calculated.

$$\Phi_x = \Phi_{ST} \left(\frac{Grad_x}{Grad_{ST}} \right) \left(\frac{\eta_x^2}{\eta_{ST}^2} \right) \quad (33)$$

The quantum yield of standard **79** is 0.11,¹⁹⁴ and the refractive indices of dichloromethane and ethanol are 1.4242 and 1.360, respectively. Therefore the quantum yield is 0.049 for **68**.

To calculate the quantum yield of **77**, rhodamine B (**80**) was chosen as the standard. Compound **80** excites at 510 nm and emits at 565 nm, compared with excitation at 522 nm and emission of 545 nm for compound **77**.



The emission spectra of both **80** and **77** are shown in Figure 3.17, Table 3.6 shows the integrated fluorescence along with the gradients produced from plots of integrated fluorescence versus absorbance (Figure 3.18).

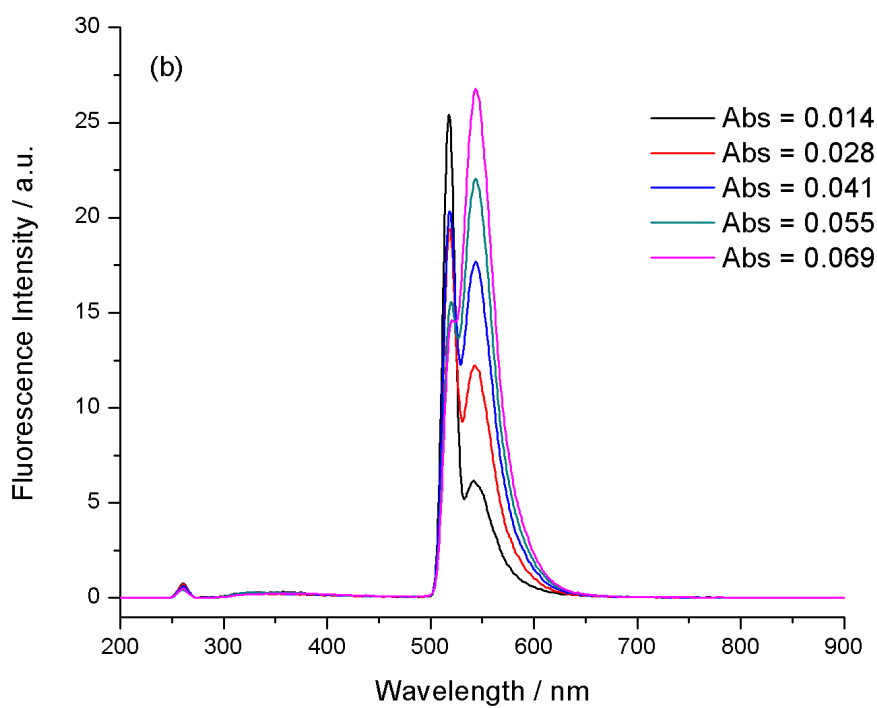
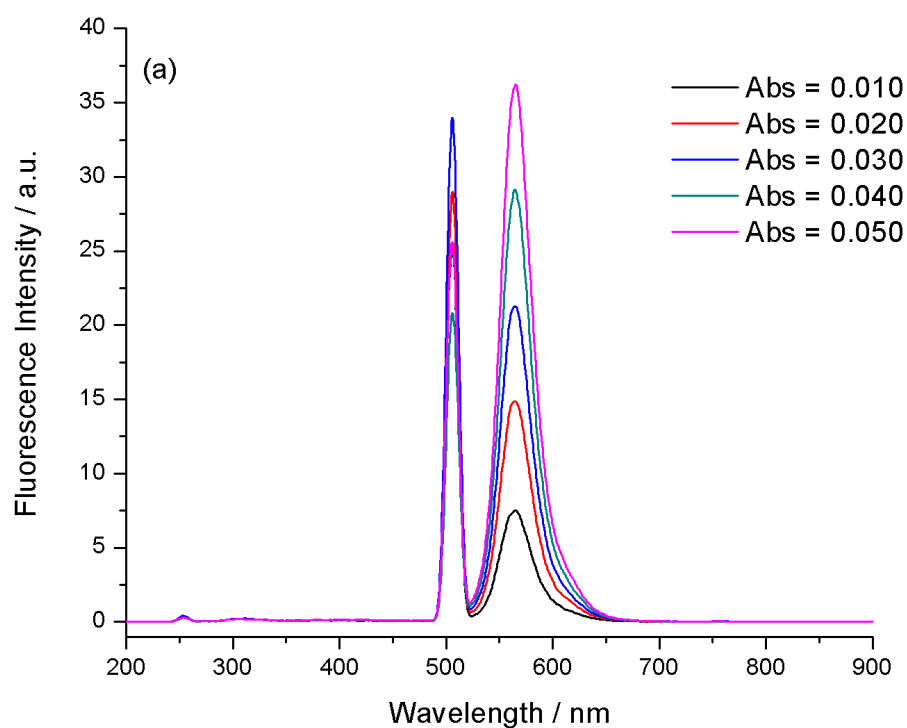
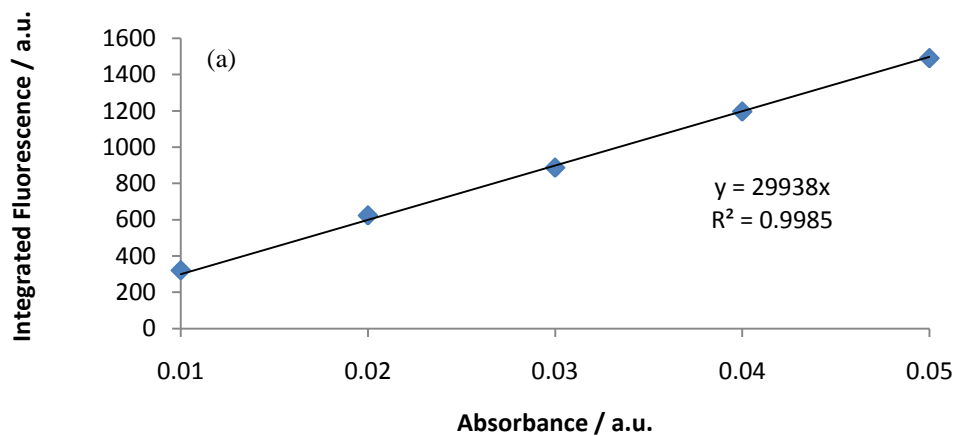


Figure 3.17 Emission spectra of (a) standard **80** and (b) **77**

Table 3.6 Emission data for **80** standard and **77**

| 80 | | 77 | |
|-----------------|-------------------------|-----------------|-------------------------|
| Absorbance | Integrated Fluorescence | Absorbance | Integrated Fluorescence |
| / a.u. | / a.u. | / a.u. | / a.u. |
| 0.01 | 320.98 | 0.014 | 228.21 |
| 0.02 | 623.46 | 0.028 | 464.57 |
| 0.03 | 887.06 | 0.041 | 683.73 |
| 0.04 | 1196.19 | 0.055 | 800.39 |
| 0.05 | 1490.36 | 0.069 | 1148.36 |
| Gradient | 29938 | Gradient | 21723 |



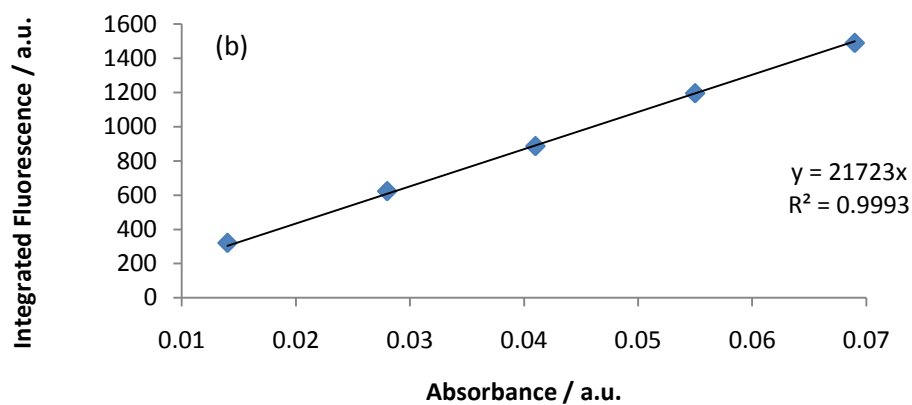


Figure 3.18 Integrated fluorescence versus absorbance for (a) **80** standard and (b) **77**.

The quantum yield of the standard **80** is 0.7,¹⁹⁴ and the refractive indices of dichloromethane and ethanol are 1.4242 and 1.360, respectively. Therefore the quantum yield calculated for **77** was 0.56. The quantum yield calculations show that addition of EDOT groups to the BODIPY core greatly decreases the luminescence efficiency of BODIPY, as seen with similar compounds.¹⁹⁰

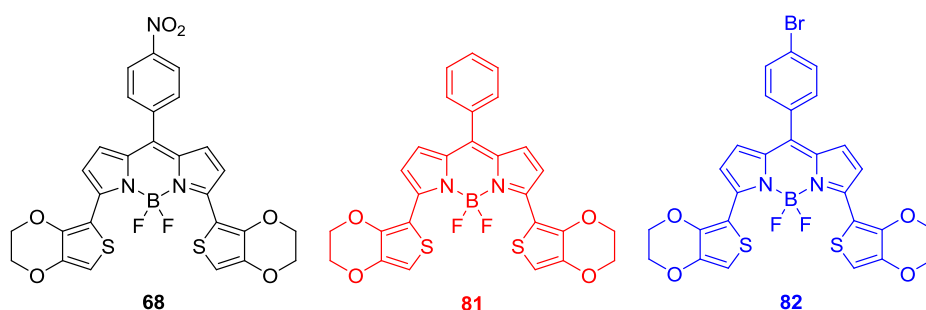
3.11 Summary

A new conjugated monomer and polymer incorporating the BODIPY unit has been created and analysed. The material is fascinating as it produces a low band gap polymer in which the oxidation and reduction processes are reversible. Despite the good colour contrast between the neutral and doped states, the polymer is not suitable for electrochromic devices as the change in absorbance is not high enough at fast switching times. However, the low band gap polymer has potential application in organic photovoltaic devices. The polymer's band gap is too narrow to give a good open circuit voltage (see section 1.15.2), but there is the possibility to modify the polymer structure for optimised properties (wider band gap) and subsequent use in OPVs.

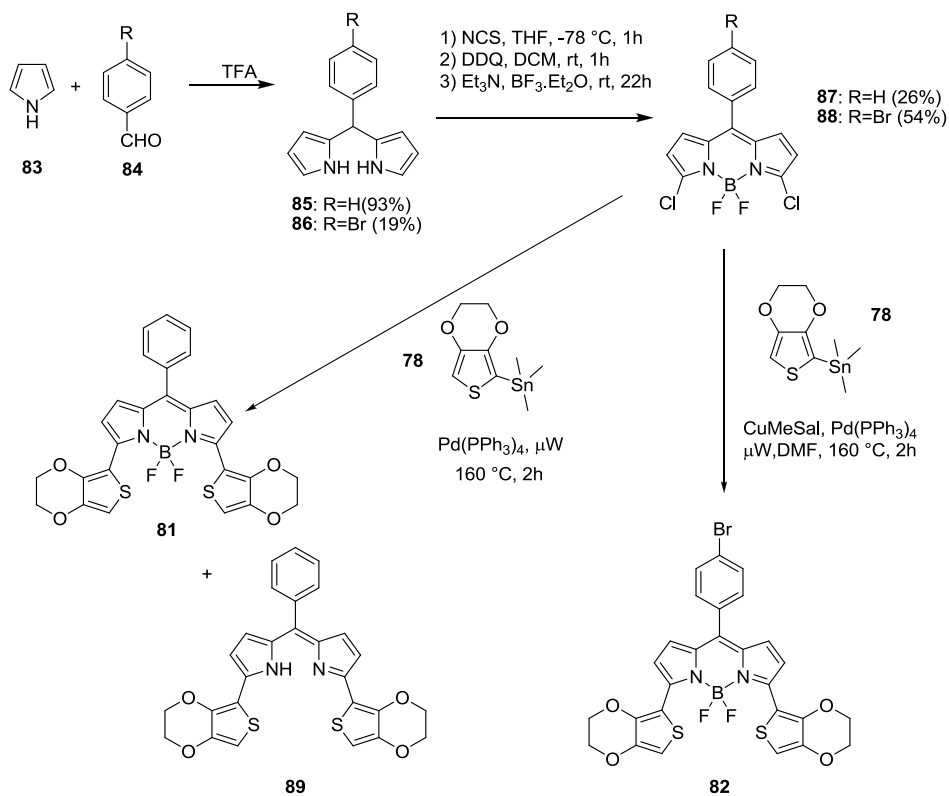
To achieve this, there are several routes that can be investigated. To increase the band gap of the polymers, the LUMO level can be raised and / or the HOMO can be lowered. Removal of the NO₂ electron withdrawing group or replacement of this with an inductive bromine group is one option to raise the LUMO level. Replacement of EDOT with EDTT is the second strategy. As explained in section 1.7, polymers incorporating EDTT in the backbone have a lower HOMO level than the analogous EDOT-containing polymer.

3.12 Modifying the LUMO level: comparison of BODIPY with NO₂, without NO₂ and with Br

Two new monomers, **81** and **82** were synthesised. As shown in Scheme 3.2, **81** has the electron-withdrawing NO₂ group removed and **82** contains an inductive bromine group. The compounds have been designed with the intention of raising the LUMO level in their homopolymers.



Scheme 3.2 Synthesis of **81** and **82**.



3.12.1 Absorption spectroscopy and Electrochemistry of the monomers

Both new monomers were analysed in dichloromethane solution. To easily compare and contrast the monomers, all the following graphs include the results of **68**. The absorption spectra (Figure 3.19) of the three monomers show similar shapes with three main absorption peaks and one shoulder; the data are summarised in Table 3.7. The noticeable difference is the π - π^* absorption band. For **68**, this transition occurs at 663 nm and this value is shifted hypsochromically for **81** and **82** to 646 and 651 nm, respectively.

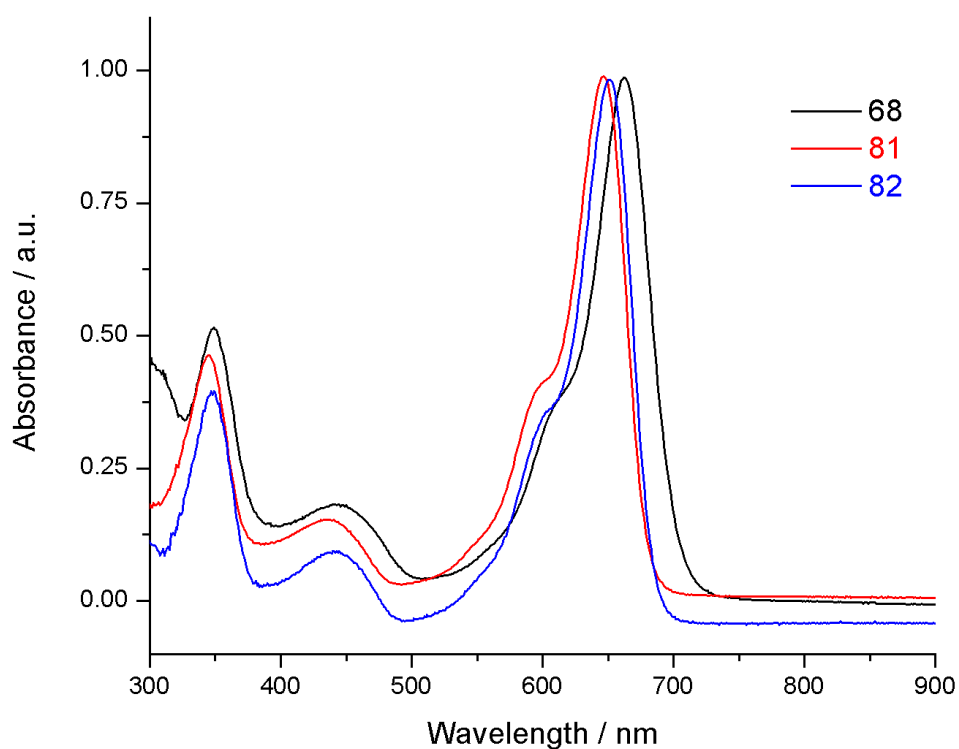
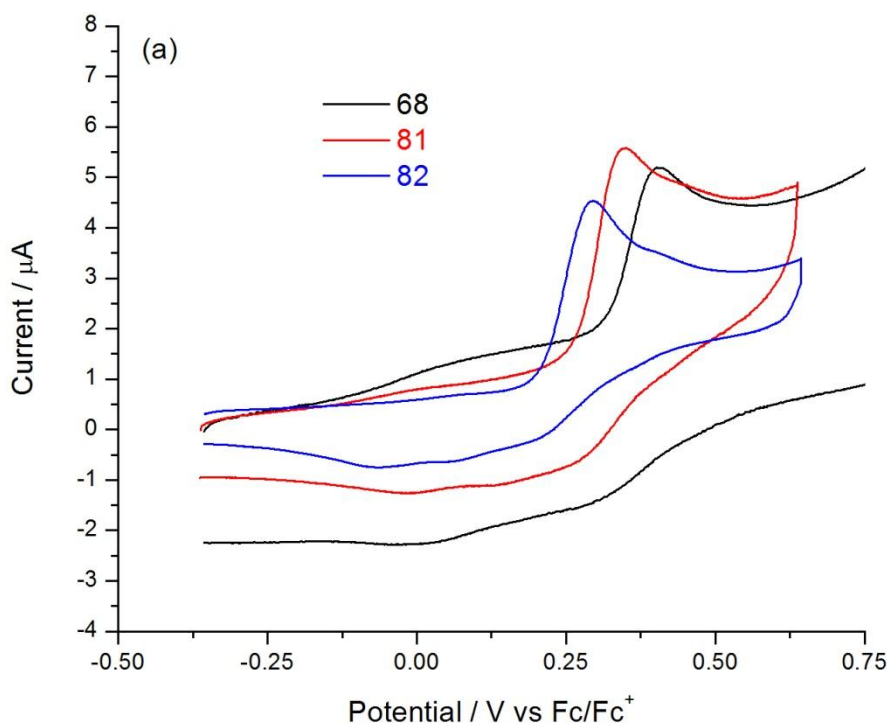


Figure 3.19 Solution state absorption spectra of **68**, **81** and **82**.

The change in the π - π^* transition also corresponds to an increase in the optical HOMO-LUMO gap. Calculated the same way as before, the HOMO-LUMO gap for

81 and **82** are 1.83 and 1.82 eV, respectively. Both are higher than the value calculated for **68** (1.70 eV).

To compare the electrochemistry of the two new monomers, cyclic voltammetry measurements were conducted under the same experimental conditions as before. The oxidation of the three monomers is shown in Figure 3.20(a). All have an irreversible oxidation wave at similar potentials. As can be seen, the electron-withdrawing NO₂ group does have an effect on the HOMO and of the three monomers, monomer **68** has the highest oxidation potential at $E^{1\text{ox}} = +0.40$ V. Without the electron-withdrawing moiety, the oxidation potential of **81** is 50 mV lower ($E^{1\text{ox}} = +0.35$ V) and the inductive Br group lowers this by a further 50 mV to $E^{1\text{ox}} = +0.30$ V for **82**.



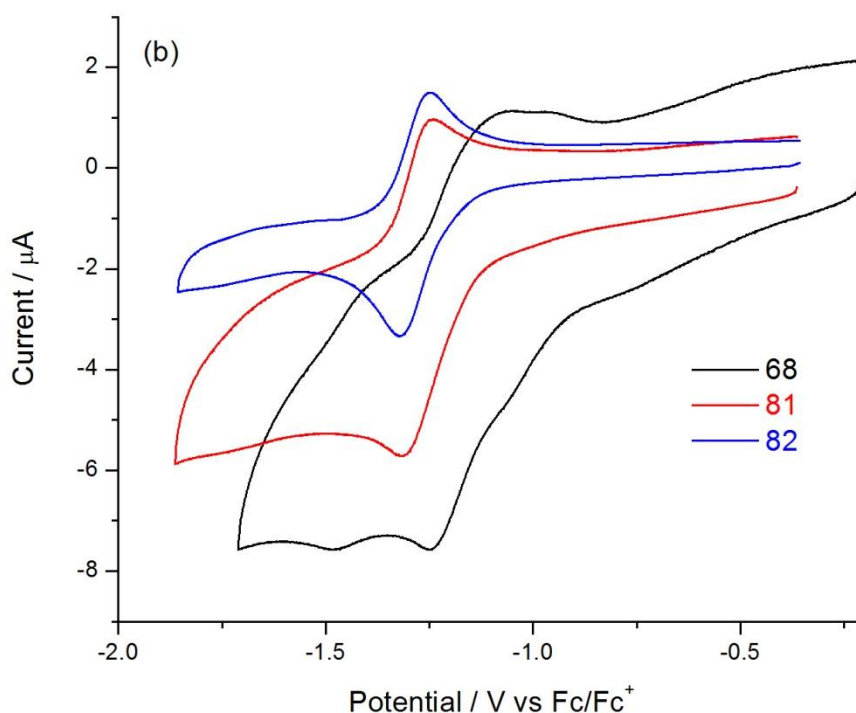


Figure 3.20 Cyclic voltammograms of (a) oxidation and (b) reduction of **68**, **81** and **82**.

Interestingly, the reduction characteristics of the monomers also significantly changes in two ways. The potential of the first reduction peak for the bromo and unsubstituted phenyl analogues has become more negative with respect to **68** ($E_{1/2}^{1\text{red}} = -1.17$, $E_{1/2}^{1\text{red}} = -1.28$, $E_{1/2}^{1\text{red}} = -1.29$ V for **68**, **81**, and **82**, respectively). Comparing **81** and **82**, the influence of the Br group actually has no effect on the reduction. In the absence of the NO_2 group there is no second reversible reduction wave ($E_{1/2}^{2\text{red}} = -1.44$ V), suggesting that this second wave is localised on the nitrophenylene group and the first is over the BODIPY core.

In the same manner as before, the electrochemical HOMO-LUMO gap was calculated from the difference in the onsets of the first oxidation and reduction

peaks. The HOMO and LUMO energy levels were calculated from the corresponding wave onsets with reference to ferrocene. The data are summarised in Table 3.7 and Table 3.8. Overall, as the electron-withdrawing NO₂ group affects both the oxidation and reduction of the monomer, removal of this results in the electrochemical HOMO-LUMO gap being very similar between the three monomers (1.46, 1.44, and 1.50 eV for **68**, **81**, and **82**, respectively).

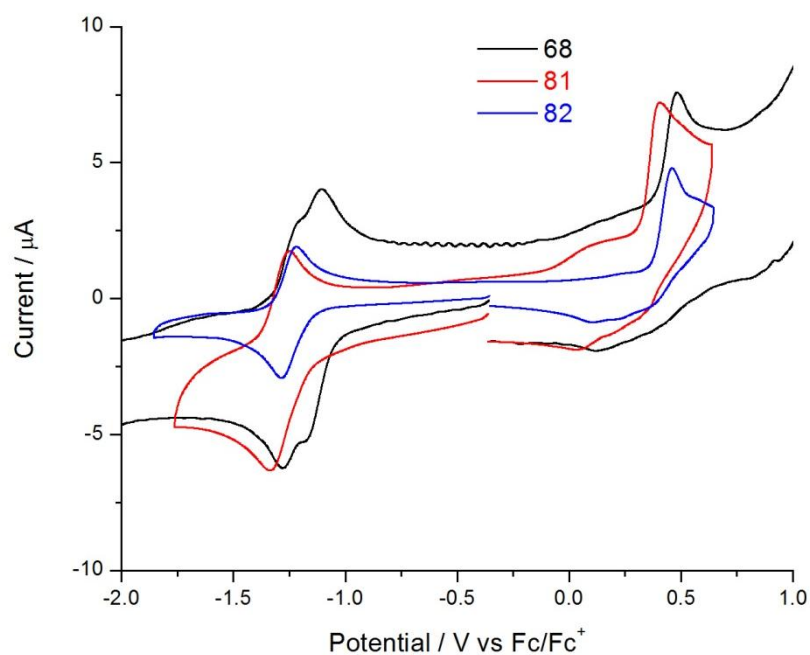


Figure 3.21 Cyclic voltammograms of **68**, **81** and **82** for energy level determination.

Table 3.7 Electronic absorption data for **68**, **81** and **82**.

| Monomer | UV Peaks / nm | | | Optical E _g / eV |
|-----------|---------------|-----|-----|--------------------------------|
| | 1 | 2 | 3 | |
| 68 | 349 | 444 | 663 | 1.70 |
| 81 | 344 | 437 | 646 | 1.83 |
| 82 | 347 | 442 | 651 | 1.82 |

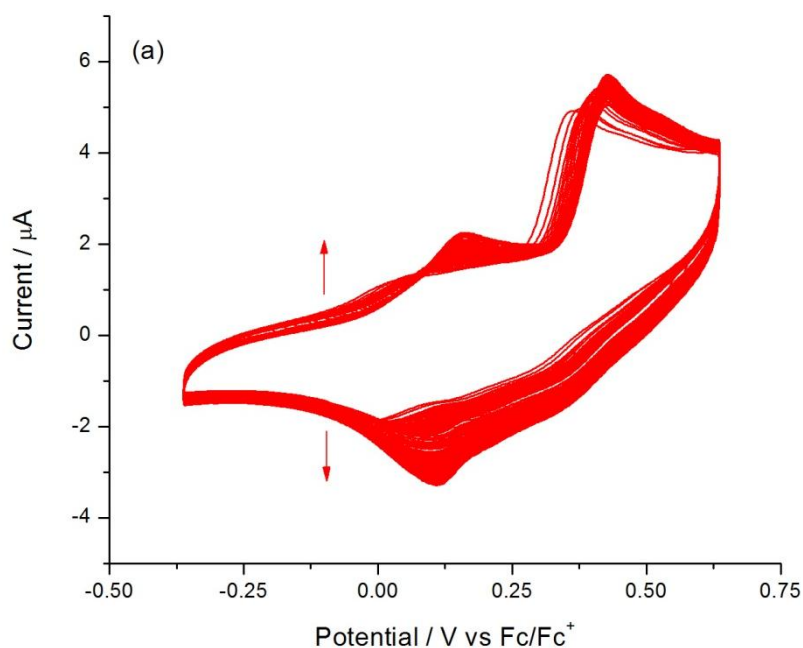
Table 3.8 Redox data for **68**, **81** and **82**.

| Monomer | E^{1ox} / V | E^{1red} / V | E^{2red} / V | HOMO / eV ^a | LUMO / eV ^a | E_g / eV^b |
|-----------|--------------------|----------------|----------------|------------------------|------------------------|--------------|
| 68 | +0.40 ⁱ | -1.25 / -1.09 | -1.48 / -1.40 | -5.20 | -3.74 | 1.46 |
| 81 | +0.35 ⁱ | -1.31 / -1.24 | - | -5.12 | -3.68 | 1.44 |
| 82 | +0.30 ⁱ | -1.32 / -1.25 | - | -5.17 | -3.67 | 1.50 |

^aHOMO and LUMO values are calculated from the onset of the first peak of the corresponding redox wave and referenced to ferrocene, which has a HOMO of -4.8 eV. ^b E_g is the HOMO-LUMO energy gap. ⁱIrreversible peak.

3.12.2 Electrochemical and Absorption Properties of Polymers

To compare the electrochemistry of the polymers, poly**81** and poly**82** were grown on the glassy carbon working electrode by repetitive cycling over the first oxidation peaks (Figure 3.22). Polymers grew readily and were detected by the development of a new peak at lower potential and increasing current response with each cycle. The growth of poly**68** is shown in Figure 3.5.



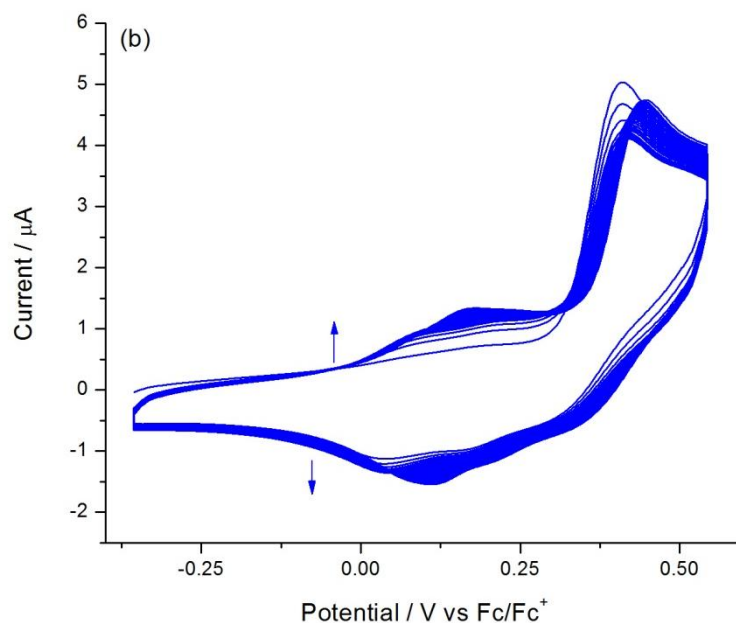


Figure 3.22 Electrochemical growth of (a) poly**81** and (b) poly**82**.

The electrochemistry of the polymers was investigated in monomer-free acetonitrile under the same experimental conditions as detailed on page 112. The oxidation of the three polymers is shown in Figure 3.23(a). The values are similar as each voltammogram represents the oxidation of the bis-EDOT units in the polymer chain ($E_{1/2}^{1ox} = +0.28, +0.29, \text{ and } +0.34 \text{ V}$, for poly**68**, poly**81**, and poly**82**, respectively).

There are two fascinating points to note. Firstly, the oxidation of poly**81** is a broad wave with $\Delta E_{pa-pc} = 30 \text{ mV}$, whereas the values for poly**68** and poly**82** are 20 mV and 8 mV, respectively. Secondly, the oxidation of **82** had the lowest potential for the monomers but its polymer has the highest oxidation half-wave potential. This, and the fact that the half-wave potentials for poly**68** and poly**81** are effectively the same, provides evidence that in the polymer form, the phenyl group has no influence on the HOMO energy levels.

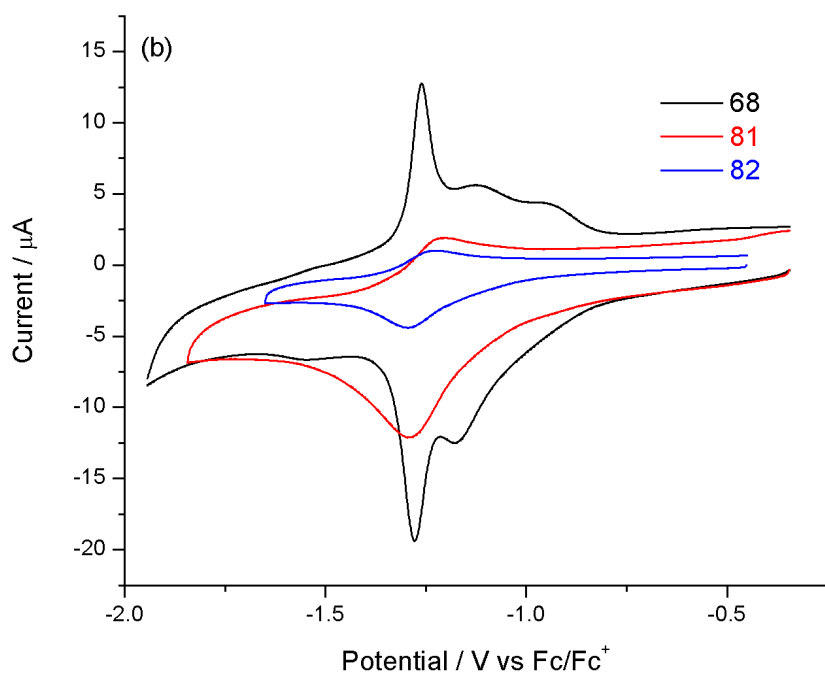
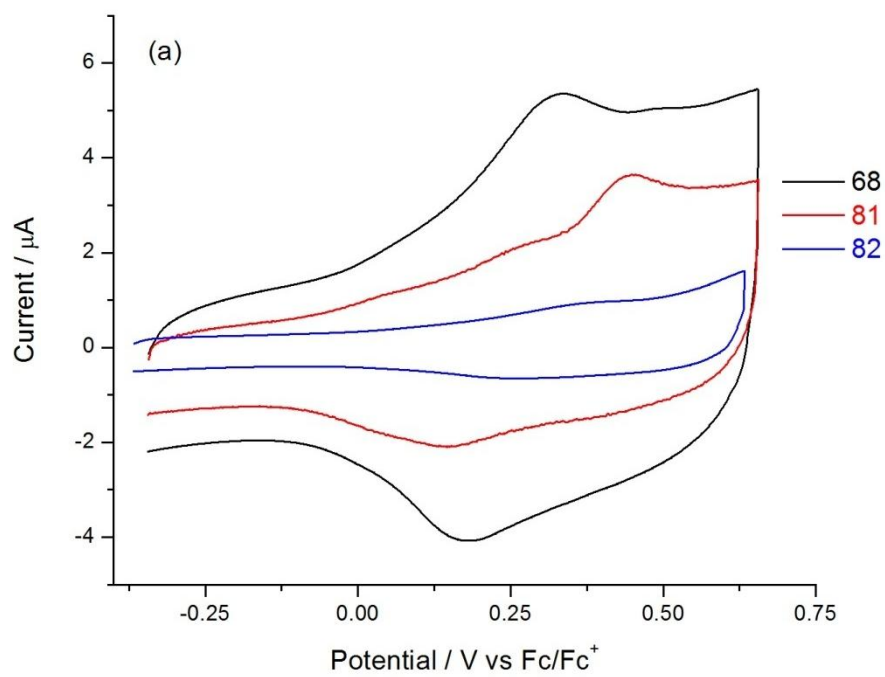


Figure 3.23 Cyclic voltammograms of (a) oxidation and (b) reduction of poly68, poly81 and poly82.

The reduction of poly**68**, poly**81**, and poly**82**, as shown in Figure 3.23(b), produces an interesting result. The first reduction wave of poly**68** as expected is of less negative potential ($E_{1/2}^{1\text{red}} = -1.17$ V compared to $E_{1/2}^{1\text{red}} = -1.28$ V for poly**81**, and $E_{1/2}^{1\text{red}} = -1.29$ V for poly**82**) due to the inclusion of the electron-withdrawing NO₂ group.

However, the second reduction wave ($E_{1/2}^{2\text{red}} = -1.27$ V) for poly**68** actually correlates better with the reduction of the other two polymers in terms of potential. It is likely therefore that in the polymer form, the nitrophenylene reduction is of less negative potential than the reduction of the pyrroles. In the monomer form, the reverse is true. This can be explained by taking into account that the bis-EDOT units have an electron-donating effect on the pyrrole groups, thus making them more difficult to reduce, whereas the nitrophenylene unit is more independent.

The electrochemical band gap of poly**81** and poly**82** were determined as described on page 114 (using onsets from Figure 3.24) and all the data including the oxidation and reduction potentials are summarised in Table 3.9. The energy levels calculated follow an expected trend: the HOMO levels become more stable and more negative with the removal of the NO₂ group and then with the addition of the Br group (-4.68, -4.76, and -4.96 eV for poly**68**, poly**81**, and poly**82**, respectively). The LUMO levels rise with the removal of the NO₂ group but there is no change observed with the addition of Br to the phenyl group (-3.88, -3.74, and -3.74 eV for poly**68**, poly**81**, and poly**82**, respectively). Consequently, the band gap increases in this series going from 0.8, 1.02, and 1.22 eV for poly**68**, poly**81**, and poly**82**, respectively.

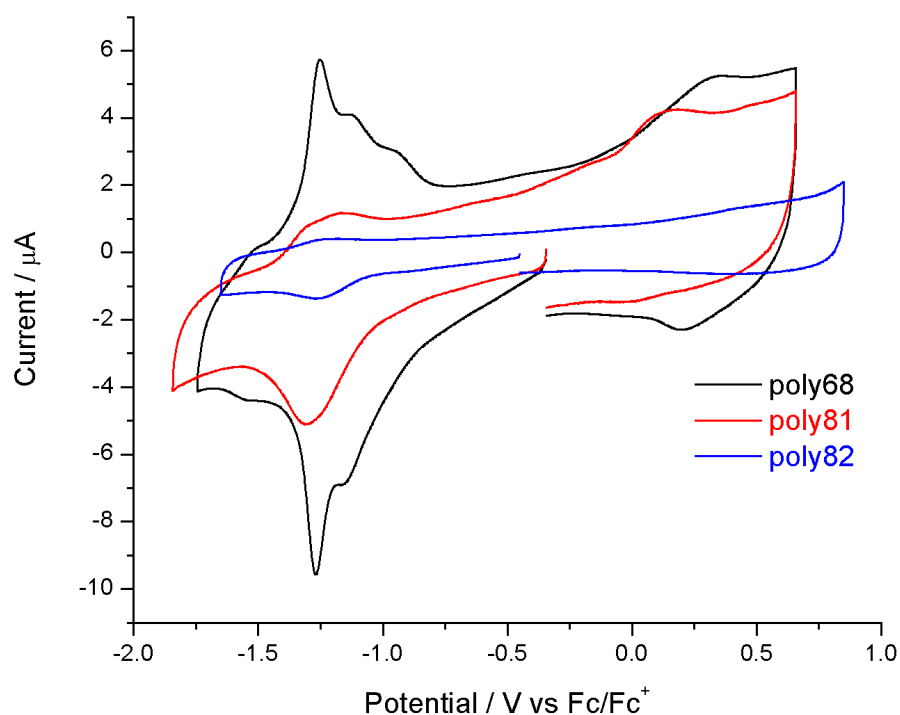


Figure 3.24 Cyclic voltammograms of poly**68**, poly**81** and poly**82** for energy level determination.

Table 3.9 Electrochemical data for poly**68**, poly**81** and poly**82**.

| Polymer | E^{1ox} / V | E^{1red} / V | E^{2red} / V | HOMO / eV ^a | LUMO / eV ^a | Band gap / eV ^b |
|----------------|------------------|-------------------|-------------------|---------------------------|---------------------------|-------------------------------|
| poly 68 | +0.38 / +0.18 | -1.13 / -1.12 | -1.28 / -1.26 | -4.68 | -3.88 | 0.8 |
| poly 81 | +0.44 / +0.14 | -1.28 / -1.21 | - | -4.76 | -3.74 | 1.02 |
| poly 82 | +0.38 / +0.30 | -1.30 / -1.23 | - | -4.96 | -3.74 | 1.22 |

^a HOMO and LUMO values are calculated from the onset of the first peak of the corresponding redox wave and referenced to ferrocene, which has a HOMO of -4.8 eV. ^b E_g is the HOMO-LUMO energy gap.

Scan rate experiments of poly**81** and poly**82** were performed on two freshly grown polymers on a glassy carbon electrode (Figure 3.25) to test if these polymers are also not diffusion limited. The scan rate experiment for poly**68** is shown in Figure 3.8. As

can be seen in Figure 3.26, R^2 values of 0.9987 for poly**81** and 0.9985 for poly**82** prove that the oxidations of the polymers are also not diffusion limited.

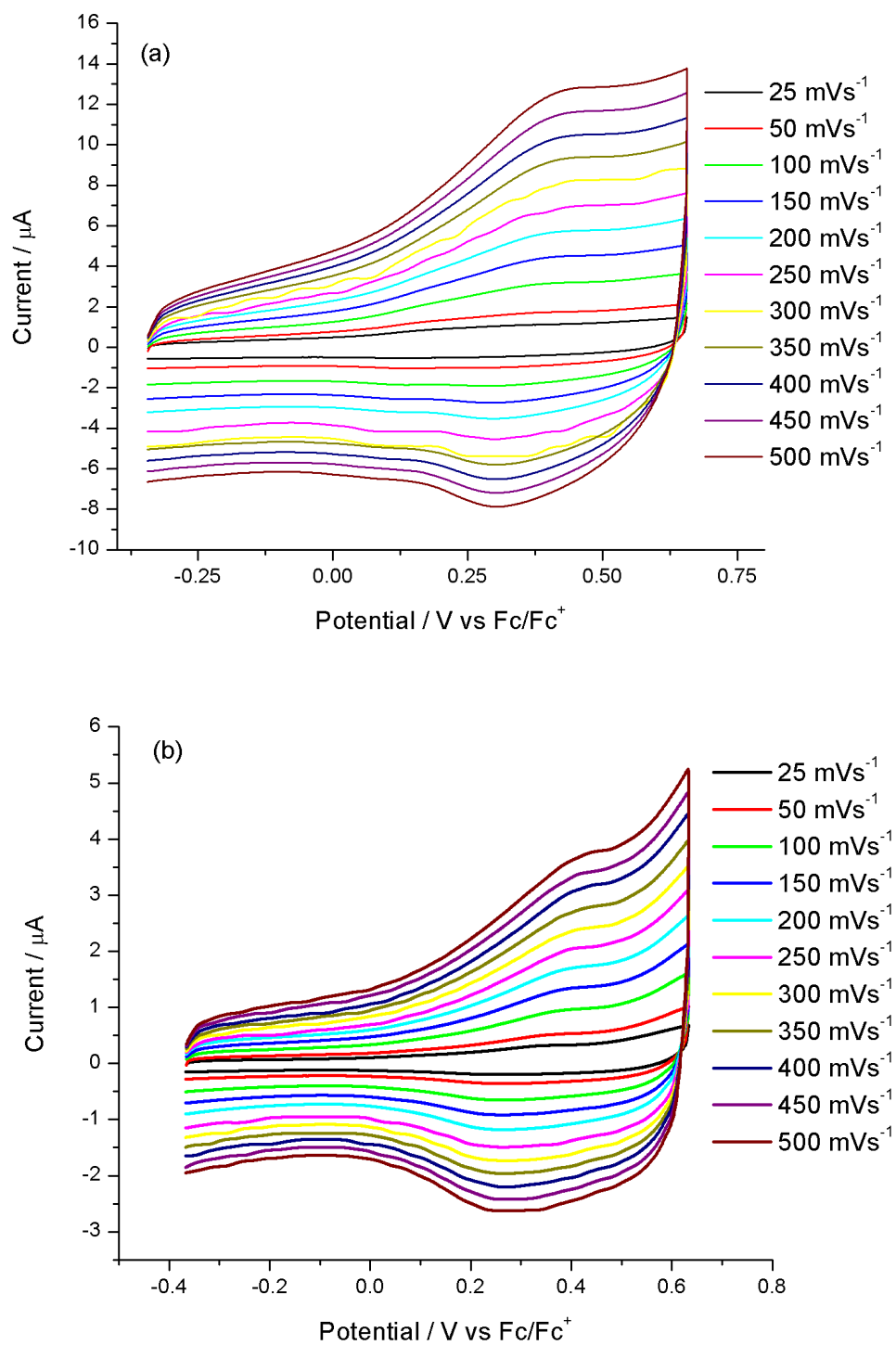


Figure 3.25 Cyclic Voltammograms with varying scan rates of (a) poly**81** and (b) poly**82**.

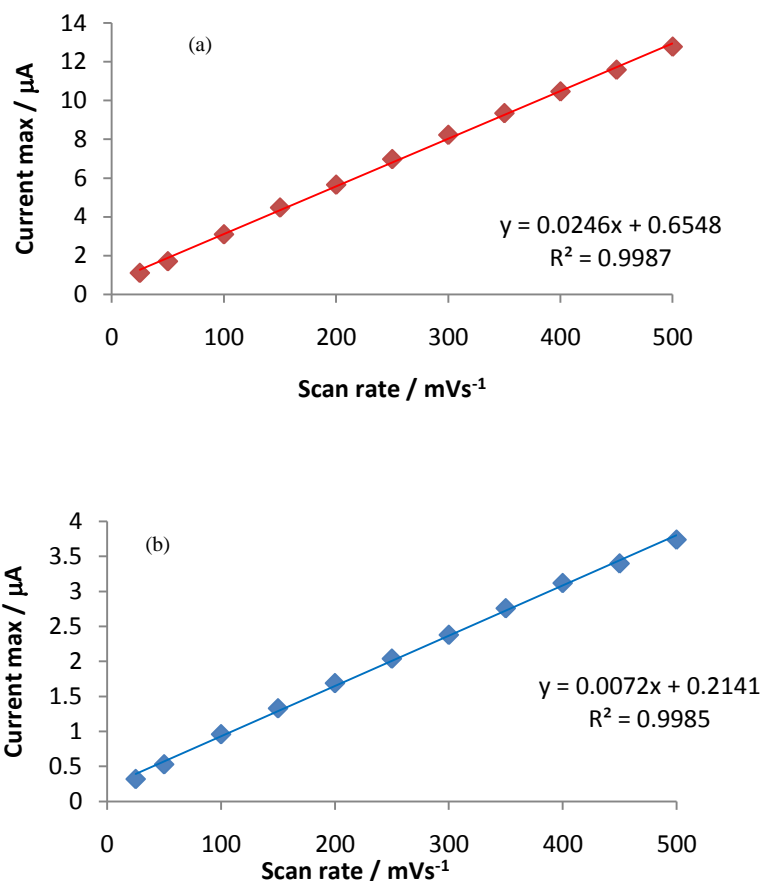


Figure 3.26 Plots of current max versus scan rate for (a) poly81 and (b) poly82.

The absorption spectra were recorded for poly81 and poly82 on ITO coated glass (but only up to 1100 nm). Figure 3.27 shows the solid state absorption of poly68, poly81 and poly82 with the data summarised in Table 3.10. Comparing the poly68 and poly81 spectra, two of the peaks have been shifted bathochromically from 419 to 441 nm and from 582 to 663 nm but the π - π^* transition peak is shifted hypsochromically (960 to 907 nm for poly68 to poly81). As the highest absorption edge does not reach baseline then no optical band gap could be calculated for poly81. Poly82 shows one main peak at 522 nm from the π - π^* transition and a small

shoulder at 658 nm. The optical band gap of this polymer was calculated to be 1.29 eV, an excellent correlation to the electrochemically determined band gap.

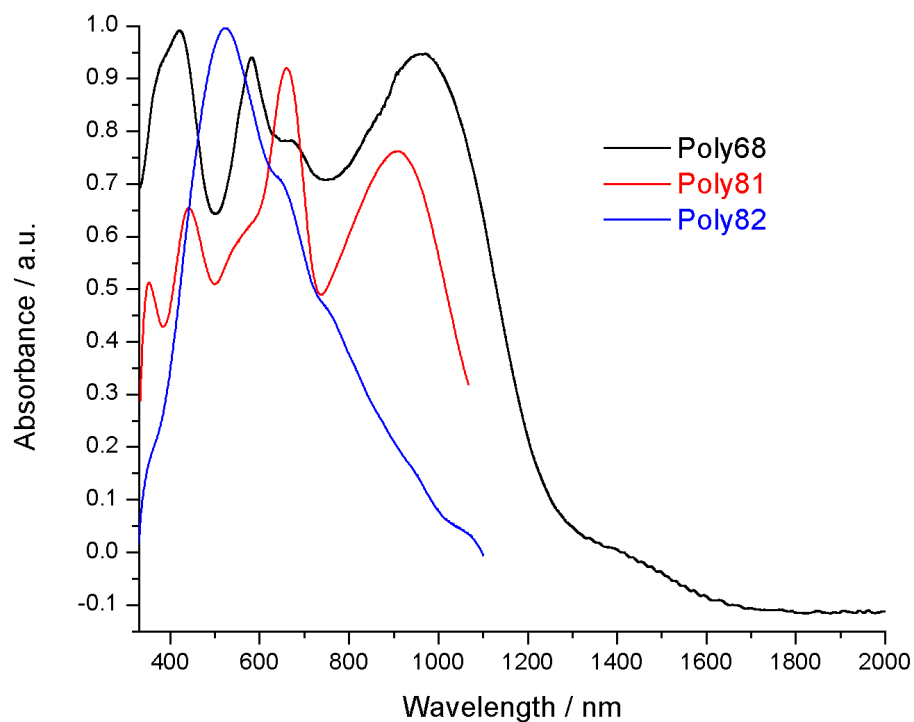


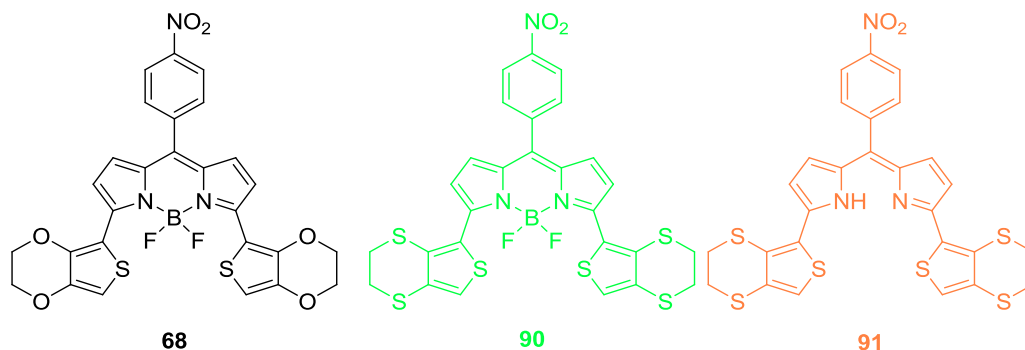
Figure 3.27 Solid state absorption spectra of poly68, poly81 and 82.

Table 3.10 Absorption data for poly68, poly81 and poly82.

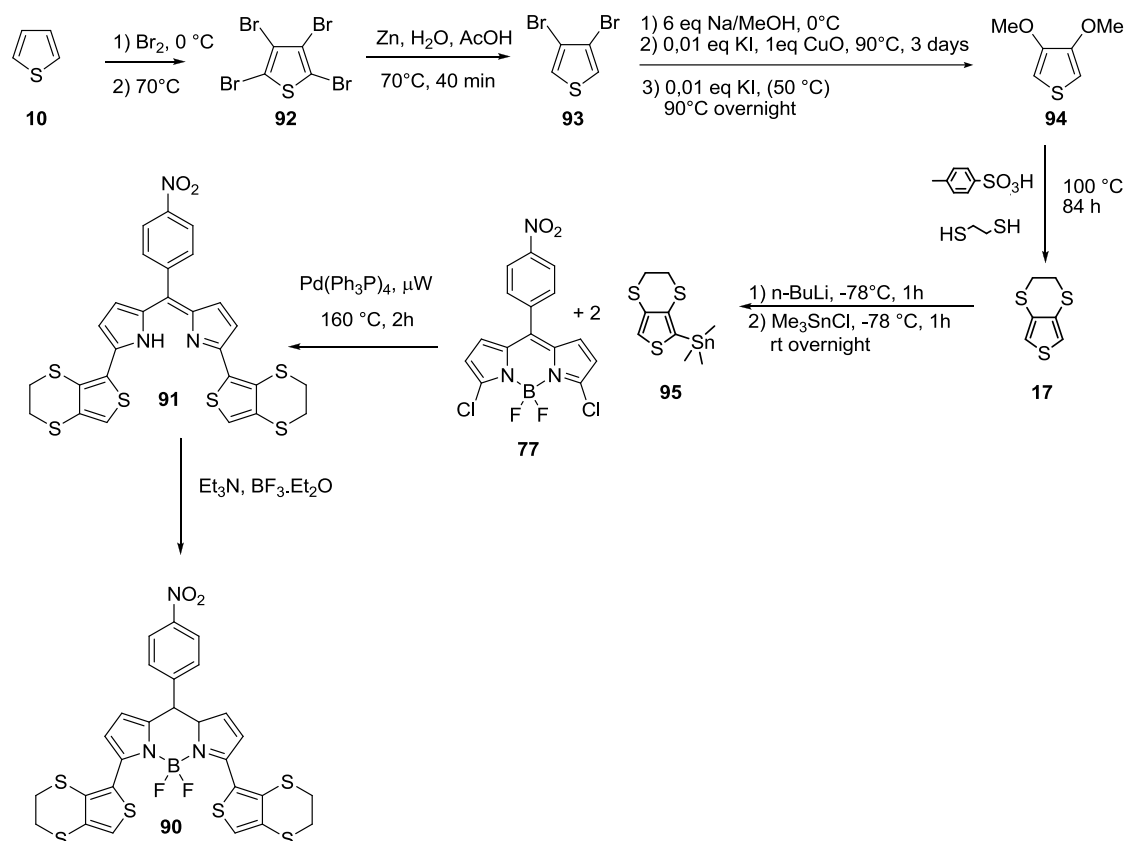
| Polymer | Absorption peaks / nm | | | Optical band gap |
|---------------|-----------------------|-----|-----|------------------|
| | 1 | 2 | 3 | / eV |
| poly68 | 419 | 582 | 960 | 0.8 |
| poly81 | 441 | 663 | 907 | - |
| poly82 | 522 | - | - | 1.29 |

3.13 Modifying the HOMO level: Comparison of BODIPY EDOT with EDTT open and closed-ring analogues

The best method for modifying the HOMO level of a donor-acceptor conjugated polymer is by manipulating the electron-rich electroactive units, which in this series of compounds is represented by the thiophene units. In molecules **90** and **91** the EDOTs have been replaced by EDTT units which should lower and stabilise the HOMO level in the polymer form. In **91**, which was a side-product from the synthesis of **90**, the BF₂ group is absent. This compound provided a means to investigate the influence of the BF₂ unit in the oxidation and reduction of the polymers presented in this chapter. The synthesis of **90** and **91** is shown in Scheme 3.3



Scheme 3.3 Synthesis of **90** and **91**.



3.13.1 Absorption spectroscopy and Electrochemistry of the monomers

The absorption spectra of monomers **90** and **91** were analysed in dichloromethane and are shown in Figure 3.28 along with the absorption spectrum of **68**. Interestingly, the peak at 444 nm for **68** and 465 nm for **90** is missing in the spectrum of **91**. Since the only structural difference between **91** and **90** is the BF_2 group, it can be said that this transition is from a lone pair on one of the fluorine atoms ($n\text{-}\pi^*$). This effect is also seen in **89** which is also without a BF_2 group (section 3.14.1).

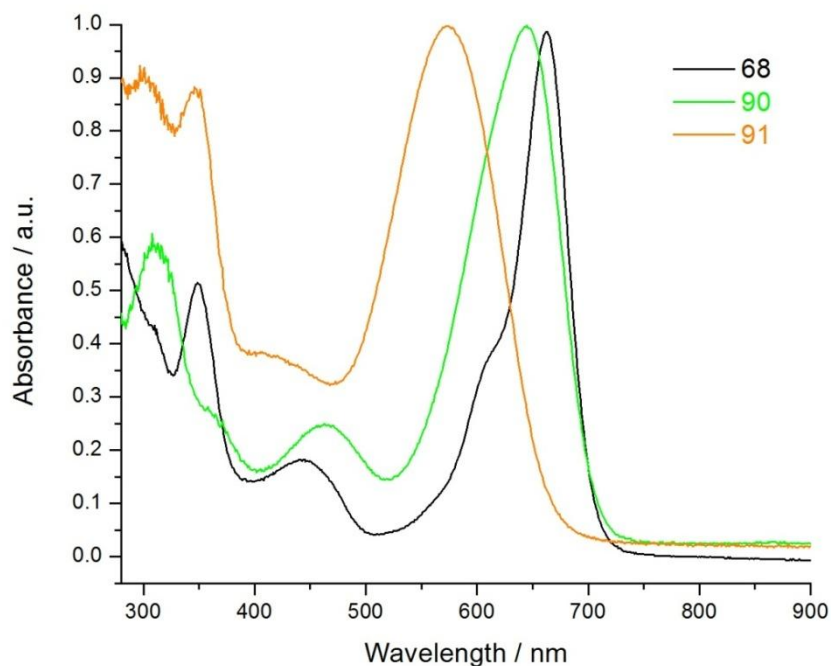


Figure 3.28 Solution state absorption spectra of **68**, **90** and **91**.

The π - π^* transition is blue-shifted for the two new monomers. The value of 663 nm for **68** has been shifted to 644 nm for **90** and 574 nm for **91**. Consequently, a range of optical HOMO-LUMO gaps is calculated for the three monomers. The HOMO-LUMO gaps determined are 1.70, 1.75, and 1.86 eV for **68**, **90**, and **91**, respectively. The effect of the BF_2 unit (or lack-of), on the energy levels will be explained later. All data are summarised in Table 3.11.

Table 3.11 Electronic and electrochemical data for **68**, **90** and **91**.

| Monomer | UV Peaks / nm | | | Optical E_g / eV |
|-----------|---------------|-----|-----|-----------------------|
| | 1 | 2 | 3 | |
| 68 | 349 | 444 | 663 | 1.70 |
| 90 | 312 | 465 | 644 | 1.75 |
| 91 | 303 | 347 | 574 | 1.86 |

Figure 3.29(a) shows the oxidation of the monomers. All three voltammograms show two irreversible waves. Unexpectedly, the oxidation of **90** is higher than the other two monomers. Monomers **68** and **91** have oxidation potentials of +0.40 and +0.45 V, respectively, whereas **90** has an oxidation potential of +0.63 V. This difference in oxidation potentials between **90** and **91** can be explained by considering the interaction between the thiophene and pyrrole groups. As seen in the computational analysis of monomer **68**, the HOMO energy level is distributed over the EDOT and pyrrole groups, despite the small twist out of planarity as a result of the fluorine / sulfur interaction. In monomer **90** it is conceivable that different non-covalent fluorine – sulfur interactions could also exist but in this case between the fluorine and a sulfur of the bridge. This could hold the thiophene group even more out of plane and consequently localise the HOMO solely on the EDTT group. Without the BF₂ groups in **91** the EDTT can align with the pyrrole through a sulfur-nitrogen interaction to once again allow the HOMO energy to be distributed over the thiophene and pyrrole groups. This explanation is theoretical and should be investigated by a computational study.

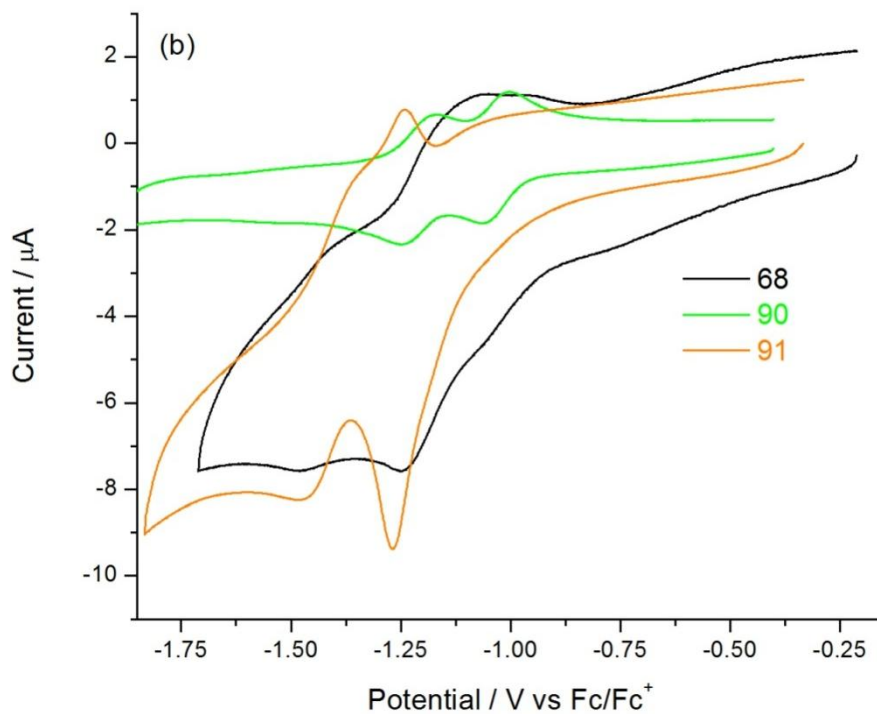
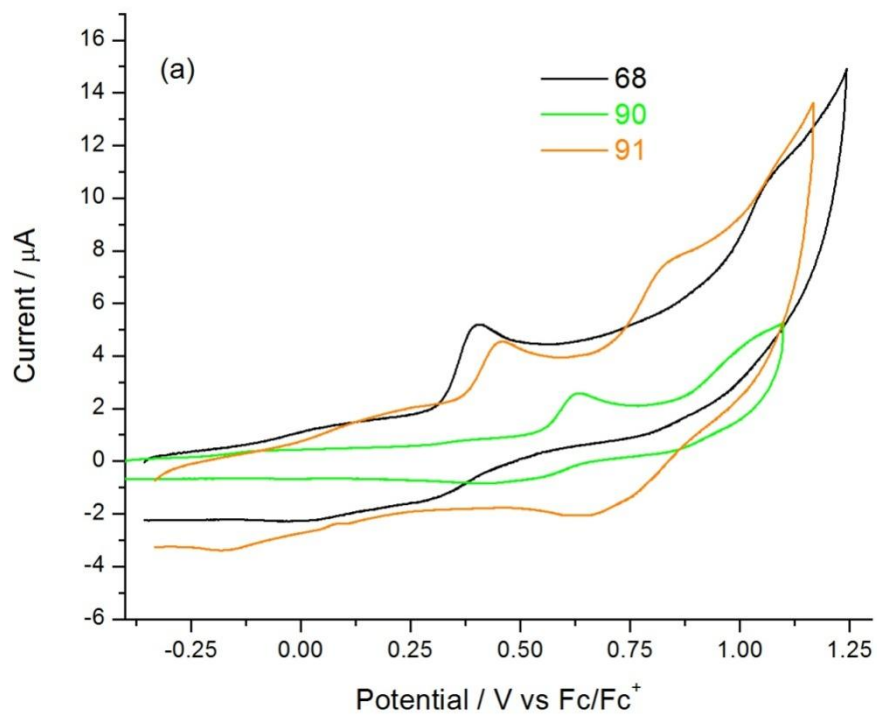


Figure 3.29 Cyclic Voltammograms of (a) oxidation and (b) reduction and **68**, **90** and **91**.

The reduction potentials are very similar for monomers **68** and **91**, with values of $E_{1/2}^{1\text{red}} = -1.17$, $E_{1/2}^{2\text{red}} = -1.44$ V for **68** and $E_{1/2}^{1\text{red}} = -1.26$, $E_{1/2}^{2\text{red}} = -1.41$ V for **91**. The reduction potentials of **90** are $E_{1/2}^{1\text{red}} = -1.04$, $E_{1/2}^{2\text{red}} = -1.21$ V; these potentials are lower than the other two monomers, because without the electron-donating effect from the EDTT groups, the pyrroles and nitrophenylene units reduce at a less negative potential.

The electrochemical HOMO-LUMO gaps of the three monomers were calculated as described on page 114 (from the onsets of first oxidation and reduction waves in Figure 3.30) and the data are summarised in Table 3.11 and Table 3.12. The HOMO level of **91** (-5.24 eV) is slightly lower than the HOMO of **68** (-5.20 eV), whilst the LUMO level is also slightly raised for **91** (-3.64 eV) compared to **68** (-3.74 eV). These values result in electrochemical band gaps of 1.60 and 1.46 eV for **91** and **68**, which is in good agreement with the optically determined HOMO-LUMO gaps. The HOMO and LUMO levels are expectedly lower for **90** but overall the HOMO-LUMO gap (1.55 eV) is in the same range as the other two monomers.

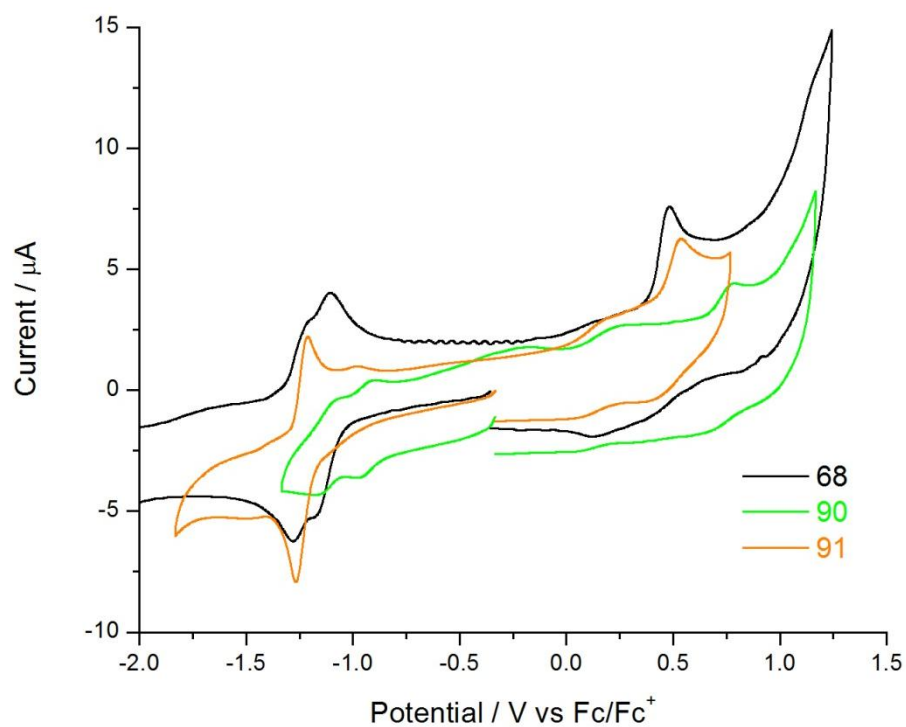


Figure 3.30 Cyclic voltammogram of **68**, **90** and **91** for energy level determination.

Table 3.12 Electrochemical data for **68**, **90** and **91**.

| Monomer | E^{1ox} / V | E^{1red} / V | E^{2red} / V | HOMO / eV ^a | LUMO / eV ^a | E_g / eV^b |
|-----------|--------------------|----------------|----------------|------------------------|------------------------|--------------|
| 68 | +0.40 ⁱ | -1.25 / -1.09 | -1.48 / -1.40 | -5.20 | -3.74 | 1.46 |
| 90 | +0.63 ⁱ | -1.07 / -1.00 | -1.25 / -1.17 | -5.40 | -3.85 | 1.55 |
| 91 | +0.45 ⁱ | -1.27 / -1.24 | -1.46 / -1.37 | -5.24 | -3.64 | 1.60 |

^aHOMO and LUMO values are calculated from the onset of the first peak of the corresponding redox wave and referenced to ferrocene, which has a HOMO of -4.8 eV. ^b E_g is the HOMO-LUMO energy gap. ⁱIrreversible peak

3.13.2 Electrochemical and Absorption Properties of Polymers

Polymers of **90** and **91** were grown onto the surface of a glassy carbon electrode and the corresponding growth traces are shown in Figure 3.31. The electrochemical growth of poly**68** was shown previously in Figure 3.5.

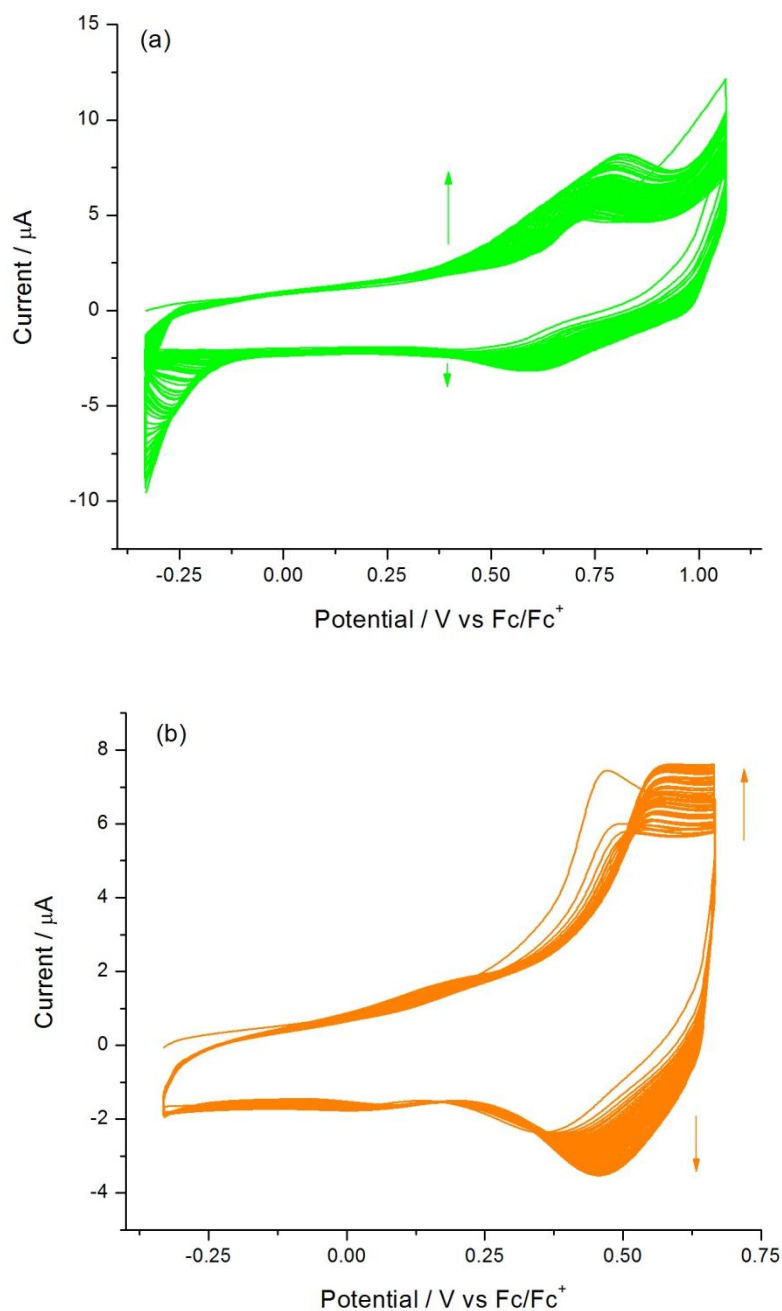


Figure 3.31 Electrochemical growth of (a) poly**90** and (b) poly**91**.

The new polymers were then analysed in monomer-free acetonitrile solution and the oxidation and reduction analyses are shown in Figure 3.32.

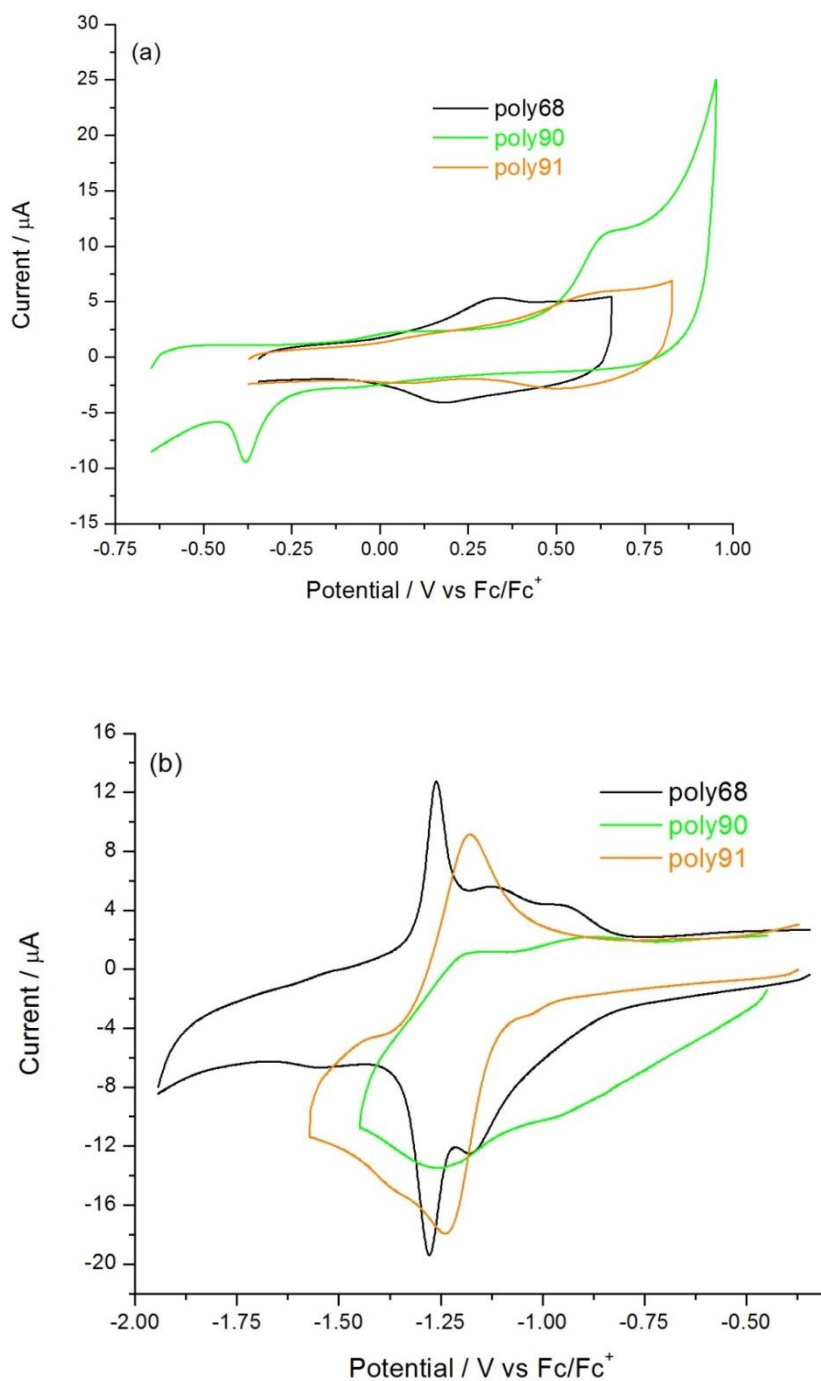


Figure 3.32 Cyclic voltammograms of (a) oxidation and (b) reduction of poly68, poly90 and poly91.

The oxidation processes for all three polymers are depicted in Figure 3.32(a). The oxidation of poly**90** is quasi-reversible, whereas the oxidation for the other two polymers is reversible. Closer examination of the oxidation of poly**90** shows a cathodic peak at -0.38 V which may be the reverse of the oxidation. The difficulty in the reversal of poly**90** could be a morphological effect rather than as a result of the EDTT groups being out of plane to the rest of the polymer, as the potential $E^{1ox} = +0.63$ is identical for both monomer and polymer. The half-wave oxidation of poly**91** was predicted to be greater and is +0.18 V higher ($E_{1/2}^{1ox} = +0.46$ V) than that of poly**68** ($E_{1/2}^{1ox} = +0.28$ V) due to the twisted nature of the bis-EDTT unit.

Examination of the polymer reduction potentials reveals an interesting anomaly. The reduction of poly**91** shows only one broad reversible wave at $E_{1/2}^{1red} = -1.20$ V, which is actually mid-way between the two reduction peaks of poly**68** ($E_{1/2}^{1red} = -1.13$ V for the nitrophenylene and $E_{1/2}^{2red} = -1.27$ V for the BODIPY/pyrrole core). It is likely therefore that this peak is a combination of these two reduction processes merged as one. This is a direct result of the removal of BF_2 group and not a switch to EDTT as poly**90** has two reduction waves ($E_{1/2}^{1red} = -0.90$ V and $E_{1/2}^{2red} = -1.22$ V).

To investigate the effect of substituting EDOT to EDTT and the removal of the BF_2 group on the energy levels and the band gap of the polymers, full cycles of the polymers (Figure 3.34) were recorded. The onsets of the first oxidation and reduction waves were subtracted from the HOMO of ferrocene (-4.8 eV) to give the HOMO and LUMO levels, respectively, for all three polymers. All data for the polymer oxidation, reduction and HOMO/LUMO energy levels are summarised in Table 3.13.

Comparison with the bis-EDOT-containing polymer poly**68** with the analogous bis-EDTT poly**90**, shows that substituting to EDTT has little effect on the LUMO level (-3.88 and -4.01 eV for poly**68** and poly**90**, respectively), but the HOMO of poly**90** is lower as a result of the non-planarity of bis-EDTT as discussed previously.

The electrochemical band gaps of poly**90** and poly**91** are identical (1.34 eV), suggesting that the removal of the BF₂ unit has no overall bearing on the band gap of the polymer. However, the HOMO and LUMO energy levels are in fact different for the polymers. The HOMO of poly**91** is higher than that of poly**90**, which implies that without the non-covalent sulfur-fluorine interaction the EDTT unit of poly**91** can align itself with the pyrrole group through non-covalent sulphur-nitrogen interactions. Such an arrangement would increase the effective conjugation length of the polymer, thereby lowering the oxidation potential and raising the HOMO level, as seen in the monomers.

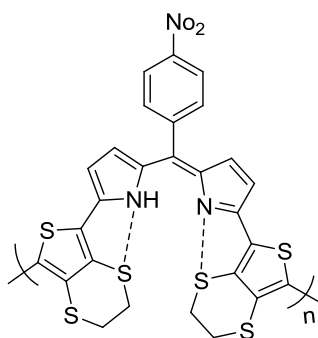


Figure 3.33 Alignment of sulfur-nitrogen interactions in poly**91**

Consequently, alignment of the EDTT with the pyrrole imparts an opposing effect on the LUMO level of the polymer. Through the electron-donating effect of the aromatic EDTT unit, the reduction of the polymer becomes more difficult and in return raises the LUMO level.

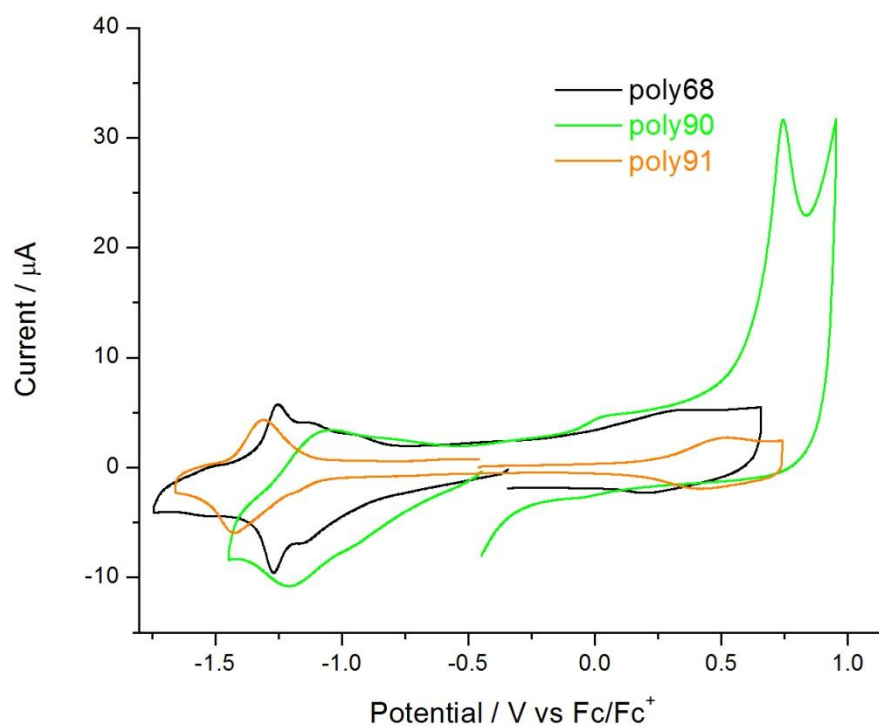


Figure 3.34 Cyclic voltammograms of poly68, poly90 and poly91 for energy level determination.

Table 3.13 Electrochemical data for poly68, poly90 and poly91.

| Polymer | E^{1ox} / V | E^{1red} / V | E^{2red} / V | HOMO / eV ^a | LUMO / eV ^a | Band gap / eV ^b |
|---------|------------------|-------------------|-------------------|---------------------------|---------------------------|-------------------------------|
| poly68 | +0.38 / +0.18 | -1.13 / -1.12 | -1.28 / -1.26 | -4.68 | -3.88 | 0.8 |
| poly90 | +0.63 / +0.38 | -0.93 / -0.88 | -1.25 / -1.18 | -5.35 | -4.01 | 1.34 |
| poly91 | +0.51 / +0.41 | -1.23 / -1.17 | - | -5.03 | -3.69 | 1.34 |

^a HOMO and LUMO values are calculated from the onset of the first peak of the corresponding redox wave and referenced to ferrocene, which has a HOMO of -4.8 eV. ^b E_g is the HOMO-LUMO energy gap.

Scan rate experiments were also performed for these two new polymers (Figure 3.35) and the resultant plots of current maximum versus scan rate are shown in Figure 3.36. The scan rate results for poly**68** are shown in Figure 3.8. The graphs show that like the other BODIPY polymers, they are not diffusion limited, $R^2 = 0.9952$, and 0.9886 for poly**90** and poly**91**, respectively.

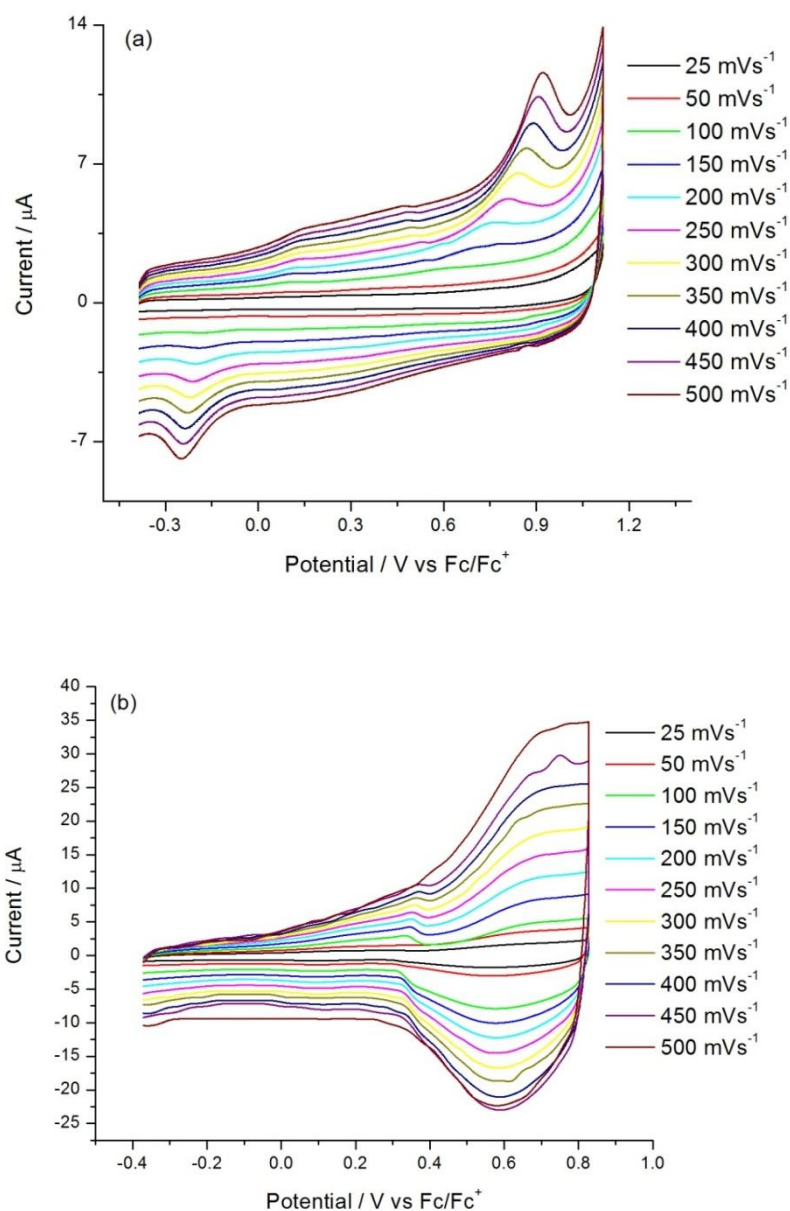


Figure 3.35 Cyclic voltammograms with varying scan rates for (a) poly**90** and (b) poly**91**.

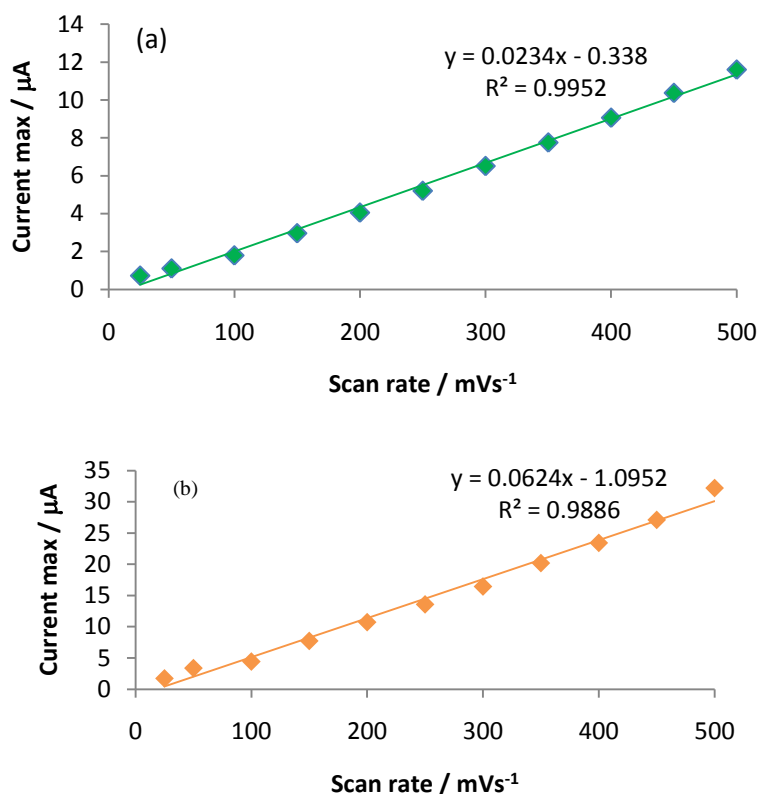


Figure 3.36 Plots of current max versus scan rate for (a) poly90 and (b) poly91.

The solid state absorption spectra of the polymers (Figure 3.37) were measured on ITO coated glass slides. Following electrodeposition, the polymers were dedoped and subsequent oxidation and reduction processes were investigated by CV. The data from these experiments are summarised in Table 3.14. The main peak for each of the two new polymers is the π - π^* transition at 634 and 614 nm for poly90 and poly91, which have been considerably blue-shifted from the π - π^* of poly68 (960 nm).

The optical band gaps of poly90 and poly91 were calculated from the onset of the longest wavelength absorption edge. For poly90, this is more difficult to determine as there is a small shoulder after the main π - π^* transition. The optical band gap is

estimated to be in the range 1.2-1.5 eV; the electrochemical band gap of poly**90** was determined to be 1.34 eV, which is in this range. It was easier to determine the optical band gap of poly**91** (1.35 eV) and this value was commensurate with that derived from electrochemical experiments.

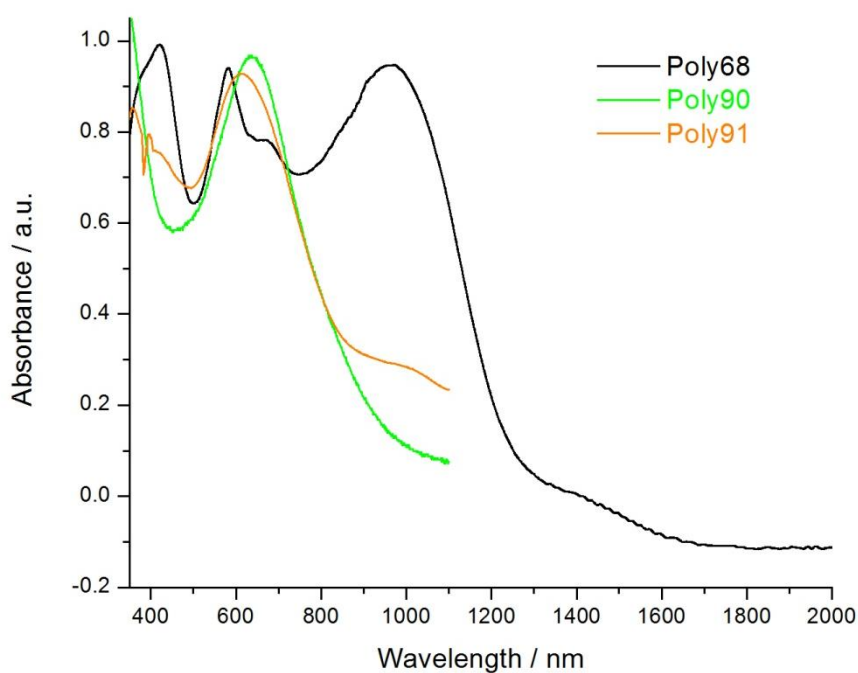


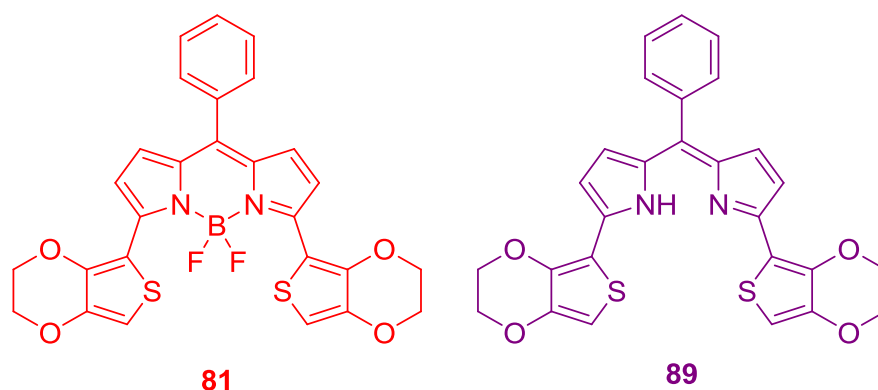
Figure 3.37 Solid state absorption spectra of poly**68**, poly**90** and poly**91**.

Table 3.14 Absorption data for poly**68**, poly**90** and poly**91**.

| Polymer | Absorption peaks / nm | | | Optical band gap / eV |
|---------------|-----------------------|-----|-----|-----------------------|
| | 1 | 2 | 3 | |
| poly68 | 419 | 582 | 960 | 0.8 |
| poly90 | 634 | - | - | 1.35 |
| poly91 | 614 | - | - | 1.2 – 1.5 |

3.14 The properties of open and closed BODIPY cores

To investigate further the effect of removing the BF₂ group from the BODIPY core in relation to the absorption properties and electrochemistry of the monomers and polymers, the following two molecules were analysed: **81** and **89**. Compound **81** was previously discussed in section 3.12.



3.14.1 Absorption spectroscopy and Electrochemistry of monomers

Figure 3.38 shows the solution state absorption spectra of monomers **81** and **89** recorded in dichloromethane. By comparing the maxima of the two compounds, it can be seen that there is a peak at 437 nm for **81** that is not seen in **89** and can be assigned to the n- π^* transition arising from the fluorine atoms in BF₂. This signature band is also seen in section 3.13.1 when comparing **90** and **91**, the low intensity of this band is typical of this type. The two other absorption peaks are also blue-shifted when comparing **89** (peaks at 331 and 574 nm) to **81** (peaks at 344 and 646 nm). As a result, the optical HOMO-LUMO gap of **89** (1.98 eV) is wider than that of **81** (1.83 eV). All data are summarised in Table 3.15.

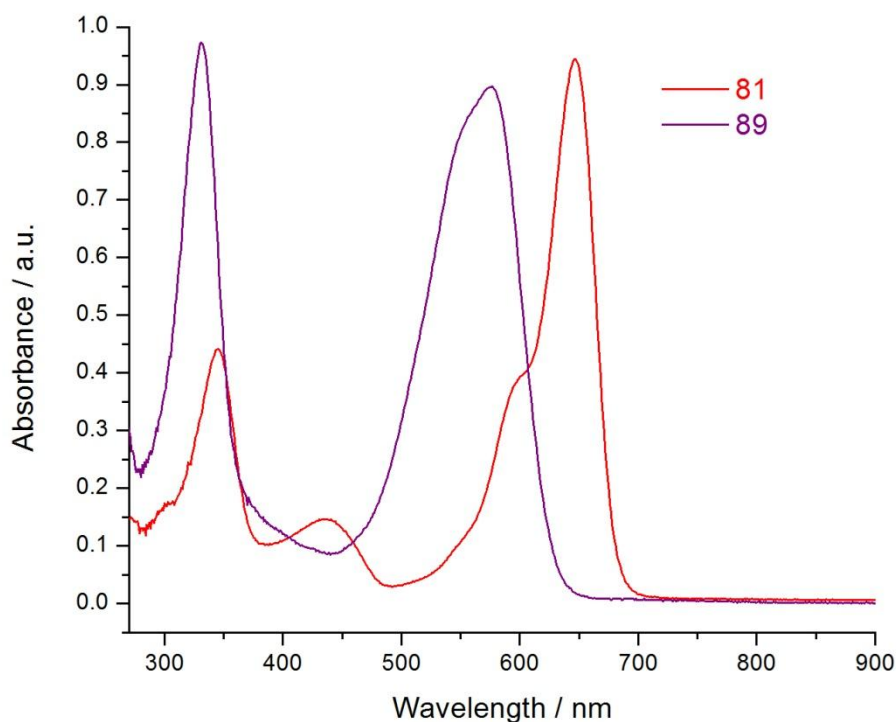


Figure 3.38 Solution state absorption spectra of **81** and **89**.

Table 3.15 Electronic absorption data for **81** and **89**.

| Monomer | UV Peaks / nm | | | Optical E_g / eV |
|-----------|---------------|-----|-----|-----------------------|
| | 1 | 2 | 3 | |
| 81 | 344 | 437 | 616 | 1.83 |
| 89 | 331 | 574 | - | 1.98 |

Cyclic voltammetry measurements were conducted for **89** (substrate concentration *ca.* 10^{-4} M) using glassy carbon, platinum wire and pseudo silver wire as the working, counter and reference electrodes, respectively. The supporting electrolyte was *n*-Bu₄NPF₆ (0.1 M) and dichloromethane was used as the solvent. The oxidation

of the two monomers is shown in Figure 3.39(a). Both compounds possess an irreversible peak at $E^{1\text{ox}} = +0.35$ V, implying that the BF_2 group has no influence on the oxidation potential of the monomers. The reduction process (Figure 3.39(b)) is considerably more negative for **89** ($E_{1/2}^{1\text{red}} = -1.54$ V), compared to **81** ($E_{1/2}^{1\text{red}} = -1.28$ V). The incorporation of the BF_2 group to the BODIPY core therefore has a stabilising effect on the reduction process.

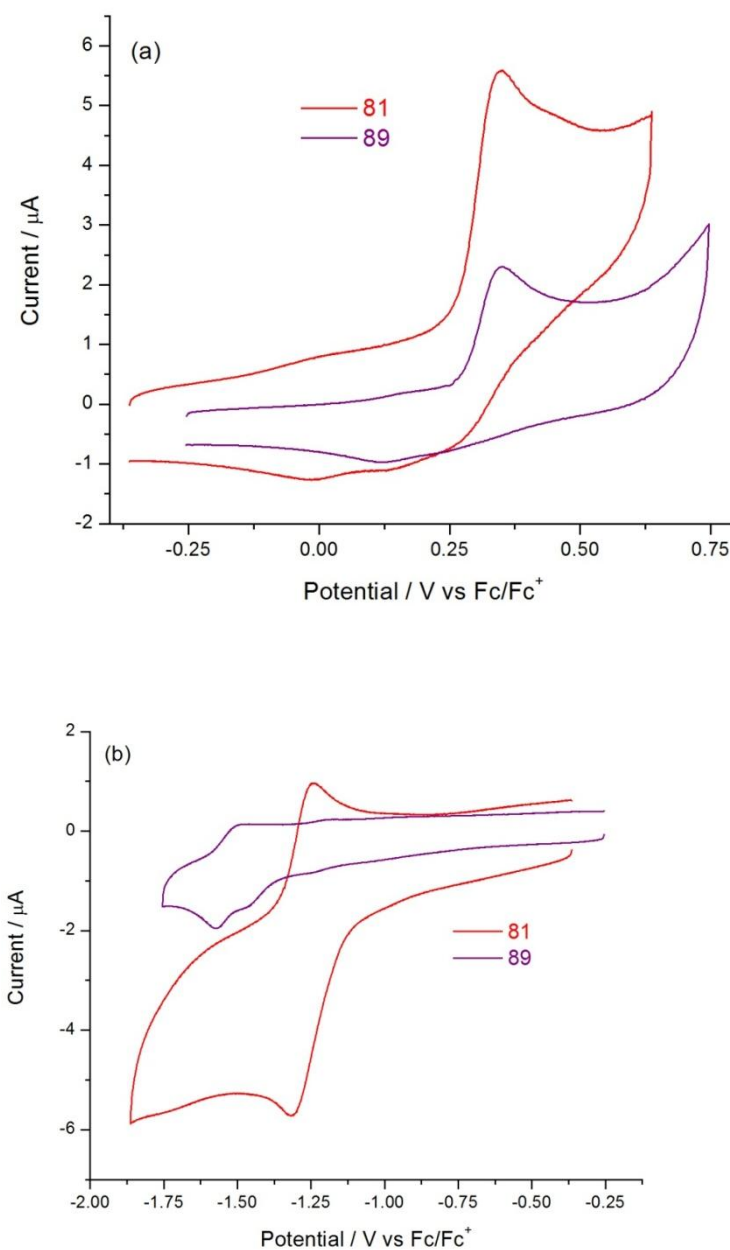


Figure 3.39 Cyclic Voltammograms of (a) oxidation and (b) reduction of **81** and **89**.

To investigate further, the electrochemical HOMO-LUMO gap of the new monomer was determined in the same manner as before by recording a cycle (Figure 3.40) containing the reduction and then oxidation of the monomer. Subtracting the onsets of the first oxidation and reduction peaks from the known HOMO of ferrocene (-4.8 eV) gives the HOMO and LUMO levels of the monomers. All data are summarised in Table 3.16.

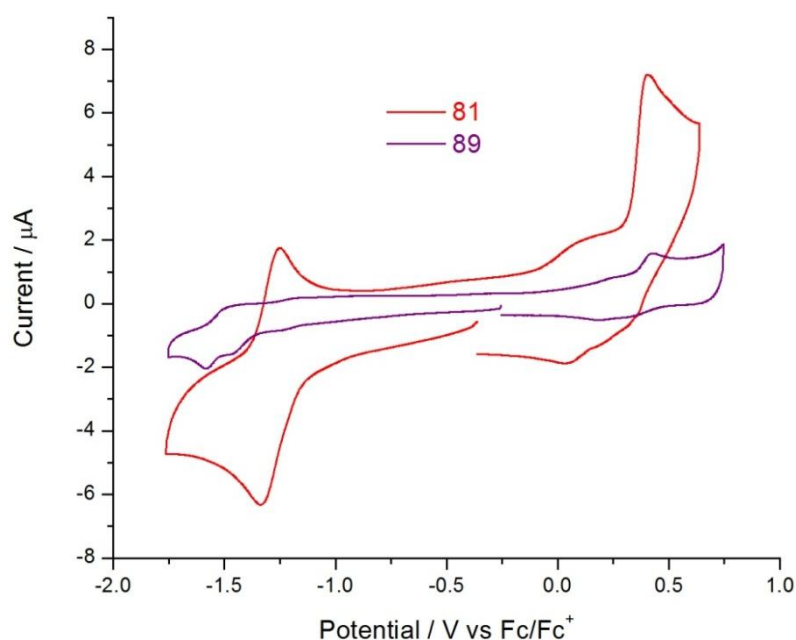


Figure 3.40 Cyclic voltammogram of **81** and **89** for energy level determination.

As expected, the HOMO energy levels for both monomers are almost identical (-5.12 and -5.13 eV for **81** and **89**, respectively), with the LUMO of **89** (-3.44 eV) higher than that of **81** (-3.68 eV). As seen in the optical HOMO-LUMO gap determination, the HOMO-LUMO gap of **89** (1.69 eV) is higher than that of **81** (1.44 eV).

Table 3.16 Electrochemical data for **81** and **89**.

| Monomer | $E^{\text{lox}} / \text{V}$ | $E^{\text{red}} / \text{V}$ | HOMO / eV ^a | LUMO / eV ^a | E_g / eV^b |
|-----------|-----------------------------|-----------------------------|------------------------|------------------------|---------------------|
| 81 | +0.35 ⁱ | -1.31/-1.24 | -5.12 | -3.68 | 1.44 |
| 89 | +0.35 ⁱ | -1.58/-1.50 | -5.13 | -3.44 | 1.69 |

^aHOMO and LUMO values are calculated from the onset of the first peak of the corresponding redox wave and referenced to ferrocene, which has a HOMO of -4.8 eV. ^b E_g is the HOMO-LUMO energy gap. ⁱIrreversible peak

3.14.2 Electrochemical and Absorption Properties of Polymers

To compare the properties of the polymers, poly**89** was grown electrochemically onto a glassy carbon working electrode (Figure 3.41). The growth of poly**81** was shown previously in Figure 3.22(a).

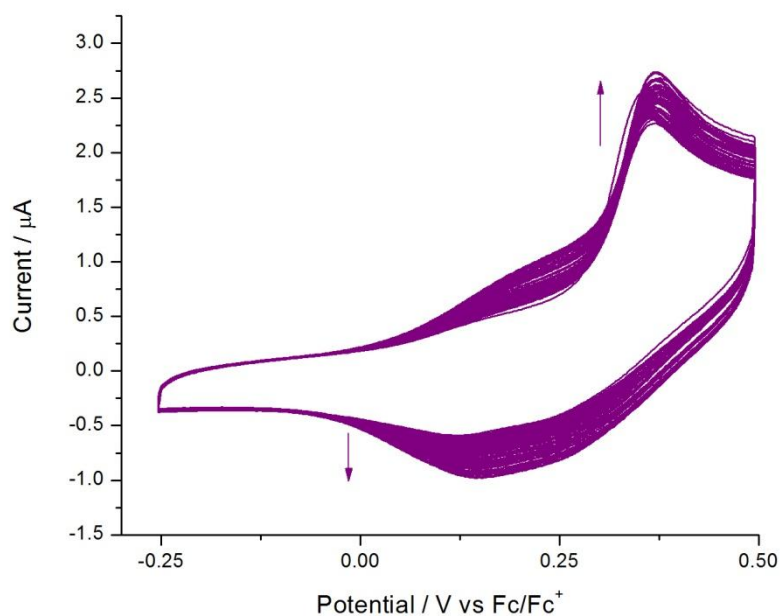
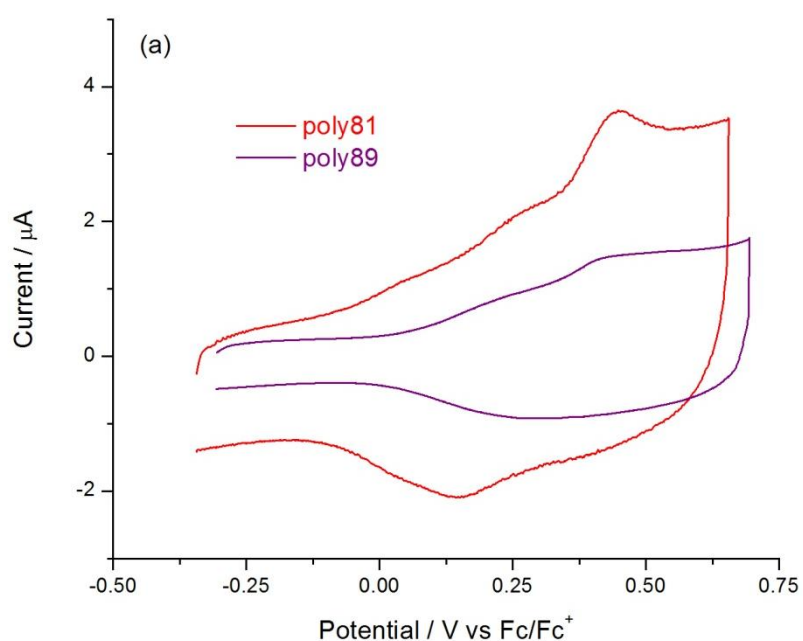


Figure 3.41 Electrochemical growth of poly**89**.

The electrochemical analyses of the polymers were performed in monomer-free acetonitrile solution. The oxidation waves for poly**81** and poly**89** are shown in Figure 3.42(a). The anodic peak of the oxidation is identical (+0.44 V) but the half-wave potential is lower for poly**81** ($E_{1/2}^{1ox} = +0.29$ V) compared to poly**89** ($E_{1/2}^{1ox} = +0.39$ V). The reduction processes of the polymers show a reversible wave and the reduction of poly**89** is at a more negative potential ($E_{1/2}^{1red} = -1.51$ V) than that of poly**81** ($E_{1/2}^{1red} = -1.25$ V).



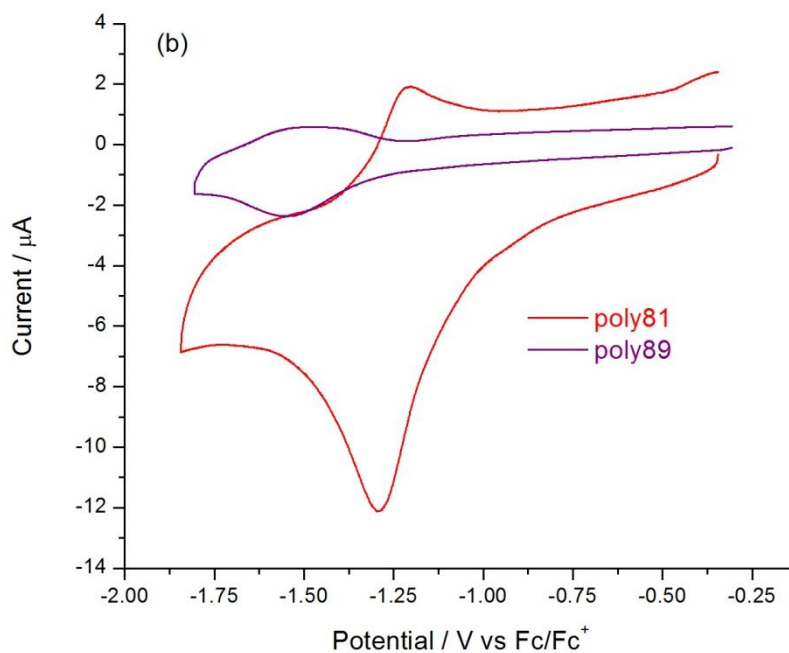


Figure 3.42 Cyclic voltammograms of (a) oxidation and (b) reduction of poly**81** and poly**89**.

The energy levels and the band gaps of the polymers were calculated using the same procedure described on page 112. The cycles for determining the onsets are shown in Figure 3.43 and the data are summarised in Table 3.17. The HOMO energy levels are similar at -4.76 eV and -4.67 eV for poly**81**, and poly**89**, respectively. Unlike the effect seen earlier (comparing **90** and **91**, where the removal of the BF₂ group allowed alignment of the EDTT group with the pyrrole which resulted in an increase in both the HOMO and LUMO levels), is not observed here. It is likely, therefore, that the bis-EDOT units does not form non-covalent (sulfur to nitrogen) interactions with the pyrrole rings. It can therefore be assumed that the sulfur in the sulfur-nitrogen interaction seen previously for poly**91** originates from the ethylenedisulfanyl bridge and not the sulfur in the thiophene ring.

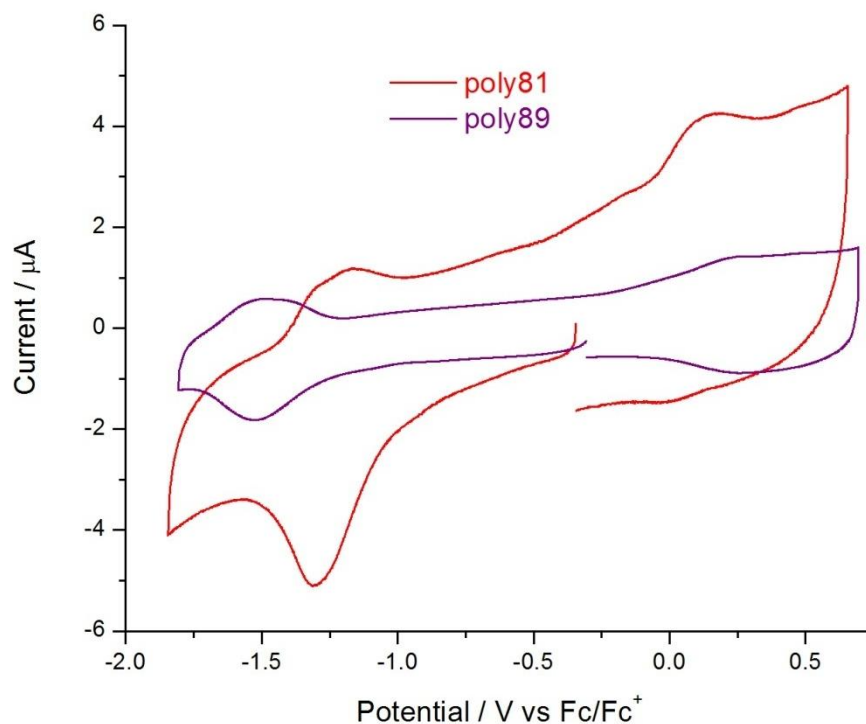


Figure 3.43 Cyclic voltammogram of poly**81** and poly**89** for energy level determination.

Table 3.17 Electrochemical data for poly**81** and poly**89**.

| Polymer | E^{1ox} / V | E^{1red} / V | HOMO / eV ^a | LUMO / eV ^a | Band gap / eV ^b |
|----------------|------------------|-------------------|---------------------------|---------------------------|-------------------------------|
| poly 81 | +0.44/+0.14 | -1.29/-1.21 | -4.76 | -3.74 | 1.02 |
| poly 89 | +0.44/+0.33 | -1.55/-1.47 | -4.67 | -3.59 | 1.08 |

^aHOMO and LUMO values are calculated from the onset of the first peak of the corresponding redox wave and referenced to ferrocene, which has a HOMO of -4.8 eV. ^b E_g is the HOMO-LUMO energy gap.

The diffusion properties of poly**89** were investigated by varying scan rates and measuring the current response (Figure 3.44(a)) of the first oxidation peak. The electrochemistry of the polymer was not diffusion limited as the R^2 value from the

plot of current versus scan rate (Figure 3.44(b)) gives a high correlation (0.9998).

The scan rate of poly**81** is shown in Figure 3.25 (a).

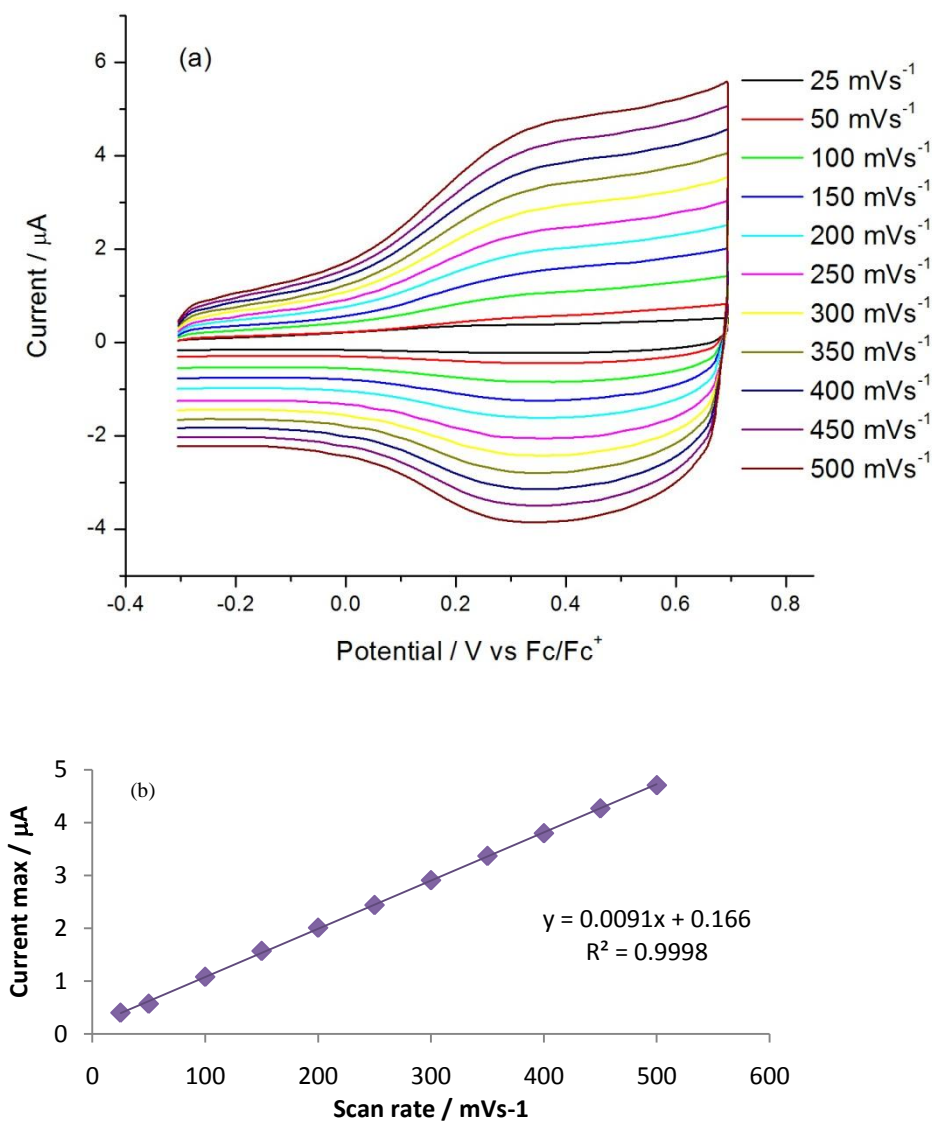


Figure 3.44 (a) Cyclic voltammograms of poly**89** with varying scan rate and (b) plot of current max vs. scan rate.

In the final comparison in this series, the absorption spectra of the polymers were recorded on ITO coated glass and dedoped (Figure 3.45 and Table 3.18). The spectrum for poly**89** show two maxima: **89** has a peak at 380 nm and a broad π - π^* transition peak (642 nm) with a small shoulder in the near-IR (*ca.* 1000 nm).

Calculating the optical band gap was difficult for these polymers, with the additional shoulders for poly**89** and poly**81** not reaching the baseline within the range of the spectrometer. Both onsets are around 1100 nm which correlates to a band gap of 1.1 eV, close to the electrochemically determined band gap.

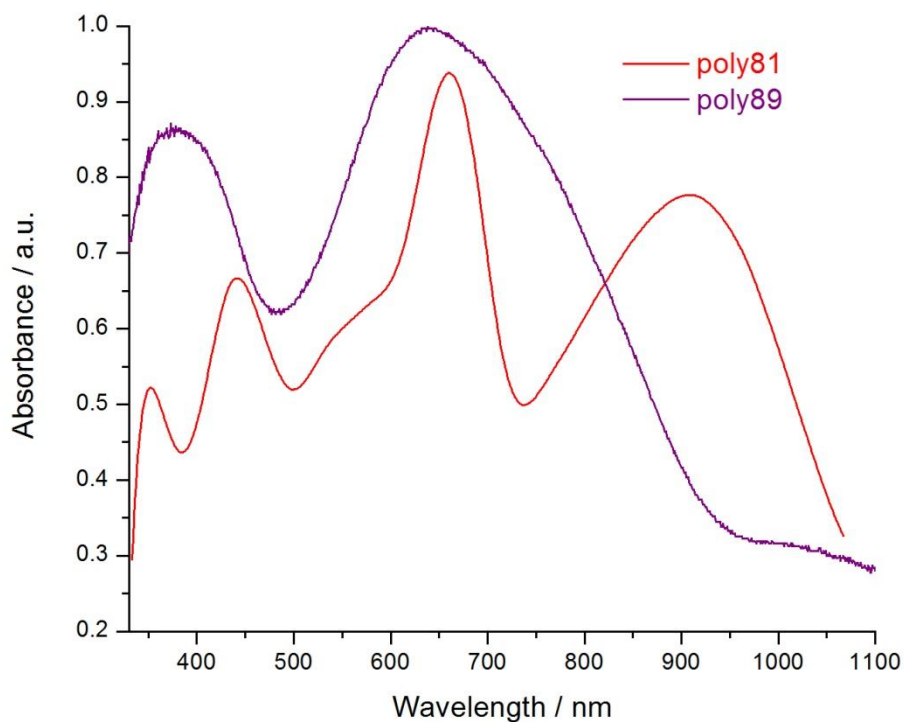


Figure 3.45 Solid state absorption spectra of poly**81** and poly**89**.

Table 3.18 Absorption data for poly**81** and poly**89**.

| Polymer | Absorption peaks / nm | | | Optical band gap / eV |
|----------------|-----------------------|-----|-----|-----------------------|
| | 1 | 2 | 3 | |
| poly 81 | 441 | 663 | 907 | 1.1 |
| poly 89 | 380 | 642 | - | 1.1 |

3.15 Conclusions and Further Work

The synthesis and analysis of a new conjugated polymer incorporating BODIPY in the main chain was successfully achieved. The highly efficient absorption characteristic of BODIPY gives attractive properties for potential use in organic photovoltaic devices. The first polymer (poly**68**) analysed gave a band gap of 0.8 eV which is too low for OPVs. An investigation was carried out into finding a more suitable polymer by modification of the structure to provide varying HOMO and LUMO levels.

The first modification was the removal of electron-withdrawing NO₂ group (**81**) and replacing it with an inductive bromine atom (**82**). The results showed that changing the properties of the nitrophenylene group through substitution affected the HOMO and LUMO characteristics. In the monomer, the oxidation potential was lowered by the addition of an inductive Br, but the reduction potential remained unchanged. In the polymers, the difference in HOMO levels was similar to those observed of the monomers, but the LUMO levels were the same for poly**81** and poly**82**.

The second modification was aimed at changing the HOMO level through replacement of the EDOT units with EDTT. The non-planar nature of the bis-EDTT repeat unit in the polymer main chain (poly**90**) provided a lowering of the HOMO level, compared to poly**68**. The effect of the BF₂ moiety was also investigated in the examination of poly**91** and was found to have a greater effect than expected. The molecular modelling of the **68** showed that a non-covalent sulphur-fluorine interaction held one thiophene above and one thiophene below the plane of the BODIPY unit. Without this interaction, the EDTT group was able to align itself with

the pyrrole group in the core to raise the HOMO level and consequently the LUMO level too.

Further investigation into the effect of removing the BF₂ group was completed with the comparison between two monomers and polymers that have EDOT as the polymerisable group (poly**81** and poly**89**). In these materials, it was found that only the monomer reduction was affected - the incorporation of the BF₂ functionality into the core facilitates the reduction of the compound.

The ideal characteristics required from a conjugated polymer for organic photovoltaic devices includes a LUMO of *ca.* -4 eV and a polymer band gap of 1.3 to 1.5 eV, if PCBM is applied as the acceptor unit.¹⁰⁵ By comparing all the polymers in this chapter, poly**90** is the best and would give a theoretical 10% power conversion efficiency in a working device (see section 1.15.2 for more details).

Further work in this project would be the development of a BODIPY polymer made chemically in bulk for device testing. The monomer will be manipulated to become more soluble by the addition of a long-chain alkyl or alkoxy group on either the pyrrole rings or in place of the NO₂ group. Other possible BODIPY monomers that could be created are ones containing 3,4-ethylenediselenothiophene (EDST), which is the selenium equivalent of EDOT, as the polymerisable group. The synthesis of a monomer with a third EDOT group in place of the NO₂ group is another possibility, from which a random cross-linked polymer may be obtained with intriguing and fascinating properties.

**Chapter 4. The Study of Unusual Extended
Conjugated Architectures.**

4.1 Abstract

In the first section, the synthesis and characterisation of two [4]-dendralene compounds incorporating thiophene-(p-nitrophenyl) donor–acceptor units are presented. The dendralenes adopt two different conformers in solution and solid state and the transformation between the structures can be controlled by light and heat. The electron donating components of the dendralenes are represented by bromothieryl (in **100**) and 3,4-ethylenedioxythiophene- (EDOT)-thieryl (in **101**) end-groups. The most facile transformation involves the isomerisation of donor–acceptor conjugated systems (**a** conformers) into structures in which only the thiophenes are conjugated (**b** conformers), and this process is driven by ambient light. The structural changes in both compounds have been monitored by absorption studies, transformations were found to be first-order processes with rate constants of $k = 0.0027 \text{ s}^{-1}$ and $k = 0.00022 \text{ s}^{-1}$ for **101** and **101**, respectively. The EDOT derivative (**101**) can be polymerised by electrochemical oxidation and a combination of cyclic voltammetry and UV-vis spectroelectrochemical experiments indicate that the a conformer can be trapped and stabilised in the solid state.

In the second section, three new diindenothienothiophene (DITT) based materials (**106 – 108**) were synthesised and their electrochemical properties investigated. The HOMO-LUMO gaps were observed to be 3.33, 3.48 and 2.81 eV, for **106**, **107** and **108**, respectively. Cyclic voltammetry results indicate increased stability for the alkylated derivatives. The dioxide exhibits strong photoluminescence, giving a photoluminescence quantum yield of 0.72 in solution and 0.14 in the solid state. Hole mobility measurements were carried out on the non-alkylated derivative and the corresponding values were $\sim 10^{-4} \text{ cm}^2 \text{ V}^{-1} \text{ s}^{-1}$.

4.2 Controlling the Conformational Changes in Donor-Acceptor [4]-Dendralenes through Intramolecular Charge-Transfer Processes

4.2.1 Introduction

Dendralenes (**96**) are a family of acyclic cross-conjugated polyenes that are known for their fascinating conformational and electronic properties.^{195, 196} The cross-conjugated nature of these molecules allows the structure to incorporate functional and unsaturated groups that are all conjugated to a central unsaturated core but not to each other. The naming of the dendralene depends on the number of C=C groups in the central core. From the figure below (Figure 4.1), the simplest dendralene, [3]-dendralene (**97**) is when $n = 1$. Expanding this structure, [4]-dendralene (**98**) is achieved from $n = 2$ and when $n = 3$, the molecule is termed a [5]-dendralene (**99**). Increasing the value of n gives higher dendralenes.

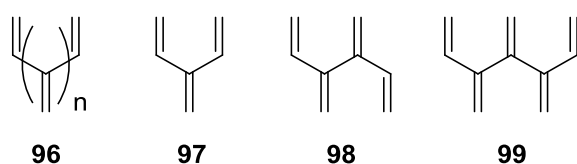
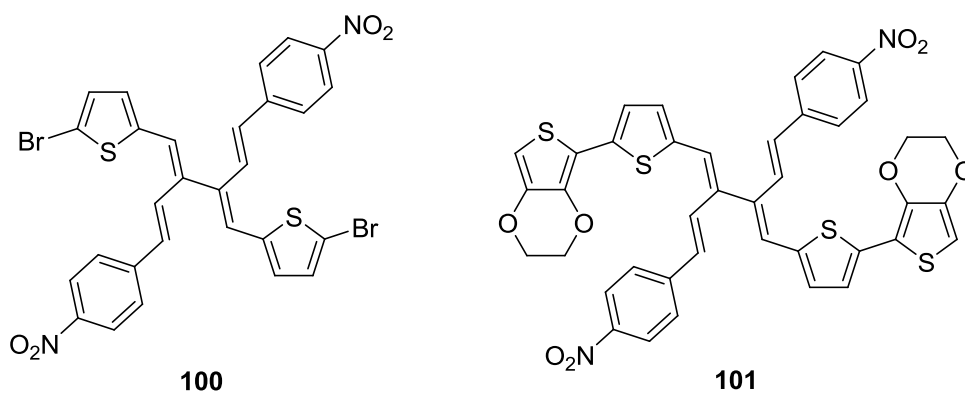


Figure 4.1 Sample structures of dendralene family

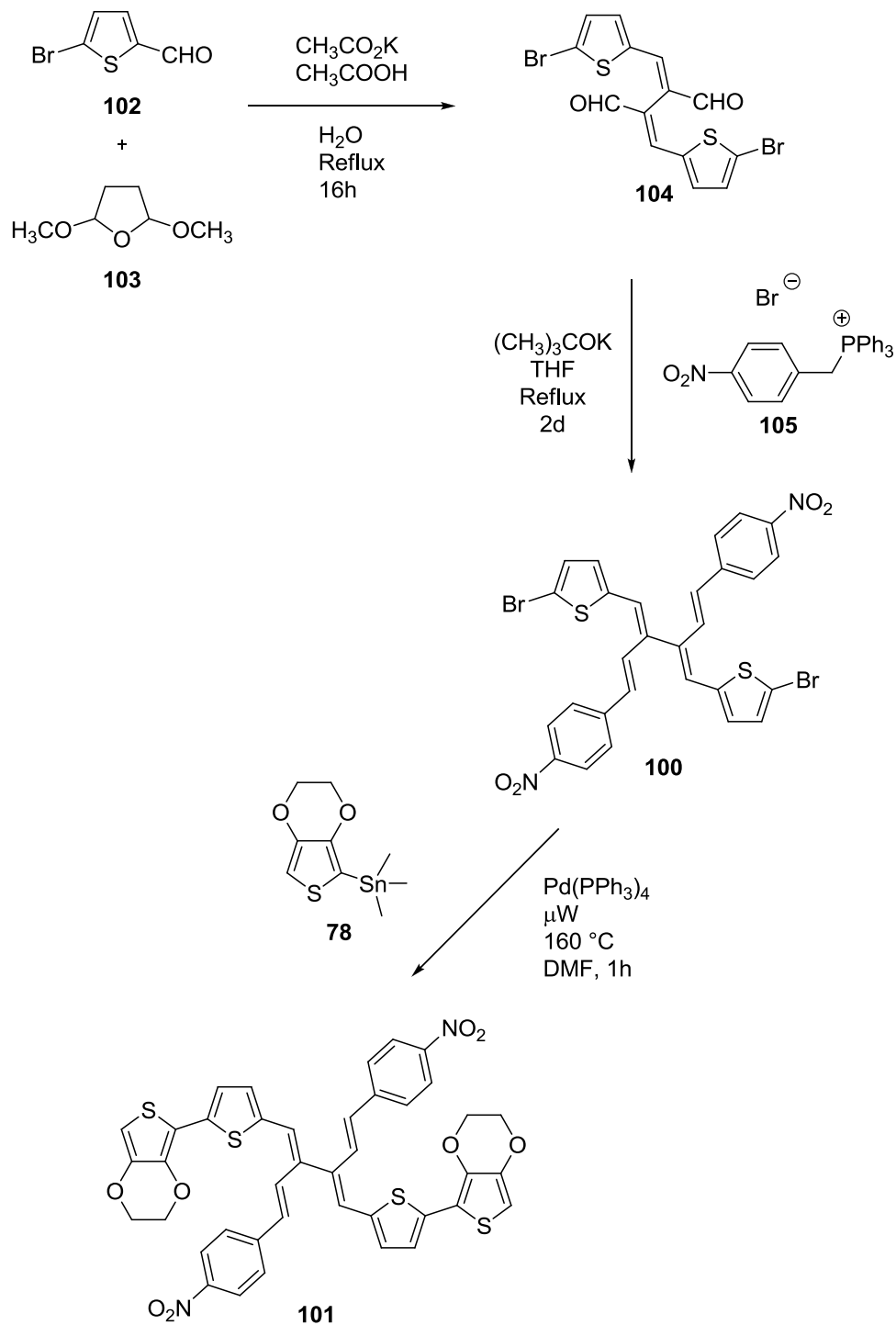
An interesting and recent study of conjugated materials has been the development of molecular and polymeric switches to control of the passage of electrons and molecular conformations through photochemical or electrochemical activation.¹⁹⁷⁻¹⁹⁹

For dendralenes, a conformational change has been shown by our group,²⁰⁰ and by others,²⁰¹ to change upon oxidation.

The first section of this chapter reports two new donor-acceptor dendralenes (**100** and **101**) that undergo a reversible conformational change from donor-acceptor to donor-donor conformations driven by light and heat. The second dendralene is extended with EDOT units to allow easy electropolymerisation,¹⁸³ and to allow investigations to ascertain which conformer is dominant in the polymer form. X-ray crystallography, evolution of absorption characteristics and electrochemistry are reported for **100**, along with a proposed mechanism for the conversion between the two conformers. Electronic and electrochemical studies for the monomer and polymer forms of **101** are also reported. The synthetic procedure for **100** and **101** are shown in Scheme 4.1.



Scheme 4.1 Synthesis of **100** and **101**.



4.2.2 Experimental

The synthesis of compounds **100** and **101** was performed by Thomas Westgate (University of Manchester), Alexander Kanibolotsky and Mir Munsif. Greg McEntee (University of Strathclyde) and Michael Auinger (Johannes Kepler University Linz) assisted with the UV absorption study. X-ray crystallographic studies were carried out by Simon Coles and Michael Hursthouse (University of Southampton).

Cyclic voltammetry measurements were performed on a CH Instruments 660A electrochemical workstation with *iR* compensation using anhydrous dichloromethane as the monomer solvent and acetonitrile for the monomer-free solvent. The electrodes were glassy carbon, platinum wire, and silver wire as the working, counter, and reference electrodes, respectively. All solutions were degassed (Ar) and contained monomer substrates at a concentration of *ca.* 10^{-4} M, together with *n*-Bu₄NPF₆ (0.1 M) as the supporting electrolyte. All measurements are referenced against the $E_{1/2}$ of the Fc/Fc⁺ redox couple. Spectroelectrochemical experiments were conducted on indium tin oxide (ITO) coated glass. Absorption spectra were recorded on a UNICAM UV 300 instrument.

4.2.3 X-ray crystallographic studies of 100

Crystals of **100** were grown using two different methods. In the first method, the crystals were grown in the dark producing **100a** (Figure 4.2 (top)) where the structure is in the donor-acceptor conformation. The second method allowed the crystals to be grown while exposed to ambient light, producing **100b** (Figure 4.2 (bottom)), a donor-donor conformation of the dendralene.

In the donor-acceptor conformation (**100a**), each bromothiophene is conjugated to a nitrobenzene unit through an all-*trans* butadiene bridge (C5-C6-C7-C8 and C19-C20-C21-C22) with a torsion angle between the two donor- π -acceptor units of $83.03(3)^\circ$. The single bond (C6-C20) that links the two orthogonal units is weakly conjugated with a C-C bond length of $1.497(3) \text{ \AA}$.

In the donor-donor conformation (**100b**), the bromothiophene units are co-planar and conjugated through an all-*trans* butadiene bridge (C5-C6-C6'-C5'). The nitrobenzene units are twisted out of plane of the bromothiophenes with a torsion angle of $99.94(4)^\circ$ (C5-C6-C7-C8). The C-C bond (C6-C7) between the styryl units and the butadiene fragment has a length of $1.481(4) \text{ \AA}$. The C=C bonds between α and β positions to the bromothiophene (C5/C6 and C19/C20 in **100a**) that possessed *cis* geometry in **100a** have changed to a *trans* geometry in **100b** (C5/C6 in **100b**).

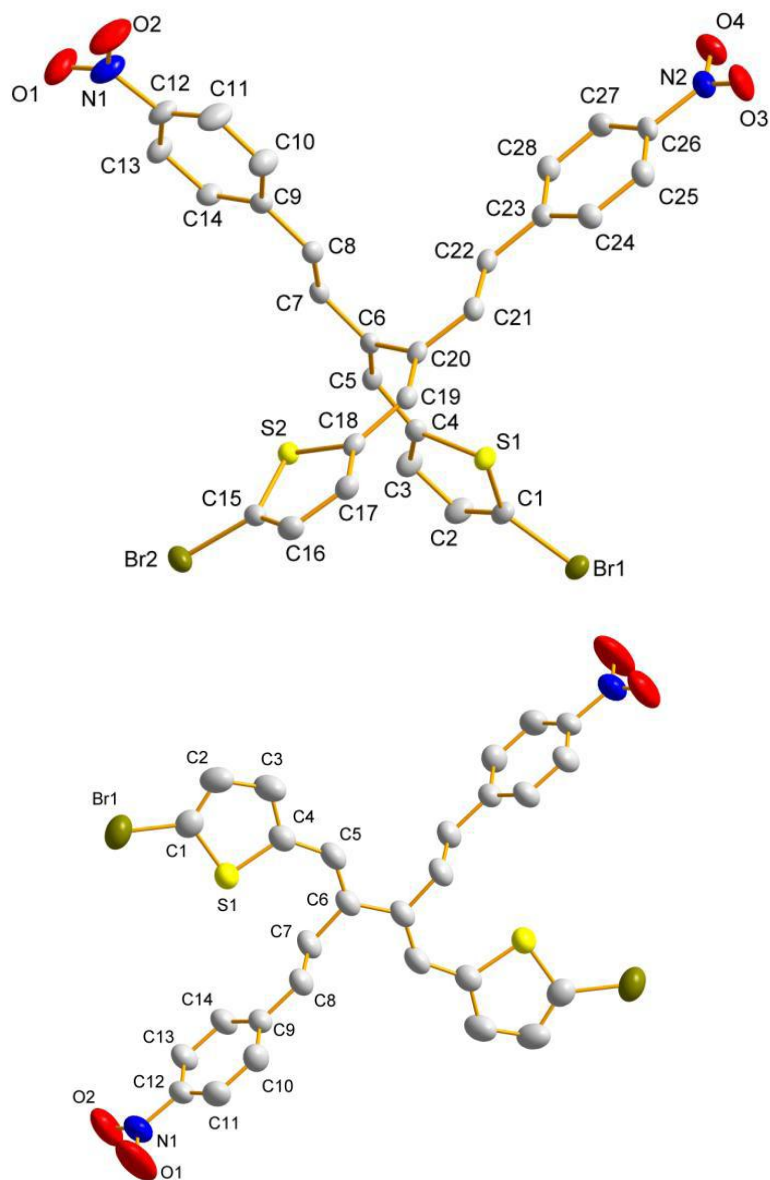


Figure 4.2 X-ray crystal structures of conformers **100a** (top) and **100b** (bottom).

4.2.4 UV-vis absorption studies of 100

The conversion of **100a** to **100b** can be observed by UV-vis spectroscopy. Crystals of **100a** were dissolved in dichloromethane in the absence of light then immediately recorded in the spectrometer. The longest wavelength absorption maximum can be seen at 403 nm and can be ascribed to an intramolecular charge transfer (ICT) process between the donor and acceptor units. If ambient light is allowed to irradiate the solution, the maximum wavelength decreases and is slightly blue-shifted by 6 nm to $\lambda = 397$ nm. The intensity of the longest wavelength band decreases with more exposure time and the decrease is accompanied with the development of a new band at $\lambda = 320$ nm. This new peak is obscured somewhat due to the intensity poor signal to noise ratio, but an isosbestic point can be seen clearly. The evolution of **100a** to **100b** over time is shown in Figure 4.3. If the solution is not exposed to light, then any point in the spectrum is repeatable during the process.

The rate of change for the absorbance at $\lambda = 403$ nm is shown in Figure 4.4. The data are a good fit to the first-order rate law and the uniformity of the transformation is reinforced by the clear presence of an isosbestic point. The first-order rate constant was solved to give values of $k = 0.161 \text{ min}^{-1}$, or 0.0027 s^{-1} . The noise levels for $\lambda = 320$ nm meant that a rate constant could not be calculated at this wavelength to confirm the rate constant calculated from the change in absorbance at 403 nm.

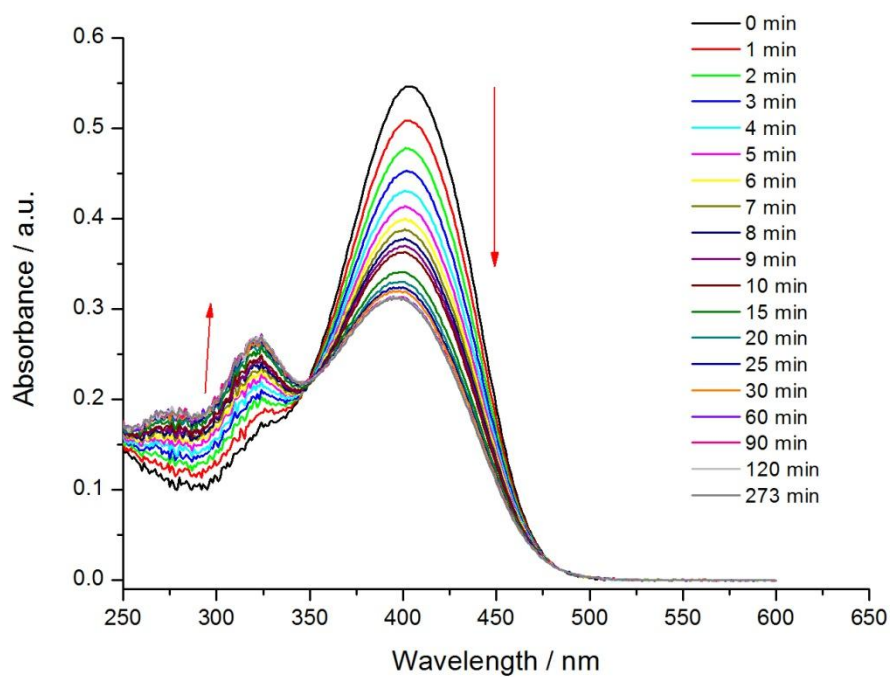


Figure 4.3 Evolution of UV-vis absorption spectra of **100a** over time whilst the sample is exposed to ambient light

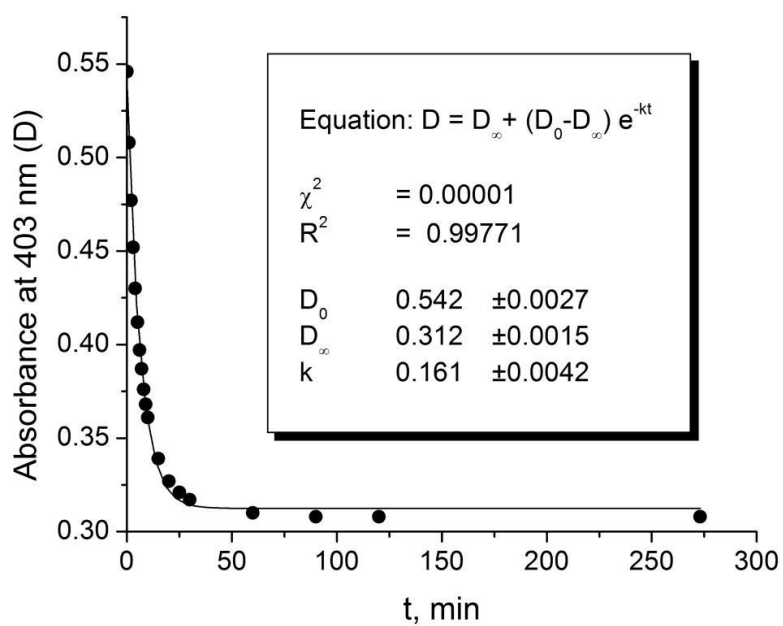


Figure 4.4 Kinetic plot of the rate change of **100**

4.2.5 Cyclic voltammetry of **100a**

A solution of **100a** (*ca.* 10^{-4} M) with supporting electrolyte was prepared with dichloromethane as the solvent in the absence of light. A cyclic voltammetry experiment was used to probe the oxidation of **100a** in the dark and then the measurement was repeated after exposure to ambient light. In the absence of light, **100a** has an oxidation potential at $E^{1\text{ox}} = +1.03$ V which shifts gradually to a lower potential with subsequent exposures of light before, stabilising at $+0.91$ V as shown in Figure 4.5.

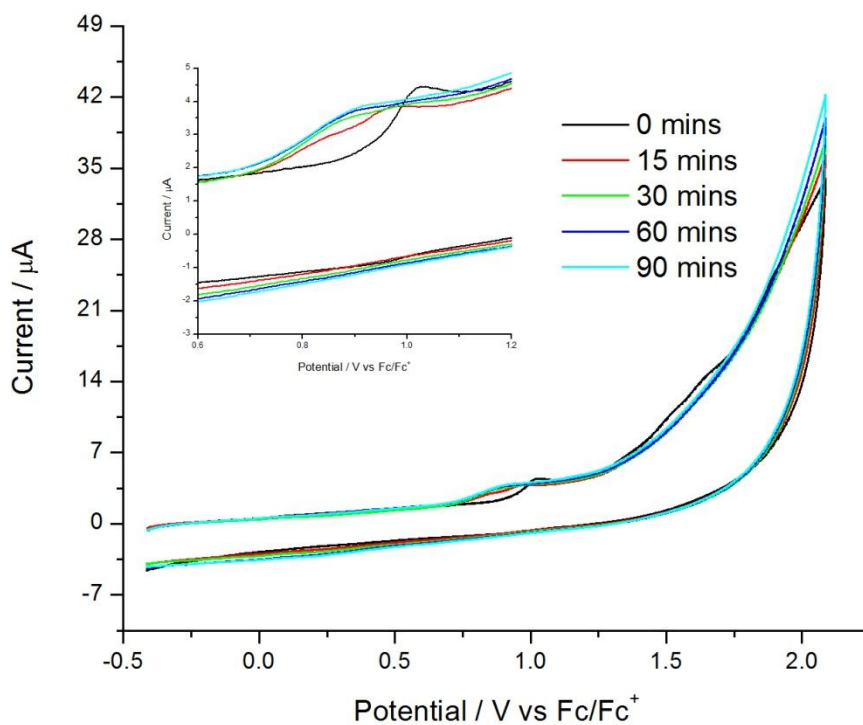


Figure 4.5 Cyclic voltammograms of **100a** over time, inset is an expansion of the oxidation peak

The reason for the change in oxidation potential can be explained by the change in conformation of **100a** towards **100b**. In the first conformer the donating bromothiophenes are both conjugated to the electron-withdrawing nitrobenzenes and as these change to a donor-donor conformation, the removal of an electron becomes easier and oxidation takes place at a lower potential. Many attempts were made at electropolymerising **100** but polymer growth was unattainable through repetitive cycling over the first oxidation peak. With each scan the current response diminished rather than increased. An example of attempted growth is shown in Figure 4.6.

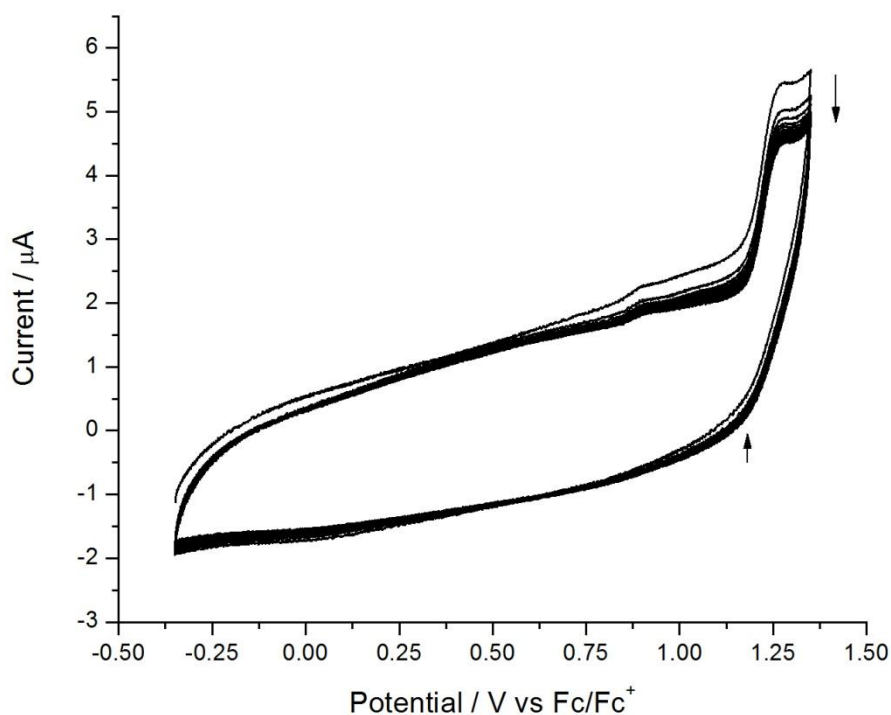
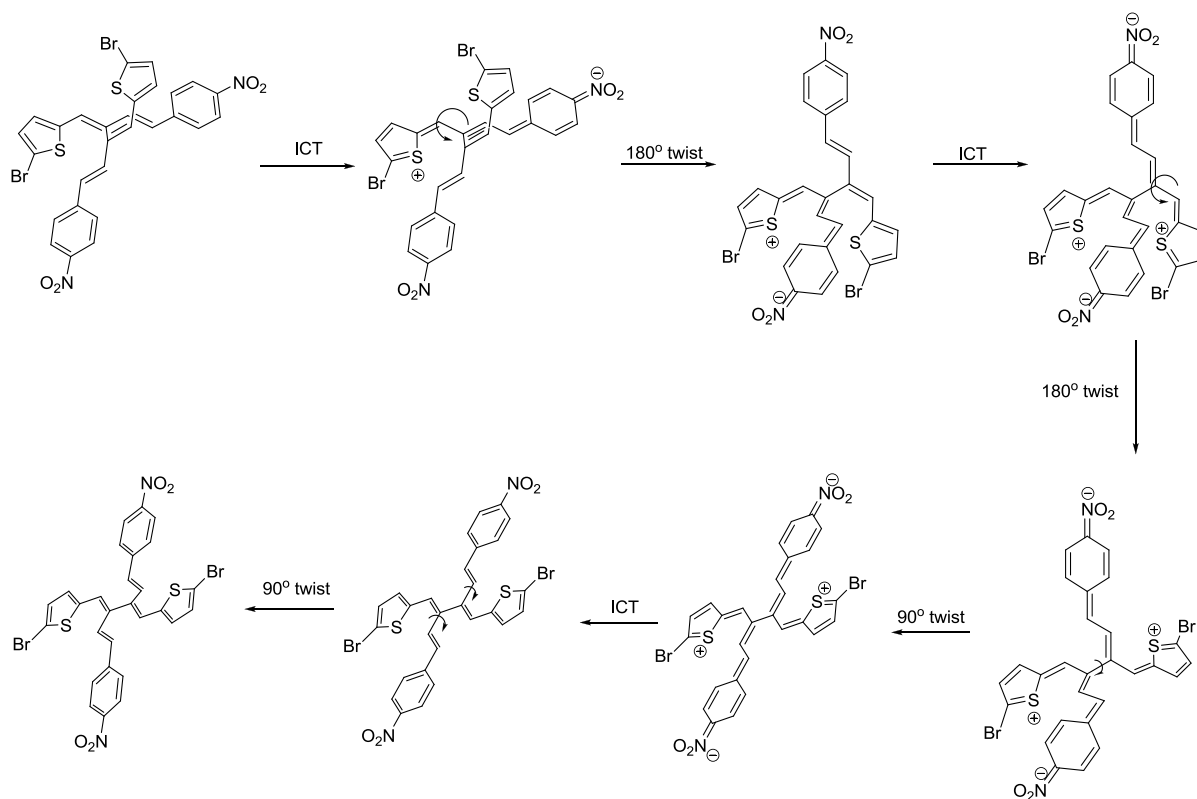


Figure 4.6 Attempted polymer growth of **100**

4.2.6 Proposed mechanism for interconversion of **100**

A mechanism for the conversion of **100a** to **100b** in solution is proposed in Scheme 4.2. The first step involves the absorption of light which induces an intramolecular charge transfer to form a charge-separated, quinoidal excited state. The newly formed single C-C bond can rotate and the molecule undergoes a 180° twist to give another excited state geometry. A second ICT process followed by two new twists (180° and 90°) gives a planar structure. Relaxation to the neutral form is possible when the excited electrons return through the conjugated framework to the thiophene group, while the nitrobenzyl groups twist out of plane to reduce steric repulsion with the thiophenes. This gives structure **100b**.

Scheme 4.2 Proposed mechanism for the interconversion of **100**



4.2.7 UV-vis absorption studies of 101

The evolution of the electronic absorption spectra of **101** in dichloromethane was monitored over time under exposure to ambient light (Figure 4.7). This dendralene showed similar behaviour to **100a**. With no exposure to light, the spectrum gives a maximum absorbance at 455 nm. The bathochromic shift of **101** compared to **100** is due to the addition of the EDOT unit which increases the conjugation length of the dendralene. As before, exposure to light causes a decrease in λ_{max} over time, accompanied with the emergence of a new band at $\lambda_{\text{max}} = 368$ nm.

The rate constants for the decreasing band at 455 nm and the increasing band at 368 nm were calculated and are shown in Figure 4.8. The first-order rate constants at each wavelength are in good agreement with each other: $k = 0.0131 \text{ min}^{-1}$ or $2.2 \times 10^{-4} \text{ s}^{-1}$ and $k = 0.0128 \text{ min}^{-1}$ or $2.1 \times 10^{-4} \text{ s}^{-1}$ for 455 and 368 nm, respectively. The rate constant for **101** is an order of magnitude lower than that of **100** ($k = 0.0027 \text{ s}^{-1}$).

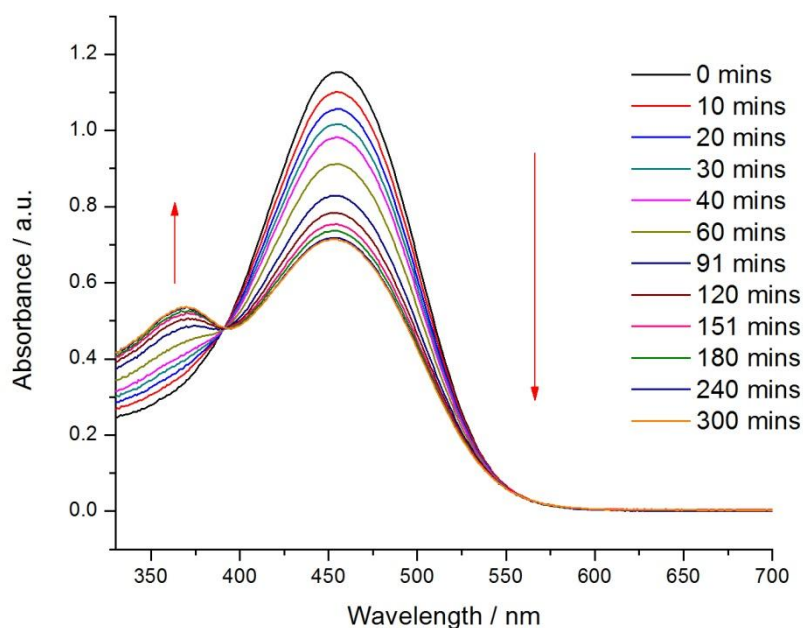


Figure 4.7 Evolution of UV-vis spectra of **101**

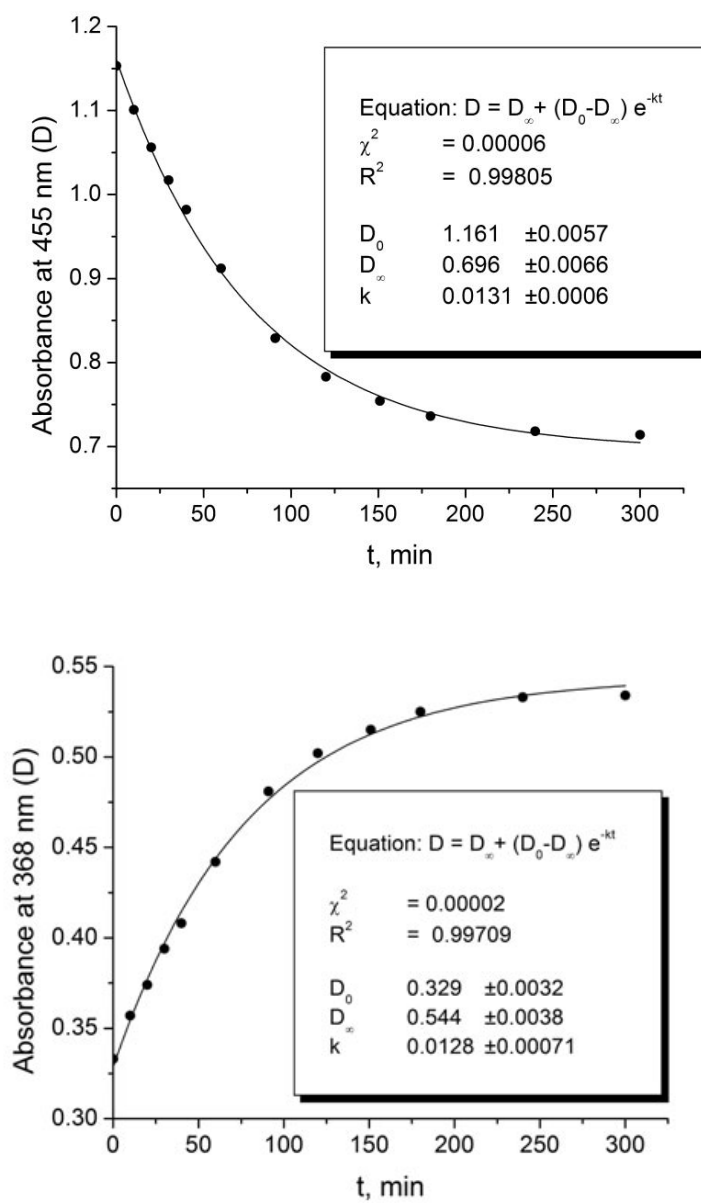
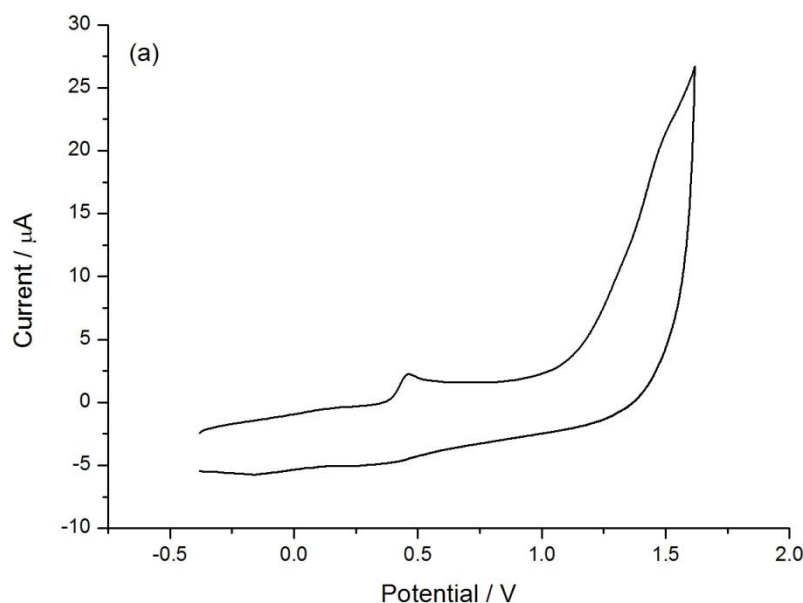


Figure 4.8 Kinetic plot of the rate change of **101** at 455 nm (top) and at 368 nm (bottom)

4.2.8 Electrochemistry of 101

Cyclic voltammetry was used to probe the electrochemical properties of **101** (in the absence of light) and its polymer. The oxidation of **101** is shown in Figure 4.9(a). The oxidation of the EDOT groups can be seen at +0.47 V; since the donor EDOT groups are not conjugated to each other, it is assumed that both are oxidised at the same potential. A second oxidation wave is seen at +1.50 V which represents the formation of dication on each donor – acceptor halves of the molecule. The reduction of **101** (Figure 4.9(b)) shows one reversible wave ($E_{1/2}^{1\text{red}} = -1.40$ V) and two irreversible waves ($E^{2\text{red}} = -1.82$ and $E^{3\text{red}} = -2.27$ V). The first reduction is a one-electron addition to each nitrobenzene unit; the second step is the addition of a second electron to the accepting nitrobenzene groups although, this results in an irreversible charged state. The third reduction, giving a trianion, is in the potential range which can be attributed to the reduction of the thiophene units.



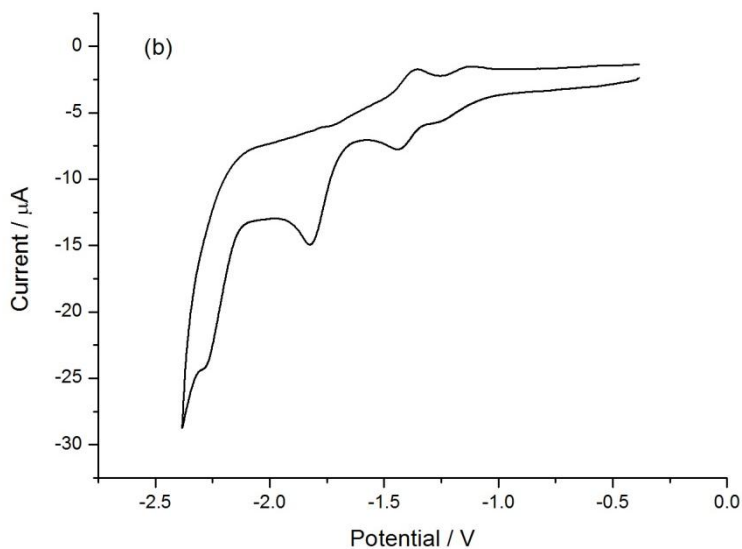


Figure 4.9 Cyclic voltammograms of (a) oxidation and (b) reduction of **101**

Electrochemical polymer growth (Figure 4.10) of **101** was achieved through repetitive cycling over the first oxidation peak to form a polymer film on the surface of the glassy carbon electrode. Growth of poly**101** can be seen with the development of a new peak between +0.2 and +0.4 V. This peak can be attributed to the oxidation of thiophene-EDOT-EDOT-thiophene units in the polymer chain.

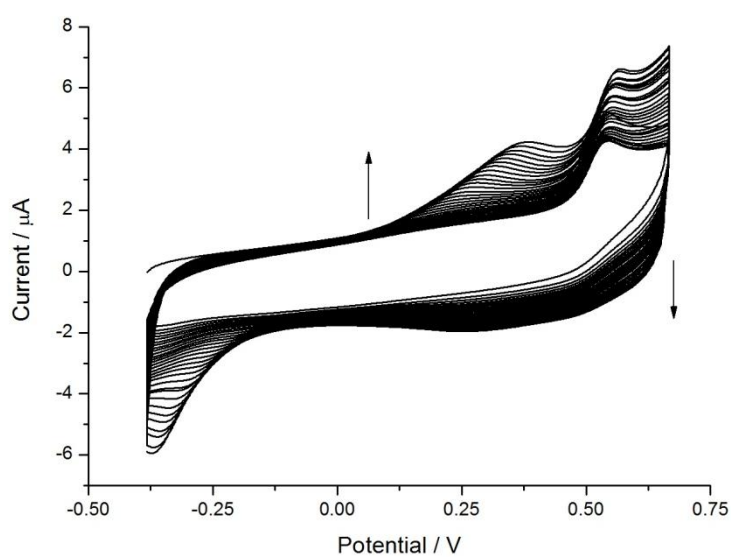


Figure 4.10 Electrochemical growth of poly**101**

The newly formed poly**101** film was analysed in a monomer-free solution. A cycle was produced (Figure 4.11) to show the oxidation and reduction characteristics of the polymer and to calculate the HOMO, LUMO and band gap. The oxidation shows two irreversible peaks. The first is a sharp peak at $E^{1ox} = +0.55$ V and the second is a broader peak between +0.7 and +1.25 V with the possibility of two peaks coalescing ($E^{2ox} = +0.79$ V and $E^{3ox} = +1.09$ V). The difference in potentials can be explained by the position of the EDOT-thiophenes units in the polymer chain. Many will exist as thiophene-EDOT-EDOT-thiophene segments in the polymer backbone but there will also be some that exist as side units to the main chain and are shorter thiophene-EDOT segments with higher oxidation potentials. The reduction shows two irreversible peaks at $E^{1red} = -1.57$ and $E^{2red} = -2.60$ V; it is possible that the wave at -1.57 V represents the loss of two electrons from the nitrobenzene groups. The reduction wave at the low potential of -2.60 V is the reduction of the thiophene-EDOT-EDOT-thiophene unit.

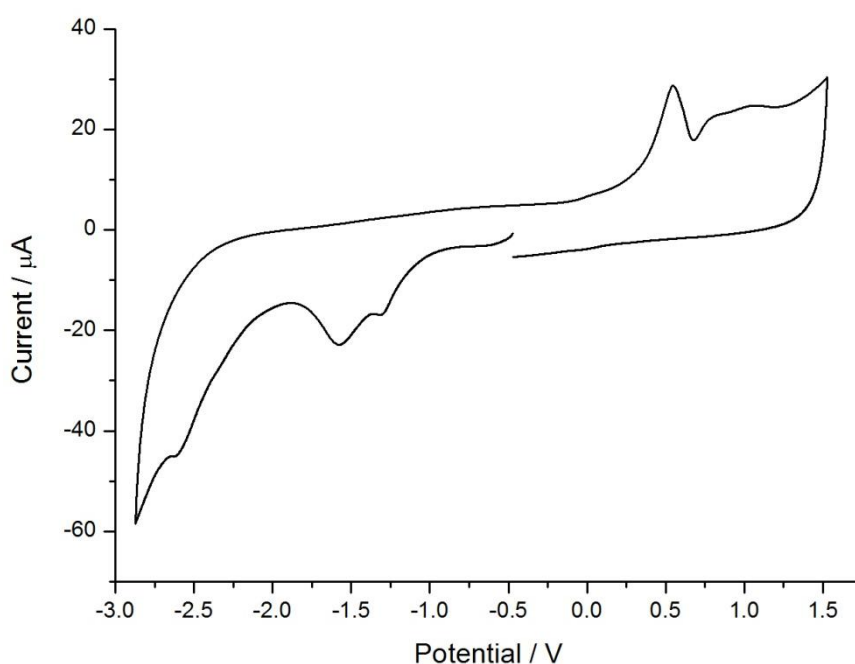


Figure 4.11 Cyclic voltammogram of poly**101**

The HOMO and LUMO energy levels of this polymer were calculated along with the band gap. The cycle is shown in Figure 4.11 and the data calculated are summarised in Table 4.1. The HOMO level was calculated by subtracting the onset of the first oxidation wave from the known HOMO of ferrocene (-4.8 eV) to give a HOMO of -5.13 eV. The LUMO was calculated in a similar manner from the onset of the first reduction peak to give a value of -3.41 eV. Therefore, the electrochemical band gap was determined to be 1.72 eV. This value is in an expected range, but lower than normal thiophene-based polymers because of the incorporation of acceptor units in the polymer chain.

Table 4.1 Energy level determination of poly101

| Onset of oxidation | HOMO | Onset of reduction | LUMO | Band gap |
|--------------------|-------|--------------------|-------|----------|
| / V | / eV | / V | / eV | / eV |
| +0.33 | -5.13 | -1.39 | -3.41 | 1.72 |

Despite degassing with argon for 20 minutes before running the scan and performing the cycle with negative potential first, there is still a persistent peak at -1.29 V which is characteristic of oxygen interference in the solution. This peak was confirmed as oxygen by running sequential differential pulse voltammetry (DPV) measurements (Figure 4.12) on a fresh polymer film with no degassing. In this more sensitive method, the peak at -1.29 V becomes more intense with each scan indicating that this peak is in fact due to oxygen interference.

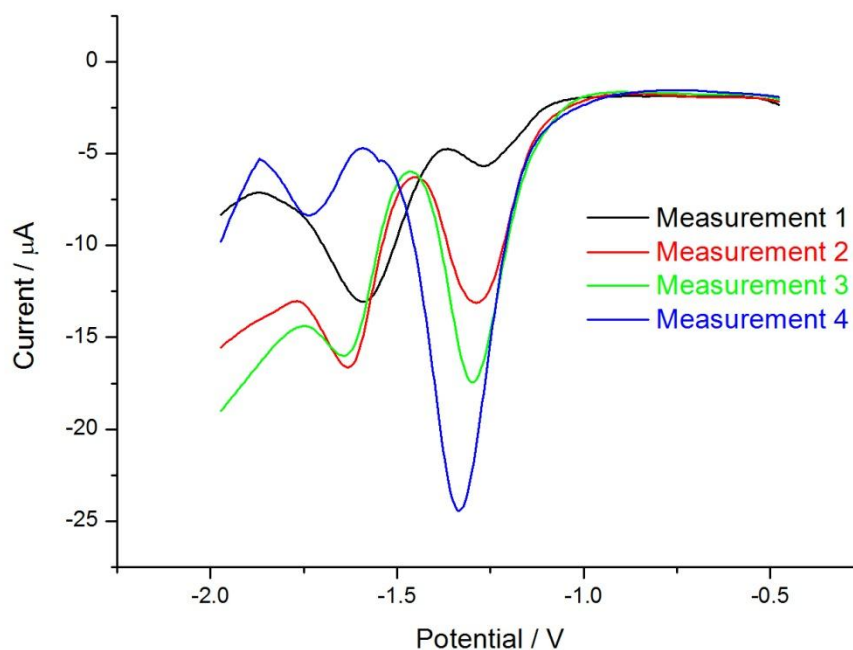


Figure 4.12 Differential pulse voltammograms of poly101 reduction

A scan rate experiment was performed on a freshly grown polymer by scanning the oxidation of the polymer at different scan rates (Figure 4.13(a)) and then plotting the current maximum of each cycle against the scan rate (Figure 4.13(b)). This determines the diffusion dependency of the polymer. A linear line with a high R^2 value of 0.9991 proves that the oxidation of this polymer is not diffusion limited. The change in oxidation potential for each scan, shifting higher with each scan is a result of the irreversibility of the oxidation process.

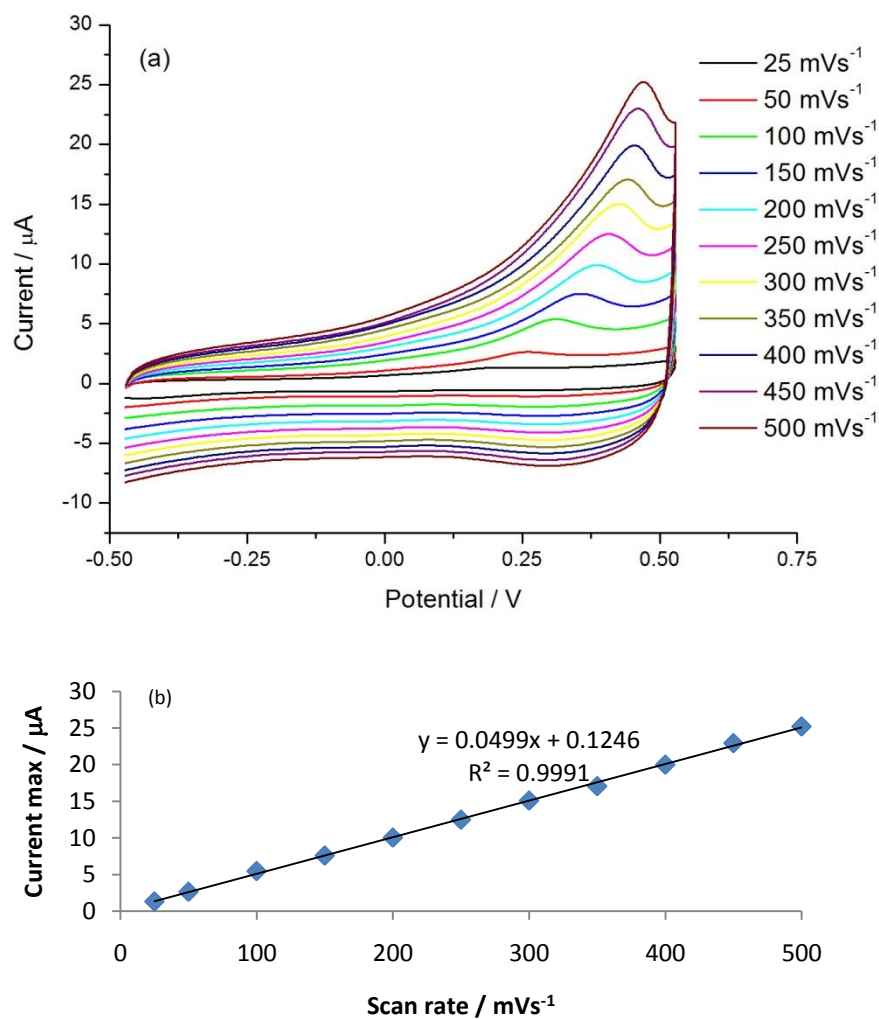


Figure 4.13 (a) Cyclic voltammograms of poly101 oxidation at varying scan rates and (b) plot of scan rate versus current maximum

To investigate the electronic properties of the polymer, a film of poly101 was grown onto an ITO-coated glass slide. The polymer film was dedoped (between -0.5 and -0.3 V for 1 hour) in monomer-free solution and then the UV-vis spectrum was recorded (Figure 4.14). The spectrum shows three main peaks at 337, 425 and 569 nm. The onset of the longest wavelength absorption edge ($\lambda_{\text{max}} = 690$ nm) was used to calculate the optical band gap. The estimated value of 690 nm corresponds to a band gap of 1.8 eV, which is in good agreement with the electrochemically determined band gap (1.72 eV).

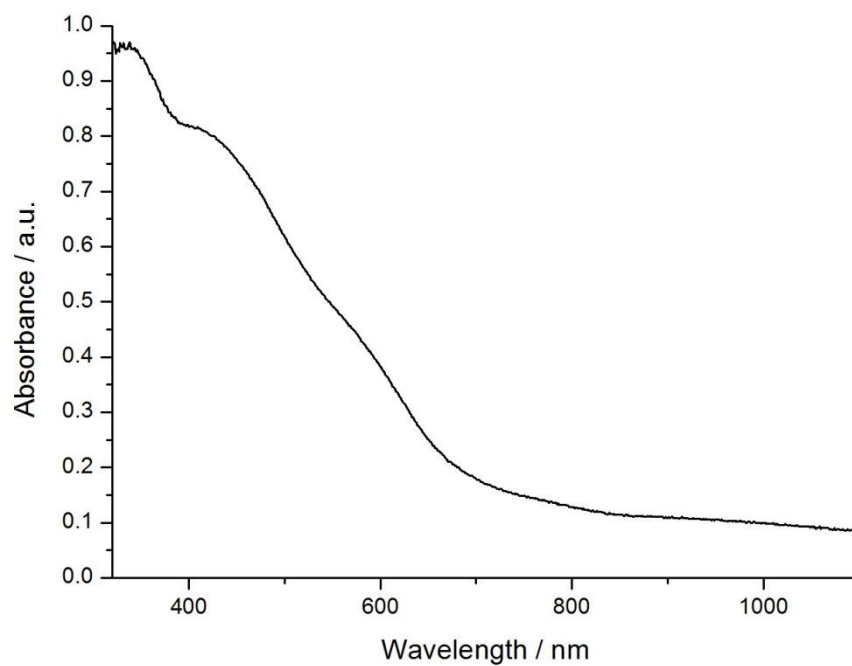


Figure 4.14 UV-vis spectrum of poly**101** in the solid state

UV-vis spectroelectrochemistry experiments were performed on poly**101** over both oxidation and reduction to investigate the changes to the absorption spectra for p- and n-doping, respectively. The oxidation spectroelectrochemical experiment is shown in Figure 4.15.

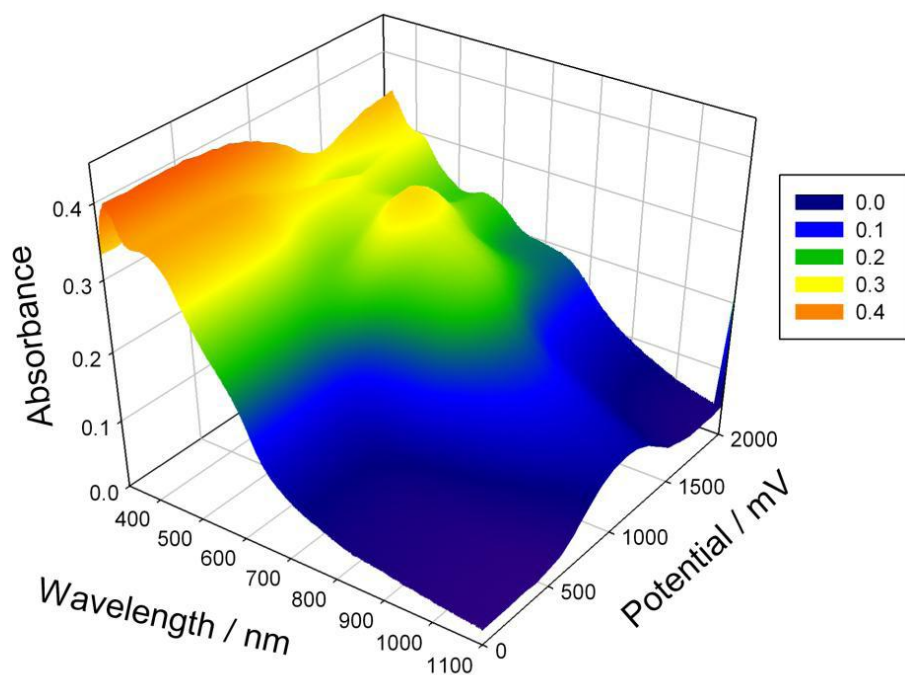


Figure 4.15 Oxidative spectroelectrochemistry of poly**101**

It can be seen that with increasing potentials beyond +0.5 V, the absorption bands at 569 and 759 nm intensify and peak at *ca.* +1.2 V. This represents the formation of polaron and is accompanied by a small decrease in the π - π^* transition. This latter does not decrease a great amount due to the localisation of the polaron over the thiophene-EDOT-EDOT-thiophene segments rather than delocalisation over the whole polymer. This localisation is also evidenced by the sharp nature of the peak at 759 nm. From +1.5 V, the bands at 337, 425, 569 and 759 nm diminish as a consequence of the generation of bipolarons and a rearrangement of the π -conjugated character of the polymer. Overall, the polymer changes from brown (neutral) to blue (doped).

The reduction spectroelectrochemical experiment, (Figure 4.16), shows less change in the absorption spectra than the oxidative spectroelectrochemical experiment. The

spectra beyond -1.0 V, show that there is an increase in the absorption in the wavelength range between 600 and 900 nm, matching well with the first reduction peak in the CV ($E^{\text{red}} = -1.5 \text{ V vs. Fc/Fc}^+$). This feature arises from the charge transfer of anion species between polymeric chains.

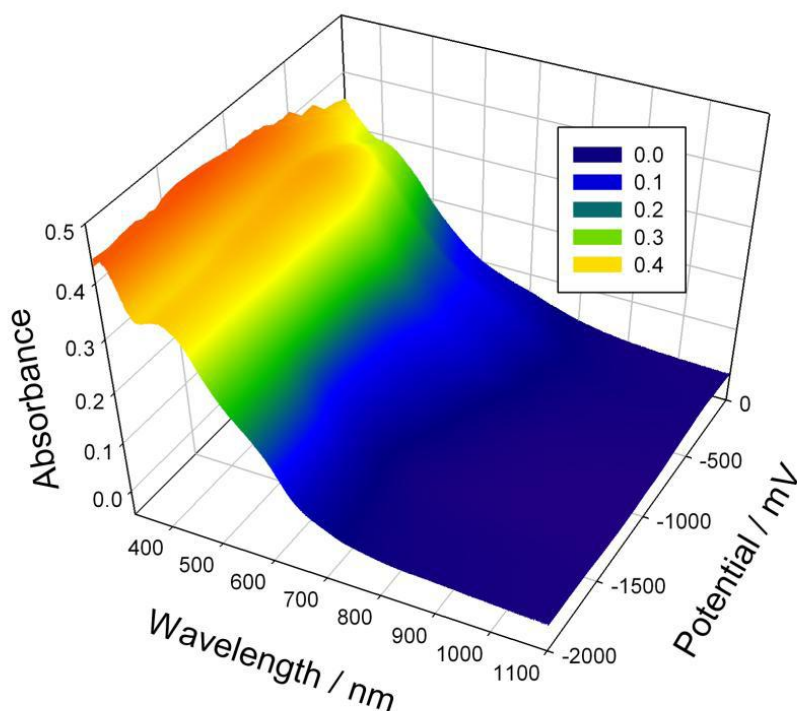


Figure 4.16 Reductive spectroelectrochemistry of poly**101**

As the oxidation potential of poly**101** is higher than that of PEDOT derivatives, together with the sharp nature of the charged states in the oxidative spectroelectrochemistry experiment along with the relatively low band gap of the polymer. It can be reasonably assumed that the conjugation path of the polymer is limited to nitrostyryl-thiophene-EDOT-EDOT-thiophene-nitrostyryl (acceptor-extended donor-acceptor) segments. This indicates that the **a** conformer has been “frozen” in the electropolymerisation experiment and that conformer is persistent in the solid state.

4.2.9 Conclusions

Two new [4]-dendralenes bearing thiophene nitrobenzene donor–acceptor units have been prepared that can exist as two different conformers. The dendralenes can adopt a donor–acceptor conformer or a donor–donor conformer. The first conformer can be maintained by excluding ambient light and can be transformed to the second conformer through irradiation of light which induces two intramolecular charge transfers and conformational twists as depicted in the proposed interconversion between the two conformers.

X-ray crystallographic studies on **100** show the difference in structures between the two conformers. UV-vis spectroscopy and cyclic voltammetry studies have shown that **100a** (donor–acceptor conformer) can transform to **100b** (donor–donor conformer) through exposure to light. Many attempts were made at polymerising **100a** to investigate if the donor-acceptor conformer remains and is persistent or can transform to the donor–donor conformer in polymeric form, but this was not accomplished.

A second dendralene (**101**) was synthesised with the attachment of EDOT groups to facilitate polymer growth. The second dendralene was also shown to be convertible from its **a** to **b** conformer through exposure to light in a UV-vis absorption study. Electropolymerisation of this monomer was achieved and the analysis of poly**101** through cyclic voltammetry and UV-vis spectroelectrochemistry experiments show that localised charged states and a relatively low band gap indicate that the **a** conformer persists in the polymer form.

4.3 Characterisation of New Diindeno[1,2-b:4,5-b']thiophene Based Materials

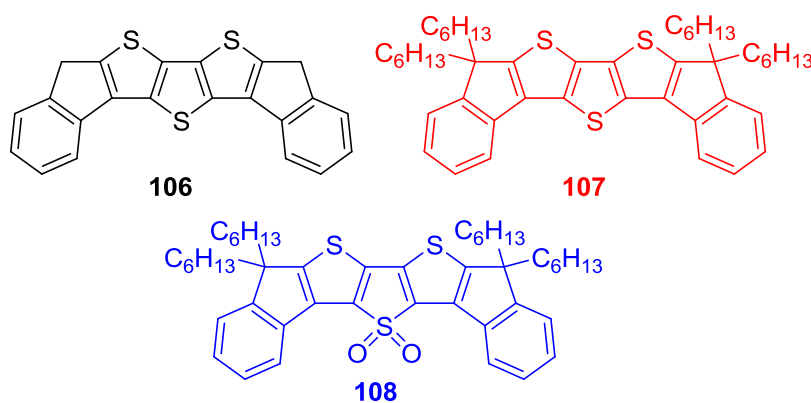
4.3.1 Introduction

The study of unusual conjugated structures for use in electronic systems is not only limited to linear and cross-conjugated molecules. The fusion of thiophene units into extended architectures has been a hot topic in recent literature for the development of a class of materials suitable for many different types of applications, especially OFET devices. The best OFET materials require good π -stacking to increase charge carrier mobility,²⁰² and traditional α -oligothiophenes suffer from a deviation from planarity through torsion around the single bonds. The fusion of the thiophene rings induces planarity as the rings have no freedom of rotation. The planarity of the fused thiophenes allows π -stacking motifs in the solid state,²⁰³ which in principle will facilitate improved charge transport through the material and increase charge-carrier mobility.²⁰⁴

Oligoacenes, such as pentacene, are well known for their high hole mobility,²⁰⁵ and fused thiophenes are considered analogues of these. However, one major difference between these two is the packing in the solid state. Some oligoacenes pack in a herringbone structure, whereas fused thiophenes pack in the more favoured π -stacked structure which allows a more superior overlap.^{206, 207} One of the disadvantages to oligoacenes is their relatively poor environmental stability and they degrade easily in oxygen environments.²⁰⁸ Fused thiophenes suffer less from this because they have larger HOMO-LUMO gaps compared to their all carbon equivalents.²⁰⁹ Oligoacenes are more quinoidal in nature whereas in contrast, fused

thiophene based materials have greater aromaticity with each thiophene having a benzoid character, which gives them lower lying HOMO levels.²¹⁰

In this section, three new compounds have been synthesised (**106**, **107** and **108**), which are extended analogues of dithienothiophene. The electrochemical and photophysical properties of these materials are reported. X-ray crystallography and field effect transistor measurements were performed on compound **106** as it was the most promising of the three materials for OFET applications.



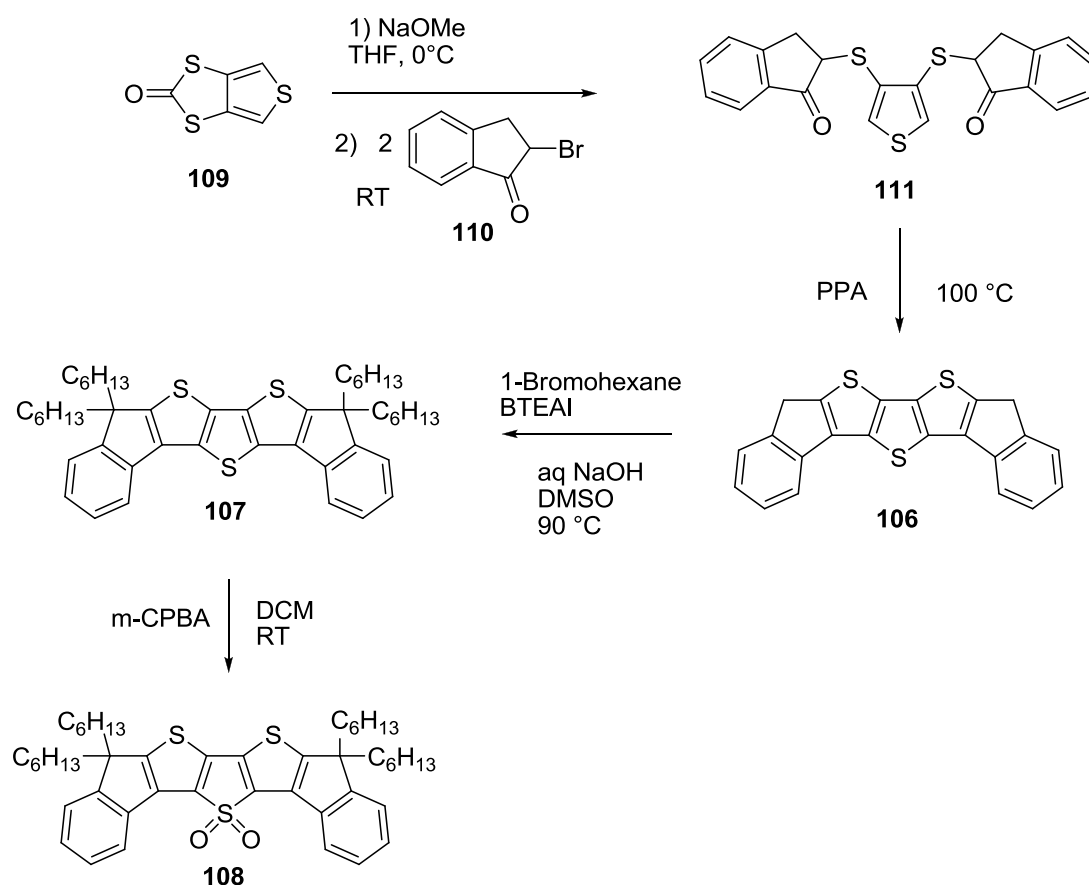
Compound **106** has poor solubility, a common problem for unsubstituted fused thiophenes.²⁰⁹ Therefore, alkylation to improve the solubility of **106** was performed, giving compound **107**. To improve the photoluminescence of this compound,²¹¹ oxidation of the central thienyl sulfur was performed to give compound **108**, the modification to the *S,S*-dioxide leads to increased electron affinity,²¹² and increased photoluminescence.²¹³

The incorporation of *S,S*-dioxide units in thiophene-based materials normally creates compounds that are more readily reduced than the parent thiophene compound,²¹²

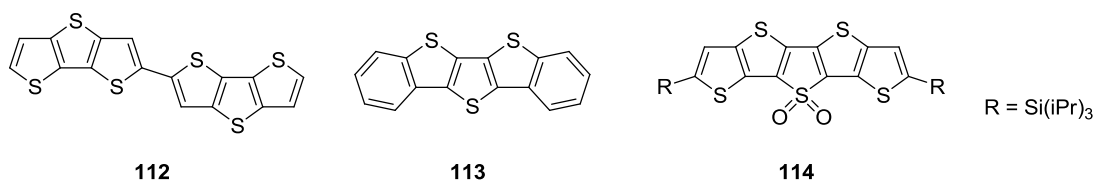
thereby affording lower HOMO-LUMO gaps from the increased delocalisation in the molecular backbone and electron-affinity of the new acceptor unit.²¹⁴ The delocalisation is due to the disruption of aromaticity in the thiophene ring, the result of the sulfur lone pair now bonding to the oxygens of the dioxide.²¹²

The synthetic procedure for the syntheses of **106**, **107** and **108** was performed by Irina Afonina and is summarised in Scheme 4.3.

Scheme 4.3 Synthesis of **106**, **107** and **108**



Previous electrochemical studies on similar compounds, **112**,²¹⁵ **113**,²¹⁶ and **114**,²¹⁷ have shown interesting results. Oxidation of **112** showed a quasi-reversible wave at +0.8 V (*vs.* Fc/Fc⁺) from the formation of a radical cation on the unsubstituted α -position on either dithienothiophene. However, the reduction showed a reversible wave at -1.5 V. Compound **113**, dithienothiophene fused with two benzene units at either side, showed a reversible oxidation process that can be attributed to the blocking of the α -positions but unusually the oxidation potential increased to +0.99 V (*vs.* Fc/Fc⁺). Oxidation and reduction of compound **114** shows reversible waves for both processes with potentials at +0.95 and -1.86 V (*vs.* Fc/Fc⁺), respectively. As expected, the incorporation of the dioxide increased the oxidation potential by 320 mV compared to the parent thiophene. **114** also featured a bathochromic shift (50 nm) in the absorption spectrum and an improved photoluminescence quantum yield of $\Phi_{\text{PL}} = 0.66$ compared to $\Phi_{\text{PL}} = 0.27$ for the thiophene analogue.



4.3.2 Experimental

The syntheses of compounds **106**, **107**, **108** were performed by Irina Afonina and Alexander Kanibolotsky. The photoluminescence quantum yield measurements were carried out by Ashu Bansal, Graham Turnbull and Ifor Samuel (University of St Andrews). X-ray crystallography was measured and solved by Simon Coles and

Michael Hursthouse (University of Southampton) and the transistor measurements were performed by John Labram and Thomas Anthopoulos (Imperial College London).

Cyclic voltammetry measurements were performed on a CH Instruments 660A electrochemical workstation with *iR* compensation using anhydrous dichloromethane and tetrahydrofuran as the solvents. The electrodes were glassy carbon, platinum wire, and silver wire as the working, counter, and reference electrodes, respectively. All solutions were degassed (Ar) and contained the substrates at concentrations of *ca.* 10^{-4} M, together with *n*-Bu₄NPF₆ as the supporting electrolyte (0.1 M). All measurements are referenced against the $E_{1/2}$ of the Fc/Fc⁺ redox couple.

4.3.3 Electronic absorption and electrochemical studies

The electronic absorption spectra for all three compounds were measured in dichloromethane and are shown on Figure 4.17. Compounds **106** and **107** show similar fine spectra, which is indicative of rigid, planar structures. Both spectra have sharp absorption maxima at 273 nm and additional peaks (π - π^* transitions) at 326 and 338 nm for **106** and 329 and 343 nm for **107**. The small red shift for **107** is due to the electron donation of the hexyl chains. The spectrum of compound **108** is quite different in comparison to the other compounds. There is a short wavelength peak at 251 nm and a more intense band centred at 420 nm. The latter is likely to involve an intramolecular charge transfer process between the thiophenes rings and the dioxide functionality.

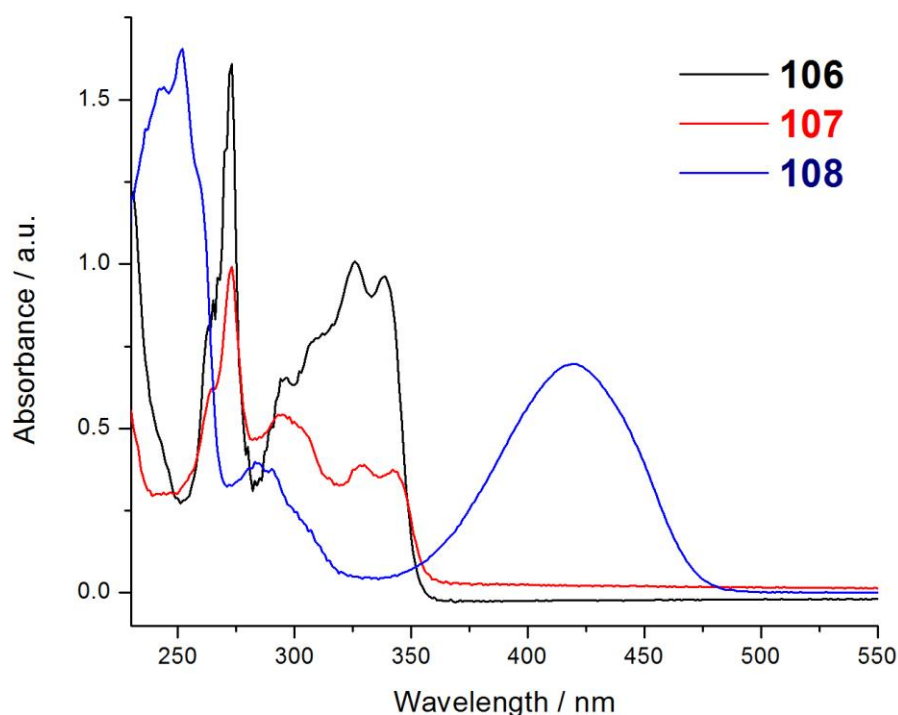


Figure 4.17 UV-vis spectra of compounds **106**, **107** and **108** in dichloromethane solutions.

To verify of the peak at 420 nm derives from an intramolecular charge transfer, solvatochromic studies were performed. Five solvents of varying polarisability (hexane, diethyl ether, tetrahydrofuran, dichloromethane and dimethyl sulfoxide) were used in this experiment and the value of λ_{max} for the longest wavelength peak was monitored as a function of the solvent's polarisability (π^*). Polarisability is a measure of the solvent to stabilize a charge or dipole by virtue of its dielectric effect.²¹⁸ Figure 4.18 and the data in Table 4.2 show that with increasing polarisability there is an increase in λ_{max} thus this positive solvatochromism proves that compound **108** does undergo an intramolecular charge transfer within the molecule.

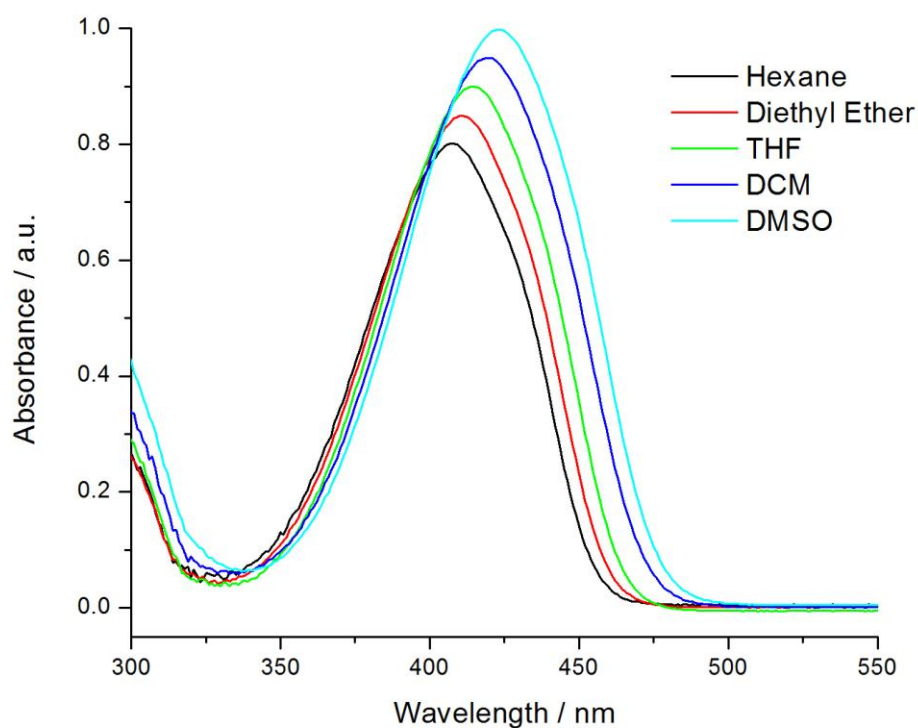


Figure 4.18 Solvatochromic effect of **108**

Table 4.2 Solvatochromic data of compound **108** in selected solvents with π^* values by Kamlet and Taft²¹⁹

| Solvent | π^* | Peak max / nm |
|--------------------|---------|---------------|
| Hexane | -0.08 | 407 |
| Diethyl Ether | 0.27 | 411 |
| Tetrahydrofuran | 0.58 | 414 |
| Dichloromethane | 0.82 | 419 |
| Dimethyl sulfoxide | 1.00 | 423 |

Cyclic voltammetry experiments were conducted on compounds **106**, **107** and **108** using dichloromethane as the solvent for oxidation and for the reduction of **108**. Tetrahydrofuran was required for the reduction of **106** and **107** at lower potentials; all graphs are shown in Figure 4.19. Glassy carbon was used as the working electrode with platinum and silver wire as the counter and pseudo reference electrodes, respectively. The supporting electrolyte was tetrabutylammonium hexafluorophosphate (0.1 M) and the graphs are referenced against the ferrocene / ferrocenium redox couple. Oxidation and reduction cycles were performed separately to avoid complications in the CV due to possible side products arising from irreversible and quasi-reversible processes.

Compounds **106** and **107** gave very similar redox potentials with the main difference being that the oxidation of **107** is reversible (**106**, $E^{1ox} = +0.72$ V; **107**, $E_{1/2}^{1ox} = +0.68$ V). The reversibility of **107** arises from the hexyl chains which block the α -position of the indene unit and prevent a chemical reaction of the intermediate radical cation. The reduction of both compounds showed irreversible behaviour (**106**, $E^{1red} = -2.86$ V; **107**, $E^{1red} = -2.95$ V), indicating that the inclusion of hexyl groups did not stabilize the formation of radical anions. Analysis of **108** showed reversible peaks for both oxidation and reduction processes ($E_{1/2}^{1ox} = +1.02$ V and $E_{1/2}^{1red} = -1.99$ V). In comparison to **107**, the decrease in reduction potential and the increase in potential for the oxidation was expected from the influence of the electron-withdrawing sulfone group.²¹²

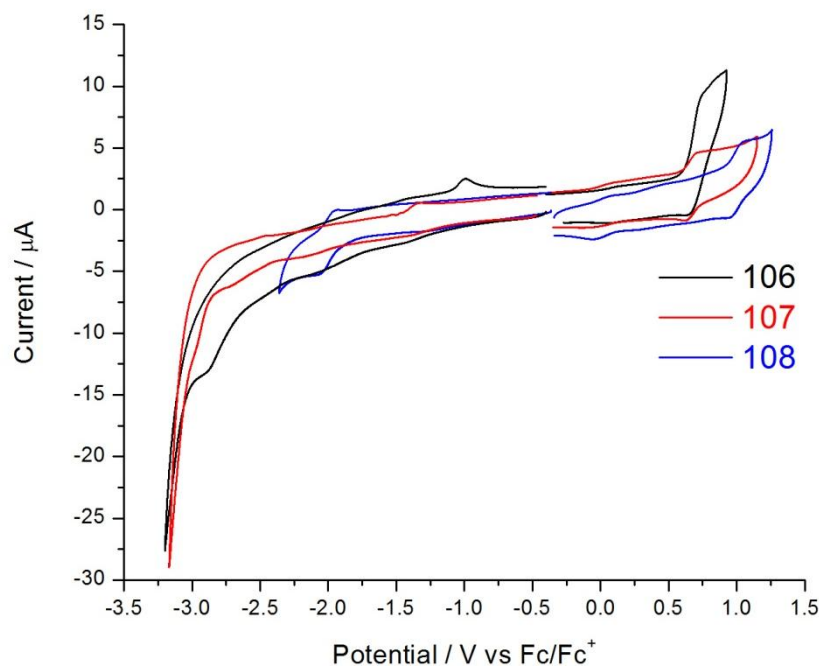


Figure 4.19 Cyclic voltammograms of **106**, **107**, and **108**

The HOMO-LUMO gaps of **106**, **107** and **108** were calculated from both the absorption spectra and electrochemical data. The edge of the longest wavelength absorption band corresponds to the optical HOMO-LUMO gap and this was similar for **106** and **107** (3.50 and 3.46 eV respectively); compound **108** produced an optical HOMO-LUMO gap of 2.62 eV. The electrochemical HOMO-LUMO gaps were calculated from the differences in the onsets of the first oxidation and reduction peaks. Using data referenced to the ferrocene/ferrocenium redox couple, HOMO and LUMO energies were calculated by subtracting the onsets from the HOMO of ferrocene which has a known value of -4.8 eV. A summary of this data can be seen in Table 4.3. All three compounds have good agreement between the electrochemically determined energy levels and the calculated optical HOMO-LUMO gap. Compound **108** has a smaller electrochemical gap of 2.81 eV compared to **106** and **107** (3.33 and 3.48 eV respectively).

Table 4.3 Electrochemical and absorption spectroscopy data for compounds **106**, **107** and **108**.

| | Absorption maxima / nm | Optical E_g / eV ^b | Oxidation Potential / V | Reduction Potential / V | HOMO / eV ^a | LUMO / eV ^a | Electrochemical E_g / eV |
|------------|---------------------------|------------------------------------|----------------------------|----------------------------|---------------------------|---------------------------|-------------------------------|
| 106 | 273 | | | | | | |
| | 326 | 3.5 | 0.72 ⁱ | -2.86 ⁱ | -5.42 | -2.09 | 3.33 |
| | 338 | | | | | | |
| 107 | 273 | | | | | | |
| | 329 | 3.46 | 0.71/0.64 | -2.95 ⁱ | -5.39 | -1.91 | 3.48 |
| | 343 | | | | | | |
| 108 | 251 | | | | | | |
| | 420 | 2.62 | 1.04/0.99 | -2.03/1.95 | -5.73 | -2.92 | 2.81 |

^aHOMO and LUMO values are calculated from the onset of the first peak of the corresponding redox wave and referenced to ferrocene, which has a HOMO of -4.8 eV. ^bOptical HOMO-LUMO gap determined from the onset of the highest absorption band. ⁱIrreversible peak.

4.3.4 Photoluminescence studies

Photoluminescence studies were performed on compounds **106**, **107** and **108** and the results are shown in Figure 4.20, Figure 4.21, and Figure 4.22, respectively, and summarised in Table 4.4. Solution studies of all three compounds were performed in dilute chloroform solution. Films of **107** and **108** were prepared on fused silica substrates by spin coating from chloroform solution; a film of **106** was unable to be prepared as it was not sufficiently soluble. The four hexyl chains in **107** increase the solubility but decrease its photoluminescence quantum yield ($\Phi_{PL} = 0.01$ and 0.004 for **106** and **107**, respectively). In the solid state, the quantum yield of **107** could not be measured due to its weak emission. The film and solution spectra of **107** are similar with the exception that the film also shows an additional peak *ca.* 540 nm, indicating the presence of excimer emission. **108** has a high PLQY in solution

(0.72), this value is higher than related non-fused oligothiophene S,S-dioxide compounds,²²⁰ and this can be attributed to the restriction of torsional flexibility.²¹¹

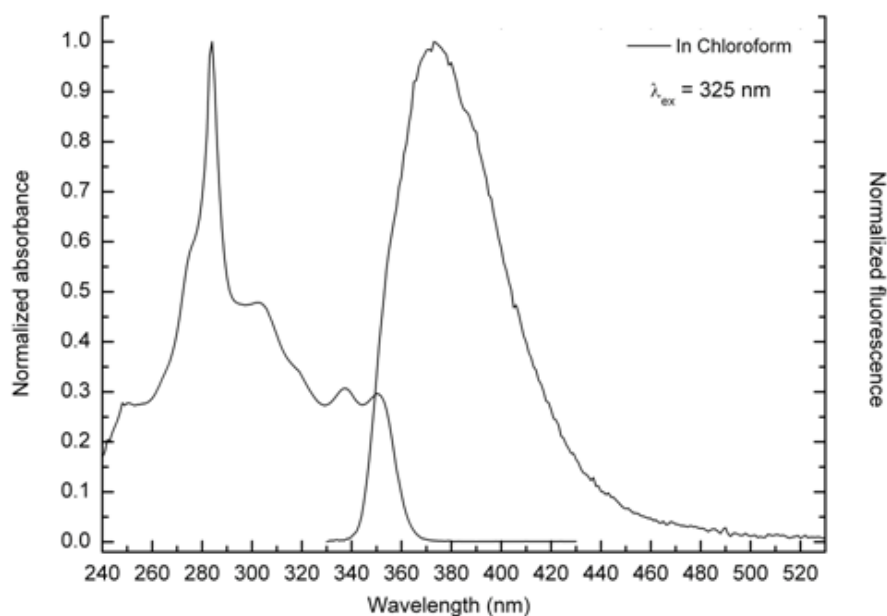


Figure 4.20 Solution state normalised absorption and emission of **106**

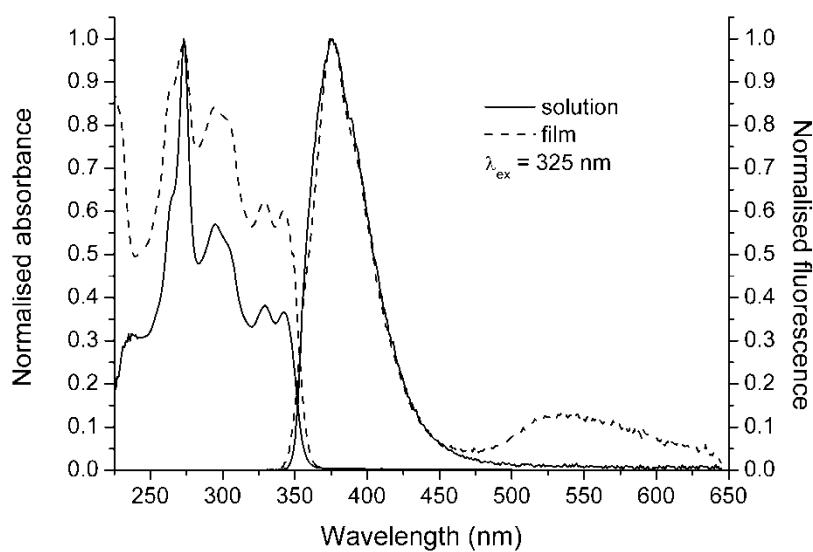


Figure 4.21 Solution and solid state normalised absorption and emission of **107**

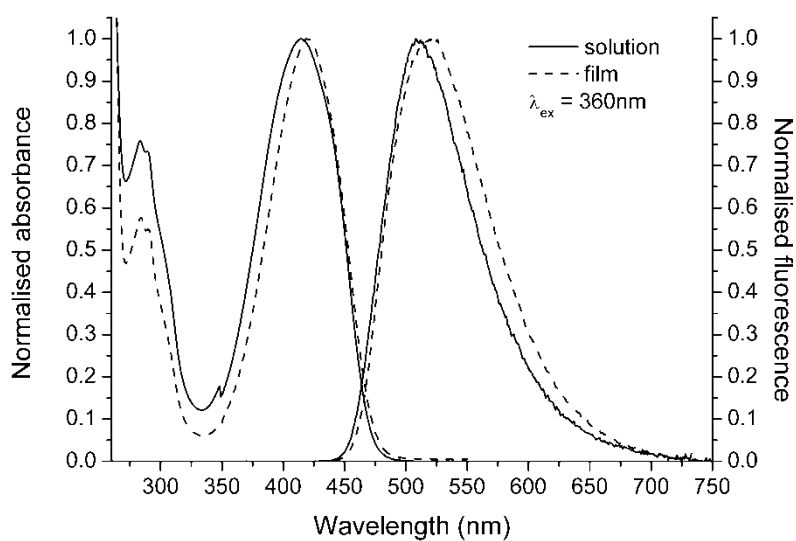


Figure 4.22 Solution and solid state normalised absorption and emission of **108**

Table 4.4 Photoluminescence data for compounds **106**, **107** and **108**

| Sample | State | λ_{\max} absorption / nm | λ_{\max} emission / nm | PLQY |
|------------|-----------------------|----------------------------------|--------------------------------|--------------------|
| 106 | Solution ^a | 284 | 373 | 0.01 ^b |
| 107 | Solution ^a | 273 | 376 | 0.004 ^b |
| | Solid | 273 | 376 | - |
| 108 | Solution ^a | 419 | 524 | 0.72 ^b |
| | Solid | 414 | 508 | 0.14 ^c |

^a Solution absorption and emission measured in chloroform. ^b Solution photoluminescence quantum yields were measured by preparing a sample in chloroform solvent with the same absorption at 360 nm as a standard solution of quinine sulphate in 0.5 M sulphuric acid. ^c The photoluminescence quantum yield of the films were determined using a He-Cd laser operating at 325nm to excite the sample and an integrating sphere to collect the resulting emission following the method of Greenham *et. al.*²²¹ The integrating sphere containing the sample was purged with nitrogen

4.3.5 X-ray crystallography

Single crystals of compound **106** were isolated by recrystallisation from toluene. The asymmetric unit is shown in Figure 4.23 and consists of seven fused rings labelled A-G. The central rings A-C represent the dithienothiophene unit and two benzene rings (F and G) are linked to this core via fused cyclopentadienes (D and E). The entire molecule is highly planar with the largest torsion angle in the structure being 2.19° within S(2)-C(2)-C(3)-C(11). In the bulk, compound **106** forms one-dimensional π - π stacks (Figure 4.24) in which adjacent molecules are inverted but otherwise eclipsed, see Figure 4.25.

Due to the curved shape of the molecules, this leads to rings A, D and E being efficiently overlapping with π - π ring centroid distances of 3.49 – 3.52 Å. Due to inversion between neighbouring molecules, rings B and C suffer from lateral displacement to give longer π - π distances (3.87 and 3.95 Å) and this is greatly exacerbated in the benzene rings F and G (5.03 and 4.75 Å), which reside at the peripheries of the curved structures.

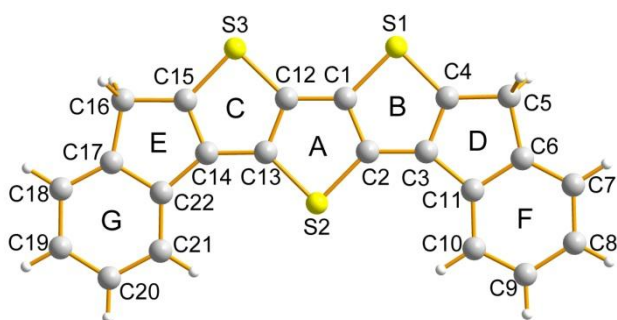


Figure 4.23 Asymmetric unit of compound **106** with labels

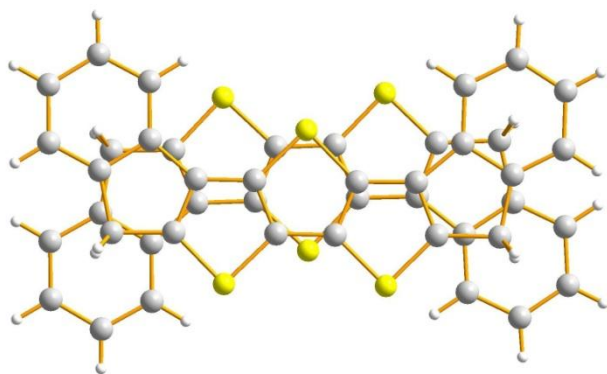


Figure 4.24 Space-filling diagram of **106** showing π - π stacking

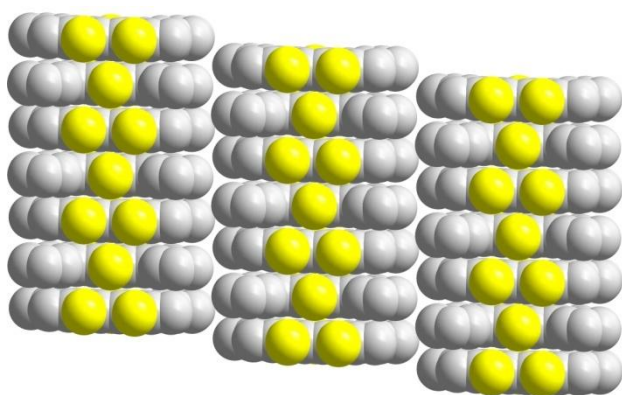


Figure 4.25 Inversion between a dimer of **106** within the one-dimensional stacks

4.3.6 Transistor fabrication and measurement

Due to the flat nature of the core structure and the absence of hexyl chains, the charge transport properties of compound **106** were investigated. The mobilities of structures **107** and **108** were not investigated, since the hexyl groups are expected to impede efficient stacking of the molecules. Field-effect transistors were fabricated from **106** using heavily doped Si^{++} substrates as the gate electrode and a 200 nm thermally oxidised SiO_2 layer as the gate dielectric. Using conventional

photolithography, gold source and drain electrodes were defined in a bottom-contact configuration to give a channel of length (L) of 15 μm and width (W) of 20 μm . The SiO_2 layer was treated with the primer hexamethyldisilazane (HMDS) to passivate the surface. A 50 nm layer of the organic semiconductor was then deposited by vacuum sublimation at a base pressure of 10^{-9} bar and a rate of 1 \AA s^{-1} . Figure 4.26 shows a polarised optical microscope image of compound **106** vacuum deposited onto an HMDS treated Si/ SiO_2 substrate, after annealing for 4 hours at 125 $^\circ\text{C}$. The devices were then annealed at 125 $^\circ\text{C}$ for 4 hours under atmospheric pressure in N_2 . Electrical characterisation was carried out in N_2 at atmospheric pressure using a Keithley 4200 semiconductor parameter analyser.

Figure 4.27 shows the transfer characteristics of a bottom-gate, bottom-contact OFET based on **106** with the inset showing the schematic of the transistor used. The transfer characteristics were obtained with the drain voltage (V_D) set to $V_D = -3 \text{ V}$ (linear regime) and $V_D = -20 \text{ V}$ (saturation regime). Using standard semiconductor equations (section 1.15.3) the hole mobility was calculated to be $\sim 10^{-4} \text{ cm}^2 \text{ V}^{-1} \text{ s}^{-1}$. From plots of $I_D^{1/2}$ against V_G (not shown) the threshold voltage was determined to be approximately -21 V. The current on/off ratio and subthreshold slope for these devices were estimated to be $\sim 10^6$ and 2 V/decade, respectively. The relatively low hole mobility is attributed partly to the deep HOMO level of **106** (-5.42 eV) and partly to the polycrystalline nature of the evaporated film (see Figure 4.26). It is anticipated that optimisation of the various evaporation conditions (*e.g.* evaporation rate, substrate temperature etc.) could yield larger crystalline domains and hence higher charge carrier mobilities.

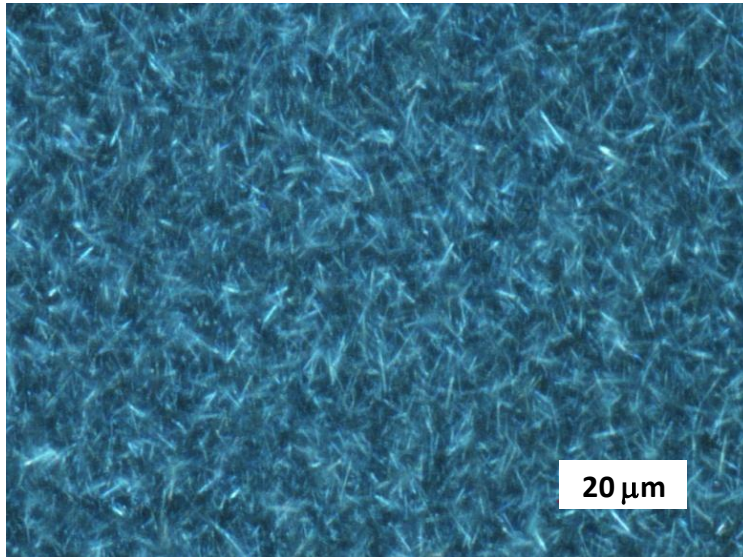


Figure 4.26 Polarised optical microscope image of material **106** vacuum deposited onto an HMDS treated Si/SiO₂ substrate, after annealing for 4 hours at 125°C in nitrogen

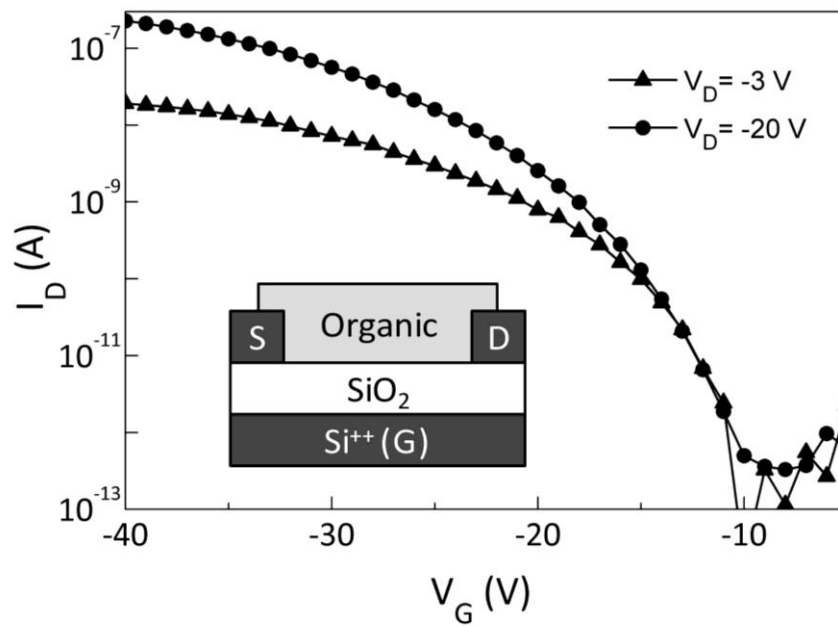


Figure 4.27 Transfer characteristics of bottom-gate, bottom-contact OFET based on **106**. Inset shows schematic representation of bottom-gate, bottom-contact transistor structure used

4.3.7 Conclusions

The synthesis, electronic, electrochemical and photoluminescence studies of three new fused oligothiophene derivatives have been reported. The first compound (**106**), with the absence of hexyl chains shows the best packing in the crystal form and is the most suitable for organic field effect transistor devices of the three. However, this compound is irreversible to oxidation and reduction processes. Addition of hexyl groups (compound **107**) allows much better solubility and stability to oxidation but decreases the photoluminescence quantum yield. Functionalisation with a sulfone group (compound **108**) has the benefit of giving a smaller HOMO-LUMO gap, reversibility to reduction as well as oxidation and a much improved quantum yield making this compound a very interesting material for possible photonic applications.

**Chapter 5. An Electronic, Electrochemical,
Spectroelectrochemical and Electrochromic Study of
Benzobisthiazole based Monomers and Polymers.**

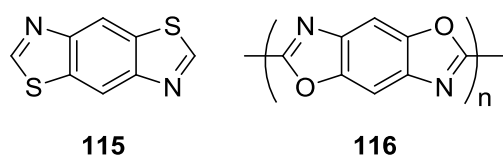
5.1 Abstract

A series of compounds that contain a benzobisthiazole (BTZ) core have been synthesised and investigated. Compound **123**, was synthesised for the sole purpose of examining the role of the BTZ core in the analysis. Three of the other four compounds have hexylthiophenes attached at either side of the core; compounds **117**, **120** and **121** differ only in the position of the hexyl chain with the influence of the positioning discussed. Compound **122** has two extra thiophenes and allowed the examination of the effect of elongation of the conjugated chain compared to **117**.

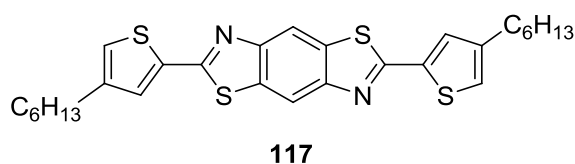
Films of poly**117**, poly**120** and poly**122** were grown electrochemically and were analysed by cyclic voltammetry, solid-state UV-vis spectroscopy, spectroelectrochemistry, electrochromic switching times, and colourimetry. Poly**122** shows the greatest contrast for spectroelectrochemistry, switching and colour change and could have potential for use in an electrochromic device. The electrochemical and optical band gaps were in good agreement for each polymer.

5.2 Introduction

Benzobisthiazole (BTZ, **115**) based polymers are part of a larger family known as poly(benzazole)s. This group also contains other heterocyclic polymers such as poly(benzobisoxazole) (**116**). These polymers have been of great interest over the last thirty years, since these rigid-rod polymers display high tensile strength and modulus with great stability in tough thermal and environmental conditions.²²²⁻²²⁴ Their excellent physical properties can be attributed to the polymers' ability to efficiently π -stack through strong intermolecular interactions in the solid state.^{225, 226}



In recent years, benzobisthiazole units have been incorporated into a wide variety of conjugated polymers to create materials for OLEDs,²²⁷ OPVs and especially OFETs,²²⁸ since BTZ-based materials exhibit the aforementioned efficient π -stacking, a desirable property for transistors. In previous research in our group,²²⁹ it was shown that compound **117**, a BTZ-thiophene, self-assembles in the solid state to give three dimensional ordering with intermolecular close contacts in all three cartesian directions (Figure 5.1 and Figure 5.2).



The orthogonal units are linked together in an infinite chain through sulfur – nitrogen non-covalent intramolecular interactions. Each molecule is planar, allowing π - π interactions, while each of the orthogonal units are linked together in a π -stacking arrangement.

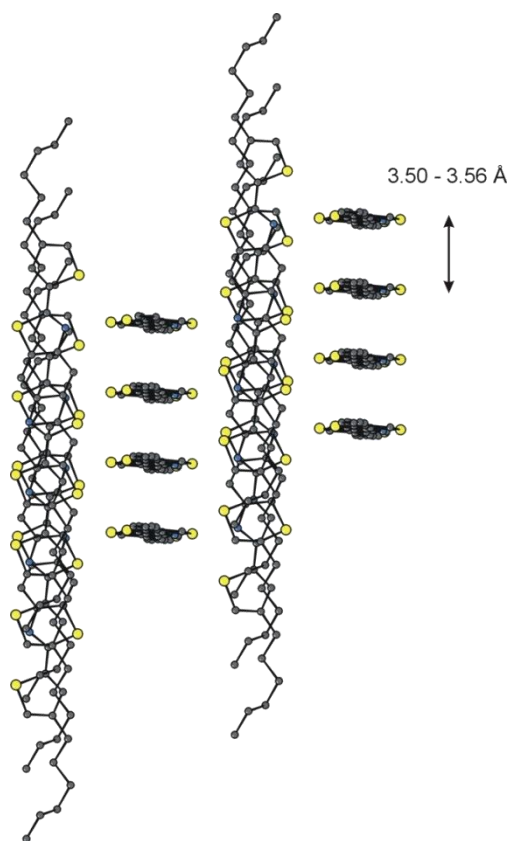


Figure 5.1 X-ray structure of **117** showing π - π stacks in two dimensions

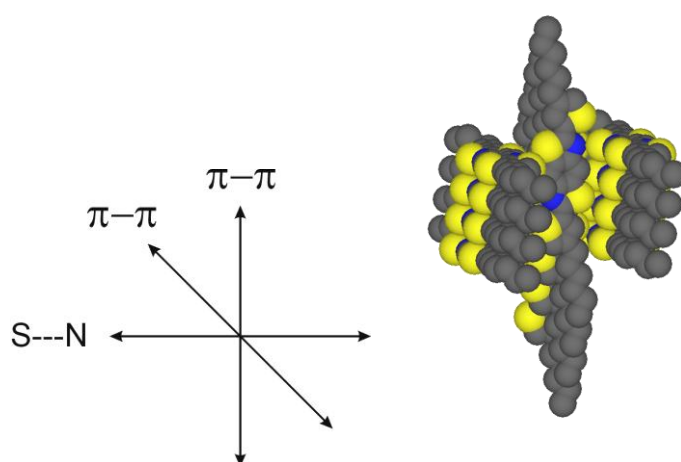
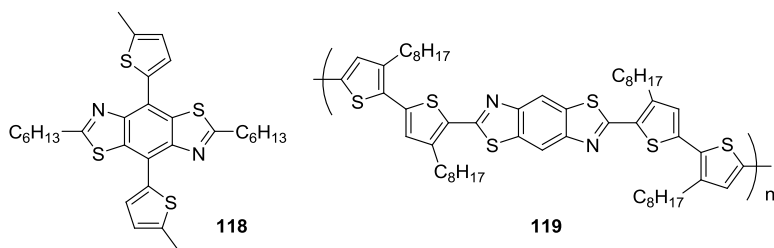
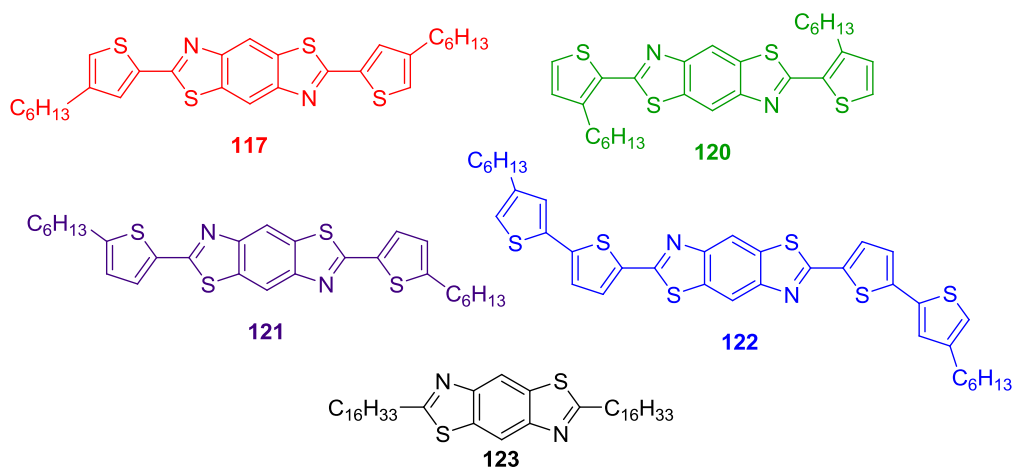


Figure 5.2 Summary of intermolecular close contacts in the X-ray structure of **117**

The planar nature and efficient packing of BTZ-thiophene compounds has been shown by other groups. The near planar compound **118** is an example by Kang *et al.*²³⁰ and Jenekhe *et al.*²²⁸ showed that in the solid state, interdigitation is present in the packing of a BTZ-thiophene copolymer (**119**).

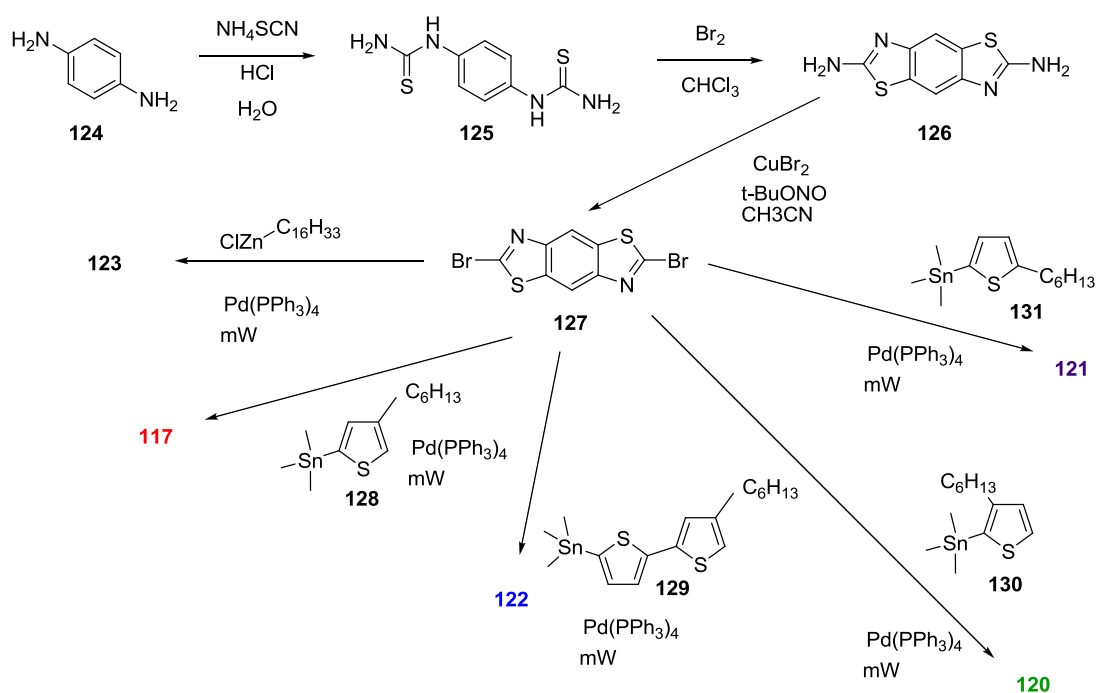


To date, the BTZ polymers in the literature have been chemically synthesised rather than electropolymerised. In this chapter, five compounds have been investigated, including the previously mentioned BTZ derivative **117**. Compounds **117**, **120** and **121** differ only in the position of the hexyl chain. The influence that the positioning has on all the experimental results will be discussed. Compound **122** has two extra thiophenes and this allows the examination of the effect of elongation of the conjugated chain compared to **117**. Compound **123** is a soluble, alkylated BTZ derivative which was synthesised to allow the optical and electrochemical analysis of the BTZ core without the presence of thiophenes.



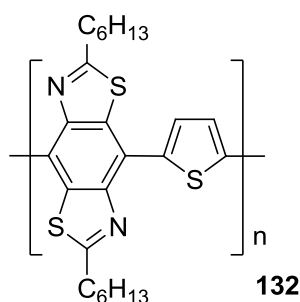
The optical and electrochemical properties of all five compounds were examined. Electrochemical polymer growth was achieved for three of these compounds (**117**, **120** and **122**) and the electrochemistry, absorption spectroscopy, UV-vis spectroelectrochemistry and electrochromic properties were investigated for all three polymers. The various synthetic routes for the BTZ compounds are summarised in Scheme 5. 1.

Scheme 5. 1 Syntheses of **117**, **120**, **121**, **122** and **123**



An interesting feature that has been observed in several papers is the difference in the absorption maxima between solution and thin film spectra of BTZ polymers. In thin films, π -stacking of the BTZ units causes a bathochromic shift in the λ_{max} . Examples can be seen in the chemically produced BTZ-thiophene copolymers, **119**,²²⁸ and **132**.²³¹ In the analysis of **119**, a 50 nm blue shift is seen going from film to solution spectra and is attributed to the loss of planarisation and π -stacking. In the

electronic absorption spectra of **132**, a 78 nm difference is observed between the two maxima: 460 nm (solution) and 538 nm (solid).



Electrochemical analysis of several BTZ polymers was performed by Osaheni and Jenekhe²³² who reported that the BTZ core affords a reversible reduction wave (*ca.* - 2.0 V *vs.* SCE) and an irreversible oxidation (*ca.* 1.5 – 1.8 V *vs.* SCE).

5.3 Experimental

The five starting compounds were prepared by Filipe Vilela and Greg McEntee (University of Strathclyde).

Cyclic voltammetry measurements were performed on a CH Instruments 660A electrochemical workstation with *iR* compensation using anhydrous dichloromethane as the monomer solvent and acetonitrile for monomer-free solvent. The electrodes were glassy carbon, platinum wire, and silver wire as the working, counter, and reference electrodes, respectively. All solutions were degassed (Ar) and contained monomer substrates at a concentration of *ca.* 10⁻⁴ M, together with *n*-Bu₄NPF₆ as the supporting electrolyte (0.1 M). All measurements are referenced against the E_{1/2} of the Fc/Fc⁺ redox couple. Spectroelectrochemical and switching experiments were

conducted on indium tin oxide (ITO) coated glass. Absorption spectra and CIE coordinates were recorded on a UNICAM UV 300 instrument.

5.4 Absorption and Cyclic Voltammetry of monomers

The electronic absorption spectra of compounds **117**, **120**, **121**, **122** and **123** recorded in dichloromethane solution are shown in Figure 5.3. Fine structures can be seen in all five spectra, indicating rigid structures. The core (**123**) shows peaks at 244, 279 and 290 nm and no further bands above 300 nm. Given their similarities in structure, the spectra of **117**, **120** and **121** all display very comparable shapes and absorption maxima. The data for all the absorption maxima are summarised in Table 5.1 for easier comparison.

There are small differences between **117**, **120** and **121**, and the three peaks of **121** are 4-5 nm higher in wavelength, possibly as a consequence of the position of the hexyl chain in the 5-position. The shoulder of **120** at 399 nm is also less pronounced than the corresponding peak for the other two compounds. As expected, the longest wavelength absorption maximum of **122** (428 nm) is bathochromically shifted due to the addition of the two thiophenes in the chain. However, the spectrum is less well-defined, which indicates that the molecule is probably less rigid in solution.

Optical HOMO-LUMO gaps of **117**, **120**, **121** and **122** were calculated from the onsets of the longest wavelength absorption peaks and are also shown in Table 5.1. As expected, the optical HOMO-LUMO gaps of **117**, **120**, and **121** are close at 3.02,

3.01, and 2.97 eV, respectively and the value of **122** is lower due to the extended conjugation (2.61 eV).

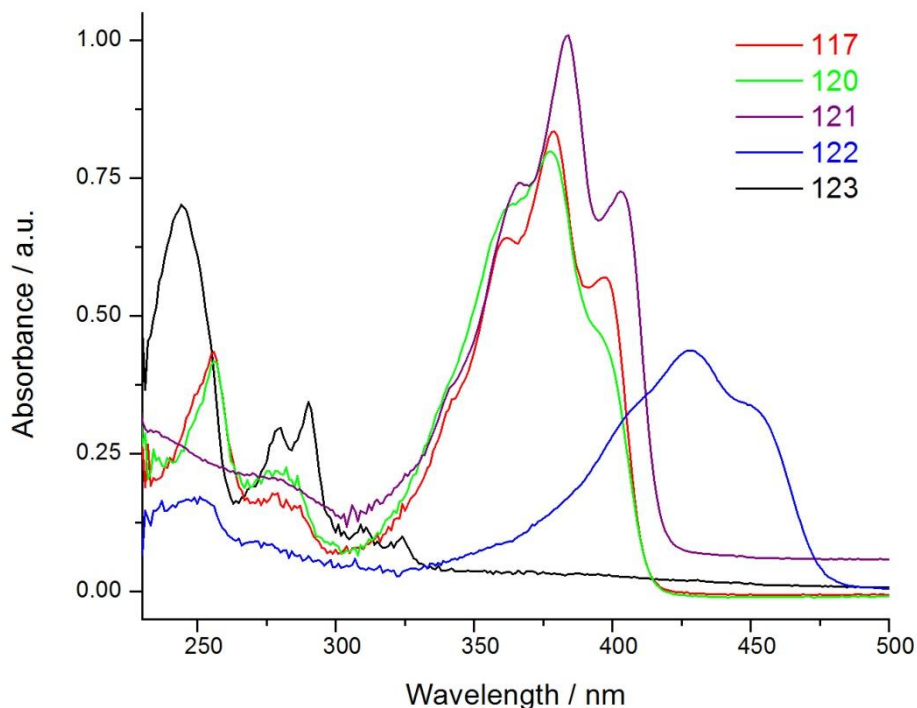


Figure 5.3 UV-vis spectra of **117**, **120**, **121**, **122** and **123**

The cyclic voltammograms of **117**, **120**, **121** and **122** were performed in dichloromethane solution with a glassy carbon working electrode and pseudo silver reference. Oxidation (Figure 5.4(a)) gives two irreversible waves for **117**, **120** and **121**, and the first process is at almost the same potential ($E^{1ox} = +0.99$ V for **117** and $+1.00$ V for **120** and **121**), producing a radical cation species in each case. The second wave occurs at a lower potential for **121** ($E^{2ox} = +1.20$ V) than it does for **117** and **120** ($E^{2ox} = +1.41$ and 1.45 V, respectively). The lower potential for **121** is from the α -positioned hexyl chains, which stabilise the formation of the dication to a greater extent than **117** and **120**. Given the structure of **121**, it would be predicted

that the blocking of the α -position would produce a reversible oxidation. When the scan rate is increased from 0.1 V s^{-1} to 1 V s^{-1} (shown in the inset of Figure 5.4(a)), the oxidation peak becomes reversible thereby inhibiting unwanted α - β' couplings.

Interestingly, the oxidation of **122** is much different to the others. The oxidation shows a quasi-reversible ($E_{1/2}^{1\text{ox}} = +0.65 \text{ V}$), reversible ($E_{1/2}^{2\text{ox}} = +1.02 \text{ V}$) and then an irreversible wave ($E^{3\text{ox}} = +1.43 \text{ V}$). The quasi-reversibility and the lower oxidation potential of the first peak can be explained by the ability of the radical cation to delocalise over a bis-thiophene, compared to a single thiophene unit in **117**, **121** and **120**. By comparing the area of the three peaks, it is worth noting that the second peak is twice the size of the first and third peaks indicating that this step is actually the removal of two electrons to form a trication radical (dication on one side and a radical cation on the other bis-thiophene). The third oxidation step then will give a quaternary cation. This hypothesis is supported by the fact that polymer growth can be achieved by cycling past the first and second waves but not past the third, suggesting that no radical exists at this stage.

The reduction processes of **117**, **120**, **121** and **122** are shown in Figure 5.4(b) with the reduction of **123** shown in the inset. By first looking at the reduction of **123**, there is a reversible wave at $E_{1/2}^{1\text{red}} = -1.73 \text{ V}$, then an irreversible wave at $E^{2\text{red}} = -2.09 \text{ V}$. Unusually, the reversible wave of the core is not seen in the reduction of the other monomers. It is possible that the radical anions of these derivatives are partially delocalised over the entire conjugated unit. The potential of the reduction processes for **117**, **120** and **121** are close in value at $E^{1\text{red}} = -2.27$, -2.11 and -2.24 V , respectively. Predictably, the reduction of **122** with its greater resonance and extended conjugation has the least negative potential ($E^{1\text{red}} = -2.04 \text{ V}$).

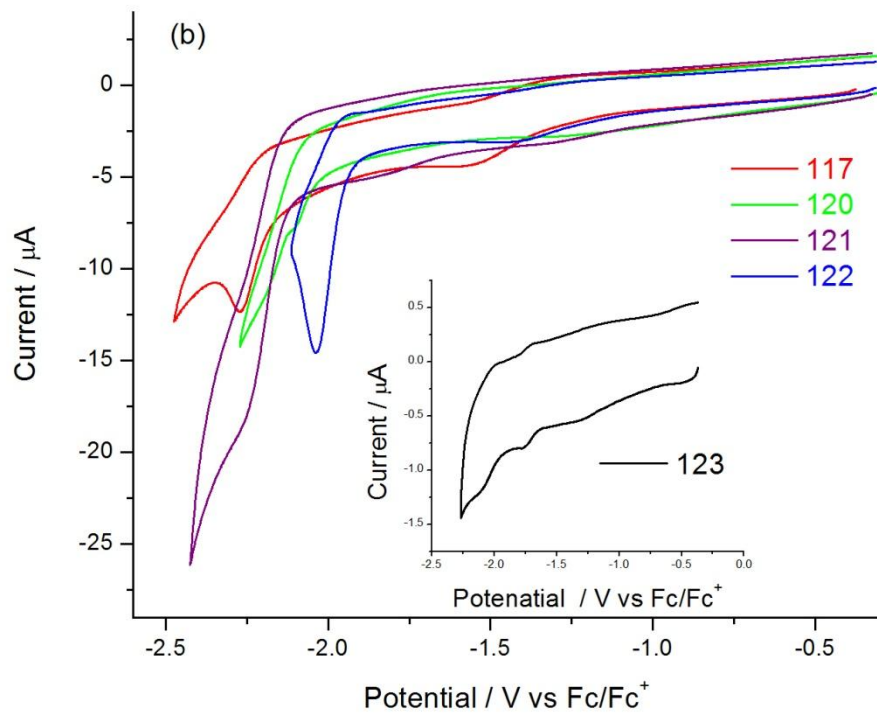
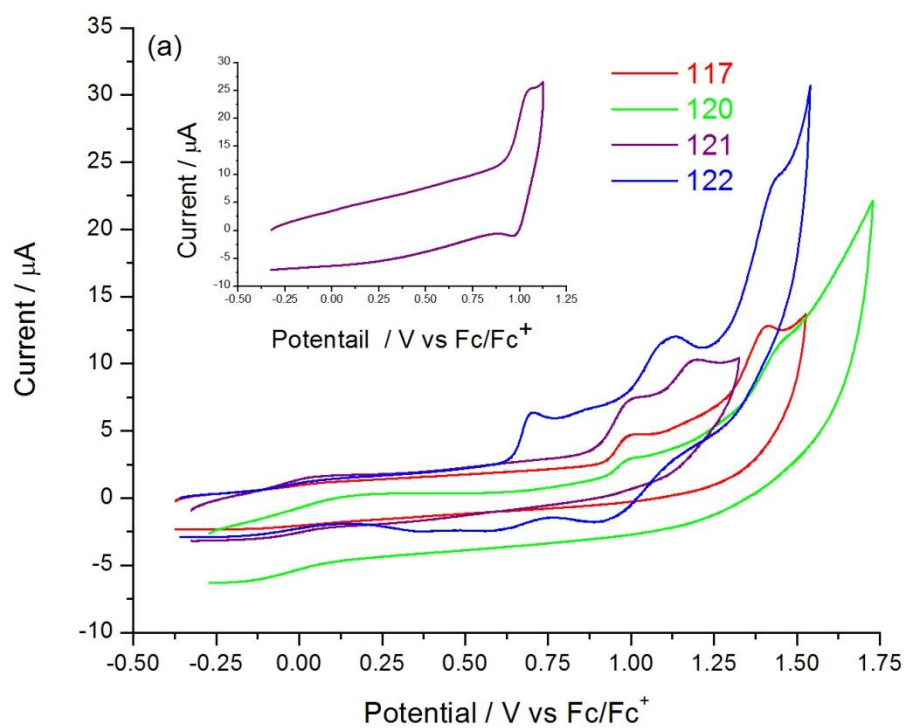


Figure 5.4 Cyclic voltammograms of (a) oxidation and (b) reduction of, **117**, **120**, **121** and **122**. The oxidation of **121** at 1 V s^{-1} is in the inset of (a) and the reduction of **123** is in the inset of (b)

Table 5.1 Absorption spectroscopy and electrochemical data for monomers **117**, **120**, **121** and **122**

| Monomer | UV-vis peaks (nm) | | | Optical E_g / eV | Oxidation / V | | | Reduction / V |
|------------|-------------------|-----------------|-----------------|-----------------------|--------------------------|--------------------|--------------------|--------------------|
| | 1 st | 2 nd | 3 rd | | 1 st | 2 nd | 3 rd | |
| 117 | 361 | 379 | 398 | 3.02 | +0.99 ⁱ | +1.41 ¹ | - | -2.27 ¹ |
| 120 | 361 | 378 | 391 | 3.01 | +1.00 ⁱ | +1.45 ⁱ | - | -2.11 ⁱ |
| 121 | 365 | 383 | 403 | 2.97 | +1.00/+0.96 ^a | +1.20 ⁱ | - | -2.24 ⁱ |
| 122 | 428 | 452 | - | 2.61 | +0.70/+0.59 ^b | +1.12/+0.91 | +1.43 ⁱ | -2.04 ⁱ |

^a only reversible with a scan rate of 1 V s⁻¹. ^b quasi-reversible peak. ⁱ Irreversible peak

To calculate the HOMO and LUMO energy levels and then the electrochemical HOMO-LUMO gap, CVs of **117**, **120**, **121** and **122** were measured (Figure 5.5). By subtracting the onset of the first oxidation and reduction waves from the HOMO of ferrocene (-4.8 eV), the HOMO and LUMO levels were determined. All data are summarised in Table 5.2. By comparing the energy levels, **122** has the highest HOMO (-5.49 eV) and the lowest LUMO (-2.88 eV) and therefore the smallest energy gap (2.61 eV). This is due to the extended conjugation afforded by the two bis-thiophene units. The monomers containing only two thiophenes have slightly differing HOMO and LUMO levels but essentially the same HOMO-LUMO gap. The HOMO-LUMO gaps for **117**, **120** and **121** are 3.07, 3.09 and 3.07 eV, respectively.

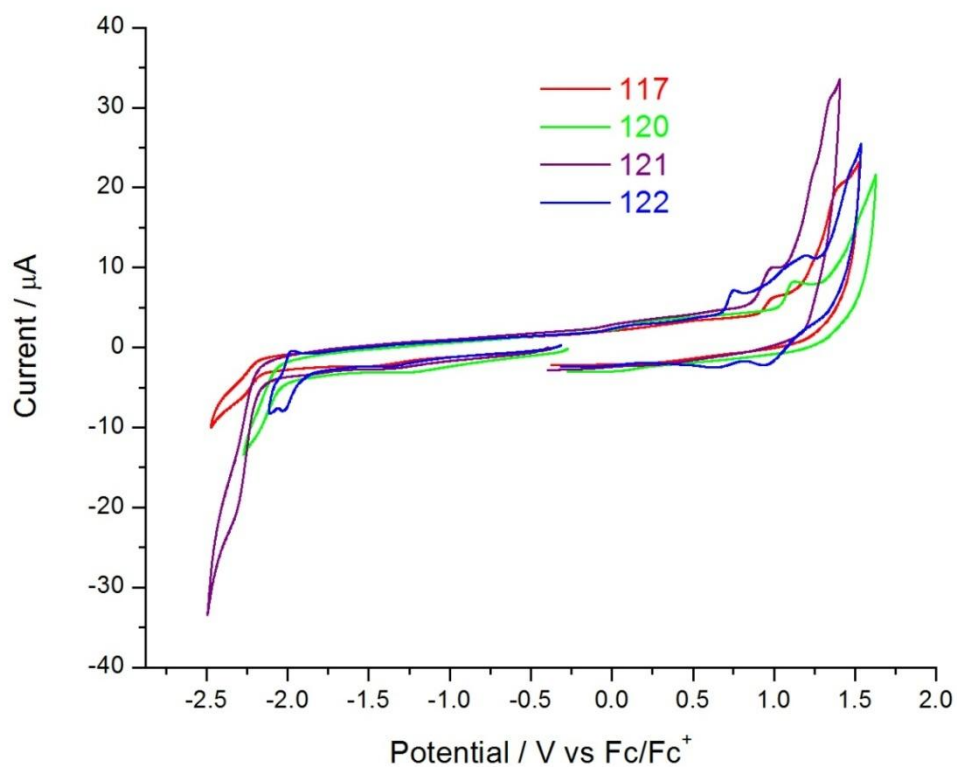


Figure 5.5 Cyclic voltammograms of **117**, **120**, **121** and **122** for energy level determination

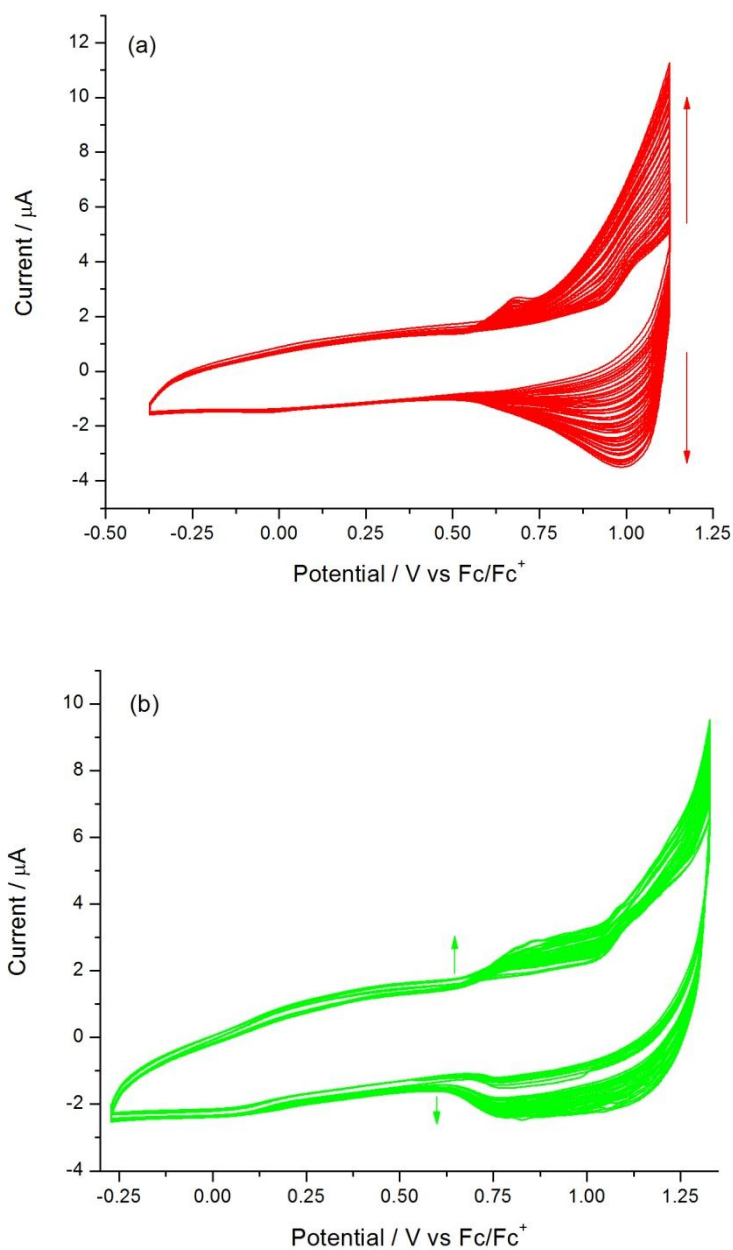
Table 5.2 Energy levels of **117**, **120**, **121** and **122**

| Monomer | HOMO / eV ^a | LUMO / eV ^a | E _g / eV ^b |
|------------|------------------------|------------------------|----------------------------------|
| 117 | -5.71 | -2.64 | 3.07 |
| 120 | -5.84 | -2.75 | 3.09 |
| 121 | -5.67 | -2.60 | 3.07 |
| 122 | -5.49 | -2.88 | 2.61 |

^a HOMO and LUMO values are calculated from the onset of the first peak of the corresponding redox wave and referenced to ferrocene, which has a HOMO of -4.8 eV. ^bE_g is the HOMO-LUMO energy gap.

5.5 Electrochemistry of the Polymers

Polymer films of **117**, **120** and **122** were produced by repetitive cycling over the first oxidation peak. The graphs produced from electrochemical growth on the glassy carbon electrodes can be seen in Figure 5.6. The development of the polymeric material can be seen with the increase in current and creation of a new peak at lower potentials.



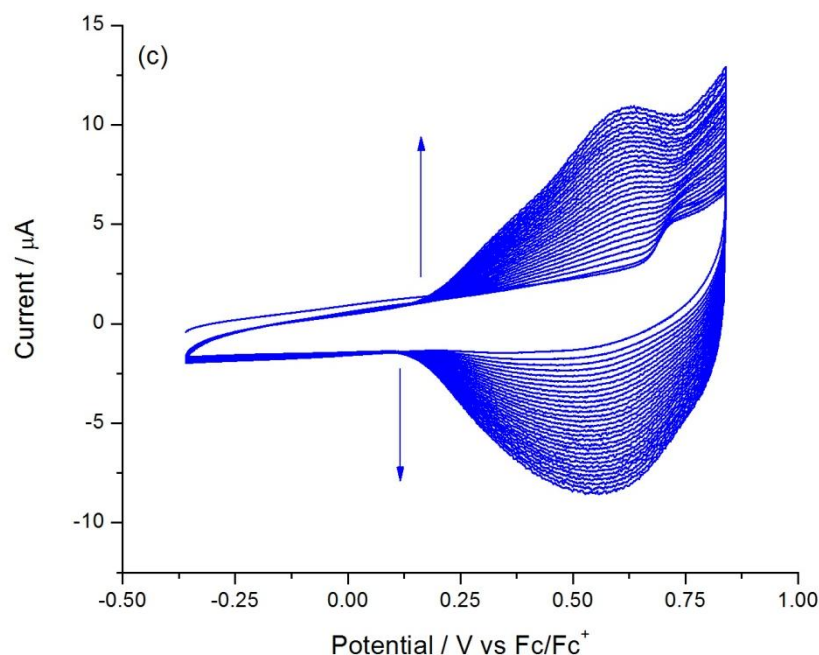


Figure 5.6 Electrochemical growth of (a) poly**117**, (b) poly**120** and (c) poly**122**

The electrochemistry of the polymers was performed in a monomer-free solution and the oxidation processes are shown in Figure 5.7(a). The oxidation curves are different for the three polymers. Poly**117** shows only an irreversible wave at $E^{1ox} = +0.82$ V. Poly**120** shows an irreversible wave at a higher potential ($E^{1ox} = +0.91$ V) but also a reversible wave at $E_{1/2}^{2ox} = +1.06$ V. Poly**122** has two reversible waves, $E_{1/2}^{1ox} = +0.61$ V and $E_{1/2}^{2ox} = +0.94$ V; the lower oxidation potential and reversibility compared to the other two polymers can be attributed to the extended conjugation of having a quarterthiophene in the polymer chain to help stabilise the loss of electrons.

Surprisingly, despite having irreversible first oxidation waves, the reduction of poly**117** and poly**120** are reversible with half-waves of $E_{1/2}^{1red} = -1.88$ V and $E_{1/2}^{1red} = -1.86$ V, respectively. The reduction of poly**122** shows two reversible waves within a similar potential window, with reduction potentials of $E_{1/2}^{1red} = -1.93$ V and $E_{1/2}^{2red}$

= -2.07 V. Fascinatingly, unlike the monomer, having extra thiophenes in the chain of poly122 actually causes the reduction potential to be at a lower potential compared to the other two polymers. All data are summarised in Table 5.3.

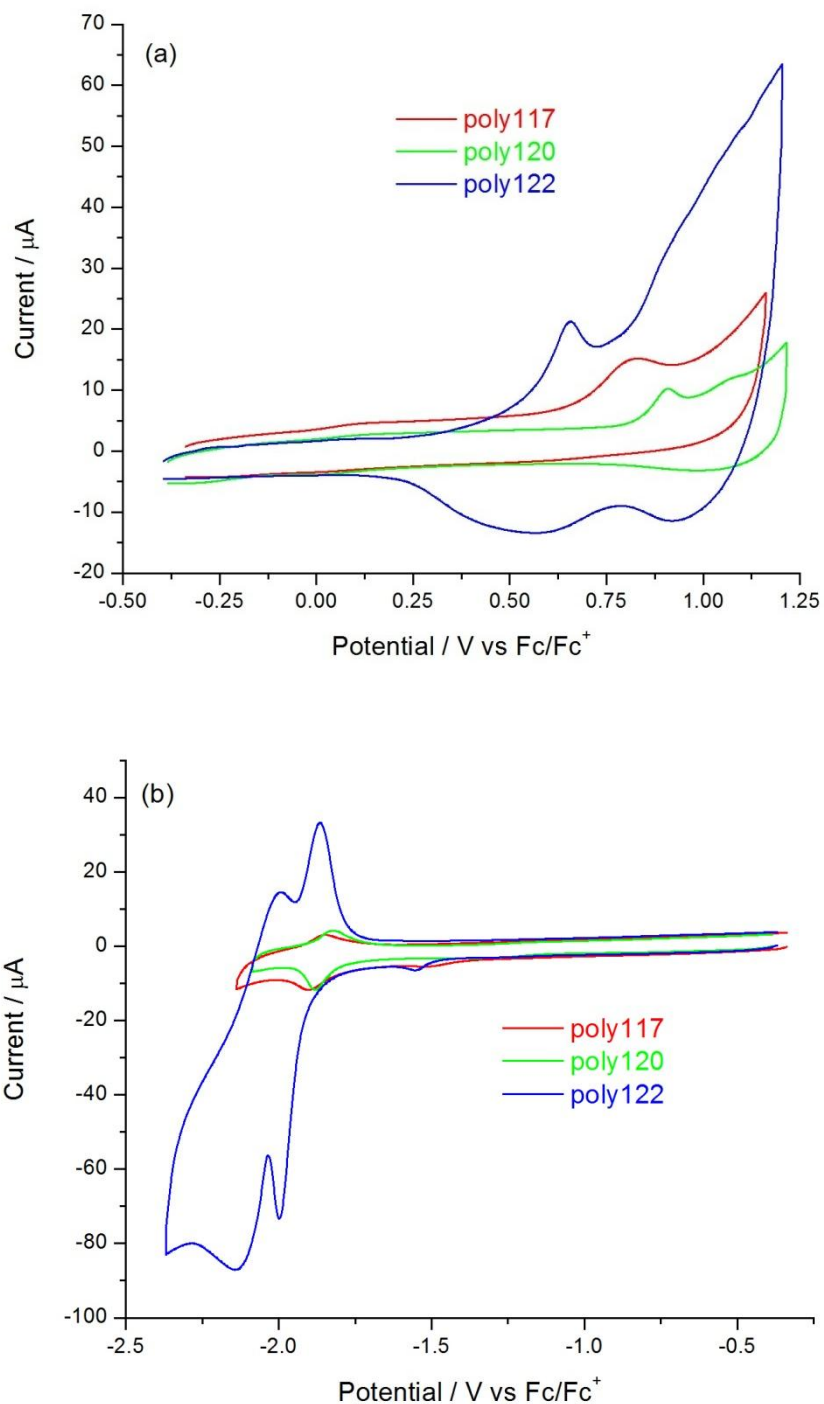


Figure 5.7 Cyclic voltammograms of (a) oxidation and (b) reduction of poly117, poly120 and poly122

Using the same procedure as before for energy level determination, cycles of the three polymers (Figure 5.8) were recorded and the onsets of oxidation and reduction subtracted from the HOMO of ferrocene (-4.8 eV). The data are summarised in Table 5.4. All three polymers have varying HOMO and LUMO levels but the band gaps (E_g) are almost identical (2.45 eV for poly**117** and poly**120** and 2.40 eV for poly**122**).

The band gaps of the polymers are in the same range seen for other BTZ polymers.²³² However, the band gaps are larger than other donor-acceptor polymers and this suggests that in these polymers there is not a significant degree of intramolecular charge transfer between the BTZ and thiophene heterocycles.²²⁸

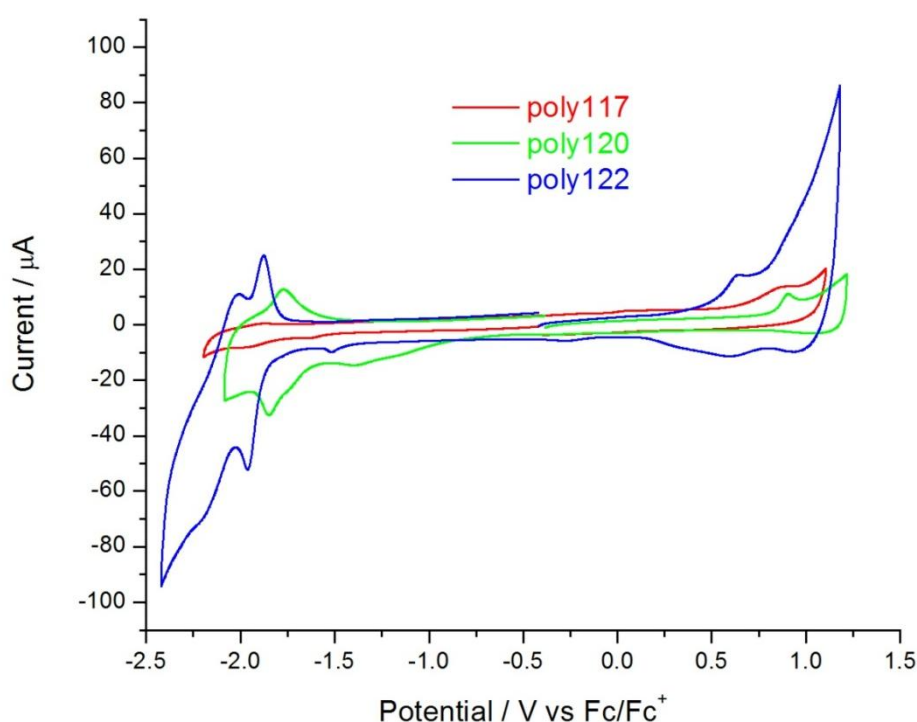


Figure 5.8 Cyclic voltammograms of poly**117**, poly**120** and poly**122** for energy level determination

Table 5.3 Electrochemical data of poly**117**, poly**120** and poly**122**

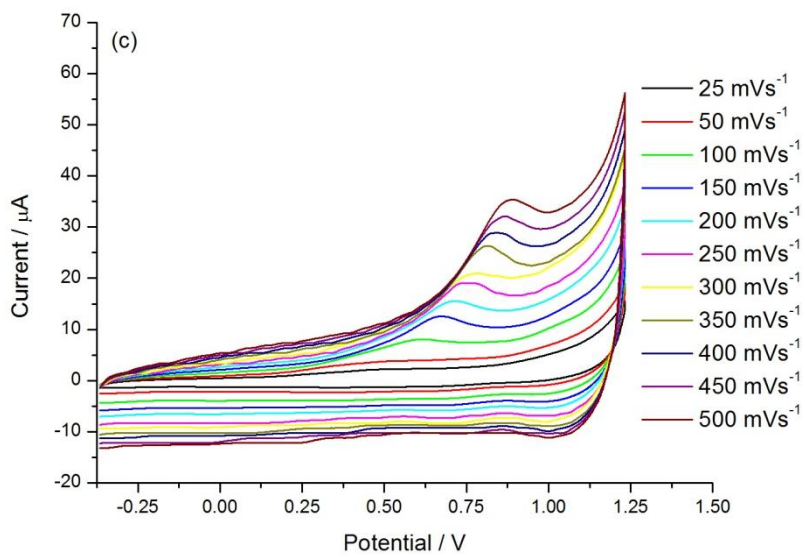
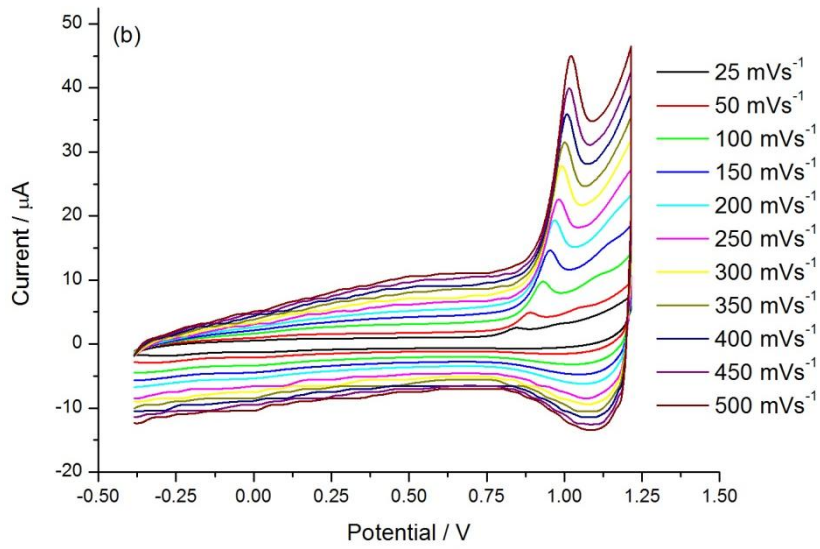
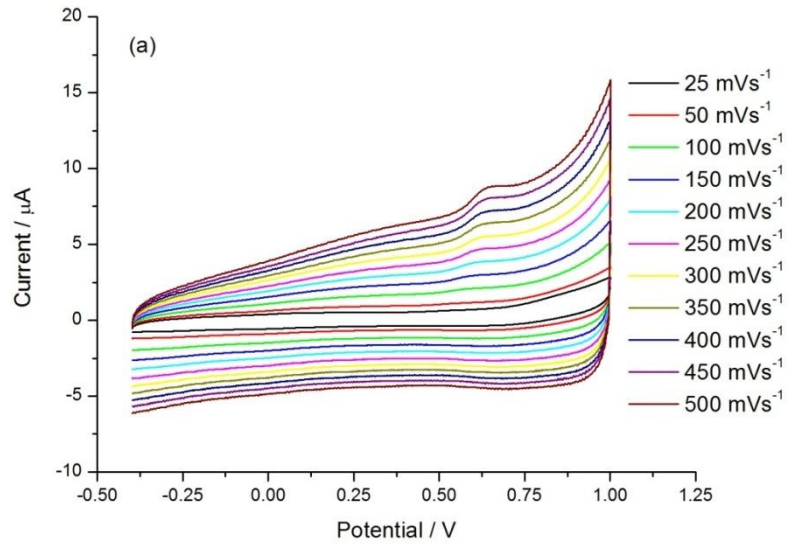
| Polymer | Oxidation / V | | Reduction / V | |
|-----------------|--------------------|-----------------|-----------------|-----------------|
| | 1 st | 2 nd | 1 st | 2 nd |
| poly 117 | +0.82 ⁱ | - | -1.90 / -1.85 | - |
| poly 120 | +0.91 ⁱ | +1.08 / +1.03 | -1.89 / -1.82 | - |
| poly 122 | +0.65 / +0.56 | +0.95 / 0.93 | -2.00 / -1.86 | -2.14 / -1.99 |

ⁱ Irreversible peak**Table 5.4** Energy level data of poly**117**, poly**120** and poly**122**

| Polymer | HOMO / eV ^a | LUMO / eV ^a | E _g / eV ^b |
|-----------------|------------------------|------------------------|----------------------------------|
| poly 117 | -5.46 | -3.01 | 2.45 |
| poly 120 | -5.63 | -3.18 | 2.45 |
| poly 122 | -5.32 | -2.92 | 2.40 |

^a HOMO and LUMO values are calculated from the onset of the first peak of the corresponding redox wave and referenced to ferrocene, which has a HOMO of -4.8 eV. ^bE_g is the HOMO-LUMO energy gap.

To evaluate the stability and electrochemical behaviour of the polymers, oxidation cycles over the first peaks were measured at increasing scan rates (Figure 5.9(a) to (c)). From these data, the plots of scan rate versus current maxima were plotted and the resulting graph is shown in Figure 5.9(d). Each polymer produced a linear fit with high R² values of 0.9994, 0.9988, and 0.9957 for poly**117**, poly**120**, and poly**122**, respectively, proving that the redox processes are not diffusion limited.



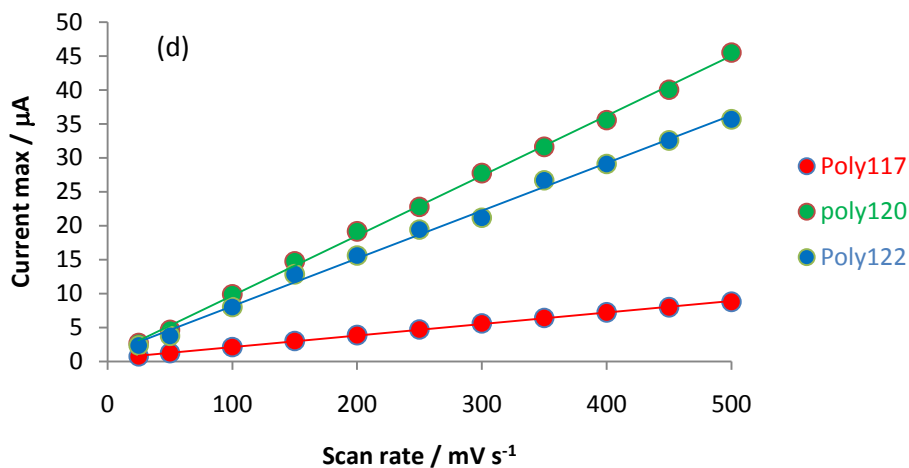
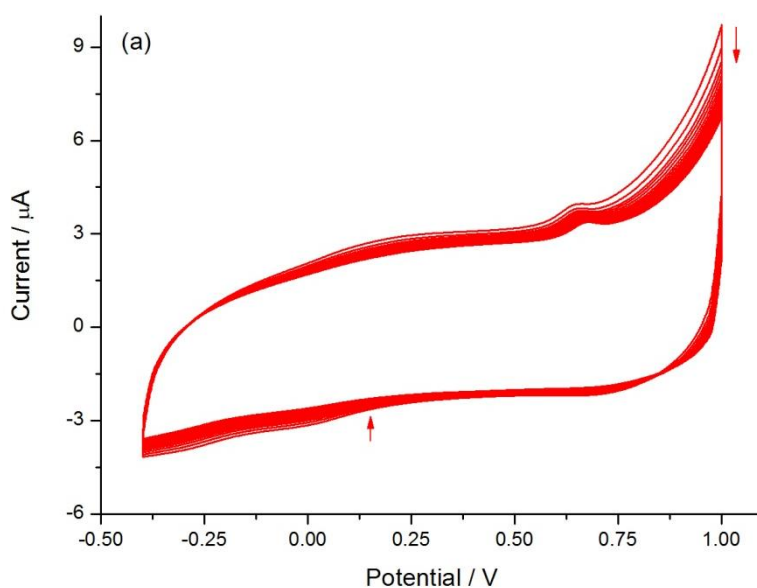


Figure 5.9 Scan rate experiments of (a) poly117, (b) poly120, (c) poly122. The plot of scan rate versus current maxima of all three polymers is shown in (d).

The stability of the polymers to adhere to the glassy carbon electrode was evaluated by cycling over the redox-active ranges for 20 cycles and measuring the percentage decrease in the current response. Poly117 showed the best stability with only a 17 and 11% decrease for oxidation and reduction, respectively. Poly120 shows an 18 and 12% decrease for oxidation and reduction, respectively and poly122 has the least stability with a 16 and 25% decrease for oxidation and reduction, respectively.



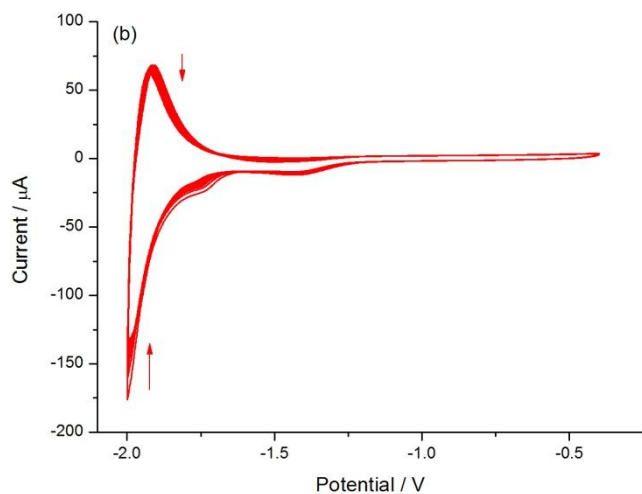


Figure 5.10 Poly117 (a) oxidation and (b) reduction stability test

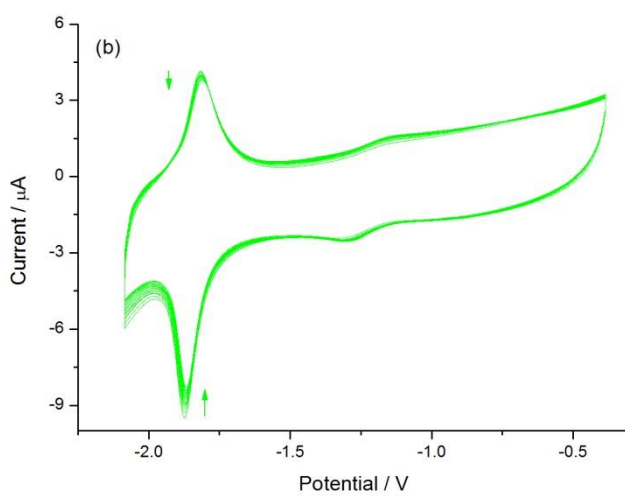
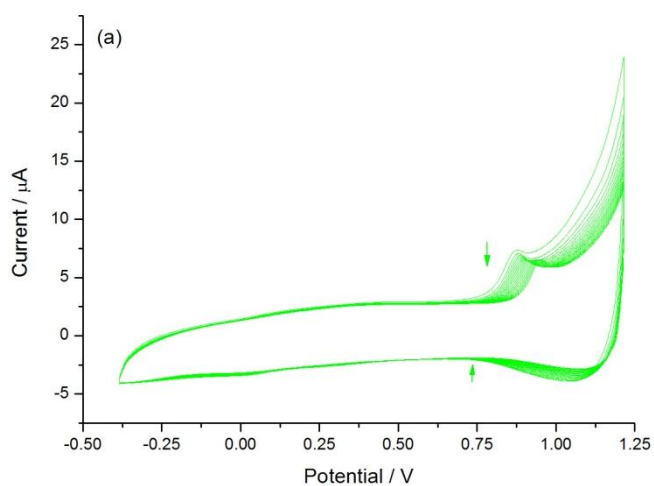


Figure 5.11 Poly120 (a) oxidation and (b) reduction stability test

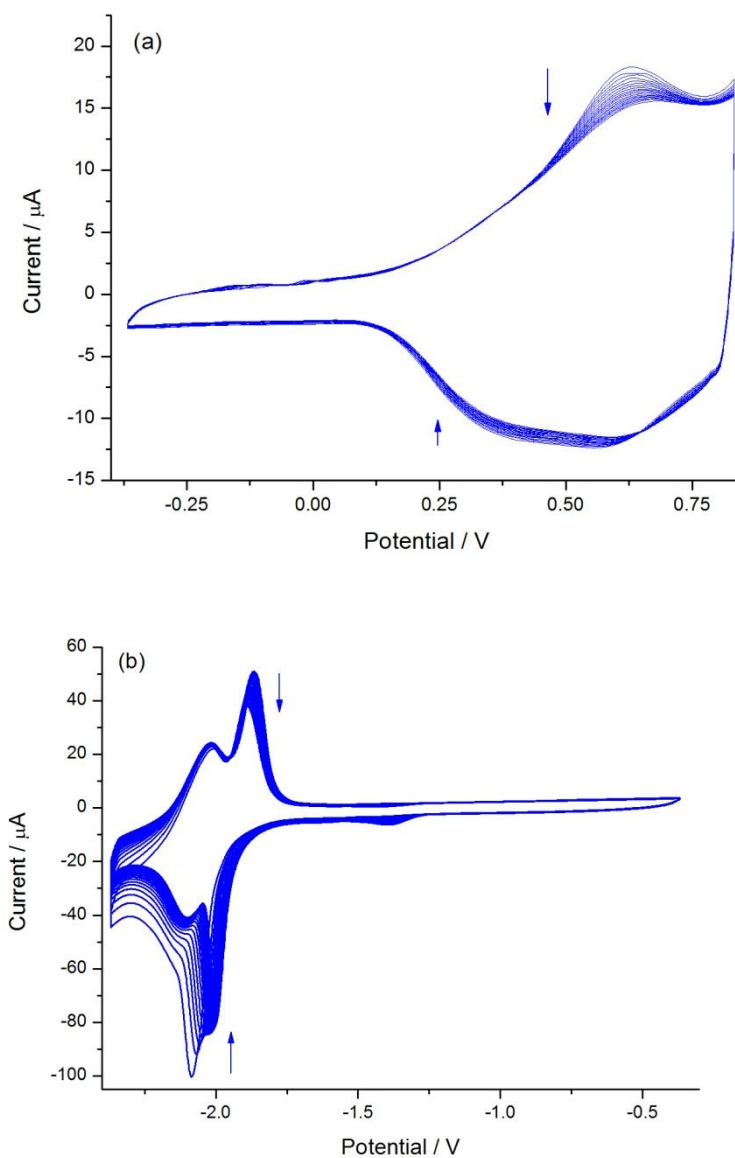


Figure 5.12 Poly122 (a) oxidation and (b) reduction stability test

5.6 Absorption spectroscopy and spectroelectrochemical analysis of the polymers

To measure the solid-state absorbance spectra of the polymers, the three polymers were grown onto the surface of ITO glass slides in higher concentration monomer solutions (1 mM) and then dedoped (-0.2 to 0 V for 30 minutes) in a region of no redox activity to expel trapped electrolyte. The spectra of the three polymers are shown in Figure 5.13. The absorption maxima and the optical band gaps, calculated from the onset of the longest wavelength absorption edge, are summarised in Table 5.5

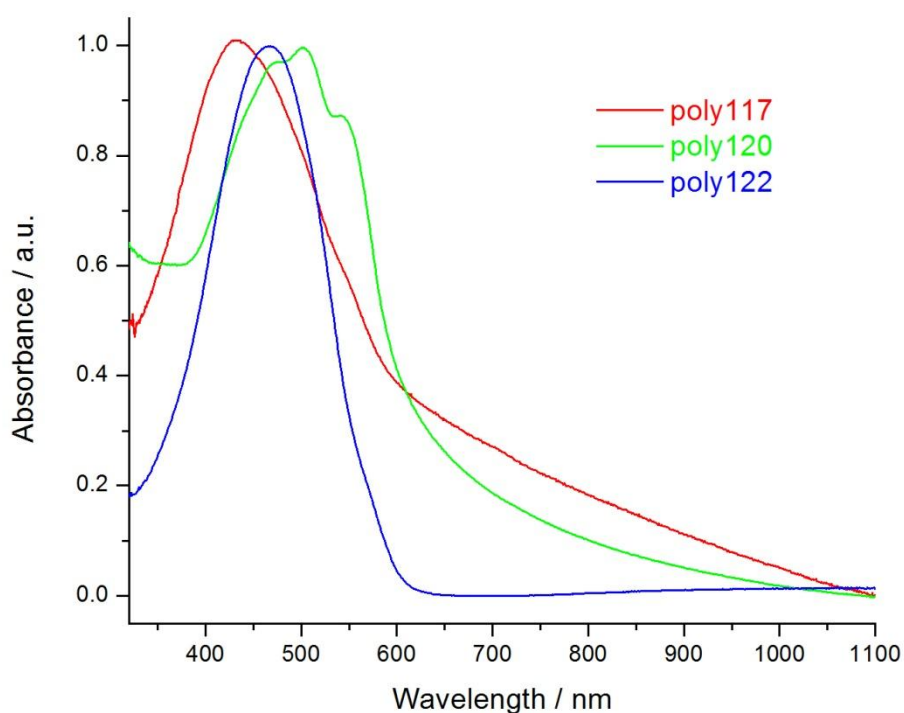


Figure 5.13 UV-vis spectra of poly117, poly120 and poly122 in the solid state

All three polymers have similar optical band gaps (2.08, 2.03, and 2.05 eV for poly**117**, poly**120** and poly**122**), but differ in shape and values for absorption maxima. Poly**117** is broad compared to poly**122** and has a λ_{max} at 432 nm (poly**122** has λ_{max} of 468nm). The absorption band for poly**120** is also broad with the longest wavelength λ_{max} at 503 nm and it is the only polymer to show a shoulder (562 nm). The optical band gaps are lower than the electrochemically determined band gaps, suggesting that the HOMOs and LUMOs are more localised rather than dispersed over the polymer chain. The optical band gap of poly**122** (2.05 eV) is very similar to that of **119** (1.97 eV).²²⁸

Table 5.5 Absorption spectroscopy data for poly**117**, poly**120** and poly**122**

| Polymer | UV-vis λ_{max} / nm | Optical E_g / eV |
|-----------------|------------------------------------|--------------------|
| poly 117 | 432 | 2.08 |
| poly 120 | 503 | 2.03 |
| poly 122 | 468 | 2.05 |

UV-vis spectroelectrochemistry experiments were performed on the three polymers to investigate the effect that p-doping has on the electronic spectra of the polymer. The results of the spectroelectrochemistry (SEC) experiments of poly**117**, poly**120**, and poly**122** are shown in Figure 5.14, Figure 5.15, and Figure 5.16, respectively. All three graphs follow very similar trends. In the SEC of poly**117** (Figure 5.14), no change occurs until around +0.9 V (coincidental with the first oxidation wave in the CV), where the π - π^* transition peak starts to decrease from the disruption of π -conjugation alongside the development of a new broad absorption band (*ca.* 750

nm). The creation of polarons and bipolarons in the polymer chain peak at +1.5 V where there is also a small absorbance extending into the near-IR

The UV-vis spectroelectrochemistry plot of poly**120** (Figure 5.15) also shows no activity until +0.9 V, whereupon the π - π^* transition decreases (to a greater extent than in poly**117**) and there is a concomitant growth of a broad wave between 350 and 900 nm and another wave extending into the near-IR. For this polymer, the new absorbance waves peak at +1.4 V and it is also worth noting that the new peaks have a greater absorbance. This is accompanied by a greater decrease in the π - π^* band, suggesting that the delocalisation is greater for poly**120** than poly**117**.

Poly**122** shows a very interesting SEC plot (Figure 5.16). Again, the shape of the absorption spectra does not change until around +0.9 V and the evolving peaks reach a maximum at +1.4 V. In this p-doping experiment, there is an even greater drop in the π - π^* transition, suggesting larger π -delocalisation, the broad absorption band starts at 600 nm and extends to the near-IR. The absorption peaks belonging to the polarons and bipolarons are more persistent and do not diminish to the same extent as they do in the other two spectroelectrochemical experiments.

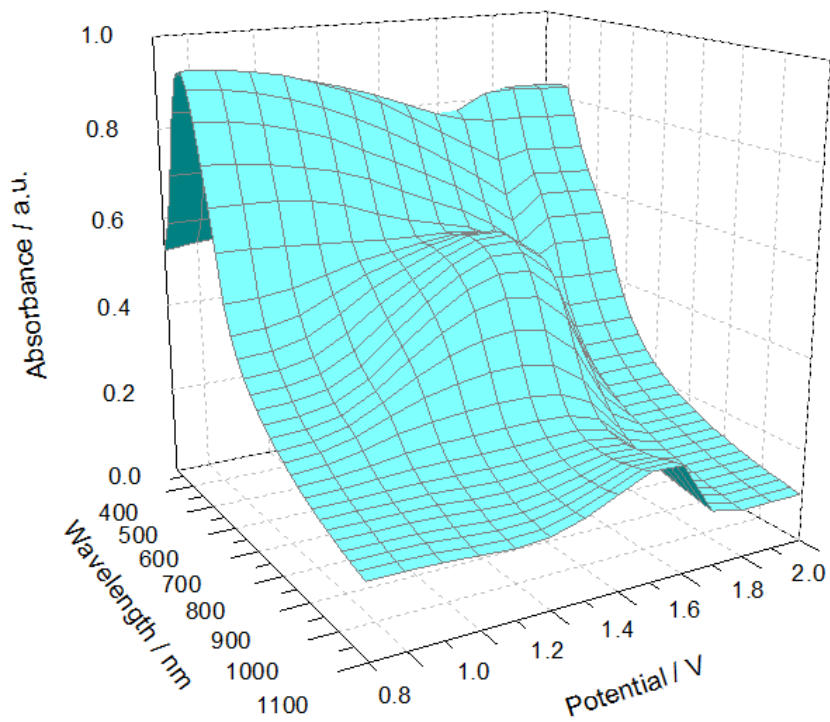


Figure 5.14 UV-vis spectroelectrochemistry of poly117 upon p-doping

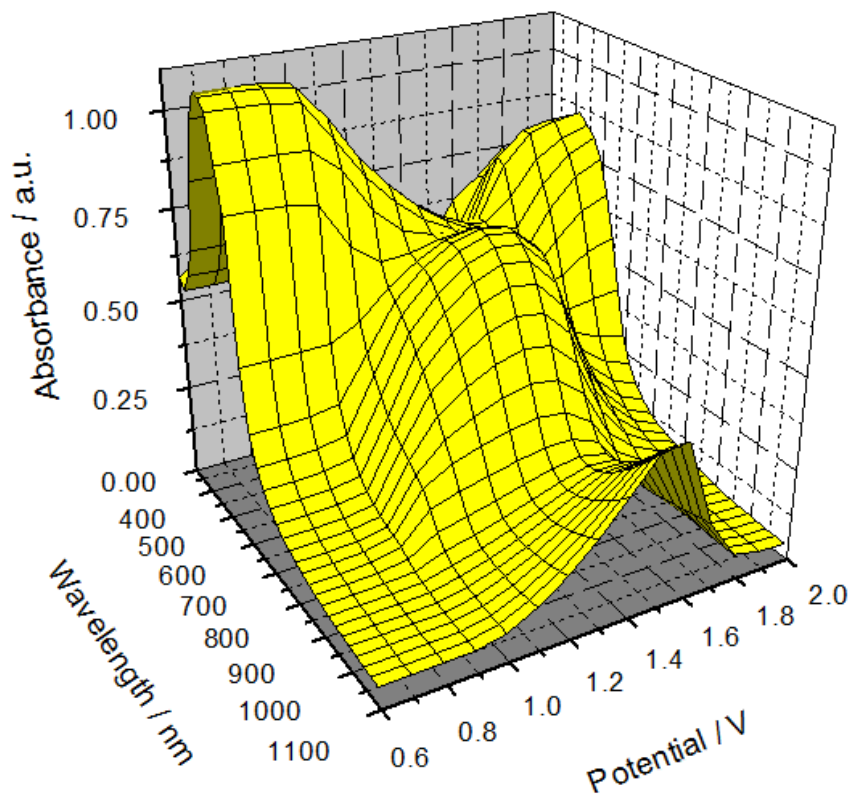


Figure 5.15 UV-vis spectroelectrochemistry of poly120 upon p-doping

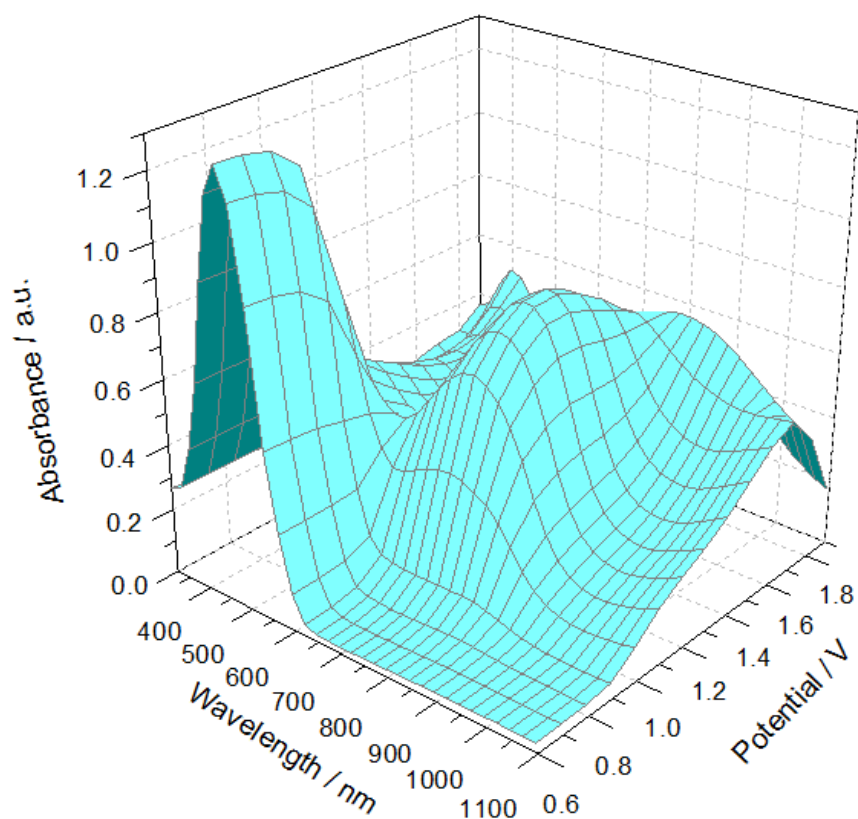


Figure 5.16 UV-vis spectroelectrochemistry of poly122 upon p-doping

From the spectroelectrochemistry experiments, it was noticed that these polymers have a large change in the electronic absorption spectra from the neutral and doped states. Each polymer has a noticeable colour change, as seen in the photographs in Figure 5.17, Figure 5.18 and Figure 5.19. The electrochromic properties of the polymers were investigated by recording the change in absorbance of peak maxima over various switching times between p-doping and dedoping; the colour coordinates were also measured.

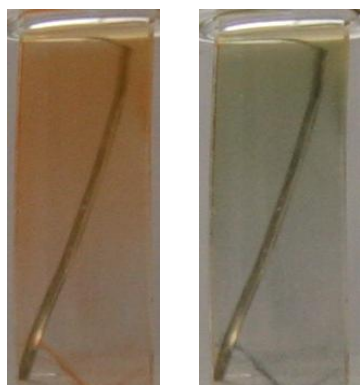


Figure 5.17 Electrochromic colour change of poly117 between neutral (left) and doped state (right)

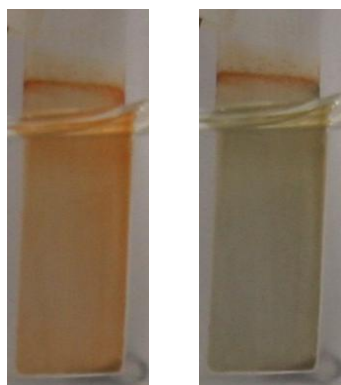


Figure 5.18 Electrochromic colour change of poly120 between neutral (left) and doped state (right)

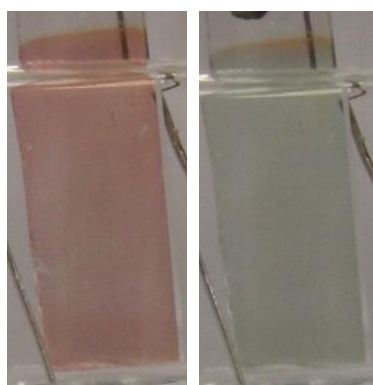
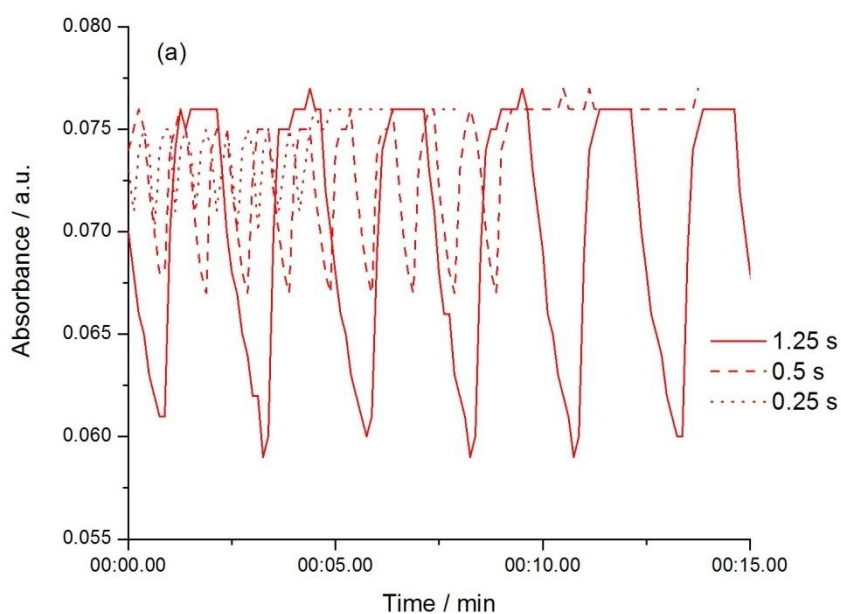
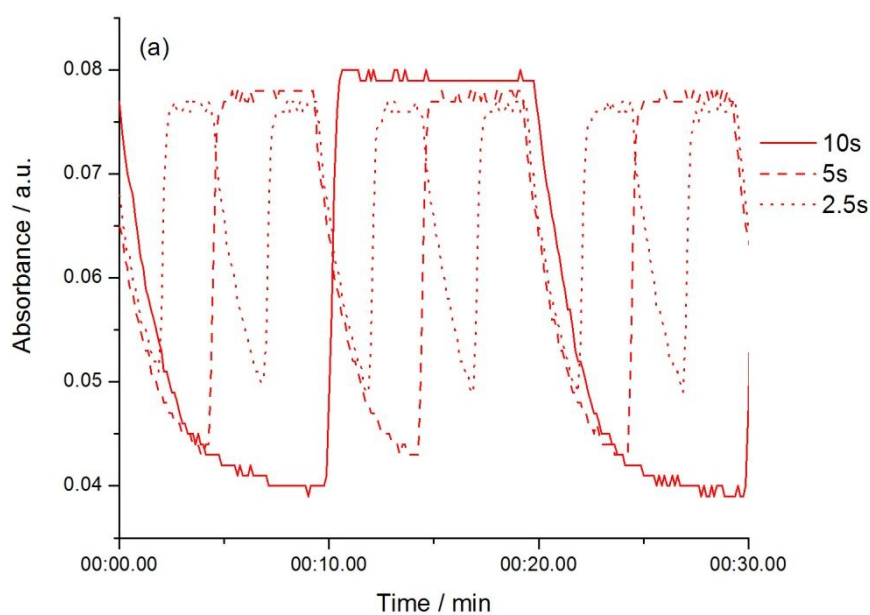
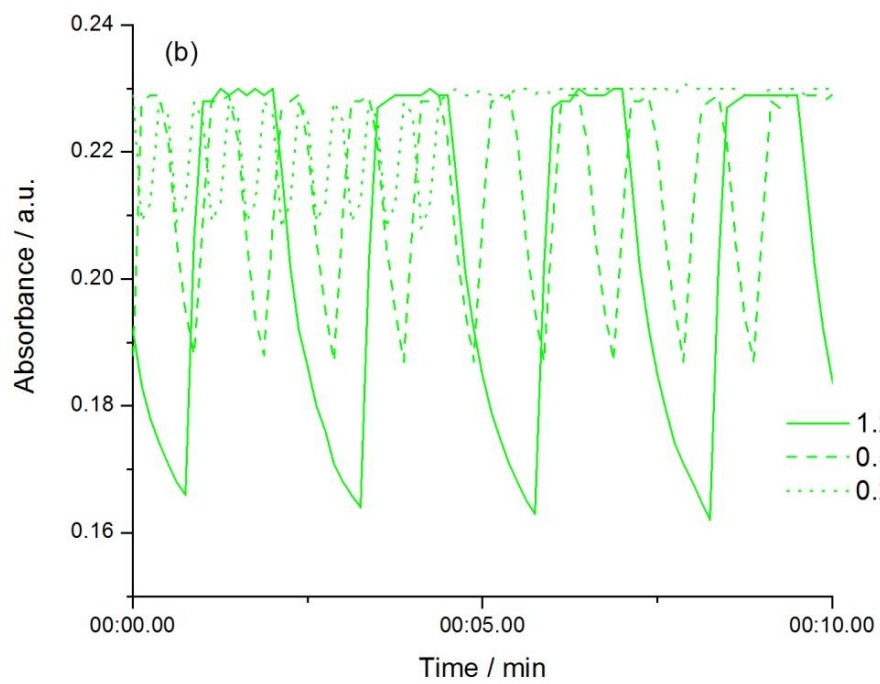
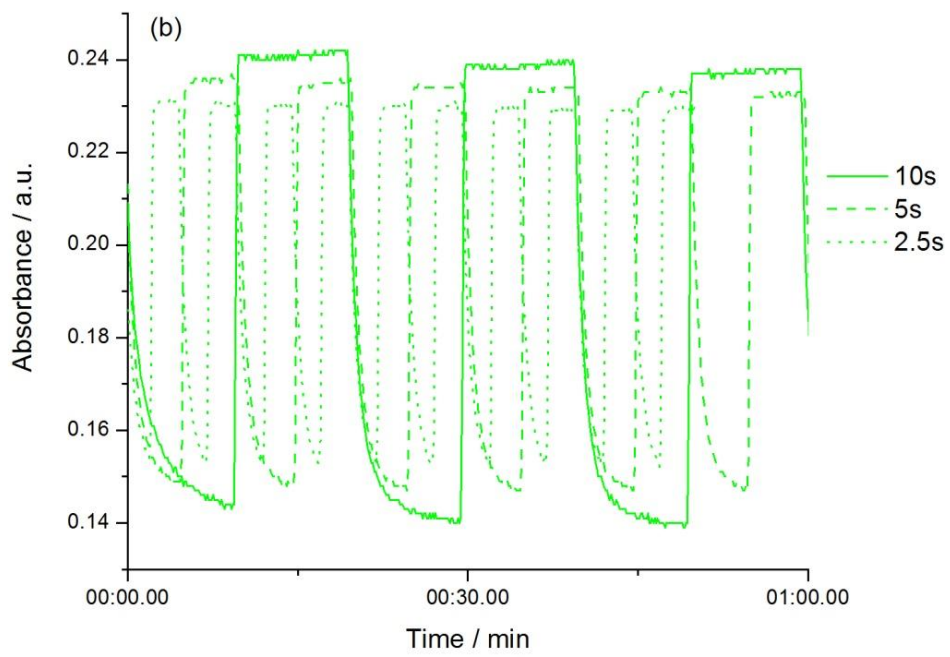


Figure 5.19 Electrochromic colour change of Poly122 between neutral (left) and doped state (right)

For the switching time measurements, fresh polymers were grown on ITO glass and dedoped. The polymers were switched between their neutral (0V) and doped (+1.5 V) states with the absorbance measured at 485, 468, and 485 nm for poly**117**, poly**120** and poly**122**, respectively, which provided the greatest change in absorbance. The switching times were measured for 10, 5, 2.5, 1.25, 0.5 and 0.25 seconds. The changes in absorbance can be seen in Figure 5.20 and are summarised in Table 5.6.





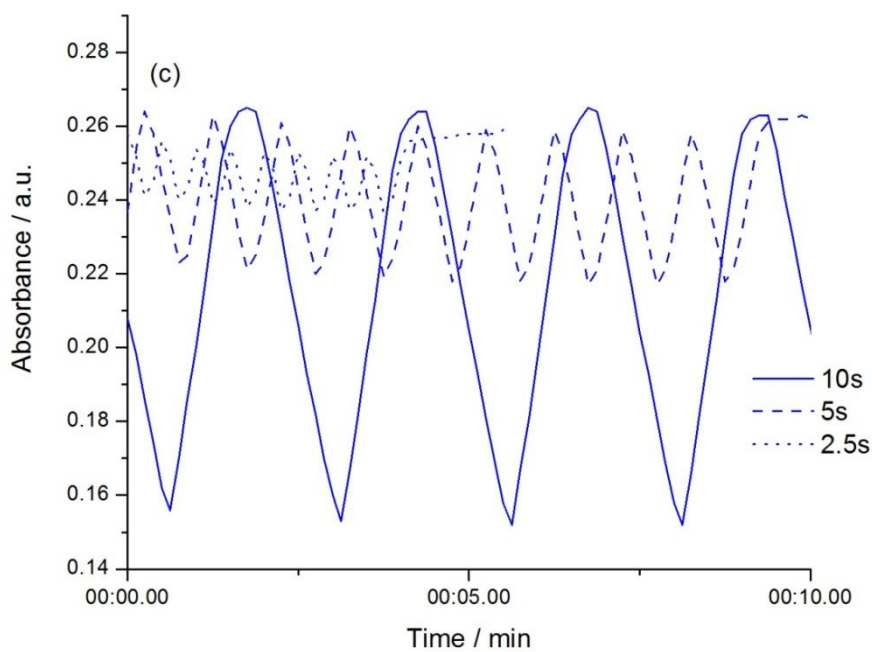
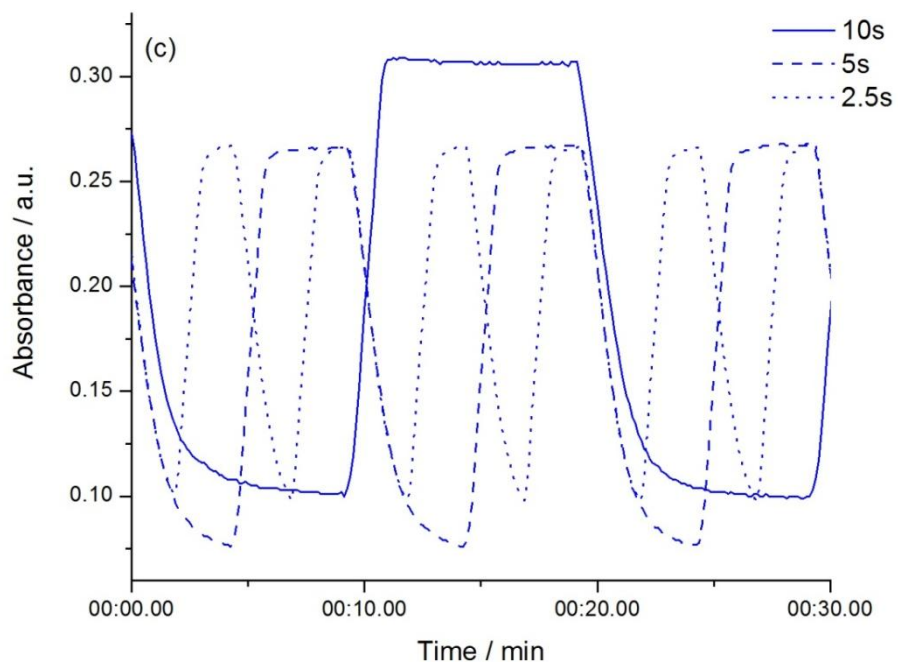


Figure 5.20 Switching times of (a) poly117, (b) poly120 and (c) poly122

Table 5.6 Switching times and percentage change in absorbance

| Switching Time / s | % change poly 117 | % change poly 120 | % change poly 122 |
|-----------------------|-----------------------------|-----------------------------|-----------------------------|
| 10 | 49.6 % | 42.1 % | 67.4 % |
| 5 | 44.5 % | 37.1 % | 71.4 % |
| 2.5 | 36.0 % | 33.3 % | 63.4 % |
| 1.25 | 22.4 % | 28.6 % | 42.2 % |
| 0.5 | 11.9 % | 18.6 % | 15.52 % |
| 0.25 | 6.7 % | 8.9 % | 6.4 % |

Comparison of the results shows, that poly**122** shows the best switching rates as it has the most delocalised π -electrons. The degree of delocalisation explains the greater switching ability seen for poly**117** compared to poly**120**. As the spectroelectrochemistry experiments suggest, poly**120** is more delocalised. This difference between two very similar structures can be explained by the positioning of the hexyl chains. Growth of poly**117** can produce a less packed polymer, allowing more facile diffusion of counter-ions in and out of the polymer film upon doping-dedoping, whereas poly**120** likely produces a more planar structure and packs more tightly.

CIE colour coordinates were measured for each polymer in the neutral and doped states using both the 1931 (Y_{xy}) and 1976 ($L^*a^*b^*$) CIE representation of colour space. Table 5.7 shows the data produced from the measurements.

Table 5.7 Y_{xy} and L^{*}a^{*}b^{*} Colour characteristics for poly**117**, poly**120** and poly**122**

| | Y | x | y | L* | a* | b* |
|-------------------------|--------|--------|--------|--------|-------|-------|
| Poly 117 neutral | 116.00 | 0.3184 | 0.3126 | 105.88 | 8.06 | -1.15 |
| Poly 117 doped | 124.77 | 0.3049 | 0.3090 | 108.11 | 2.52 | -4.45 |
| Poly 120 neutral | 90.30 | 0.3617 | 0.3434 | 96.12 | 12.93 | 18.49 |
| Poly 120 doped | 93.75 | 0.3340 | 0.3341 | 97.53 | 4.46 | 9.92 |
| Poly 122 neutral | 73.34 | 0.3545 | 0.3306 | 88.61 | 14.86 | 11.52 |
| Poly 122 doped | 106.20 | 0.3012 | 0.3179 | 102.35 | -4.53 | -2.13 |

Poly**117** and poly**120** go from an orange / red colour to a green colour, although for poly**120** the orange colour still remains to a small extent. The colour transition for poly**122** is from pink to turquoise as seen in the change of a^{*} and b^{*} coordinates. Of the three polymers, poly**122** gives the greatest visual colour change.

5.7 Conclusions

Five new compounds incorporating benzobisthiazole (BTZ) cores have been characterised by UV-vis absorption spectroscopy and cyclic voltammetry. One compound, **123**, was synthesised for the sole purpose of examining the role of the BTZ core in the analysis. Three of the other four compounds have hexylthiophenes attached at either side with varying positions of the hexyl chain on the thiophenes (2-, 3- and 4-positions of **121**, **117** and **120**, respectively). The last compound has a bis-thiophene at either end and was included in the study to measure the effect of extending the conjugation of these monomers.

In the monomer analysis, the position of the hexyl chain has very little influence for λ_{max} and the extended conjugation of **122** gives a bathochromic shift. In the cyclic voltammetry analysis, only the second oxidation wave is influenced by the hexyl position: the end-capped thiophene (**121**) stabilises the dication and permits oxidation at a lower potential. Monomer **122**, with a longer conjugated chain, shows three oxidation waves in the same electrochemical window with two of them being reversible. In addition, **122** also has the lowest reduction potential and therefore overall has the lowest electrochemical HOMO-LUMO gap.

Only three of the monomers were able to be polymerised. The polymers were measured by cyclic voltammetry, solid-state UV-vis spectroscopy, spectroelectrochemistry, electrochromic switching times, and colourimetry. There were some minor differences between poly**117** and poly**120**. Poly**120** is more delocalised, giving two oxidation waves compared to a single wave for poly**117**. Poly**120** has a greater change in absorbance in the spectroelectrochemistry experiment. Poly**117**, however, is more stable and is more likely to have an open structure, as it has a greater switching ability. Poly**122** shows the greatest contrast for spectroelectrochemistry, switching and colour change, with potential for use in an electrochromic device. The electrochemical and optical band gaps were in good agreement for each polymer.

Chapter 6. The Study of Conjugated Polymers in Biological Applications.

6.1 Abstract

Bio-sensors require polymers with biological-active units, compounds that can electro-polymerise to produce a polymer with a bio-active side group are ideal. In the first section, compound **135** which is based on the biological active group flavin but with terthiophene group attached instead of a benzene ring is analysed. This compound was found not to be able to polymerise, due to an intramolecular charge transfer process occurring which leaves one thiophene electron-deficient and one out of plane of the rest of the molecule. It is postulated that only the twisted thiophene undergoes oxidative coupling, resulting in the formation of a dimer species.

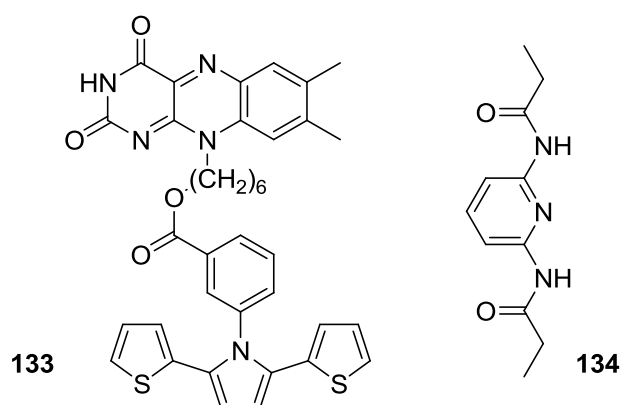
In the second section, a prototype NO sensor was constructed using a nickel porphyrin polymer as the active material. The monomer (**146**) was polymerised first onto the surface of a glassy carbon electrode, the resultant polymer showed a redox response to the addition of NO to the solution. The polymer was grown onto a prototype sensor with carbon fibre as the electrode, these polymer films are stable and can be grown with ease. However, when developing these into sensors for the biological detection of NO *in situ*, a coating of Nafion is required to block out unwanted analytes. This coating makes simple detection of NO difficult and the connection to a NO sensor gives an overflow in current output.

6.2 Biological Sensor Based on Flavin

6.2.1 Introduction

As discussed in section 1.15.5, the ability of an immobilised conducting polymer on an electrode surface that can detect or sense ions through a change in redox or optical properties is a growing field. If the sensing part of the polymer was functionalised to recognise bio-active materials then the polymer has the potential to be used as a bio-sensor.^{233, 234}

Of particular interest in this chapter is the use of a flavin-based sensor that is formed through electropolymerisation. Previous examples of these types of polymers have been shown by the groups of Karyakin,^{235, 236} and Cooke.²³⁷ The research by Cooke *et al.* is the basis for the work in this chapter. A flavin derivative (**133**) was shown to electropolymerise. The polymer's reduction potential shifted to a less negative voltage by the addition of 2,6-diethylamidopyridine (**134**), a consequence of intermolecular hydrogen bonding and the formation of an adduct (Figure 6.1).²³⁷



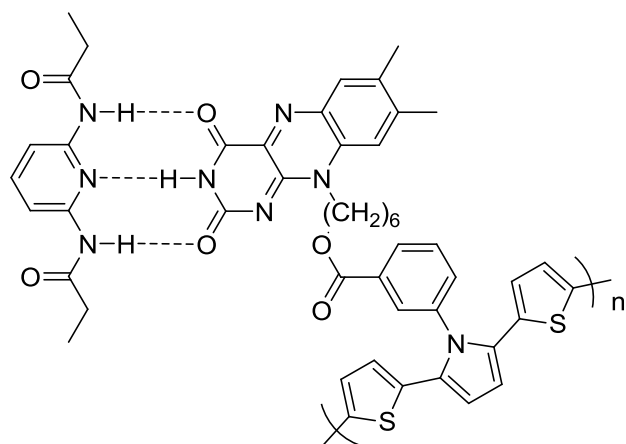
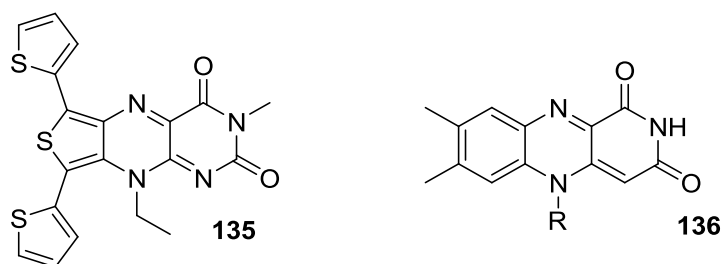


Figure 6.1 Hydrogen bonding between poly**133** and **134**

The compound of interest in this chapter (**135**) is also a flavin derivative but this time fused directly to terthiophene to allow electropolymerisation to produce a much simpler polymer. Flavin (**136**) itself is an isoalloxazine ring found as the redox centre in many enzymes such as flavin adenine dinucleotide, flavin mononucleotide, and the flavoproteins.²³⁸ Flavins are known to catalyse oxidation and reduction in biological systems and act as redox mediators that can easily exchange electrons with proteins and electrodes.²³⁹



The redox potential of flavins are very environment dependent.²⁴⁰ However, most flavin derivatives show that they can be reversibly oxidised (Figure 6.2),²⁴¹ or reduced in either a 1 or 2 step electron addition process (Figure 6.3).²⁴² The singly

reduced state of flavin is known as the semiquinone and the doubly reduced state is the hydroquinone state.²⁴³

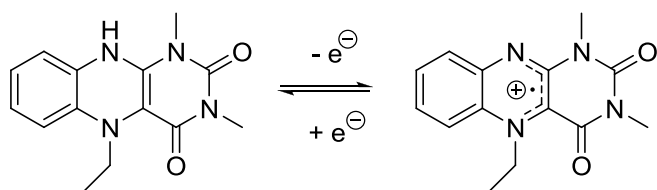


Figure 6.2 Oxidation of flavin

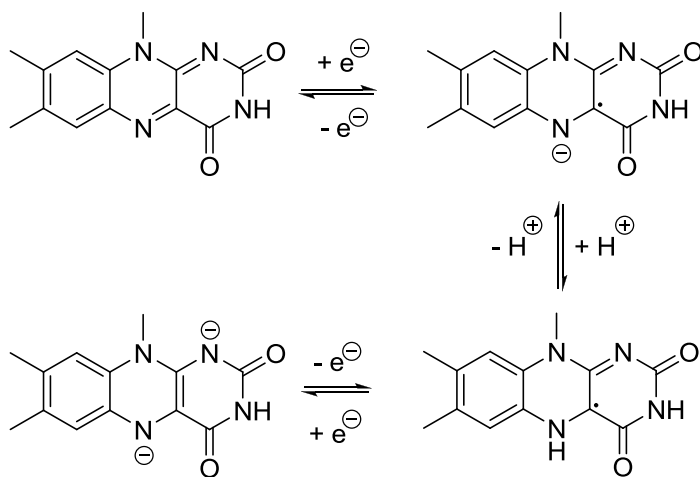
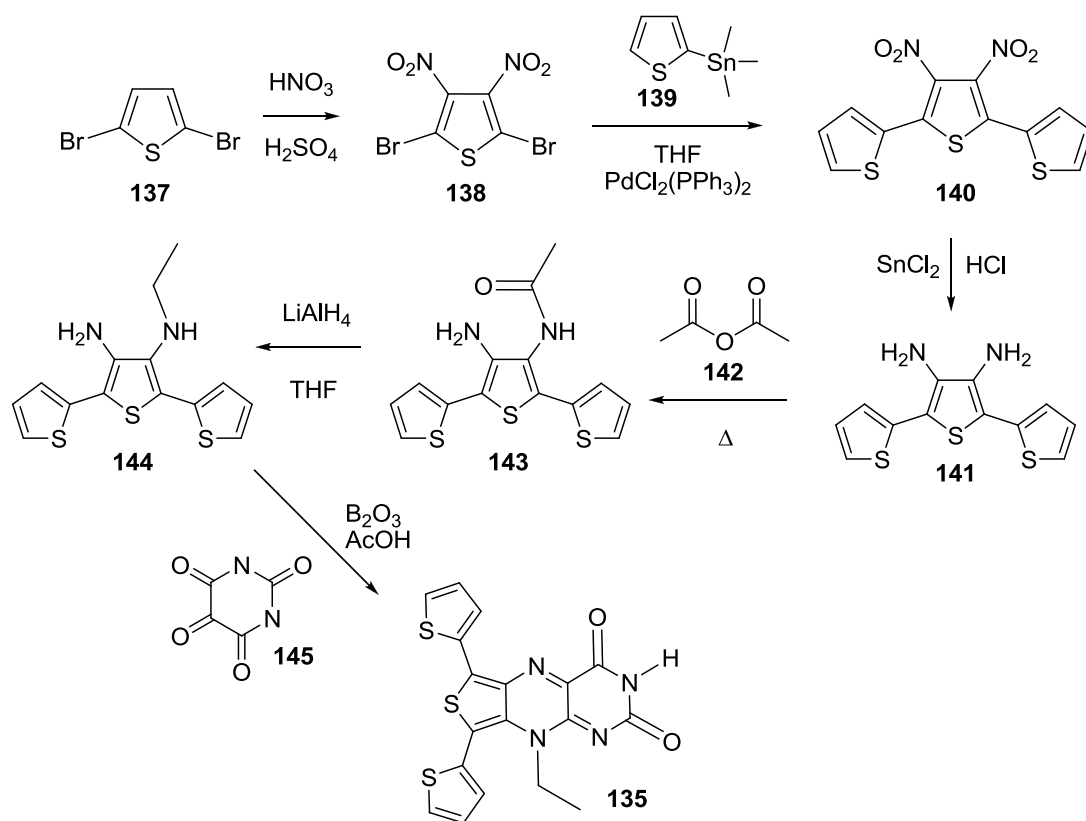


Figure 6.3 Reduction of flavin

In this chapter computational, electronic and electrochemical analysis of **135** is reported along with the attempted polymer growth. The synthetic route to produce **135** is summarised in Scheme 6.1.

Scheme 6.1 Synthesis of **135**



6.2.2 Experimental

The synthesis of compound **135** was performed by Niall McDonald from Dr Cooke's group in the University of Glasgow and the computational analysis was performed by Peter Skabara.

Cyclic voltammetry measurements were performed on a CH Instruments 660A electrochemical workstation with *iR* compensation using anhydrous acetonitrile as the monomer solvent. The electrodes were glassy carbon, platinum wire, and silver wire as the working, counter, and reference electrodes, respectively. All solutions were degassed (Ar) and contained monomer substrates in a concentration of *ca.* 10^{-4}

M, together with $n\text{-Bu}_4\text{NPF}_6$ as the supporting electrolyte (0.1 M). All measurements are referenced against the $E_{1/2}$ of the Fc/Fc^+ redox couple. Absorption spectra were recorded on a UNICAM UV 300 instrument.

6.2.3 Computational analysis

Using Hyperchem, a semi-empirical PM3 calculation was performed to show the most stable conformation of the compound. The result (Figure 6.4) shows that one of the thiophene groups is twisted out of plane and perpendicular to the other two thiophenes by the bulky ethyl group.

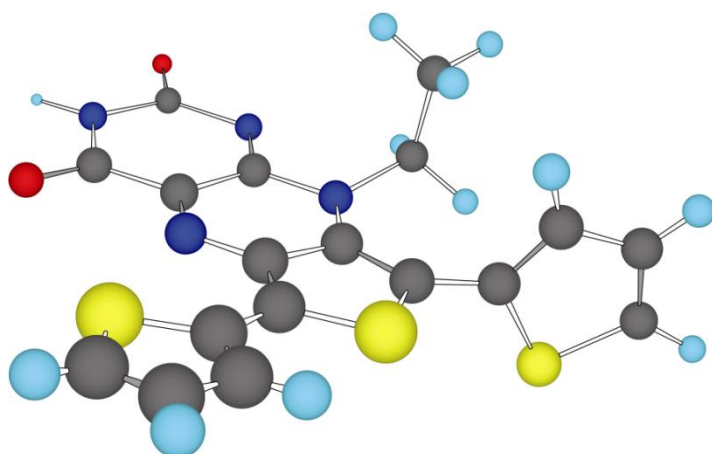


Figure 6.4 Computational analysis of **135**

6.2.4 UV-vis absorption spectroscopy and cyclic voltammetry

The electronic absorption spectrum of **135** was recorded in dichloromethane solution and shown in Figure 6.5. The spectrum shows four main peaks at 260, 303, 437, and

555 nm, also accompanied by a shoulder at 465 nm. The peaks at 260 and 303 nm are characteristic of low energy $n-\pi^*$ transitions from either nitrogen or oxygen heteroatoms in the molecule. The peak at 437 nm is the known absorbance of the flavin part of the compound,²⁴⁴ and the broad peak of low absorbance between 500 and 650 nm can be attributed to an intramolecular charge transfer (ICT) process.

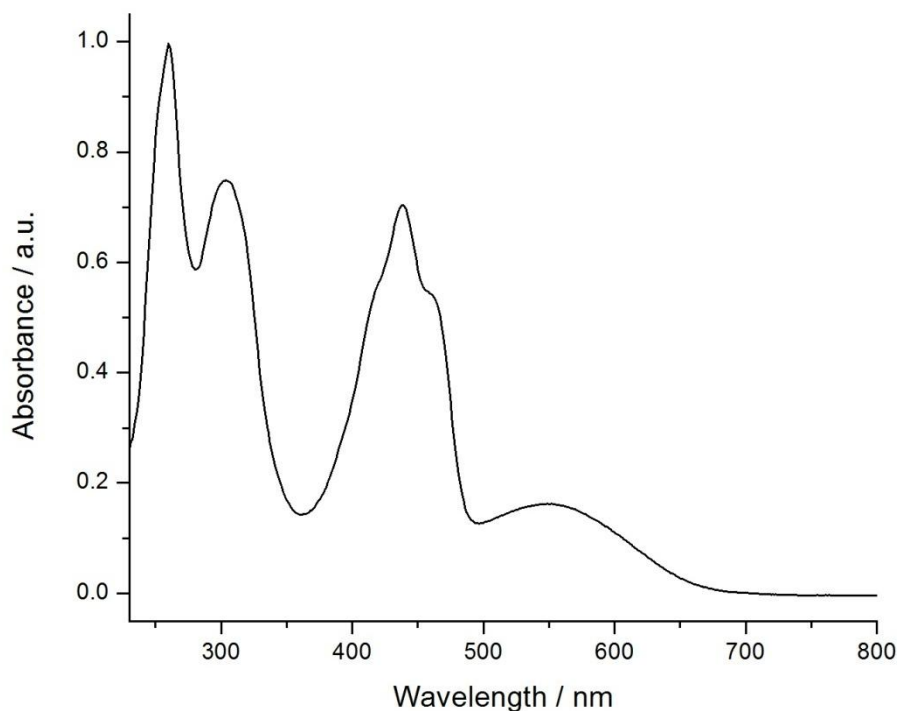
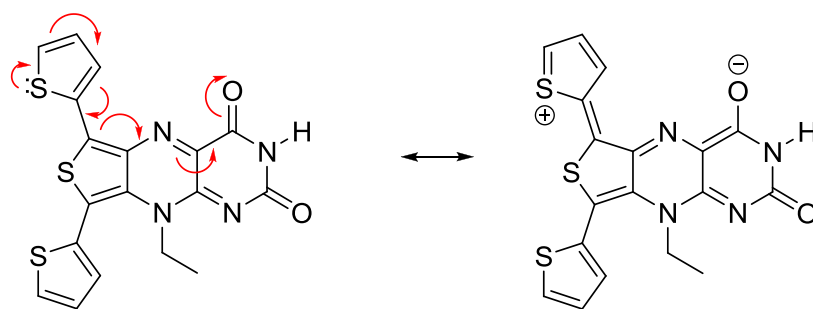


Figure 6.5 UV-vis absorbance of **135**

The mechanism for the ICT process can be seen in Scheme 6.2. The lone pair of electrons from the top thiophene can transfer to one of the oxygens of the carbonyl groups as shown. Transfer to the other oxygen is also possible (not shown). The result of the ICT process is that the thiophene taking part in the charge transfer is electron-deficient and unlikely to oxidise in the electrochemical window. With only one thiophene (the bottom twisted) group likely to form a radical cation upon oxidation this will greatly hinder the possibility of polymer growth.

Scheme 6.2 ICT process of **135**



Cyclic voltammetry measurements of **135** were performed and shown in Figure 6.6. The oxidation (Figure 6.6(a)) shows two irreversible peaks, $E^{1\text{ox}} = +1.05$ and $E^{2\text{ox}} = +1.30$ V. The first oxidation will be the removal of an electron from the twisted thiophene group forming a radical cation. The second oxidation could be one of three possibilities, either the removal of a second electron to give the dication, oxidation of the electron-deficient thiophene or more likely the oxidation of the flavin unit. The reduction (Figure 6.6(b)) shows two reversible waves, $E_{1/2}^{1\text{red}} = -0.83$ V and $E_{1/2}^{2\text{red}} = -1.46$ V. The reduction is two step process, the first electron gain gives a radical anion (semiquinone) and the second electron gain gives a dianion (hydroquinone) species.

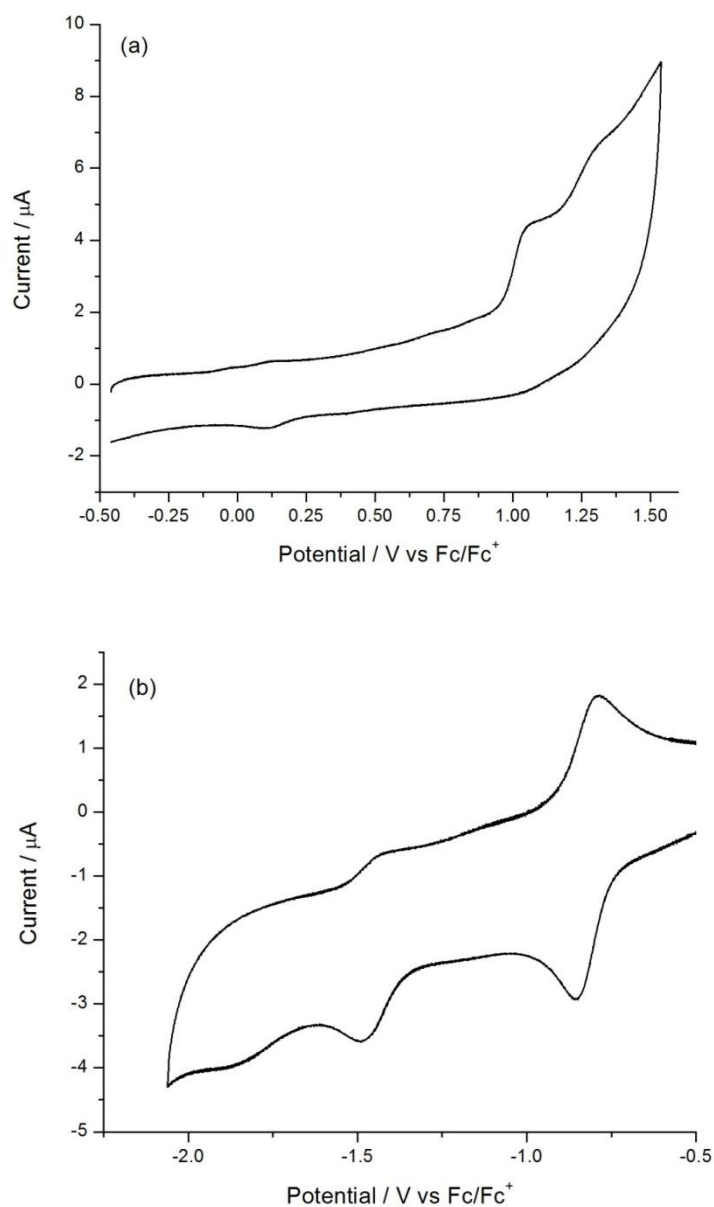


Figure 6.6 Cyclic voltammograms of (a) oxidation and (b) reduction of **135**

The HOMO-LUMO gap of **135** was calculated by cyclic voltammetry (Figure 6.7), by determining the onsets of both oxidation and reduction to give the HOMO and LUMO energy levels, respectively, when subtracted from the known HOMO of ferrocene (-4.8 eV). All data are summarised in Table 6.1. This monomer has both donor and acceptor units and therefore has a smaller band gap of 1.73 eV, compared

to other terthiophenes such as monomers **55** (2.93 eV) and **56** (2.89 eV) in Chapter 2.

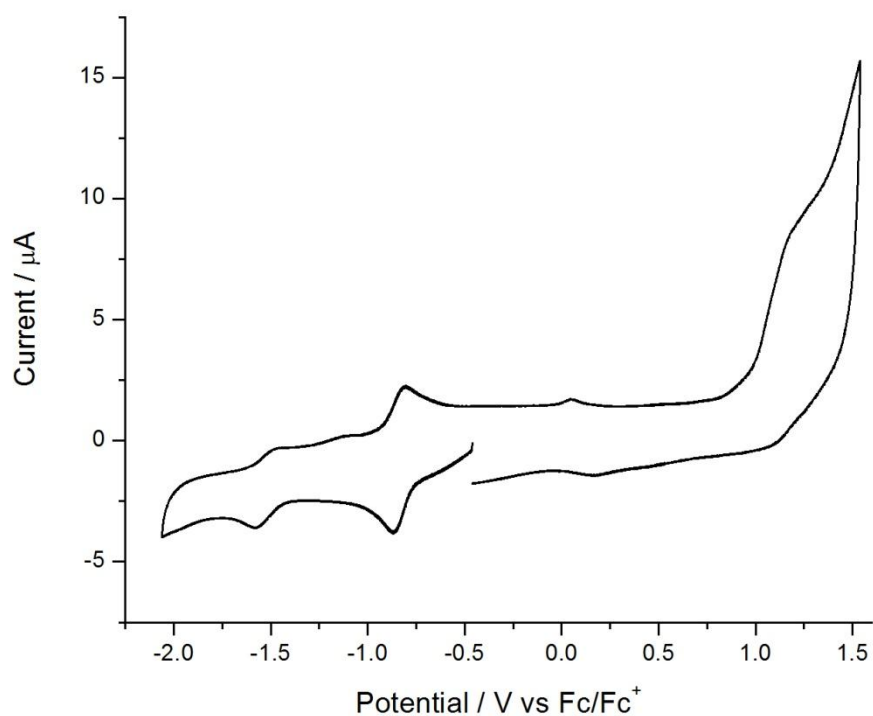


Figure 6.7 Cyclic voltammogram of **135** for energy level determination

Table 6.1 Energy levels for **135** derived from cyclic voltammetry

| Onset of oxidation | HOMO | Onset of reduction | LUMO | HOMO-LUMO |
|--------------------|-------|--------------------|-------|-----------|
| / V | / eV | / V | / eV | gap / eV |
| +0.97 | -5.77 | -0.76 | -4.04 | 1.73 |

Many attempts were made at electropolymerising the monomer, using different potentials, concentrations, and number of cycles. None however were successful. Each attempt showed no increase in current or the development of a new peak at a lower potential (Figure 6.8). With the inability to grow a polymer, it can be

concluded that the second oxidation peak is in fact from the flavin part of the molecule. If the oxidation was derived from the electron-deficient thiophene then polymer growth from radical cations at either end of the terthiophene would be expected.

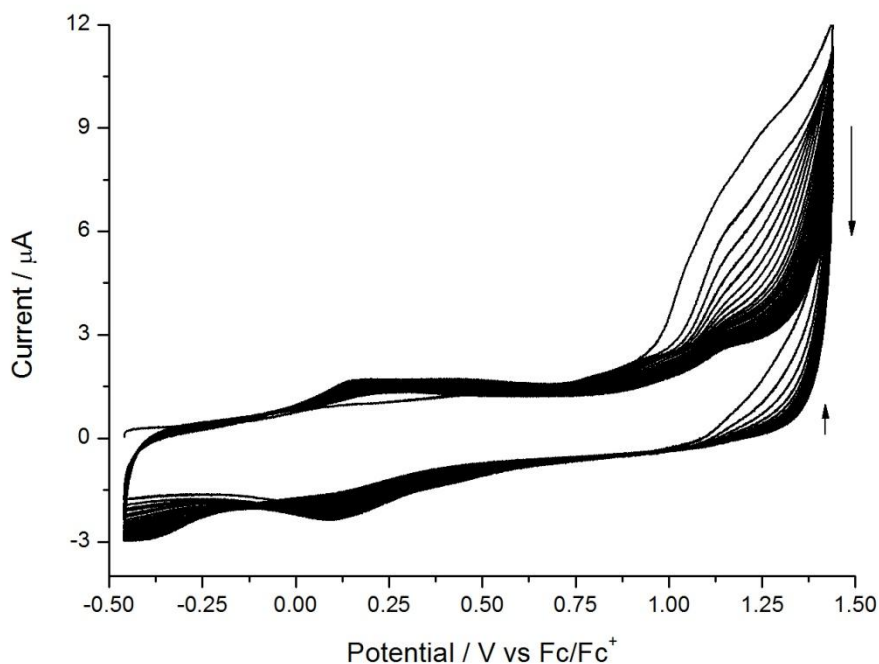


Figure 6.8 Attempted polymer growth of **135**

Despite no growth trace being produced using cyclic voltammetry, there was a deposition of a film being produced on the electrode surface. The experiment was repeated using ITO coated glass slide as the working electrode and a thin film was produced. The absorption spectrum of this new electrochemically formed film was recorded and compared against a drop-cast monomer film on ITO coated glass. The comparison is shown in Figure 6.9.

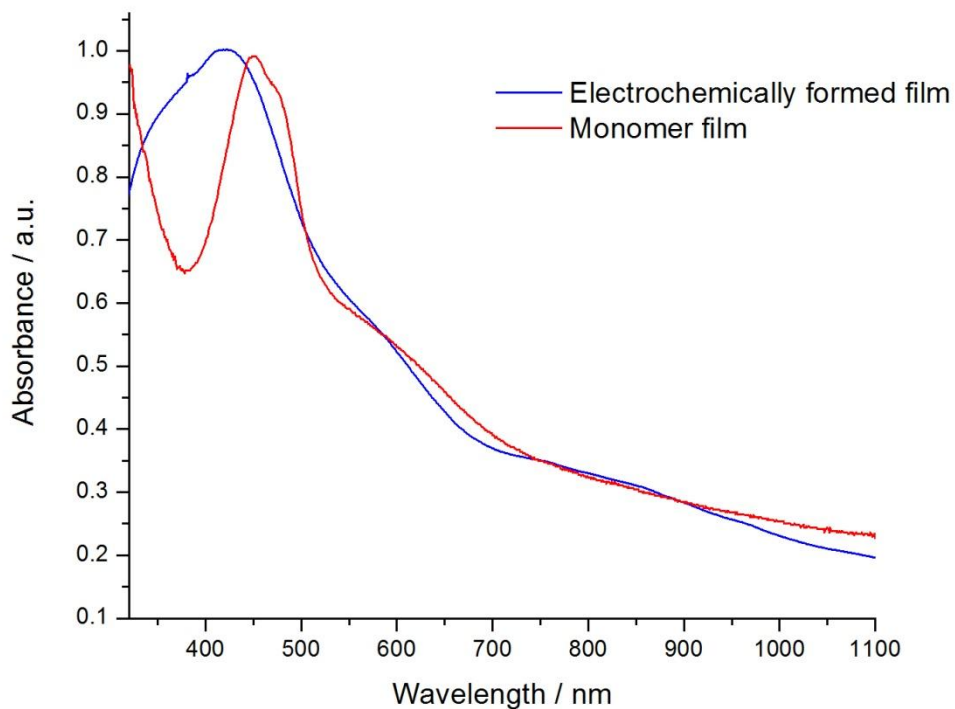


Figure 6.9 UV-vis absorption spectrum of electrochemically formed film growth and monomer film of **135**

The small shift of 30 nm in the absorption maxima of the electrochemically formed film (422 nm) and monomer film (452 nm) suggests that a dimer is actually being produced on the electrode upon oxidation. The structure of the proposed dimer is shown in Figure 6.10. Unfortunately, as no polymer was able to be produced, no further work on this compound as a possible sensor was investigated.

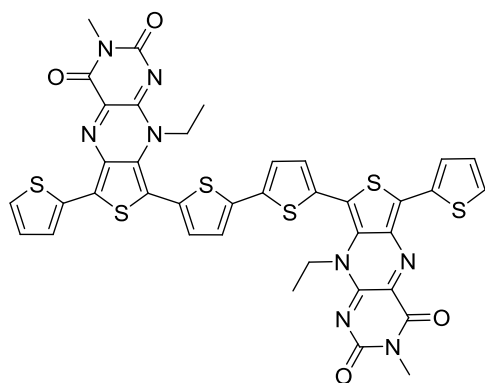


Figure 6.10 Dimer of **135**

6.2.5 Conclusions

The possibility of a flavin-based biosensor is an interesting topic with many examples already published. The research in this chapter was to produce a much simpler polymer through electropolymerisation. Unfortunately, this was not possible with this compound, due to an intramolecular charge transfer process occurring, which leaves one thiophene electron-deficient and one out of plane of the rest of the molecule. It is postulated that only the twisted thiophene undergoes oxidative coupling, resulting in the formation of a dimer species. A dimer is unsuitable for biosensing applications as it still will be redox active, producing possible irreversible chemical or electrochemical reactions.

6.3 The development of a nitric oxide sensor

6.3.1 Introduction

Nitric oxide (NO) is an important molecule in the human body with many roles such as regulation of blood flow and signalling in the central nervous system. However, increased amount of NO in the body can result in serious states such as hypertension and strokes. The detection and quantification of NO has been an ongoing research topic for over twenty years. There are several ways to detect nitric oxide such as electron paramagnetic resonance spectroscopy,²⁴⁵ UV-vis spectrophotometry,²⁴⁶ and chemiluminescence, either through a reaction of NO with ozone,²⁴⁷ or hydrogen peroxide and luminol to generate light.²⁴⁸

The best method developed involves an electrochemical technique,²⁴⁹ using voltammetry or amperometry to satisfy the sensitive and real time analysis of biological materials *in situ*. Voltammetry is used to confirm the identity of NO, anodic peak at 0.63 vs. SCE.²⁵⁰ For amperometry, the working electrode is set to a suitable poise potential relative to the reference electrode (usually a silver wire). In direct amperometry, the poise potential is set to its optimum and the generated current is measured continuously and with differential amperometry, two set potentials are rapidly switched between and the current difference recorded.²⁵¹

The use of carbon fibres coated with a polymeric nickel porphyrin to detect NO was first published in 1992,²⁵² and nowadays there are commercial sensors available based on this methodology. These sensors are also coated with an outer layer of Nafion (perfluorinated sulfonic acid isomer), a cationic exchange membrane used to

block unwanted interfering analytes such as nitrites,¹⁸ and to increase sensitivity.^{253,}

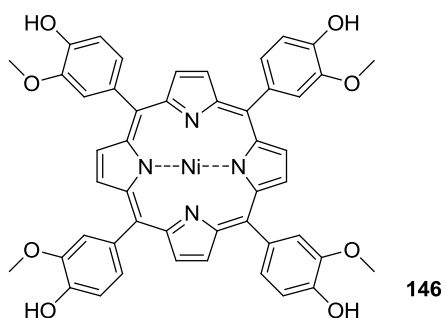
254

Metal porphyrins were the natural choice for NO sensing due to their similarity to the protein haemoglobin. Haemoglobin found in red blood cells is known to react with NO, forming diamagnetic complexes with the main interaction taking place on the iron core of the protein. - during this association, the iron changes from a high spin to a low spin configuration.²⁵⁵

One disadvantage associated with the commercial sensors is the lack of reproducibility. The results differ between sensors from the same batch that have been made according to a standard fabrication protocol. The aim in this section, which is in collaboration with Prof Wadsworth in the University of Strathclyde's *Institute of Pharmacy and Biomedical Science department* is to try and fabricate NO sensors with greater reproducibility using cyclic voltammetry to electropolymerise films onto the electrode surface. The monomer chosen was nickel(II)tetrakis(3-methoxy-4-hydroxyphenyl)porphyrin (**146**). The construction of the prototype sensor was a carbon fibre (either a single filament approx 6 micrometre diameter, or a group of such filaments) connected to a copper wire using silver epoxy and held within a pulled glass capillary tube. A thin prototype sensor will be possible to fit in a catheter and brought in to close proximity to a cell, allowing amperometry measurements to determine the measurement of NO in a living animal or man.²⁵¹

Films were first grown onto the surface of a glassy carbon electrode to optimise growth conditions and to test the polymers redox response to NO. After successful growth onto the surface of the glassy carbon electrode, the film was then grown onto

the surface of a carbon fibre prototype sensor and tested with a NO solution to monitor any redox change.



6.3.2 Experimental

Cyclic voltammetry measurements were performed on a CH Instruments 660A Electrochemical Workstation with iR compensation, using a 0.1 M NaOH solution. The electrodes were glassy carbon or carbon fibre as the working electrode, platinum wire and Ag/AgCl as the counter and reference electrodes, respectively. All solutions were degassed (Ar) and contained monomer substrates in a concentration of *ca.* 10^{-4} M.

6.3.3 Electropolymerisation onto glassy carbon electrodes

Polymer growth was achieved by repetitive cycling over the redox active range of the porphyrin (between 0 and +0.8 V), as reported by Malinski *et al.*²⁵⁶ The growth of the polymer can be seen with the development of two new peaks at +0.5 V and

+0.36 V (Figure 6.11). The shape and positioning of the peaks matches well with other publications that reported polymer growth from porphyrins.²⁵⁷

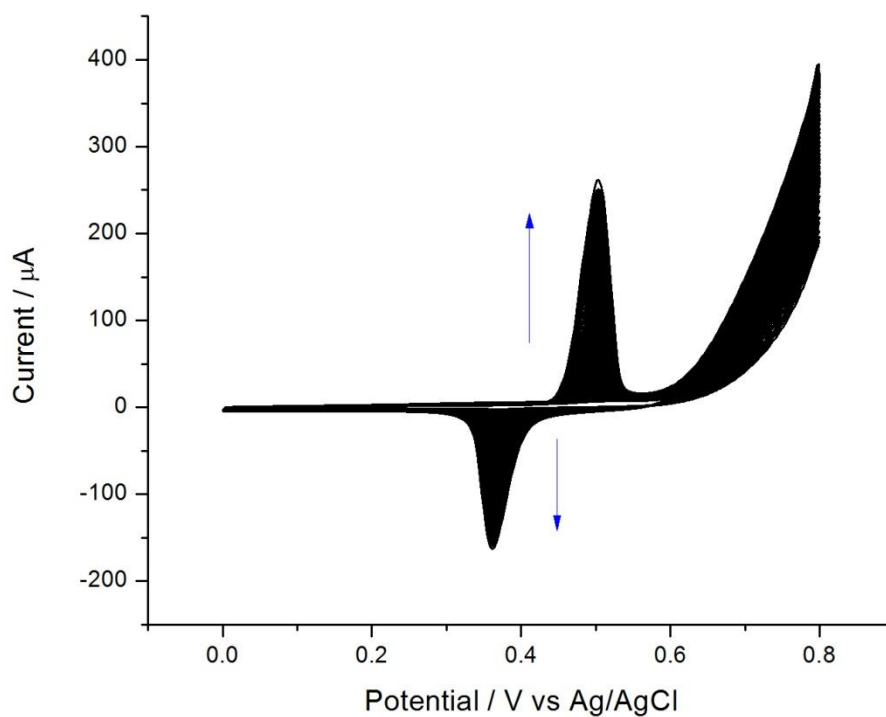


Figure 6.11 Electrochemical growth onto a glassy carbon electrode

Oxidation of the polymer was measured in a monomer free solution (0.1 M NaOH). The polymer gave an oxidation peak at +0.57 V with a reverse peak to the neutral polymer at +0.38 V as shown in Figure 6. 12.

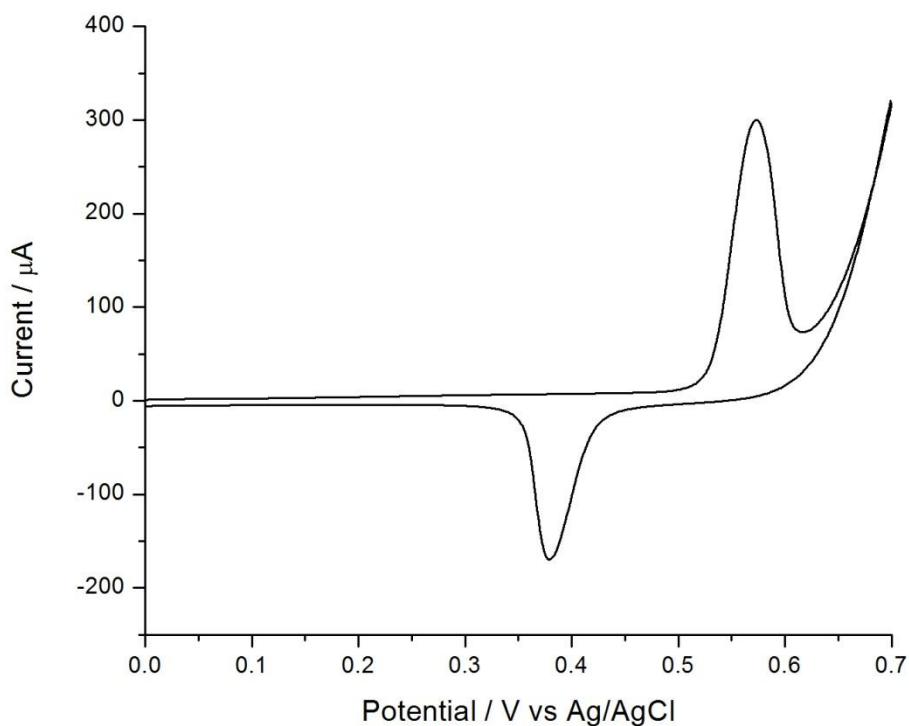


Figure 6. 12 Cyclic voltammograms of polymer in monomer-free solution

To test the response to NO, 1 mL of a solution of 2 mM NO in 0.1 M NaOH was added to the monomerfree solution after 5 cycles on a 15 cycle measurement. It can be seen that with the introduction of NO into the system, the redox response of the polymer changes (Figure 6.13). On addition of NO, there is an increase in potential and current for the oxidation segment with a small change in the reduction. The peak maximum potential changes from +0.58 to +0.60 V for oxidation and +0.46 to +0.47 V for the reduction. It can be noted that, after the addition, the redox properties of the polymer return to normal. This result is reproducible.

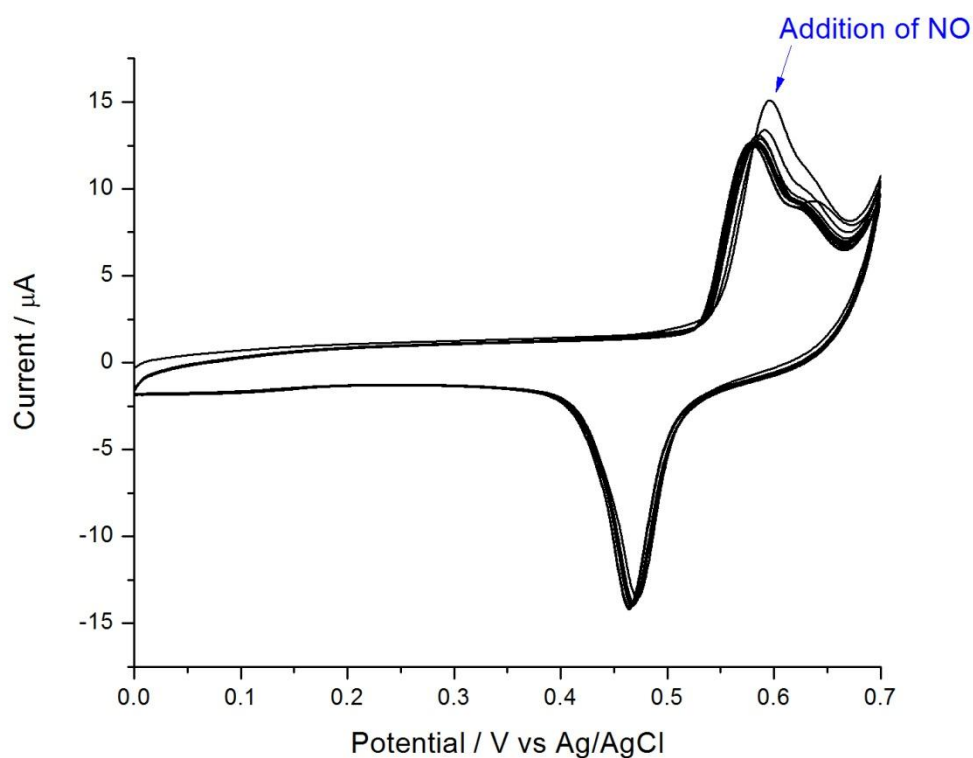


Figure 6.13 Cyclic voltammogram showing the addition of NO to the polymer film

To measure the stability of the polymer on the carbon electrode, a fresh polymer was grown and cycled 500 times. This resulted in an increase in current response for the oxidation and reduction as well as a shift to a higher potential for the oxidation (Figure 6.14). The peak maximum shifted from +0.63 to +0.66 V. Despite the change, the polymer still shows electroactivity in the desired potential window and a response to NO.

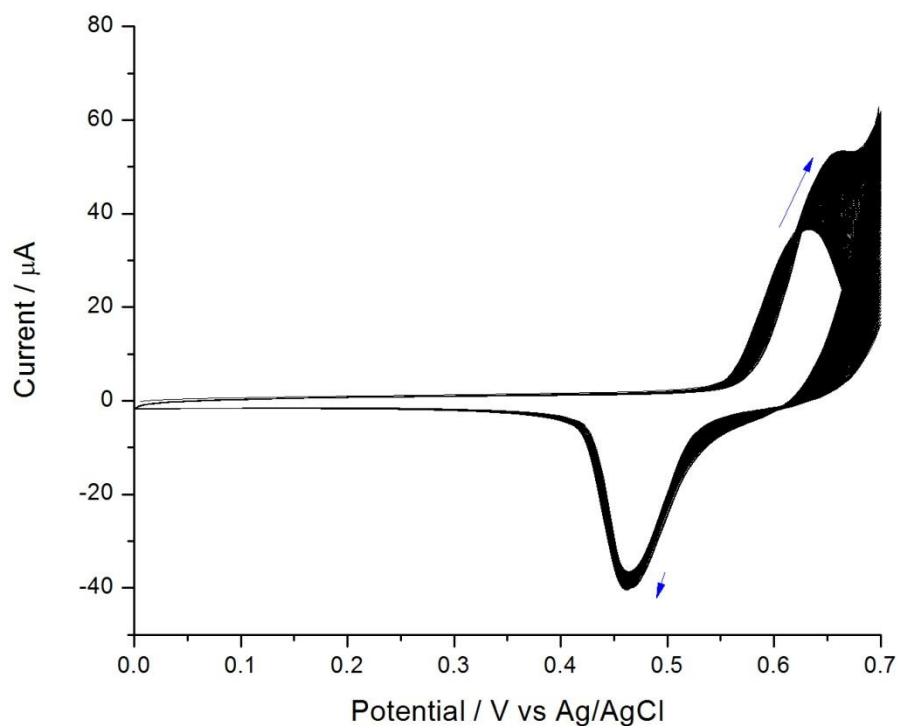


Figure 6.14 Stability test of the polymer on glassy carbon electrode to 500 oxidative cycles

After successful analysis on a glassy carbon electrode, the next step was to repeat the measurements on the prototype devices containing carbon fibre as the active electrode.

6.3.4 Electropolymerisation onto a carbon fibre electrode

Polymer growth was again achieved using the same conditions as before (0 to +0.8 V, 200 cycles, Figure 6.15).

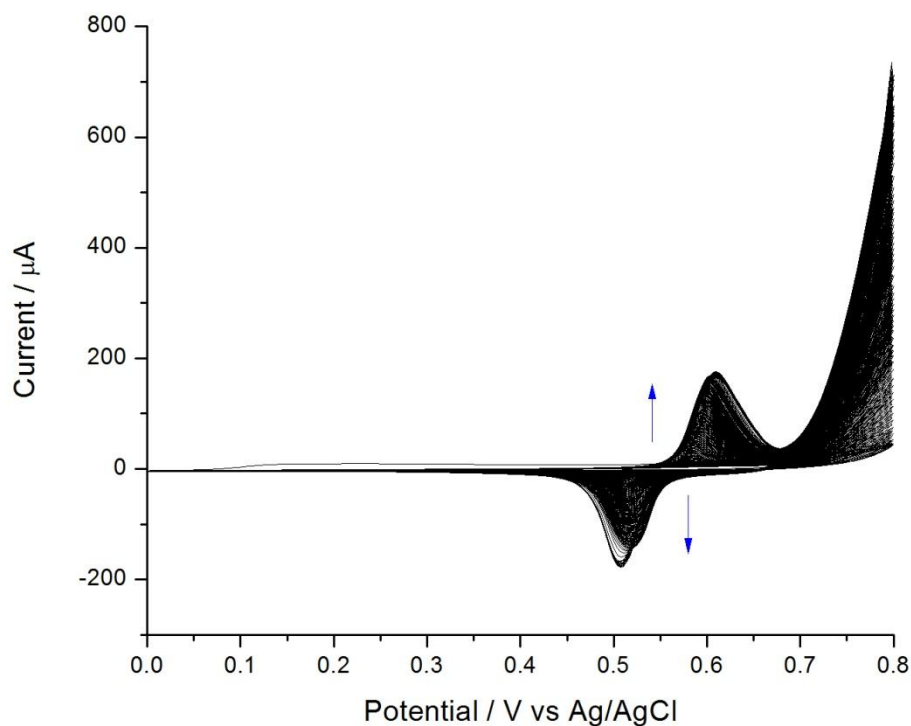


Figure 6.15 Electrochemical growth of the porphyrin onto a carbon fibre electrode

Addition of NO to this electrode had a different effect. The application of 1 mL of NO solution (2 mM NO in 0.1 M NaOH) increased the oxidation potential as before but instead of returning to normal, the redox response remained at the new potential. In Figure 6.16, NO was injected into the system every 5 cycles in a 20 cycle run. With each addition, the potential increased by *ca.* 7 mV.

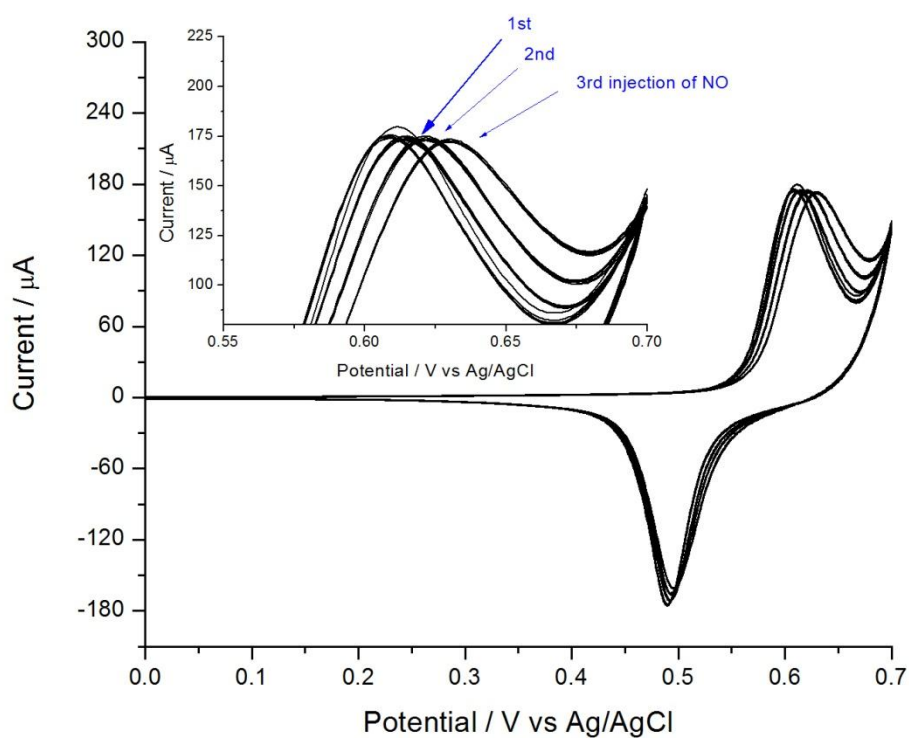


Figure 6.16 Cyclic voltammograms of the polymer film with injection of NO; the inset shows magnification of the active area

The stability of the polymer on the carbon fibre electrode was measured again with 500 cycles between 0 and +0.8 V. Once again this resulted in an increase in potential and current for the oxidation and reduction responses as indicated by the arrows on Figure 6.17.

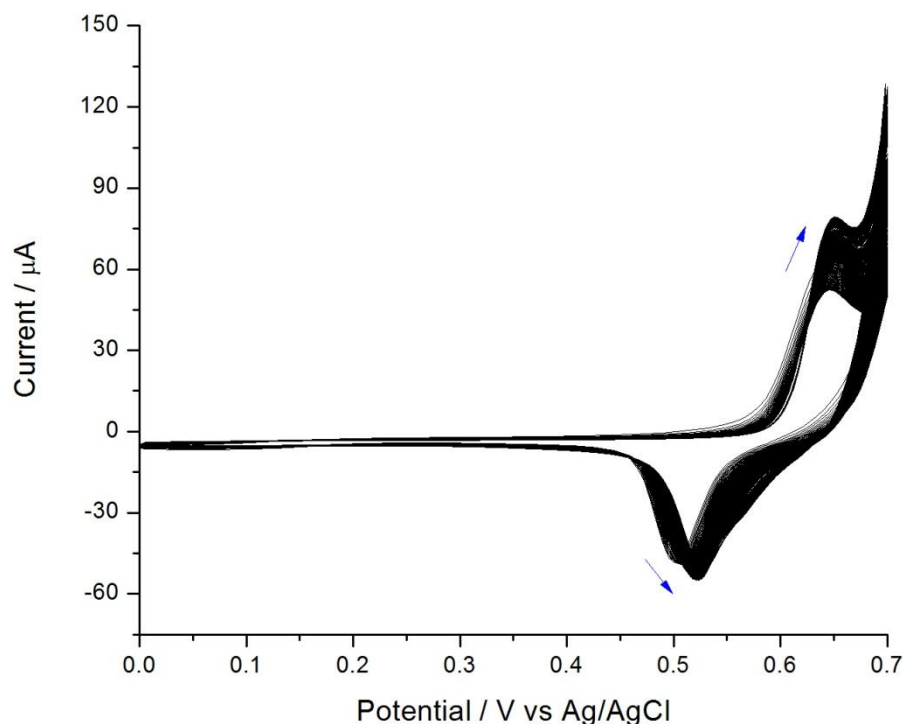


Figure 6.17 Stability test of polymer on carbon fibre electrode to 500 oxidative cycles

The next stage of the investigation was to coat a freshly grown polymer with Nafion. This was achieved by dipping the polymer into the Nafion solution and then leaving the polymer to dry. From this point, all electrochemical analysis was unable to be performed as the Nafion coat did not allow counter ions to reach the electrode to balance the charge in the redox measurement.

Several prototype sensors were fabricated with varying number of carbon fibre strands and the number of cycles for polymer growth. Unfortunately, in these preliminary results the sensors tested in phosphate buffered saline solution (NaCl 0.9 g/L, plus approx 20 mM phosphate, pH 7.4) at room temperature all gave high current readings above the available output range of the NO meter used at the *Strathclyde Institute of Pharmacy and Biomedical Science department*.

6.3.5 Conclusions and Further Work

In this section, it has been shown that a polymeric nickel porphyrin film can be grown onto either the surface of a glassy carbon electrode or on carbon fibre strands in a prototype sensor that can detect the presence of nitric oxide in solution through a change in the redox response of the polymer. These polymer films are stable and can be grown with ease. The problem develops when developing these into sensors for the biological detection of NO *in situ* where a coating of Nafion is required to block out unwanted analytes. This coating makes simple detection of NO difficult and the connection to a NO sensor gives an overflow in current output.

These trials have shown that a simple swap of the new sensors for the commercially available sensors does not work. However, a disadvantage of this approach is that the circuit and capabilities of the NO meter are unknown. It might be better to use a generic high quality amplifier and ammeter to test the sensors. That may enable offsetting any background current or using a 3 electrode configuration.

There are many possibilities for the continuation of this project involving variables that can be modified, such as the type of monomer, control of polymer thickness and choice of membrane when fabricating sensors.

Publications

- A. L. Kanibolotsky, J. C. Forgie, S. Gordeyev, F. Vilela, P. J. Skabara, J. E. Lohr, B. M. Petersen and J. O. Jeppesen *The Introduction of Pyrrolotetrathiafulvalene into Conjugated Architectures: Synthesis and Electronic Properties* *Macromolecular Rapid Communications*, **2008**, 29 (14), 1226-1230
- J. C. Forgie, A. L. Kanibolotsky, P. J. Skabara, S. J. Coles, M. B. Hursthouse, R. W. Harrington and W. Clegg, *Electrochemical, Spectroelectrochemical, and Comparative Studies of Novel Organic Conjugated Monomers and Polymers Featuring the Redox-Active Unit Tetrathianaphthalene*, *Macromolecules*, **2009**, 42 (7), 2570-2580
- L. Li, F. Vilela, J. Forgie, P. J. Skabara, and D. Uttamchandani *A Miniature Humidity Microsensor Based on Organic Conductive Polymer - poly(3,4-ethylenedioxythiophene)*, *Micro & Nanoletters*, **2009**, 4 (2), 84-87
- J. C. Forgie, P. J. Skabara, I. Stibor, F. Vilela and Z. Vobecka *New Redox Stable Low Band Gap Conjugated Polymer Based on an EDOT-BODIPY-EDOT Repeat Unit*, *Chemistry of Materials*, **2009**, 21 (9), 1784-1786
- K. Zhang, B. Tieke, J. C. Forgie and P. J. Skabara, *Electrochemical Polymerisation of N-Arylated and N-Alkylated EDOT-Substituted Pyrrolo[3,4-c]pyrrole-1,4-dione (DPP) Derivatives: Influence of Substitution Pattern on Optical and Electronic Properties*, *Macromolecular Rapid Communications*. **2009**, 30 (21), 1834-1840
- A.L. Kanibolotsky, J. C. Forgie, G. J. McEntee, M. M. A. Talpur, P. J. Skabara, T. D. J. Westgate, J. J. W. McDouall, M. Auinger, S. J. Coles, and M. B. Hursthouse, *Controlling the Conformational Changes in Donor-Acceptor [4]-Dendralenes Through Intramolecular Charge-Transfer Processes*. *Chemistry - A European Journal*. **2009**, 15 (43), 11581-11593
- K. D. Trotter, J. Reglinski, K. Robertson, J. C. Forgie, J. A. Parkinson, A. R. Kennedy, D. R. Armstrong, R. J. Strowden, C. M. Spickett, *Structural Studies of Trans-N₂S₂ Copper Macrocycles*. *Inorganica Chimica Acta*. **2009**, 362 (11), 4065-4072
- I. Afonina, P. J. Skabara, F. Vilela, A. L. Kanibolotsky, J. C. Forgie, A. K. Bansal, G. A. Turnbull, I. D. W. Samuel, John G. Labram, T. D. Anthopoulos, S. J. Coles and M. B. Hursthouse, *Synthesis and Characterisation of New Diindeno[1,2-b:3,4-b']thiophene (DITT) Based Materials*. *Journal of Materials Chemistry*. **2010**, 20, 1112-1116

- K. D. Trotter, M.K. Taylor, J.C. Forgie, J. Reglinski, L.E.A. Berlouis, A.R. Kennedy, C.M. Spickett, R.J. Sowden, *The Structural and Electrochemical Consequences of Hydrogenating Copper N₂S₂ Schiff Base Macrocycles*, *Inorganica Chimica Acta*, **2010**, 363 (7), 1529-1538
- I. A. Wright, P. J. Skabara, J. C. Forgie, A. L. Kanibolotsky, B. González, S. J. Coles, M. B. Hursthouse, S. Gambino and I. D. W. Samuel, *Electronic, redox and charge transport properties of an unusual hybrid structure: a bis(septathiophene) bridged by a fused tetrathiafulvalene (TTF)*, *Journal of Materials Chemistry*, **Accepted**
- A. L. Kanibolotsky, F. Vilela, J. C. Forgie, P. J. Skabara, K. Zhang, B. Tieke, D. C. C. Bradley, J. McGurk, *Well-defined and monodisperse linear and star-shaped quaterfluorene-DPP molecules: the significance of conjugation and dimensionality*, *Journal of American Chemical Society*, **Submitted**
- K. Zhang, B. Tieke, J. C. Forgie, F. Vilela and P. J. Skabara, *Cross-linked Conjugated Polymers based on 2,3,5,6-tetra-Substituted Pyrrolo[3,4-c]pyrrole-1,4(2H,5H)-dione (DPP): Synthesis, Optical and Electronic Properties*, **In preparation**
- K. Zhang, B. Tieke, J. C. Forgie, F. Vilela and P. J. Skabara, *Donor-Acceptor Conjugated Polymers based on Benzodifuranone and Thiophene Derivatives: Electrochemical Preparation, Optical and Electronic Properties*, **In preparation**

References

1. C. K. Chiang, C. R. Fincher, Y. W. Park, A. J. Heeger, H. Shirakawa, E. J. Louis, S. C. Gau and A. G. Macdiarmid, *Physical Review Letters*, 1977, **39**, 1098-1101.
2. A. F. Diaz, K. K. Kanazawa and G. P. Gardini, *J. Chem. Soc.-Chem. Commun.*, 1979, 635-636.
3. G. Tourillon and F. Garnier, *J. Electroanal. Chem.*, 1982, **135**, 173-178.
4. A. Tsumura, H. Koezuka and T. Ando, *Appl. Phys. Lett.*, 1986, **49**, 1210-1212.
5. J. H. Burroughes, D. D. C. Bradley, A. R. Brown, R. N. Marks, K. Mackay, R. H. Friend, P. L. Burns and A. B. Holmes, *Nature*, 1990, **347**, 539-541.
6. J. Roncali, *Chem. Rev.*, 1997, **97**, 173-205.
7. J. P. Lowe and S. A. Kafafi, *J. Am. Chem. Soc.*, 1984, **106**, 5837-5841.
8. V. Hernandez, C. Castiglioni, M. Delzoppo and G. Zerbi, *Phys. Rev. B*, 1994, **50**, 9815-9823.
9. P. M. Grant and I. P. Batra, *Solid State Commun.*, 1979, **29**, 225-229.
10. J. L. Bredas, *J. Chem. Phys.*, 1985, **82**, 3808-3811.
11. *Fundamentals and Applications: A Practical Approach*, Kluwer Academic Publishers, London, 1999.
12. F. Wudl, M. Kobayashi and A. J. Heeger, *J. Org. Chem.*, 1984, **49**, 3382-3384.
13. C. Pozo-Gonzalo, T. Khan, J. J. W. McDouall, P. J. Skabara, D. M. Roberts, M. E. Light, S. J. Coles, M. B. Hursthouse, H. Neugebauer, A. Cravino and N. S. Sariciftci, *J. Mater. Chem.*, 2002, **12**, 500-510.
14. S. S. Zade and M. Bendikov, *Org. Lett.*, 2006, **8**, 5243-5246.
15. S. S. Zade and M. Bendikov, *Chem.-Eur. J.*, 2007, **13**, 3688-3700.
16. M. R. Bryce, *Chem. Soc. Rev.*, 1991, **20**, 355-390.
17. C. H. Hamann, A. Hamnett and W. Vielstich, *Electrochemistry*, Second edn., WILEY-VCH, 2007.
18. J. Koryta and J. Dvořák, *Principles of Electrochemistry*, John Wiley & Sons Ltd., 1987.
19. R. J. Mortimer, A. L. Dyer and J. R. Reynolds, *Displays*, 2006, **27**, 2-18.
20. J. Roncali, *Chem. Rev.*, 1992, **92**, 711-738.
21. C. P. Andrieux, P. Audebert, P. Hapiot and J. M. Saveant, *J. Phys. Chem.*, 1991, **95**, 10158-10164.
22. S. Roquet, P. Leriche, I. Perepichka, B. Joussetme, E. Levillain, P. Frere and J. Roncali, *J. Mater. Chem.*, 2004, **14**, 1396-1400.
23. G. Tourillon and F. Garnier, *J. Phys. Chem.*, 1983, **87**, 2289-2292.
24. J. Roncali, F. Garnier, R. Garreau and M. Lemaire, *J. Chem. Soc.-Chem. Commun.*, 1987, 1500-1502.
25. K. Gurunathan, A. V. Murugan, R. Marimuthu, U. P. Mulik and D. P. Amalnerkar, *Materials Chemistry And Physics*, 1999, **61**, 173-191.
26. J. Roncali, *J. Mater. Chem.*, 1999, **9**, 1875-1893.
27. G. A. Sotzing, C. A. Thomas, J. R. Reynolds and P. J. Steel, *Macromolecules*, 1998, **31**, 3750-3752.
28. A. Ajayaghosh, *Chem. Soc. Rev.*, 2003, **32**, 181-191.

29. C. L. Pai, C. L. Liu, W. C. Chen and S. A. Jenekhe, *Polymer*, 2006, **47**, 699-708.
30. C. J. DuBois, K. A. Abboud and J. R. Reynolds, *J. Phys. Chem. B*, 2004, **108**, 8550-8557.
31. J. M. Raimundo, P. Blanchard, H. Brisset, S. Akoudad and J. Roncali, *Chem. Commun.*, 2000, 939-940.
32. I. H. Jung, J. Yu, E. Jeong, J. Kim, S. Kwon, H. Kong, K. Lee, H. Y. Woo and H. K. Shim, *Chem.-Eur. J.*, **16**, 3743-3752.
33. S. Akoudad and J. Roncali, *Chem. Commun.*, 1998, 2081-2082.
34. F. Jonas and L. Schrader, *Synth. Met.*, 1991, **41**, 831-836.
35. S. Y. Hong, *Synth. Met.*, 2003, **135**, 439-441.
36. G. Heywang and F. Jonas, *Adv. Mater.*, 1992, **4**, 116-118.
37. S. Kirchmeyer and K. Reuter, *J. Mater. Chem.*, 2005, **15**, 2077-2088.
38. C. G. Wang, J. L. Schindler, C. R. Kannewurf and M. G. Kanatzidis, *Chem. Mat.*, 1995, **7**, 58-68.
39. J. M. Raimundo, P. Blanchard, P. Frere, N. Mercier, I. Ledoux-Rak, R. Hierle and J. Roncali, *Tetrahedron Lett.*, 2001, **42**, 1507-1510.
40. H. C. Li and C. Lambert, *J. Mater. Chem.*, 2005, **15**, 1235-1237.
41. P. Blanchard, A. Cappon, E. Levillain, Y. Nicolas, P. Frere and J. Roncali, *Org. Lett.*, 2002, **4**, 607-609.
42. M. Turbiez, P. Frere, M. Allain, N. Gallego-Planas and J. Roncali, *Macromolecules*, 2005, **38**, 6806-6812.
43. H. J. Spencer, P. J. Skabara, M. Giles, I. McCulloch, S. J. Coles and M. B. Hursthouse, *J. Mater. Chem.*, 2005, **15**, 4783-4792.
44. J. Roncali, P. Blanchard and P. Frere, *J. Mater. Chem.*, 2005, **15**, 1589-1610.
45. A. Kumar, D. M. Welsh, M. C. Morvant, F. Piroux, K. A. Abboud and J. R. Reynolds, *Chem. Mat.*, 1998, **10**, 896-902.
46. H. W. Heuer, R. Wehrmann and S. Kirchmeyer, *Adv. Funct. Mater.*, 2002, **12**, 89-94.
47. L. Groenendaal, G. Zotti, P. H. Aubert, S. M. Waybright and J. R. Reynolds, *Adv. Mater.*, 2003, **15**, 855-879.
48. A. Elschner, H. W. Heuer, F. Jonas, S. Kirchmeyer, R. Wehrmann and K. Wussow, *Adv. Mater.*, 2001, **13**, 1811-1814.
49. D. J. Crouch, P. J. Skabara, M. Heeney, I. McCulloch, S. J. Coles and M. B. Hursthouse, *Chem. Commun.*, 2005, 1465-1467.
50. N. Hergue, P. Leriche, P. Blanchard, M. Allain, N. Gallego-Planas, P. Frere and J. Roncali, *New J. Chem.*, 2008, **32**, 932-936.
51. I. F. Perepichka, E. Levillain and J. Roncali, *J. Mater. Chem.*, 2004, **14**, 1679-1681.
52. P. Schottland, K. Zong, C. L. Gaupp, B. C. Thompson, C. A. Thomas, I. Giurgiu, R. Hickman, K. A. Abboud and J. R. Reynolds, *Macromolecules*, 2000, **33**, 7051-7061.
53. A. Patra, Y. H. Wijsboom, S. S. Zade, M. Li, Y. Sheynin, G. Leitun and M. Bendikov, *J. Am. Chem. Soc.*, 2008, **130**, 6734-6736.
54. H. Pang, P. J. Skabara, S. Gordeyev, J. J. W. McDouall, S. J. Coles and M. B. Hursthouse, *Chem. Mat.*, 2007, **19**, 301-307.
55. *Instrumental Methods in Electrochemistry*, Horwood publishing Limited, Chichester, 1985.
56. A. J. Bard and L. R. Faulkner, *Electrochemical Methods Fundamentals and Applications*, Second edn., John Wiley & Sons, Inc., 2001.

57. P. M. S. Monk, R. J. Mortimer and D. R. Rosseinsky, *Electrochromism and Electrochromic Devices*, Cambridge University Press, Cambridge, 2007.
58. J. Heinze, *Angew. Chem.-Int. Edit. Engl.*, 1984, **23**, 831-847.
59. G. Gritzner and J. Kuta, *Pure Appl. Chem.*, 1984, **56**, 461-466.
60. D. H. Williams and I. Fleming, *Spectroscopic Methods in Organic Chemistry*, Fifth edn., McGraw-Hill, 1995.
61. C. R. Mason, P. J. Skabara, D. Cupertino, J. Schofield, F. Meghdadi, B. Ebner and N. S. Sariciftci, *J. Mater. Chem.*, 2005, **15**, 1446-1453.
62. Y. H. Pang, X. Y. Li, H. L. Ding, G. Y. Shi and L. T. Jin, *Electrochim. Acta*, 2007, **52**, 6172-6177.
63. J. P. McEvoy and J. S. Foord, *Electrochim. Acta*, 2005, **50**, 2933-2941.
64. *Spectroelectrochemistry*, Royal Society of Chemistry, Cambridge, 2008.
65. T. C. Chung, J. H. Kaufman, A. J. Heeger and F. Wudl, *Phys. Rev. B*, 1984, **30**, 702-710.
66. J. D. Coyle, *Introduction to Organic Photochemistry*, Wiley, New York, 1986.
67. J. R. Lakowicz, *Principles of Fluorescence Spectroscopy*, Kulwer Academic / Plenum Press, New York, 1989.
68. S. Dhami, A. J. Demello, G. Rumbles, S. M. Bishop, D. Phillips and A. Beeby, *Photochem. Photobiol.*, 1995, **61**, 341-346.
69. A. T. R. Williams, S. A. Winfield and J. N. Miller, *Analyst*, 1983, **108**, 1067-1071.
70. S. J. Higgins, *Chem. Soc. Rev.*, 1997, **26**, 247-257.
71. I. Schwendeman, J. Hwang, D. M. Welsh, D. B. Tanner and J. R. Reynolds, *Adv. Mater.*, 2001, **13**, 634-637.
72. A. Cirpan, A. A. Argun, C. R. G. Grenier, B. D. Reeves and J. R. Reynolds, *J. Mater. Chem.*, 2003, **13**, 2422-2428.
73. G. Sonmez, H. B. Sonmez, C. K. F. Shen, R. W. Jost, Y. Rubin and F. Wudl, *Macromolecules*, 2005, **38**, 669-675.
74. A. Kraft, A. C. Grimsdale and A. B. Holmes, *Angew. Chem.-Int. Edit.*, 1998, **37**, 402-428.
75. D. Dini, *Chem. Mat.*, 2005, **17**, 1933-1945.
76. U. Mitschke and P. Bauerle, *J. Mater. Chem.*, 2000, **10**, 1471-1507.
77. S. R. Forrest, *Nature*, 2004, **428**, 911-918.
78. C. D. Dimitrakopoulos and P. R. L. Malenfant, *Adv. Mater.*, 2002, **14**, 99-+.
79. G. Horowitz, *Adv. Mater.*, 1998, **10**, 365-377.
80. Z. N. Bao, J. A. Rogers and H. E. Katz, *J. Mater. Chem.*, 1999, **9**, 1895-1904.
81. M. M. Ling and Z. N. Bao, *Chem. Mat.*, 2004, **16**, 4824-4840.
82. C. J. Brabec, N. S. Sariciftci and J. C. Hummelen, *Adv. Funct. Mater.*, 2001, **11**, 15-26.
83. J. L. Segura, N. Martin and D. M. Guldi, *Chem. Soc. Rev.*, 2005, **34**, 31-47.
84. A. Cravino and N. S. Sariciftci, *J. Mater. Chem.*, 2002, **12**, 1931-1943.
85. L. M. Goldenberg, P. J. Skabara, D. M. Roberts, R. Berridge, E. Orti, P. M. Viruela and R. Pou-Amerigo, *J. Mater. Chem.*, 2000, **10**, 2458-2465.
86. T. M. Swager and M. J. Marsella, *Adv. Mater.*, 1994, **6**, 595-597.
87. D. T. McQuade, A. E. Pullen and T. M. Swager, *Chem. Rev.*, 2000, **100**, 2537-2574.
88. K. J. Albert, N. S. Lewis, C. L. Schauer, G. A. Sotzing, S. E. Stitzel, T. P. Vaid and D. R. Walt, *Chem. Rev.*, 2000, **100**, 2595-2626.

89. C. L. Gaupp, D. M. Welsh, R. D. Rauh and J. R. Reynolds, *Chem. Mat.*, 2002, **14**, 3964-3970.
90. G. Sonmez, H. Meng, Q. Zhang and F. Wudl, *Adv. Funct. Mater.*, 2003, **13**, 726-731.
91. S. A. Sapp, G. A. Sotzing and J. R. Reynolds, *Chem. Mat.*, 1998, **10**, 2101-2108.
92. A. A. Argun, P. H. Aubert, B. C. Thompson, I. Schwendeman, C. L. Gaupp, J. Hwang, N. J. Pinto, D. B. Tanner, A. G. MacDiarmid and J. R. Reynolds, *Chem. Mat.*, 2004, **16**, 4401-4412.
93. G. Sonmez, H. B. Sonmez, C. K. E. Shen and F. Wudl, *Adv. Mater.*, 2004, **16**, 1905-1908.
94. G. Sonmez and F. Wudl, *J. Mater. Chem.*, 2005, **15**, 20-22.
95. F. Carpi and D. De Rossi, *Optics And Laser Technology*, 2006, **38**, 292-305.
96. P. M. Beaujuge, S. Ellinger and J. R. Reynolds, *Adv. Mater.*, 2008, **20**, 2772-2776.
97. B. C. Thompson, P. Schottland, K. W. Zong and J. R. Reynolds, *Chem. Mat.*, 2000, **12**, 1563-1571.
98. R. D. Rauh, F. Wang, J. R. Reynolds and D. L. Meeker, *Electrochim. Acta*, 2001, **46**, 2023-2029.
99. A. F. B. Braga, S. P. Moreira, P. R. Zampieri, J. M. G. Bacchin and P. R. Mei, *Sol. Energy Mater. Sol. Cells*, 2008, **92**, 418-424.
100. W. L. Ma, C. Y. Yang, X. Gong, K. Lee and A. J. Heeger, *Adv. Funct. Mater.*, 2005, **15**, 1617-1622.
101. G. Yu, J. Gao, J. C. Hummelen, F. Wudl and A. J. Heeger, *Science*, 1995, **270**, 1789-1791.
102. C. J. Brabec, *Sol. Energy Mater. Sol. Cells*, 2004, **83**, 273-292.
103. R. Kroon, M. Lenes, J. C. Hummelen, P. W. M. Blom and B. De Boer, *Polym. Rev.*, 2008, **48**, 531-582.
104. V. Shrotriya, G. Li, Y. Yao, T. Moriarty, K. Emery and Y. Yang, *Adv. Funct. Mater.*, 2006, **16**, 2016-2023.
105. W. Shockley and H. J. Queisser, *J. Appl. Phys.*, 1961, **32**, 510-519.
106. G. Dennler, M. C. Scharber and C. J. Brabec, *Adv. Mater.*, 2009, **21**, 1323-1338.
107. M. C. Scharber, D. Wuhlbacher, M. Koppe, P. Denk, C. Waldauf, A. J. Heeger and C. L. Brabec, *Adv. Mater.*, 2006, **18**, 789-794.
108. H. Hoppe and N. S. Sariciftci, *J. Mater. Chem.*, 2006, **16**, 45-61.
109. S. E. Shaheen, C. J. Brabec, N. S. Sariciftci, F. Padinger, T. Fromherz and J. C. Hummelen, *Appl. Phys. Lett.*, 2001, **78**, 841-843.
110. C. Winder and N. S. Sariciftci, *J. Mater. Chem.*, 2004, **14**, 1077-1086.
111. Y. Y. Liang, Y. Wu, D. Q. Feng, S. T. Tsai, H. J. Son, G. Li and L. P. Yu, *J. Am. Chem. Soc.*, 2009, **131**, 56-57.
112. S. H. Park, A. Roy, S. Beaupre, S. Cho, N. Coates, J. S. Moon, D. Moses, M. Leclerc, K. Lee and A. J. Heeger, *Nat. Photonics*, 2009, **3**, 297-U295.
113. http://www.pv-tech.org/news/a/solarmer_breaks_organic_solar_pv_cell_conversion_efficiency_record_hits_nre/. (accessed 24/07/2010)
114. C. R. McNeill, A. Abrusci, J. Zaumseil, R. Wilson, M. J. McKiernan, J. H. Burroughes, J. J. M. Halls, N. C. Greenham and R. H. Friend, *Appl. Phys. Lett.*, 2007, **90**.

115. M. Lenes, G. Wetzelaer, F. B. Kooistra, S. C. Veenstra, J. C. Hummelen and P. W. M. Blom, *Adv. Mater.*, 2008, **20**, 2116-2119.
116. B. Joussetme, P. Blanchard, E. Levillain, R. de Bettignies and J. Roncali, *Macromolecules*, 2003, **36**, 3020-3025.
117. J. Roncali, *Chem. Soc. Rev.*, 2005, **34**, 483-495.
118. M. L. Chabinyk and A. Salleo, *Chem. Mat.*, 2004, **16**, 4509-4521.
119. T. P. I. Saragi, T. Spehr, A. Siebert, T. Fuhrmann-Lieker and J. Salbeck, *Chem. Rev.*, 2007, **107**, 1011-1065.
120. M. Mas-Torrent and C. Rovira, *Chem. Soc. Rev.*, 2008, **37**, 827-838.
121. H. E. Katz and J. Huang, *Ann. Rev. Mater. Res.*, 2009, **39**, 71-92.
122. Y. Kunugi, K. Takimiya, N. Negishi, T. Otsubo and Y. Aso, *J. Mater. Chem.*, 2004, **14**, 2840-2841.
123. C. R. Newman, C. D. Frisbie, D. A. da Silva, J. L. Bredas, P. C. Ewbank and K. R. Mann, *Chem. Mat.*, 2004, **16**, 4436-4451.
124. D. A. Scherlis and N. Marzari, *J. Am. Chem. Soc.*, 2005, **127**, 3207-3212.
125. H. Klauk, M. Halik, U. Zschieschang, G. Schmid, W. Radlik and W. Weber, *J. Appl. Phys.*, 2002, **92**, 5259-5263.
126. H. Sirringhaus, P. J. Brown, R. H. Friend, M. M. Nielsen, K. Bechgaard, B. M. W. Langeveld-Voss, A. J. H. Spiering, R. A. J. Janssen, E. W. Meijer, P. Herwig and D. M. de Leeuw, *Nature*, 1999, **401**, 685-688.
127. V. C. Sundar, J. Zaumseil, V. Podzorov, E. Menard, R. L. Willett, T. Someya, M. E. Gershenson and J. A. Rogers, *Science*, 2004, **303**, 1644-1646.
128. D. M. deLeeuw, M. M. J. Simenon, A. R. Brown and R. E. F. Einerhand, *Synth. Met.*, 1997, **87**, 53-59.
129. H. E. Katz, A. J. Lovinger, J. Johnson, C. Kloc, T. Siegrist, W. Li, Y. Y. Lin and A. Dodabalapur, *Nature*, 2000, **404**, 478-481.
130. S. Handa, E. Miyazaki, K. Takimiya and Y. Kunugi, *J. Am. Chem. Soc.*, 2007, **129**, 11684-11685.
131. S. Handa, E. Miyazaki and K. Takimiya, *Chem. Commun.*, 2009, 3919-3921.
132. T. D. Anthopoulos, S. Setayesh, E. Smits, M. Colle, E. Cantatore, B. de Boer, P. W. M. Blom and D. M. de Leeuw, *Adv. Mater.*, 2006, **18**, 1900-+.
133. J. Zaumseil and H. Sirringhaus, *Chem. Rev.*, 2007, **107**, 1296-1323.
134. A. R. Murphy and J. M. J. Frechet, *Chem. Rev.*, 2007, **107**, 1066-1096.
135. A. C. Grimsdale, K. L. Chan, R. E. Martin, P. G. Jokisz and A. B. Holmes, *Chem. Rev.*, 2009, **109**, 897-1091.
136. M. R. Andersson, O. Thomas, W. Mammo, M. Svensson, M. Theander and O. Inganäs, *J. Mater. Chem.*, 1999, **9**, 1933-1940.
137. H. Spreitzer, H. Becker, E. Kluge, W. Kreuder, H. Schenk, R. Demandt and H. Schöo, *Adv. Mater.*, 1998, **10**, 1340-1343.
138. U. Scherf and E. J. W. List, *Adv. Mater.*, 2002, **14**, 477-487.
139. T. Zyung, J. J. Kim, W. Y. Hwang, D. H. Hwang and H. K. Shim, *Synth. Met.*, 1995, **71**, 2167-2169.
140. H. S. Woo, S. C. Graham, D. A. Halliday, D. D. C. Bradley, R. H. Friend, P. L. Burn and A. B. Holmes, *Phys. Rev. B*, 1992, **46**, 7379-7389.
141. M. Leclerc, *J. Polym. Sci. Pol. Chem.*, 2001, **39**, 2867-2873.
142. B. W. D'Andrade and S. R. Forrest, *Adv. Mater.*, 2004, **16**, 1585-1595.
143. A. R. Brown, D. D. C. Bradley, J. H. Burroughes, R. H. Friend, N. C. Greenham, P. L. Burn, A. B. Holmes and A. Kraft, *Appl. Phys. Lett.*, 1992, **61**, 2793-2795.

144. M. Yan, L. J. Rothberg, F. Papadimitrakopoulos, M. E. Galvin and T. M. Miller, *Mol. Cryst. Liq. Cryst. Sci. Technol. Sect. A-Mol. Cryst. Liq. Cryst.*, 1994, **256**, 17-25.
145. L. M. Goldenberg, M. R. Bryce and M. C. Petty, *J. Mater. Chem.*, 1999, **9**, 1957-1974.
146. D. Demeter, P. Blanchard, I. Grosu and J. Roncali, *J. Incl. Phenom. Macrocycl. Chem.*, 2008, **61**, 227-239.
147. D. Demeter, P. Blanchard, I. Grosu and J. Roncali, *Electrochem. Commun.*, 2007, **9**, 1587-1591.
148. I. F. Perepichka, M. Besbes, E. Levillain, M. Salle and J. Roncali, *Chem. Mat.*, 2002, **14**, 449-457.
149. J. L. Segura and N. Martin, *Angew. Chem.-Int. Edit.*, 2001, **40**, 1372-1409.
150. J. Ferraris, V. Walatka, Perlstei.Jh and D. O. Cowan, *J. Am. Chem. Soc.*, 1973, **95**, 948-949.
151. P. Frere and P. J. Skabara, *Chem. Soc. Rev.*, 2005, **34**, 69-98.
152. X. K. Gao, W. F. Qiu, Y. Q. Liu, G. Yu and D. B. Zhu, *Pure Appl. Chem.*, 2008, **80**, 2405-2423.
153. O. Aleveque, P. Frere, P. Leriche, T. Breton, A. Cravino and J. Roncali, *J. Mater. Chem.*, 2009, **19**, 3648-3651.
154. R. Berridge, P. J. Skabara, C. Pozo-Gonzalo, A. Kanibolotsky, J. Lohr, J. J. W. McDouall, E. J. L. McInnes, J. Wolowska, C. Winder, N. S. Sariciftci, R. W. Harrington and W. Clegg, *J. Phys. Chem. B*, 2006, **110**, 3140-3152.
155. C. Thobiegautier, A. Gorgues, M. Jubault and J. Roncali, *Macromolecules*, 1993, **26**, 4094-4099.
156. L. Huchet, S. Akoudad and J. Roncali, *Adv. Mater.*, 1998, **10**, 541-545.
157. J. Garin, R. Andreu, J. Orduna and J. M. Royo, *Synth. Met.*, 2001, **120**, 749-750.
158. P. J. Skabara, R. Berridge, K. Prescott, L. M. Goldenberg, E. Orti, R. Viruela, R. Pou-Amerigo, A. S. Batsanov, J. A. K. Howard, S. J. Coles and M. B. Hursthouse, *J. Mater. Chem.*, 2000, **10**, 2448-2457.
159. S. Seong and D. S. Marynick, *J. Phys. Chem.*, 1994, **98**, 13334-13338.
160. K. Kobayashi and C. L. Gajurel, *Sulfur Rep. FIELD Full Journal Title:Sulfur Reports*, 1986, **7**, 123-152.
161. R. Berridge, I. M. Serebryakov, P. J. Skabara, E. Orti, R. Viruela, R. Pou-Amerigo, S. J. Coles and M. B. Hursthouse, *J. Mater. Chem.*, 2004, **14**, 2822-2830.
162. D. C. Green, *J. Org. Chem.*, 1979, **44**, 1476-1479.
163. W. Schroth, R. Borsdorf, Herzschu.R and J. Seidler, *Zeitschrift Fur Chemie*, 1970, **10**, 147.
164. P. R. Moses, R. M. Harnden and J. Q. Chambers, *J. Electroanal. Chem.*, 1977, **84**, 187-194.
165. R. M. Harnden, P. R. Moses and J. Q. Chambers, *J. Chem. Soc.-Chem. Commun.*, 1977, 11-12.
166. T. Sugimoto, I. Sugimoto, A. Kawashima, Y. Yamamoto, Y. Misaki and Z. Yoshida, *Heterocycles*, 1987, **25**, 83-88.
167. C. Pozo-Gonzalo, R. Berridge, P. J. Skabara, E. Cerrada, M. Laguna, S. J. Coles and M. B. Hursthouse, *Chem. Commun.*, 2002, 2408-2409.
168. P. J. Skabara, C. Pozo-Gonzalo, N. L. Miazza, M. Laguna, E. Cerrada, A. Luquin, B. Gonzalez, S. J. Coles, M. B. Hursthouse, R. W. Harrington and W. Clegg, *Dalton Trans.*, 2008, 3070-3079.

169. R. Berridge, S. P. Wright, P. J. Skabara, A. Dyer, T. Steckler, A. A. Argun, J. R. Reynolds, W. H. Ross and W. Clegg, *J. Mater. Chem.*, 2007, **17**, 225-231.
170. M. E. G. Lyons, *Charge Percolation in Electroactive Polymers in Electroactive Polymer Chemistry, Part 1 Fundamentals*, Plenum Press, New York, 1994.
171. Q. B. Pei, G. Zuccarello, M. Ahlskog and O. Inganas, *Polymer*, 1994, **35**, 1347-1351.
172. P. J. Skabara, R. Berridge, E. J. L. McInnes, D. P. West, S. J. Coles, M. B. Hursthouse and K. Mullen, *J. Mater. Chem.*, 2004, **14**, 1964-1969.
173. A. Loudet and K. Burgess, *Chem. Rev.*, 2007, **107**, 4891-4932.
174. A. Treibs and F. H. Kreuzer, *Justus Liebigs Ann. Chem.*, 1968, **718**, 208.
175. L. Bonardi, H. Kanaan, F. Camerel, P. Jolinat, P. Retailleau and R. Ziessel, *Adv. Funct. Mater.*, 2008, **18**, 401-413.
176. S. Erten-Ela, M. D. Yilmaz, B. Icli, Y. Dede, S. Icli and E. U. Akkaya, *Org. Lett.*, 2008, **10**, 3299-3302.
177. S. Y. Moon, N. R. Cha, Y. H. Kim and S. K. Chang, *J. Org. Chem.*, 2004, **69**, 181-183.
178. M. Yee, S. C. Fas, M. M. Stohlmeyer, T. J. Wandless and K. A. Cimprich, *J. Biol. Chem.*, 2005, **280**, 29053-29059.
179. I. J. Arroyo, R. R. Hu, G. Merino, B. Z. Tang and E. Pena-Cabrera, *J. Org. Chem.*, 2009, **74**, 5719-5722.
180. E. Vosdewael, J. A. Pardoën, J. A. Vankoevinge and J. Lugtenburg, *Recl. Trav. Chim. Pays-Bas-J. Roy. Neth. Chem. Soc.*, 1977, **96**, 306-309.
181. R. Ziessel, L. Bonardi, P. Retailleau and G. Ulrich, *J. Org. Chem.*, 2006, **71**, 3093-3102.
182. M. Kollmannsberger, K. Rurack, U. Resch-Genger and J. Daub, *J. Phys. Chem. A*, 1998, **102**, 10211-10220.
183. B. L. Groenendaal, F. Jonas, D. Freitag, H. Pielartzik and J. R. Reynolds, *Adv. Mater.*, 2000, **12**, 481-494.
184. G. Ulrich and R. Ziessel, *J. Org. Chem.*, 2004, **69**, 2070-2083.
185. R. Y. Lai and A. J. Bard, *J. Phys. Chem. B*, 2003, **107**, 5036-5042.
186. F. Algi and A. Cihaner, *Org. Electron.*, 2009, **10**, 704-710.
187. A. Cihaner and F. Algi, *React. Funct. Polym.*, 2009, **69**, 62-67.
188. T. Atalar, A. Cihaner and F. Algi, *Turk. J. Chem.*, 2009, **33**, 313-319.
189. H. C. Kang and R. P. Haughland, *US Patent 5451663*, 1993.
190. H. C. Kang and R. P. Haughland, *US Patent 5433896*, 1995.
191. S. Zrig, P. Remy, B. Andrioletti, E. Rose, I. Asselberghs and K. Clays, *J. Org. Chem.*, 2008, **73**, 1563-1566.
192. A. Cihaner and F. Algi, *Electrochim. Acta*, 2008, **54**, 786-792.
193. A. Bondi, *J. Phys. Chem. A*, 1964, **68**, 441-451.
194. H. Du, R. C. A. Fuh, J. Z. Li, L. A. Corkan and J. S. Lindsey, *Photochem. Photobiol.*, 1998, **68**, 141-142.
195. H. Hopf, *Angew. Chem.-Int. Edit.*, 2001, **40**, 705-707.
196. S. Fielder, D. D. Rowan and M. S. Sherburn, *Angew. Chem.-Int. Edit.*, 2000, **39**, 4331-4333.
197. J. Otsuki, M. Tsujino, T. Iizaki, K. Araki, M. Seno, K. Takatera and T. Watanabe, *J. Am. Chem. Soc.*, 1997, **119**, 7895-7896.
198. K. Sendt, L. A. Johnston, W. A. Hough, M. J. Crossley, N. S. Hush and J. R. Reimers, *J. Am. Chem. Soc.*, 2002, **124**, 9299-9309.
199. A. C. Benniston, *Chem. Soc. Rev.*, 2004, **33**, 573-578.

200. R. Berridge, P. J. Skabara, R. Andreu, J. Garin, J. Orduna and M. Torra, *Tetrahedron Lett.*, 2005, **46**, 7871-7875.
201. S. Amriou, I. F. Perepichka, A. S. Batsanov, M. R. Bryce, C. Rovira and J. Vidal-Gancedo, *Chem.-Eur. J.*, 2006, **12**, 5481-5494.
202. J. G. Laquindanum, H. E. Katz, A. J. Lovinger and A. Dodabalapur, *Chem. Mat.*, 1996, **8**, 2542-2544.
203. M. D. Curtis, J. Cao and J. W. Kampf, *J. Am. Chem. Soc.*, 2004, **126**, 4318-4328.
204. J. L. Bredas, J. P. Calbert, D. A. da Silva and J. Cornil, *Proc. Natl. Acad. Sci. U. S. A.*, 2002, **99**, 5804-5809.
205. K. Xiao, Y. Q. Liu, T. Qi, W. Zhang, F. Wang, J. H. Gao, W. F. Qiu, Y. Q. Ma, G. L. Cui, S. Y. Chen, X. W. Zhan, G. Yu, J. G. Qin, W. P. Hu and D. B. Zhu, *J. Am. Chem. Soc.*, 2005, **127**, 13281-13286.
206. X. N. Zhang, A. P. Cote and A. J. Matzger, *J. Am. Chem. Soc.*, 2005, **127**, 10502-10503.
207. E. G. Kim, V. Coropceanu, N. E. Gruhn, R. S. Sanchez-Carrera, R. Snoberger, A. J. Matzger and J. L. Bredas, *J. Am. Chem. Soc.*, 2007, **129**, 13072-13081.
208. M. M. Payne, S. A. Odom, S. R. Parkin and J. E. Anthony, *Org. Lett.*, 2004, **6**, 3325-3328.
209. M. Q. He and F. X. Zhang, *J. Org. Chem.*, 2007, **72**, 442-451.
210. K. Yamada, T. Okamoto, K. Kudoh, A. Wakamiya, S. Yamaguchi and J. Takeya, *Appl. Phys. Lett.*, 2007, **90**.
211. G. Barbarella, L. Favaretto, G. Sotgiu, L. Antolini, G. Gigli, R. Cingolani and A. Bongini, *Chem. Mat.*, 2001, **13**, 4112-4122.
212. G. Barbarella, L. Favaretto, M. Zambianchi, O. Pudova, C. Arbizzani, A. Bongini and M. Mastragostino, *Adv. Mater.*, 1998, **10**, 551-554.
213. A. Bongini, G. Barbarella, L. Favaretto, G. Sotgiu, M. Zambianchi and D. Casarini, *Tetrahedron*, 2002, **58**, 10151-10158.
214. L. S. Miguel and A. J. Matzger, *J. Org. Chem.*, 2008, **73**, 7882-7888.
215. X. C. Li, H. Sirringhaus, F. Garnier, A. B. Holmes, S. C. Moratti, N. Feeder, W. Clegg, S. J. Teat and R. H. Friend, *J. Am. Chem. Soc.*, 1998, **120**, 2206-2207.
216. T. Okamoto, K. Kudoh, A. Wakamiya and S. Yamaguchi, *Org. Lett.*, 2005, **7**, 5301-5304.
217. Y. Suzuki, T. Okamoto, A. Wakamiya and S. Yamaguchi, *Org. Lett.*, 2008, **10**, 3393-3396.
218. M. J. Kamlet, J. L. Abboud and R. W. Taft, *J. Am. Chem. Soc.*, 1977, **99**, 6027-6038.
219. M. J. Kamlet, J. L. M. Abboud, M. H. Abraham and R. W. Taft, *J. Org. Chem.*, 1983, **48**, 2877-2887.
220. L. Antolini, E. Tedesco, G. Barbarella, L. Favaretto, G. Sotgiu, M. Zambianchi, D. Casarini, G. Gigli and R. Cingolani, *J. Am. Chem. Soc.*, 2000, **122**, 9006-9013.
221. N. C. Greenham, I. D. W. Samuel, G. R. Hayes, R. T. Phillips, Y. Kessener, S. C. Moratti, A. B. Holmes and R. H. Friend, *Chem. Phys. Lett.*, 1995, **241**, 89-96.
222. J. F. Wolfe, B. H. Loo and F. E. Arnold, *Macromolecules*, 1981, **14**, 915-920.
223. J. F. Wolfe and F. E. Arnold, *Macromolecules*, 1981, **14**, 909-915.

224. J. F. Wolfe, *Encyclopedia of Polymer Science and Engineering*, Wiley, New York, 1988.
225. J. A. Osaheni and S. A. Jenekhe, *J. Am. Chem. Soc.*, 1995, **117**, 7389-7398.
226. J. F. Mike, A. J. Makowski and M. Jeffries-El, *Org. Lett.*, 2008, **10**, 4915-4918.
227. J. A. Osaheni and S. A. Jenekhe, *Macromolecules*, 1993, **26**, 4726-4728.
228. E. Ahmed, F. S. Kim, H. Xin and S. A. Jenekhe, *Macromolecules*, 2009, **42**, 8615-8618.
229. H. Pang, F. Vilela, P. J. Skabara, J. J. W. McDouall, D. J. Crouch, T. D. Anthopoulos, D. D. C. Bradley, D. M. De Leeuw, P. N. Horton and M. B. Hursthouse, *Adv. Mater.*, 2007, **19**, 4438-4442.
230. J. G. Kang, H. G. Cho, S. K. Kang, C. Park, S. W. Lee, G. B. Park, J. S. Lee and I. T. Kim, *J. Photochem. Photobiol. A-Chem.*, 2006, **183**, 212-217.
231. I. T. Kim, S. W. Lee, S. Y. Kim, G. B. Park, S. H. Lee, S. K. Kang, J. G. Kang, C. M. Park and S. H. Jin, *Synth. Met.*, 2006, **156**, 38-41.
232. J. A. Osaheni and S. A. Jenekhe, *Chem. Mat.*, 1995, **7**, 672-682.
233. D. J. Kim, N. E. Lee, J. S. Park, I. J. Park, J. G. Kim and H. J. Cho, *Biosens. Bioelectron.*, 2010, **25**, 2477-2482.
234. A. Uygun, *Talanta*, 2009, **79**, 194-198.
235. Y. N. Ivanova and A. A. Karyakin, *Electrochem. Commun.*, 2004, **6**, 120-125.
236. A. A. Karyakin, Y. N. Ivanova, K. V. Revunova and E. E. Karyakina, *Anal. Chem.*, 2004, **76**, 2004-2009.
237. G. Cooke, J. Garety, S. Mabruk, V. Rotello, G. Surpateanu and P. Woisel, *Chem. Commun.*, 2004, 2722-2723.
238. S. Ghisla and V. Massey, *Eur. J. Biochem.*, 1989, **181**, 1-17.
239. H. Durliat and M. Comtat, *J. Biol. Chem.*, 1987, **262**, 11497-11500.
240. Y. M. Legrand, M. Gray, G. Cooke and V. M. Rotello, *J. Am. Chem. Soc.*, 2003, **125**, 15789-15795.
241. A. A. Linden, N. Hermans, S. Ott, L. Kruger and J. E. Backvall, *Chem.-Eur. J.*, 2005, **11**, 112-119.
242. J. J. Hasford and C. J. Rizzo, *J. Am. Chem. Soc.*, 1998, **120**, 2251-2255.
243. A. Niemz and V. M. Rotello, *Accounts Chem. Res.*, 1999, **32**, 44-52.
244. C. Bonazzola and E. J. Calvo, *J. Electroanal. Chem.*, 1998, **449**, 111-119.
245. S. Venkataraman, S. M. Martin, F. Q. Schafer and G. R. Buettner, *Free Radic. Biol. Med.*, 2000, **29**, 580-585.
246. F. Bedioui, S. Trevin, V. Albin, M. G. G. Villegas and J. Devynck, *Anal. Chim. Acta*, 1997, **341**, 177-185.
247. R. M. J. Palmer, A. G. Ferrige and S. Moncada, *Nature*, 1987, **327**, 524-526.
248. D. C. Yao, A. G. Vlessidis, N. P. Evmiridis, A. Evangelou, S. Karkabounas and S. Tsampalas, *Anal. Chim. Acta*, 2002, **458**, 281-289.
249. H. H. Shim, H. Do and Y. Lee, *Electroanalysis*, 2010, **22**, 359-366.
250. Z. Taha, F. Kiechle and T. Malinski, *Biochem. Biophys. Res. Commun.*, 1992, **188**, 734-739.
251. R. Wadsworth, E. Stankevicius and U. Simonsen, *J. Vasc. Res.*, 2006, **43**, 70-85.
252. T. Malinski and Z. Taha, *Nature*, 1992, **358**, 676-678.
253. E. N. Navera, M. Suzuki, E. Tamiya, T. Takeuchi and I. Karube, *Electroanalysis*, 1993, **5**, 17-22.

254. X. J. Zhang, L. Cardoso, M. Broderick, H. Fein and J. Lin, *Electroanalysis*, 2000, **12**, 1113-1117.
255. B. B. Wayland and L. W. Olson, *J. Am. Chem. Soc.*, 1974, **96**, 6037-6041.
256. T. Malinski, A. Ciszewski, J. Bennett, J. R. Fish and L. Czuchajowski, *J. Electrochem. Soc.*, 1991, **138**, 2008-2015.
257. F. Bedioui, S. Trevin, J. Devynck, F. Lantoine, A. Brunet and M. A. Devynck, *Biosens. Bioelectron.*, 1997, **12**, 205-212.